Subfertility in male and female mice with mutations in *Cecr2*

by

Kacie Ann Norton

A thesis submitted in partial fulfillment of the requirements for the degree of

Doctor of Philosophy

in

Molecular Biology and Genetics

Department of Biological Sciences
University of Alberta

Abstract

In both mice and humans, defects in spermatogenesis, oogenesis, and pregnancy can all affect fertility. Spermatogenesis requires the constant renewal of spermatogonial stem cells, completion of meiosis, and an intricate remodeling process to form functional spermatozoa. Oogenesis similarly requires an amplification of germ cells followed by meiosis and oocyte maturation, but occurs largely during embryogenesis to establish the pool of oocytes available for a female's entire reproductive life. As females must additionally support the developing embryo, female infertility can also be caused by defects affecting pregnancy such as those disrupting implantation and placentation. Chromatin remodelers have been shown to have diverse functions in these processes, including roles in meiosis and regulation of gene expression.

CECR2 is part of a chromatin remodeling complex with known roles in neural tube closure, stereocilia organization within the inner ear, and kidney development. It has also been shown that male mice homozygous for the hypomorphic $Cecr2^{GT}$ allele are subfertile. The overall goal of this work was to investigate the role of $Cecr2$ in reproduction in both sexes. Since complete loss of $Cecr2$ results in perinatal death due to a neural tube defect, this study was accomplished by using mice of two $Cecr2$ genotypes: previously studied $Cecr2^{GT/GT}$ mice and compound heterozygote $Cecr2^{GT/Del}$ mice, which have a lower level of CECR2 due to the presence of one copy of the presumptive null $Cecr2^{Del}$ allele.

This work showed that in males, CECR2 is localized to gonocytes in embryonic day 18.5 testes and spermatogonia in adult testes. Fertility testing experiments revealed that both $Cecr2^{GT/GT}$ and $Cecr2^{GT/Del}$ subfertility is age-dependent. Mutant males sired few pups just after sexual maturity and their litter size improved significantly with age, although never reaching normal levels. $Cecr2^{GT/Del}$ males also have corresponding defects in testis histology and size, sperm concentration and motility, and the frequency at which they fertilize oocytes *in vivo,* phenotypes that all improve with age. Histological abnormalities in the testis first became apparent in 24 day old $Cecr2^{GT/Del}$ mice, but $Cecr2^{Del/Del}$ testes have fewer seminiferous cords at embryonic day 18.5. An RNA-seq analysis comparing $Cecr2^{+/+}$ and $Cecr2^{GT/Del}$ testes at P24 revealed 387 differentially expressed genes. Strikingly, while overall only 149 (39%) genes had higher transcript levels in $Cecr2^{GT/Del}$ testes, sex chromosome genes were exclusively found at increased levels in comparison to $Cecr2^{+/+}$ testes. This suggested a possible defect in meiotic sex chromosome inactivation, which was supported by the detection of increased autosomal asynapsis in mutant spermatocytes of 24-28 day old but not 142-149 day old males.

In females, *Cecr2* is expressed in the ovary, oviduct, and uterus at embryonic day 18.5. Both $Cecr2^{GT/GT}$ and $Cecr2^{GT/Del}$ females are subfertile with an approximately 50% reduction in litter size, but no change in litter size was observed with age. $Cecr2^{GT/GT}$ females ovulated a normal number of oocytes after superovulation, and there was no difference from wild-type in the percentage of those oocytes that were fertilized *in vivo*. In addition, they had a normal number of implantation sites at embryonic day 5.5, but embryo death occurred around day 9.5-10.5 and was accompanied by increased vaginal

blood. In contrast, *Cecr2*^{GT/Del} females had fewer implantation sites at embryonic day 5.5 despite normal ovarian histology. This is unlikely due to a defect in oocyte transport through the oviduct, as cilia function appeared normal in *Cecr2*^{GT/Del} females. However, decidual tissue was prematurely lost in some *Cecr2*^{GT/Del} females after artificially induced decidualization. As defects in decidualization can result in both the failure of implantation and embryonic loss later in gestation, abnormal decidualization in *Cecr2* mutants could play a role in both of these phenotypes.

Given that male *Cecr2* mutants have defects in spermatogenesis but female subfertility is likely due to uterine defects, *Cecr2* appears to have a sexually dimorphic role in reproduction. Additionally, *Cecr2* likely has a particularly important function in prepubertal spermatogenesis, as mutants are most severely subfertile just after sexual maturity. These intriguing phenotypes merit further investigation, as do changes in the transcriptome of *Cecr2*^{GT/Del} testes that may help explain *Cecr2's* function in spermatogenesis. Overall, this work has strengthened our understanding of the role *Cecr2* plays in reproduction in both males and females and has provided the foundation for future studies.

Preface

The research conducted in this thesis involved the use of mice. Research ethics approval was obtained from the Animal Care and Use Committee of the University of Alberta, AUP 00000094. The author has met the Canadian Council on Animal Care mandatory training requirements for all procedures and has completed the University of Alberta's Basic Surgical Skills course.

A version of Chapter 2 has been submitted and is currently in the revision process as Norton, K.A., Niri, F., Humphreys, R., Weatherill, C., Duong, K. Nguyen, V.V., Kommadath, A. Stothard, P. and McDermid, H. E., "Subfertility in young male mice mutant for chromatin remodeler CECR2". Some of the work presented was done in collaboration with the other authors. Kacie A. Norton wrote the manuscript, performed most of the experiments, and supervised the undergraduate students working on the project. The specific details are as follows:

> Dr. Farshad Niri generated the CECR2 antibody and did the western blots shown in Figure 2.1 B-C and Figure 2.2 O. Undergraduate student Ross Humphreys aided in collecting the testis weight data for Figure 2.3 F. Undergraduate students Ross Humphreys, Chelsey Weatherill, and Vivian V. Nguyen characterized histological abnormalities in the testis shown in Figure 2.5. Undergraduate student Kevin Duong assisted with RNA extractions and performed qPCR on a small portion of the genes. Drs. Arun Kommadath and Paul Stothard analyzed the RNA-seq data to generate the list of differentially expressed genes and the heat map shown in Figure 2.8. Dr. Heather E. McDermid contributed to conceptualization of some experiments and to the histological analysis of embryonic testes shown in Figure 2.6. Kacie A. Norton conceptualized and designed the experiments, performed all experiments not mentioned above, supervised all undergraduates and wrote the first draft of the manuscript.

A version of Chapter 3 is in preparation for submission as Norton, K.A., Weatherill, C., Williams, C.E., Duong, K., and McDermid, H.E., "Subfertility in female mice mutant for

chromatin remodeler *Cecr2*". Some of the work presented was done in collaboration with the other authors. Kacie A. Norton wrote the manuscript, performed most of the experiments, and supervised the undergraduate students working on the project. The specific details are as follows:

> Undergraduate student Chelsey Weatherill collected the ovary weight data mentioned in section 3.3.6 and the follicle counts shown in Figure 3.6 A. Graduate student Christine E. Williams did the X-Gal staining shown in Figure 3.2. Undergraduate student Kevin Duong assisted in the initial characterization of the histology of artificially decidualized uteri. Dr. Heather E. McDermid contributed to conceptualization of some experiments and did the uterine histology shown in Figure 3.8. Kacie A. Norton conceptualized and designed the experiments, performed all experiments not mentioned above, supervised both undergraduate students and wrote the first draft of the manuscript.

In the appendix, Dr. Arun Kommadath also generated the MDS plot shown in Figure B.1 and Figure B.2 comparing *Cecr2* expression levels as part of the RNA-seq analysis. Another graduate student, Niall Pollock, assisted with the DAVID analysis shown in Table B.2 and B.3.

Acknowledgements

I also wish to thank all my friends and family who have been by my side through these years. They not only gave me an escape from work at times, but also encouraged me to talk about my research even though the details were sometimes gory. In particular, my partner Adam has been amazingly supportive and has kept me going through difficult times. Thank you for making our lives at home relaxing, for convincing me to take breaks, and for bringing the perfect furry thesis-writing companion into our lives.

Table of Contents

List of Tables

List of Figures

List of symbols, nomenclature, and abbreviations

%	Percentage
~	Approximately
>	Greater than
≥	Greater than or equal to
<	Less than
≤	Less than or equal to
±	Plus or minus
°C	Degrees Celsius
μl	Microliter
ΔΔCT	Delta-delta cycle threshold (method for qPCR analysis)
αGSU	Glycoprotein hormone α subunit
A_S	Type A spermatogonia- single (undifferentiated)
A_{pr}	Type A spermatogonia- paired (undifferentiated)
A_{al}	Type A spermatogonia- aligned (undifferentiated)
A_{1-4}	Type A spermatogonia, subtypes 1-4 (differentiating)
A2m	Alpha-2-macroglobulin
ACF	ATP-dependent chromatin assembly factor
Adm	Adrenomedullin
AE	Axial element
AITF	Alberta Innovates Technology Futures
Amhr2	Anti-mullerian hormone receptor type 2
AT hook	Adenosine Thymine DNA binding hook
ATCC	American Type Culture Collection
ATM	Ataxia telangiectasia mutated
ATP	Adenosine triphosphate
ATR	Ataxia telangiectasia and Rad3 related
ATRX	Alpha thalassemia/mental retardation syndrome X-linked
BAF	BRG1/BRM associated factor (BAF)
Bax	BCL2-associated X protein
BAZ1A	Bromodomain adjacent to zinc finger domain, 1A
BAZ1B	Bromodomain adjacent to zinc finger domain, 1B
BET	Bromodomain and extraterminal domain
β-gal	Beta-galactosidase
Bmp2	Bone morphogenetic protein 2
Bmp7	Bone morphogenetic protein 7
Bmpr2	Bone morphogenetic protein receptor, type II (serine/threonine kinase)
bp	Base pair
BRCA1	Breast cancer 1, early onset
Brd2	Bromodomain containing 2

Brd3	Bromodomain containing 3
Brd4	Bromodomain containing 4
Brdt	Bromodomain, testis specific
BRG1	SWI/SNF related, matrix associated, actin dependent regulator of chromatin, subfamily a, member 4 (aka SMARCA4)
Ca^{2+}	Calcium ion
Cbs	Cystathionine beta-synthase
Ccnb3	Cyclin B3
cDNA	Complementary deoxyribonucleic acid
Cecr2	Cat eye syndrome chromosome region, candidate 2
Cecr2+	Wild-type allele of *Cecr2*
Cecr2GT	*Cecr2Gt(pGT1)1Hemc* hypomorphic genetrap allele of *Cecr2*
Cecr2Del	*Cecr2tm.1.1Hemc* presumptive null allele of *Cecr2*
Cecr2tm2a(EUCOMM)Hmgu	*Cecr2* allele with loxP sites flanking exon 4
Cecr2tm2b(EUCOMM)Hmgu	*Cecr2tm2a(EUCOMM)Hmgu* allele post-Cre excision (exon 4 excised)
CERF	CECR2-containing Remodeling Factor
CHD	Chromodomain, helicase, DNA binding
Chd5	Chromodomain helicase DNA binding protein 5
ChIP-seq	Chromatin immunoprecipitation with massively parallel DNA sequencing
CHRAC	Chromatin accessibility complex
CO_2	Carbon dioxide
CPM	Counts per million
Cre	Cre recombinase
C-terminal	Carboxyl-terminal
CV	Coefficient of variation
DAPI	4',6-diamidino-2-phenylindole
DAVID	Database for annotation, visualization, and integrated discovery
DDT domain	DNA binding homeobox and different transcription factors
DIC	Differential interference contrast
Dlx1	Distal-less homeobox 1
DM	Days of Mating
DMC1	DNA meiotic recombinase 1
DMSO	Dimethylsulfoxide
DNA	Deoxyribonucleic acid
dNTPs	Deoxyribonucleotide triphosphate
DSB	Double strand break
E	Embryonic day
EDTA	Ethylenediaminetetraacetic acid
ELISA	Enzyme-linked immunosorbent assay

ES cells	Embryonic stem cells
FACS	Fluorescence activated cell sorting
Fancb	Fanconi anemia, complementation group B
FC	Fold change
FDR	False discovery rate
Fgr	FGR proto-oncogene, Src family tyrosine kinase
FSH	Follicle stimulating hormone
Gapdh	Glyceraldehyde-3-phosphate dehydrogenase
GC1	Germ cell 1 cell line (immortalized type B spermatogonia)
GC2	Germ cell 2 cell line (immortalized spermatocytes)
GFRA1	Glial cell line derived neurotrophic factor family receptor alpha 1
Glp1	Zinc finger, GATA-like protein 1 (aka *Zglp1*)
GnRH	Gonadotrophin-releasing hormone
GO	Gene ontology
H	Hours
H&E	Hematoxylin and Eosin
H2AX	H2A.X variant histone
γH2AX	H2A.X variant histone, phosphorylated at serine 139
H_2O	Water
HEK-293T	Human embryonic kidney 293 cells
Hfm1	Helicase for meiosis 1
Hormad1	HORMA domain containing 1
Hormad2	HORMA domain containing 2
Hoxa10	Homeobox A10
IGEPAL CA-630	Octylphenoxy poly(ethyleneoxy)ethanol, branched
In	Intermediate (spermatogonia)
INO80	Inositol-requiring 80
ISWI	Imitation switch chromatin remodeler family
KCl	Potassium chloride
kDa	kilodaltons
KIT	KIT proto-oncogene receptor tyrosine kinase
KO	Knockout
Lgals1	Lectin, galactose binding, soluble 1
LH	Luteinizing Hormone
loxP	Locus of X-over P1 (target sites for Cre recombinase)
MBSU	Molecular biology service unit
MDC1	Mediator of DNA damage checkpoint 1
MDS	Multi-dimensional scaling
Meiob	Meiosis specific with OB domains
MEM	Minimum essential medium
mg	Milligrams

MgCl$_2$	Magnesium chloride
min	Minutes
mL	Milliliters
MLH1	mutL homolog 1
MLH3	mutL homolog 3
mM	Millimolar
mm	Millimeters
mRNA	Messenger Ribonucleic acid
MSCI	Meiotic Sex Chromosome Inactivation
Msh4	mutS homolog 4
MSUC	Meiotic Silencing of Unsynapsed Chromosomes
MT	Mutant
N	ploidy
n	Sample number
NaCl	Sodium chloride
NaOH	Sodium hydroxide
Ngn3	Neurogenin 3
NSERC	Natural sciences and engineering research council
Ni-NTA	Nickel-Nitrilotriacetic acid
N-terminal	Amino terminal
Oct4	aka *Pou5f1,* POU domain, class 5, transcription factor 1
p	p-value
P	Postnatal day
PCR	Polymerase chain reaction
PBS	Phosphate buffered saline
PFA	Paraformaldehyde
pH	Potential hydrogen
PLCζ	Phospholipase C zeta
PMSC	Post-meiotic sex chromatin
Pou5f1	POU domain, class 5, transcription factor 1, aka *Oct4*
PR	Progesterone receptor
Prkaa2	Protein kinase, AMP-activated, alpha 2 catalytic subunit
Ptchd3	Patched domain containing 3
PVA	Polyvinyl alcohol
QEII	Queen Elizabeth II scholarship
qPCR	Quantitative polymerase chain reaction
RAD18	RAD18 E3 ubiquitin protein ligase
RAD51	RAD51 recombinase
Radil	Ras association and DIL domains
Raptor	Regulatory associated protein of MTOR, complex 1
Rbpj	Recombination signal binding protein for immunoglobulin kappa J region

Rhox13	Reproductive homeobox 13
RNA	Ribonucleic acid
RNA-FISH	Ribonucleic acid- Fluorescence in situ hybridization
RNA-seq	Ribonucleic acid- massively parallel DNA sequencing
S.E.M.	Standard error of the mean
SASS	Science animal support services
Scml2	Scm polycomb group protein like 2
SDS	Sodium dodecyl sulfate
SF9 cells	Spodoptera frugiperda insect cell line
siRNA	Small interfering ribonucleic acid
Slx2	SYCP3-like X-linked 2
SNF2L	aka SMARKA1, SWI/SNF related, matrix associated, actin dependent regulator of chromatin, subfamily a, member 1
SNF2H	aka SMARKA5, SWI/SNF related, matrix associated, actin dependent regulator of chromatin, subfamily a, member 5
Sox3	SRY (sex determining region Y)-box 3
Spata22	Spermatogenesis associated 22
SPO11	SPO11 meiotic protein covalently bound to DSB
Sry	Sex determining region of Chr Y
STAR	Spliced Transcripts Alignment to a Reference (software)
STRA8	Stimulated by retinoic acid gene 8
SUMO-1	Small ubiquitin-like modifier 1
SWI/SNF	Switching defective/sucrose nonfermenting
SYCP1	aka SCP1, synaptonemal complex protein 1
SYCP2	aka SCP2, synaptonemal complex protein 2
SYCP3	aka SCP3, synaptonemal complex protein 3
Taf7l	TATA-box binding protein associated factor 7 like
TBP	TATA-Box bind protein
Tex11	Testis expressed gene 11
TMM	Trimmed mean of M-values
TNAP	Tissue non-specific alkaline phosphatase
Trp63	Transformation related protein 63
U/mL	Units per milliliter
UV	Ultraviolet
V	Volts
v/v	Volume per volume (percentage by volume)
vs	Versus
w/v	Weight per volume (percentage by weight)
WICH	WSTF-ISWI chromatin remodeling complex
Wnt5a	Wingless-type MMTV integration site family, member 5A
WT	Wild-type
XMR	Xlr-related, meiosis regulated

X-Gal	BCIG for 5-bromo-4-chloro-3-indolyl-β-D-galactopyranoside
Zfy2	Zinc finger protein 2, Y-linked
ZP1	Zona pellucida glycoprotein 1
ZP2	Zona pellucida glycoprotein 2
ZP3	Zona pellucida glycoprotein 3
µg	Micrograms
µm	Micrometer

Chapter 1 Introduction

1.1 Fertility

Infertility is defined as the failure to establish a clinical pregnancy after 1 year of regular unprotected intercourse, whereas sterility is the permanent condition of infertility (Vander Borght and Wyns, 2018). Infertility affects approximately 8-12% of couples globally, and many causes including genetic abnormalities and environmental factors have been identified (Vander Borght and Wyns, 2018). A recent meta-analysis estimates that the percentage of these cases due solely to male factor infertility ranges from 20-70% worldwide, with the percentage of men reported as infertile ranging from 2.5-12% (Agarwal et al., 2015). Even with genetic testing, the cause of infertility remains undetermined in approximately 72% of infertile men (Tüttelmann et al., 2018). The number of genes potentially involved in spermatogenesis is staggering; it has been estimated that >2300 genes or ~4% of the mouse genome is specifically expressed in male germ cells (Schultz et al., 2003). This is in addition to the multitude of genes that play a role in spermatogenesis but are not testis specific. Female factor infertility is estimated to account for ≥35% of infertility cases, with ~10% of women of reproductive age unable to produce children (Yatsenko and Rajkovic, 2019). Genetic mutations affecting sex determination, oogenesis, hormonal signaling, fertilization, implantation, and embryonic growth have all been found to contribute to female factor infertility (reviewed in Yatsenko and Rajkovic, 2019).

The identification of genes causing infertility in humans is limited due to small sample sizes, insufficient phenotypic information, and ethical constraints (Jamsai and O'Bryan, 2011). Despite this, over 60 candidate genes have been identified that are thought to cause spermatogenic failure in humans (reviewed in Cannarella et al. 2019). Over 90 genes have been strongly implicated in human female infertility (reviewed in Yatsenko and Rajkovic 2019). These discoveries have been aided by the use of animal models, particularly mouse models. The combination of genetic tools available for use in mice and their highly similar reproductive systems makes them ideal for these studies. Both forward and reverse genetic screens have proven useful in identifying genes essential for fertility in mice, many of which have also been identified as important in human studies

(reviewed in Ward et al. 2003; Furnes and Schimenti 2007; Jamsai and O'Bryan 2011; Lessard et al. 2007; Lee et al. 2007). The remainder of this work is focused on mouse studies, although examples of human diseases or comparisons to humans are sometimes given for context.

1.2 Spermatogenesis

1.2.1 Prenatal development of the testis

The continuous production of spermatozoa during adulthood is dependent first on the establishment of the gonocyte population during embryogenesis and development of the seminiferous tubules. Primordial germ cells are specified between embryonic day 6.5 (E6.5) and E7.25 during embryonic development of both sexes (Ginsburg et al., 1990), and migrate into the genital ridges around E10-10.5 (Molyneaux et al., 2001). In males, the expression of *Sry* between E10.5 and E12.5 leads to the development the testis (Koopman et al., 1991). Male primordial germ cells proliferate until E14.5 (Noguchi and Stevens, 1982), during which time they become enveloped by Sertoli cells to form seminiferous cords. At this point the germ cells are referred to as gonocytes or prospermatogonia, and they then undergo a period of quiescence until after birth (reviewed in Zhao and Garbers 2002; Furnes and Schimenti 2007). See 1.2.8 *Unique first wave of spermatogenesis* for events occurring after birth, including the transformation of gonocytes into spermatogonia.

1.2.2 Overview of adult sperm production

Overall, the process of generating spermatozoa from spermatogonial stem cells can be divided into 3 phases: proliferative, meiotic, and spermiogenic (reviewed in Russell et al., 1990). In the proliferative phase, spermatogonia undergo mitosis to both self-renew and amplify their numbers. Spermatocytes then undergo meiosis I and II to form haploid

3

spermatids. Finally, these spermatids must undergo a dramatic remodeling process known as spermiogenesis to form spermatozoa.

These three phases all occur within the seminiferous tubules, with more differentiated germ cells found progressively closer to the lumen (Figure 1.1). The organization and timing of this process is carefully controlled in a cyclical manner, such that a new "cycle" begins roughly every 8.6 days. However, since it takes around 34.5 days to produce spermatozoa, multiple generations of germ cells can be seen within a single tubule with cells from older cycles found towards the lumen (Figure 1.2 A) (Oakberg, 1956). The precise timing of the cycle ensures that a distinct set of cell types are always found together, allowing the classification of seminiferous tubules into 12 stages (Figure 1.2 B, Roman numerals). The stage of the cycle is most easily identified by which of the 16 types of spermatids are present (Figure 1.2 B, Arabic numerals). For example, stage I of a normal tubule will always contain pachytene spermatocytes, as well as step 1 and 13 spermatids. To ensure the constant production of spermatozoa, this cycle initiates as a "wave" through the length of the seminiferous tubule. Therefore, in cross-sections of whole testes, seminiferous tubules of all 12 stages can be visualized. Of the germ cells, only type A spermatogonia are found at every stage of the cycle.
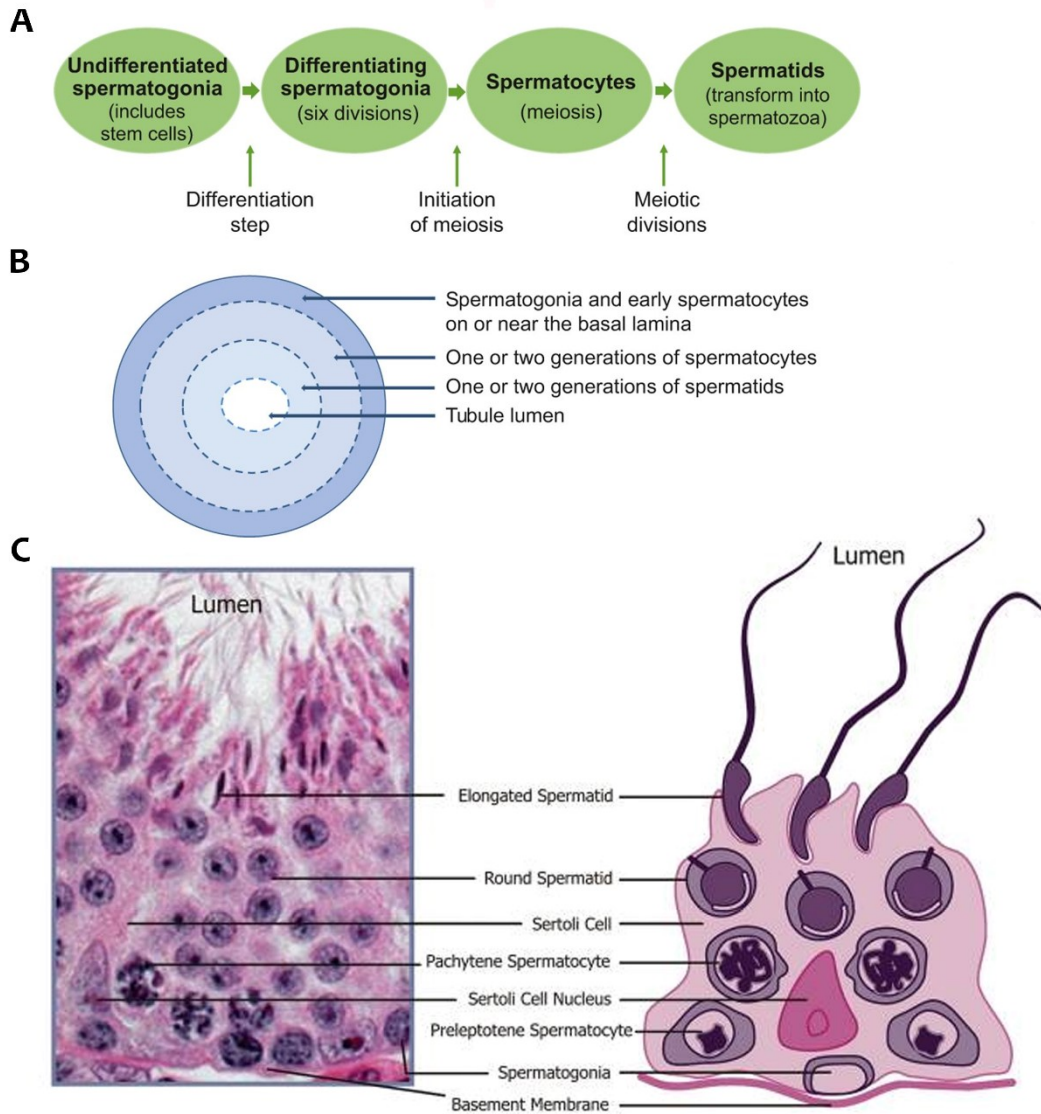
Figure 1.1: Steps of spermatogenesis and organization of the seminiferous epithelium.
(A) Overview of the major events and cell types of spermatogenesis. (B) Diagram showing the broad organization of seminiferous tubules. In a cross section, spermatogonia and early spermatocytes are found near the outer edge of each tubule and more mature germ cells are found progressively towards the lumen. (C) Partial cross section of a seminiferous tubule with major cell types identified. Each Sertoli cell envelops all layers of germ cells. *(Figure parts A, B reused with permission from Development (de Rooij 2017). Figure part C reused from Human Reproduction Update (Borg et al. 2009) by permission of Oxford University Press on behalf of the European Society of Human Reproduction and Embryology).*
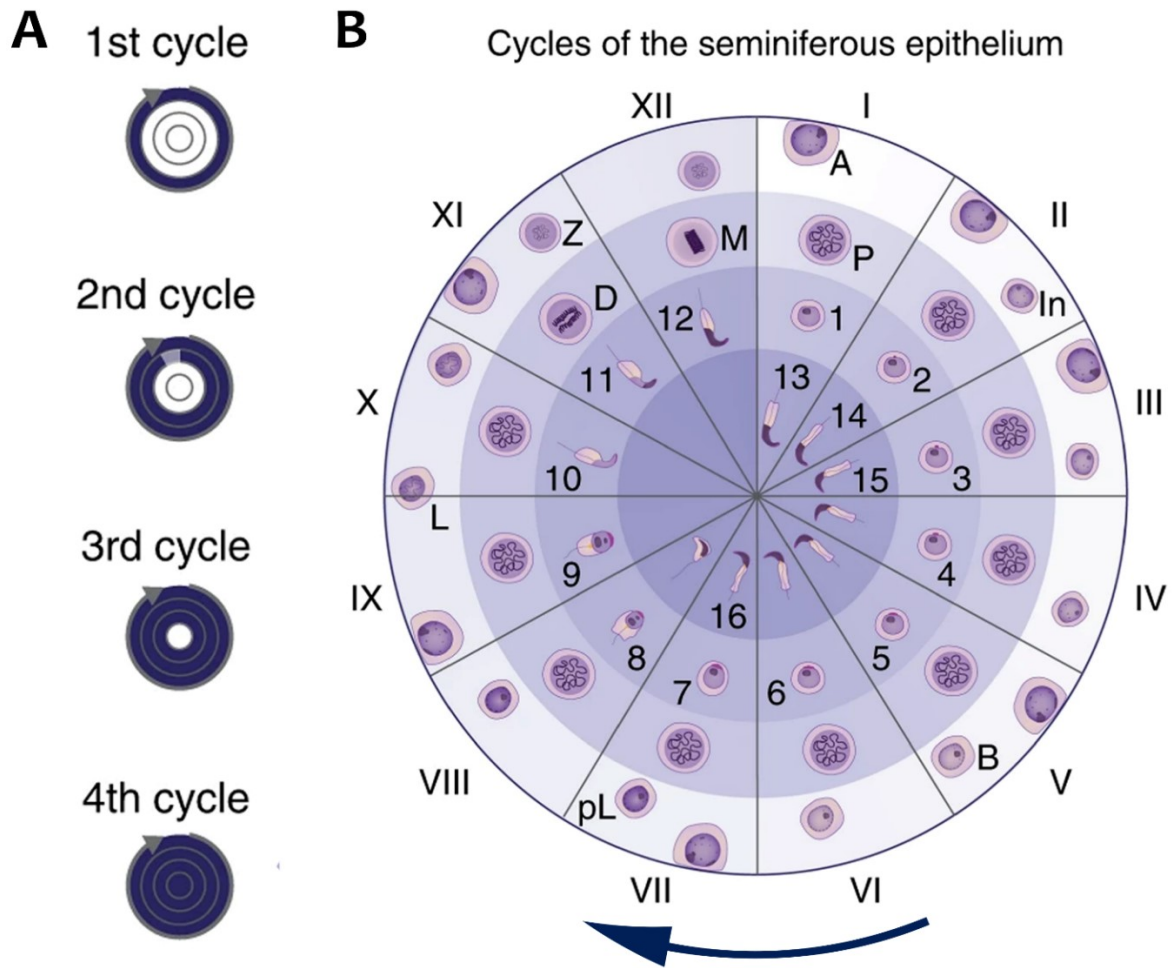
Figure 1.2: Cycle of the seminiferous epithelium. (A) Since spermatogenesis takes approximately 34.5 days to complete but a new cycle begins roughly every 8.6 days, germ cells that were initiated in the previous cycles are found in layers progressively closer to the lumen. (B) Illustration showing the 12 stages (Roman numerals) of the cycle of the seminiferous epithelium. Each slice of the diagram represents the cell types that are associated with each other at that stage. The 16 steps of spermiogenesis (Arabic numerals) are also shown. A= type A spermatogonia, In= Intermediate spermatogonia, B= type B spermatogonia, pL= preleptotene spermatocytes, L= leptotene spermatocytes, Z= zygotene spermatocytes, P=pachytene spermatocytes, D= diplotene spermatocytes, M= metaphase spermatocytes, 1-8= round spermatids, 9-16= elongating spermatids. *(Figure modified from Ernst et al. 2019 under a Creative Commons Attribution 4.0 International License: http://creativecommons.org/licenses/by/4.0/).*

1.2.3 Spermatogonial proliferation

The first several cell divisions of adult spermatogenesis serve to both increase the number of germ cells and renew the stem cell population for ongoing spermatogenesis. Within the proliferative phase, spermatogonia can be further classified into 9 types (reviewed in Russell et al. 1990). Early type A spermatogonia are termed single (A_s), paired (A_{pr}), or aligned (A_{al}) based on how many cell divisions have occurred, as up to 16 cells can remain connected to each other through intercellular bridges. Although it has been commonly accepted that A_s are the only true spermatogonial stem cells, it has now been suggested that all of these cell types may be capable of self-renewal through fragmentation of A_{al} chains to form more A_s and A_{pr} spermatogonia (Hara et al., 2014). As such, the dynamics of spermatogonial stem cell self-renewal and differentiation are still under investigation (Mäkelä and Hobbs, 2019). Nonetheless, there appears to be an epigenetically heterogenous population of undifferentiated spermatogonia that have varying capacity for self-renewal (reviewed in De Rooij 2017). A_{al} spermatogonia then differentiate to become A_1, followed by five more successive divisions to become A_2, A_3, A_4, Intermediate (In), and finally type B spermatogonia. These cell types are collectively referred to as differentiated spermatogonia. The commitment to begin this differentiation is triggered by retinoic acid, which transcriptionally activates genes required for meiosis (Busada and Geyer, 2015). While type A spermatogonia can be histologically differentiated from Intermediate and type B spermatogonia based on the amount of heterochromatin along the nuclear envelope, more precise histological identification relies on the stage of the seminiferous cycle as seen in Figure 1.2 (Russell et al., 1990).

1.2.4 Meiotic recombination and synapsis

Meiosis is essential for producing the genetically diverse haploid gametes necessary for sexual reproduction. Meiotic recombination through the formation and resolution of DNA double strand breaks (DSBs) is critical not only to generate this diversity, but also to

ensure correct synapsis and segregation of homologous chromosomes (Handel and Schimenti, 2010).

The meiotic phase of spermatogenesis begins when type B spermatogonia divide to become primary spermatocytes, which can then be defined by the stage of meiotic prophase I they are in (Figure 1.3). During leptotene stage, chromosomes condense and SPO11 topoisomerase creates 200-250 DSBs in the genome to be used for meiotic recombination (Kauppi et al., 2011; Keeney et al., 1997). This triggers the phosphorylation of H2AX by ATM and the recruitment of homologous recombination repair proteins. RAD51 and DMC1 facilitate homologous strand invasion, which allows for the pairing of homologous chromosomes and the initiation of synaptonemal complex formation (Brown and Bishop, 2015; Plug et al., 1996). Synapsis is initiated in zygotene spermatocytes and is complete by pachytene. Defects in synapsis are observed when a low number of DSBs are generated (Kauppi et al., 2013). By the end of pachytene, recombination intermediates are resolved to form either crossovers or non-crossovers (Guillon et al., 2005). MLH1 and MLH3 stabilize chiasmata and mark sites of crossovers (Baker et al., 1996; Lipkin et al., 2002). Although less than 10% of recombination events result in crossovers, these pathways are regulated to ensure at least 1 crossover event per homologous pair (Baudat et al., 2013). This is critical for the correct orientation of homologous chromosomes at metaphase, as the sites of recombination (chiasmata) hold the homologous chromosomes together after desynapsis occurs at diplotene stage (Handel and Schimenti, 2010).

Meiotic prophase I lasts approximately 3 weeks, after which primary spermatocytes undergo the first meiotic division to become secondary spermatocytes. Meiosis II occurs rapidly, and results in haploid germ cells referred to as round spermatids (Russell et al., 1990). The maturation of round spermatids into spermatozoa is discussed later (see 1.2.6 *Spermiogenesis and epididymal maturation*).
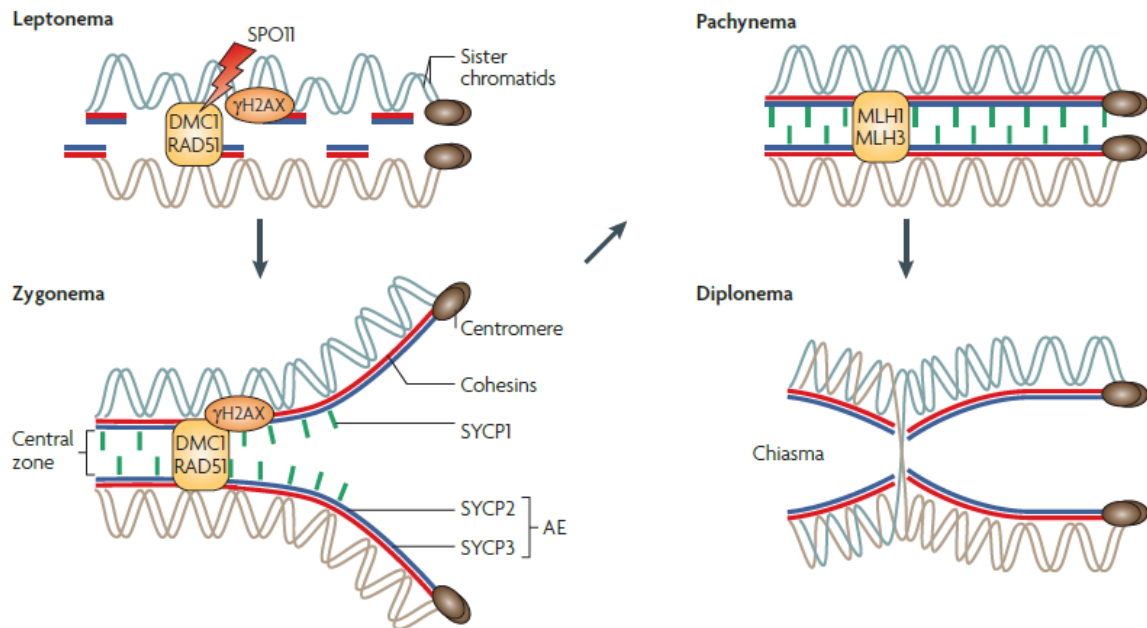
Figure 1.3: Substages of meiotic prophase I. The major events of prophase I and synaptonemal complex formation are shown. The DSBs are induced and the chromosomal scaffold begins to form during leptonema. Synapsis begins at zygotene stage and is complete by pachytene stage. At diplotene stage, the chromosomes are held together at the sites of recombination (chiasma). SYCP1 is part of the central zone of the synaptonemal complex, while SYCP2 and SYCP3 are part of the axial elements (AEs). *(Figure reprinted by permission from Springer Nature Customer Service Centre GmbH: Springer Nature, Nature Reviews Genetics, Handel and Schimenti © 2010, which was previously modified with permission from Morelli and Cohen, © 2005, Society for Reproduction and Fertility).*

1.2.5 Meiotic silencing of unsynapsed chromatin (MSUC)

During pachytene of meiosis I, when synapsis should be complete, the unsynapsed regions of the male sex chromosomes undergo transcriptional silencing and exclusion into a subnuclear domain through a process known as Meiotic Sex Chromosome Inactivation (MSCI) (Figure 1.4) (Turner et al., 2005). While it was at first thought that this silencing was unique to sex chromosomes, the discovery that asynapsed meiotic chromosome regions are also silenced in *Neurospora crassa* and other species suggested otherwise

(Bean et al., 2003; Shiu and Raju, 2001). Later experiments addressed this using mice with autosomal translocations or modified sex chromosomes that prevent full synapsis (Baarends et al., 2005; Homolka et al., 2007; Turner et al., 2005). This work confirmed that MSCI is a specific application of a much broader meiotic silencing mechanism targeting asynapsed chromosomes in both male and female meiosis. Molecularly, this transcriptional silencing occurs through a series of "sensors" and "effectors" (Figure 1.5). The DNA is organized in loops and attached to axial elements, structures that form part of the synaptonemal complex (Page and Hawley, 2004). Unsynapsed axial elements are recognized by "sensor" proteins including BRCA1, HORMAD1, and HORMAD2, which then help recruit ATR to the axial elements (Turner, 2015). ATR then translocates to the DNA loops, where it phosphorylates H2AX at serine 139 (γH2AX) and triggers the transcriptional silencing of DNA in these regions (Royo et al., 2013). Other "effectors" have also been identified, including DNA damage response proteins RAD18 (Inagaki et al., 2011) and MDC1 (Ichijima et al., 2011). Chromosomes silenced in this manner remain largely transcriptionally inactive, although some X-linked genes are reactivated in post-meiotic germ cells (Sin and Namekawa, 2013). In cases of autosomal asynapsis, MSCI proteins may be sequestered away from the sex chromosomes resulting in less efficient MSCI (Mahadevaiah et al., 2008).

The purpose of meiotic silencing remains somewhat unclear, but several hypotheses have been suggested (reviewed in Turner, 2015). One idea is that it may be a mechanism to prevent DSBs present on unsynapsed chromosomes from undergoing ectopic recombination. It has also been suggested to play a role in triggering the pachytene checkpoint, ensuring that cells with asynapsis are arrested. Alternatively, cell death could occur through a more direct method, where the abnormal silencing of asynapsed autosomes leads to "transcriptional starvation" (Turner, 2015). Importantly, failure to effectively silence the sex chromosomes also leads to cell death through the expression of pachytene-lethal Y-linked gene *Zfy2* (Royo et al., 2010).
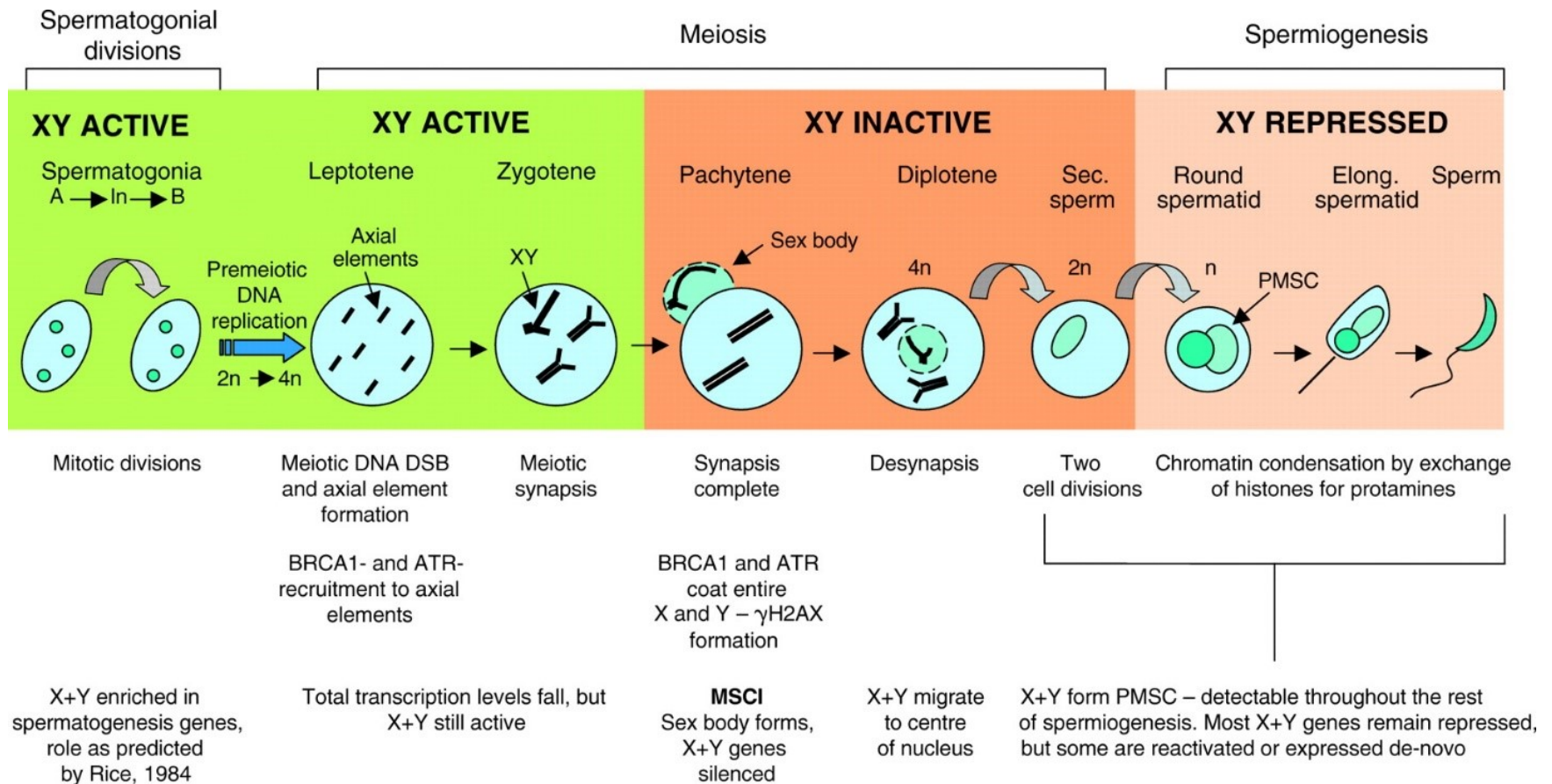
Figure 1.4: Transcriptional activity of sex chromosomes during spermatogenesis and MSCI. The major events of MSCI are shown in the context of spermatogenesis. The changing transcriptional level of the sex chromosomes during these steps is summarized along the bottom of the figure. PMSC = post-meiotic sex chromatin, the heterochromatic form of the repressed sex chromosomes. *(Figure reproduced with permission from Development, J. M. A. Turner 2007)*
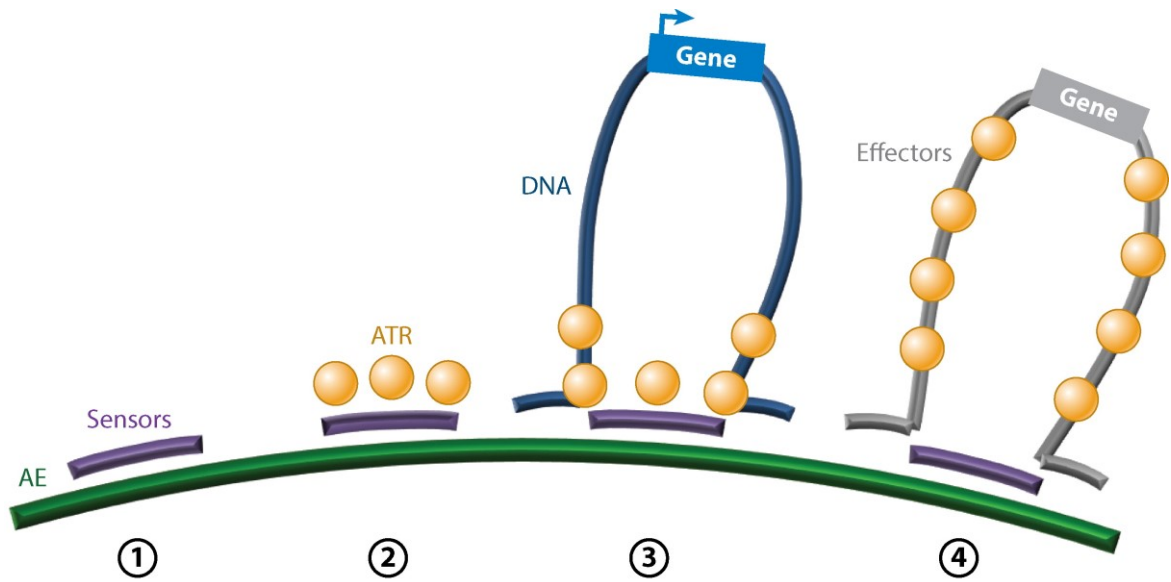
Figure 1.5: Model of meiotic silencing. Sensor proteins bind to unsynapsed axial elements (AE). ATR colocalizes with these sensors, then translocates outwards along DNA loops where it and other effectors cause meiotic silencing. *(Figure republished with permission from Annual Reviews, Inc, from James M.A. Turner 2015; permission conveyed through Copyright Clearance Center Inc.)*

1.2.6 Spermiogenesis and epididymal maturation

Following the completion of meiosis, round spermatids undergo an intricate cytodifferentiation process known as spermiogenesis to transform into elongated spermatids (reviewed in Russell et al. 1990; Toshimori and Eddy 2014). This process, which can be divided morphologically into 16 steps (Figure 1.2 B), is necessary but not sufficient for spermatids to gain motility and fertilization potential. A major part of this process is formation of the sperm tail, which includes both the microtubule-based axoneme and secondary structures necessary for flagella function. The fibrous sheath and outer dense fibers both provide structural rigidity that is important for motility and surviving the female reproductive tract, while the mitochondrial sheath is critical for ATP generation. The acrosome, a membrane-bound organelle that is necessary for sperm penetration through the zona pellucida, forms opposite the tail. Histones are replaced by transition proteins and eventually protamines, resulting in nuclear compaction to ~5% the nuclear volume of a somatic cell (Sassone, 2002). This extreme chromatin condensation results in transcriptional silencing, therefore most RNAs necessary for spermiogenesis are transcribed in a massive wave early in spermiogenesis and their translation is delayed until they are required at a later step (Braun, 1998).

As spermiogenesis completes, the cytoplasm of elongated spermatids is condensed and removed with the aid of Sertoli cells (reviewed in Russell et al. 1990). This final remodeling and subsequent release of spermatids into the lumen is known as spermiation. To become fertilization-competent, spermatozoa must undergo extra-testicular maturation in the epididymis. Within the epididymis, they become capable of progressive movement upon later capacitation in the female reproductive tract (Visconti et al., 1995) (see 1.4: *Fertilization* for more information about capacitation). They also acquire new proteins and post-translational modifications to existing proteins, including modifications to the sperm surface that are needed to bind the zona pellucida (Lakoski et al., 1988), undergo the acrosome reaction (Busso et al., 2007), and bind to the oolemma (Rochwerger et al., 1992). As epididymal spermatozoa are transcriptionally and

13

translationally inactive, these changes are dependent on epididymal epithelial secretions (reviewed in Gervasi and Visconti 2017).

1.2.7 Somatic cells of the testis

Although the testis is largely composed of germ cells, there are several types of somatic cells that also play key roles in spermatogenesis both within and between the seminiferous tubules. Sertoli cells are large cells found at the basement membrane within the seminiferous tubules, enveloping germ cells as they develop (Figure 1.1 C) (reviewed in Russell et al. 1990). Each Sertoli cell is in contact with 4-5 layers of germ cells and 5-6 other Sertoli cells, and these connections are critical to their functions (reviewed in Borg et al. 2009). Tight junctions between Sertoli cells separate the seminiferous epithelium into two compartments: the basal compartment that houses spermatogonia and spermatocytes up to early leptotene stage, and the adluminal compartment that contains meiotic and post-meiotic cells (reviewed in Russell et al. 1990). This compartmentalization is known as the blood-testis barrier or Sertoli cell barrier, and it acts as a critical immunological barrier to protect the adluminal compartment germ cells which are highly antigenic (reviewed in Borg et al. 2009). Sertoli cells also play several other support roles, including secreting luminal fluid, phagocytosing degenerating germ cells and cellular debris, and releasing mature spermatozoa into the lumen (known as spermiation). They provide nutrients to the germ cells they envelop, which is particularly critical for the germ cells of the adluminal compartment that are removed from the vascular system (Russell et al., 1990). In addition, Sertoli cells are involved in regulating the spermatogenic cycle through cyclical changes in the expression of genes such as galectin 1 (*Lgals1*) during the 12 stages of the cycle (Timmons et al., 2002). Galectin 1 is expressed in a pulse between seminiferous tubule stage VIII and IX, with the highest accumulation of transcript occurring between stage X and XII (Timmons et al., 2002).

The interstitial space between the seminiferous tubules contains Leydig cells and blood vessels as well as immune cells and connective tissue. Of these, the Leydig cells are the most abundant, and play a critical role in the hormonal control of spermatogenesis

(reviewed in Borg et al. 2009). Briefly, gonadotrophin-releasing hormone (GnRH) released by the hypothalamus stimulates the pituitary gland to secrete both follicle stimulating hormone (FSH) and luteinizing hormone (LH), which act on Sertoli and Leydig cells, respectively. Leydig cells respond to LH by producing testosterone, which stimulates Sertoli cell activity along with FSH from the pituitary gland. The release of these hormones is controlled by negative feedback: the release of GnRH from the hypothalamus and LH from the pituitary gland is inhibited by testosterone, and inhibin B produced by Sertoli cells reduces FSH production. Disruption of this hormonal control through surgical means (removal of the pituitary gland) or mutations commonly leads to germ cell degeneration and infertility (Ma et al., 2004; Wang et al., 2009).

Finally, peritubular smooth muscle cells make up the outer border of the seminiferous tubules, dividing the tubules and interstitial space. They are also thought to have some paracrine function, particularly in secreting factors that act on Sertoli cells (Skinner et al., 1985; Skinner and Fritz, 1985; Welsh et al., 2012). In addition, they can contract to produce peristalsis-like waves that assist the transport of spermatozoa and fluid within the lumen (Romano et al., 2005).

1.2.8 Unique first wave of spermatogenesis

During the first postnatal week, the gonocytes migrate from the middle to the periphery of the seminiferous cords. There, they transform into spermatogonia at around Postnatal day (P)3-P6 (Bellve et al., 1977). During the first wave of spermatogenesis, some gonocytes bypass the undifferentiated spermatogonia stage to directly become differentiating spermatogonia, and therefore do not undergo self-renewal (Niedenberger et al., 2015; Yoshida et al., 2006). While it was originally unclear whether or not spermatozoa formed in the first wave lacked fertilization potential, it was confirmed that spermatozoa from this lineage are able to produce offspring from *in vivo* matings at the first days of sexual maturity (P40 and P41 males) (Yoshida et al., 2006). The gonocytes that do not differentiate in this first wave establish the self-renewing spermatogonia population (Niedenberger et al., 2015; Yoshida et al., 2006). This also may be when the

spermatogenic wave is first established, as the gonocytes which divide directly into differentiating spermatogonia are found preferentially in segments with high galectin 1 (Yoshida et al., 2006). The time at which each germ cell type first appears during the initial wave has been well defined (Table 1.1), although it can vary slightly between mouse strains. The first spermatozoa appear at approximately P35 (Kramer and Erickson, 1981), and the wave nature of the cycle of the seminiferous epithelium allows for constant production from that point on.

Table 1.1: Time of first appearance of germ cells during testis development.

Cell Type	Time of first appearance
Gonocyte	E12 – P1
Undifferentiated spermatogonia (A_s, A_{pr}, A_{al})	P6
Differentiating spermatogonia (A_{1-4}, In, B)	P8
Meiosis I Leptotene spermatocytes	P10
Meiosis I Zygotene spermatocytes	P12
Meiosis I Pachytene spermatocytes	P14
Meiosis I Diplotene spermatocytes	P17 – P18
Meiosis II (secondary) spermatocytes	P18
Round spermatids	P20
Condensing spermatids	P30
Spermatozoa	P35

 E= embryonic day, P= postnatal day. *(Table adapted from Human Reproduction Update (Borg et al. 2009) by permission of Oxford University Press on behalf of the European Society of Human Reproduction and Embryology).*

The first wave of spermatogenesis is also characterized by a wave of apoptosis occurring largely between postnatal weeks 1 and 4 (Rodriguez et al., 1997; Russell et al., 2002). This apoptosis occurs in both spermatogonia and spermatocytes, and is estimated to result in a 70-80% reduction of germ cells in normal mice (Mori et al., 1997; Rodriguez et al., 1997). The purpose of this loss is not completely understood, but it appears to be critical for maintaining the proper ratio of germ cells to Sertoli cells. When this wave of apoptosis is prevented by altering the expression of critical proteins, this ratio is disrupted leading to abnormal adult spermatogenesis. For example, decreased apoptosis in *Bax*-deficient mice at this time leads to hypercellular tubules caused by increased numbers of type A spermatogonia followed by increased pre-meiotic spermatocytes (Russell et al., 2002). Later in pubertal development (P20-30), these mice show massive degeneration of spermatogenic cells, leading to an almost complete absence of mature sperm (Russell et al., 2002). As developing germ cells are highly dependent on Sertoli cells, maintaining their ratio may be important simply due to spatial and nourishment constraints (Kierszenbaum, 2001; Rodriguez et al., 1997; Russell et al., 2002). However, it has also been suggested that this early wave of apoptosis may act as an early quality control mechanism by targeting abnormal germ cells and the spermatogonium giving rise to them, as they remain connected by syncytium during these early divisions (Rodriguez et al., 1997).

1.3 Oogenesis

1.3.1 Early ovary development and establishment of the primordial follicle pool

As mentioned above, mouse primordial germ cells are established by E7.5 and migrate to the genital ridge at approximately E10.5 (Ginsburg et al., 1990; Molyneaux et al., 2001). In females, they then undergo mitotic divisions with incomplete cytokinesis to form germ cell cysts or nests (reviewed in Pepling 2006). These germ cells then initiate meiosis and become primary oocytes (Ginsburg et al., 1990). However, they only progress

to the diplotene stage of prophase I before entering a resting phase called dictyate, where they will remain until they are induced in adulthood to mature (Borum, 1966). Meiotic arrest occurs around the time of birth in mice, and follicle formation is also initiated at this time by the breakdown of germ cell cysts. Primordial follicles are formed when oocytes are surrounded by somatic pre-granulosa cells (reviewed in Pepling 2006). Many oocytes are lost at this point, as those that are not surrounded by pre-granulosa cells undergo apoptosis (Pepling and Spradling, 2001). The pool of primordial follicles that is established at this time is thought to act as the reservoir of germ cells available for a female's entire reproductive life. However, this pool is much larger than the number of oocytes that are eventually ovulated, as most follicles undergo atresia either prior to activation or during folliculogenesis (reviewed in Findlay et al. 2019). In fact, approximately 155 primordial follicles per ovary per day undergo atresia in P6-P19 mice (Tingen et al., 2009). This wave of death is thought to act as quality control for oocytes that have not recruited sufficient granulosa cells or have damaged genomes (Tilly, 2001).

1.3.2 Folliculogenesis

The process by which primordial germ cells are activated and develop into ovulatory follicles is known as folliculogenesis (Figure 1.6). This takes 2-4 weeks in the mouse and involves the acquisition of both meiotic and developmental competence (reviewed in Sánchez and Smitz 2012; Findlay et al. 2019). Meiotic competence refers to the ability of the oocyte to resume meiosis, while developmental competence refers to the ability of the oocyte to be fertilized and develop into a viable embryo. These changes are highly dependent on interactions between oocytes and their surrounding somatic cells.

Recruitment of oocytes into folliculogenesis occurs in cohorts, and many oocyte and somatic cell derived factors are involved in balancing the number of follicles that are activated (reviewed in Sánchez and Smitz 2012; Findlay et al. 2019). For example, the production of anti-Mullerian hormone by growing follicles has been shown to suppress the activation of nearby primordial follicles (Durlinger et al., 1999). Upon activation, the flattened granulosa cells of primordial follicles become cuboidal, characteristic of primary

follicles (Figure 1.6). Early follicle growth also consists of the formation of a basement membrane surrounding the follicle and formation of a zona pellucida around the oocyte (Findlay et al., 2019). The transition from primary to secondary follicles is seen as the recruitment of thecal cells and proliferation of granulosa cells to form multiple layers, and is dependent on intraovarian paracrine factors produced by the developing follicles (reviewed in Kol and Adashi 1995). Continued proliferation of granulosa cells leads to a drastic increase in follicular size and eventually the development of an antral cavity, at which time they are referred to as antral follicles. The granulosa cells then differentiate into cumulus cells (surrounding the oocyte) and mural granulosa cells (surrounding the antrum). While mural granulosa cells play a role in endocrine function, cumulus cells mainly nurture the developing oocyte (reviewed in Findlay et al. 2019). At this stage, follicle growth becomes dependent on gonadotropins secreted from the pituitary. FSH drives antral development and leads to the expression of LH receptors in mural granulosa cells, which is critical to allow follicles to respond to LH for final follicle maturation and ovulation (Burns et al., 2001). LH stimulates thecal cells to produce androgens, which granulosa cells then use to produce estrogens with stimulation of FSH (Hillier et al., 1994). Estradiol, the predominant estrogen produced by granulosa cells, is critical for follicle maturation past the early antral stage (Lubahn et al., 1993).
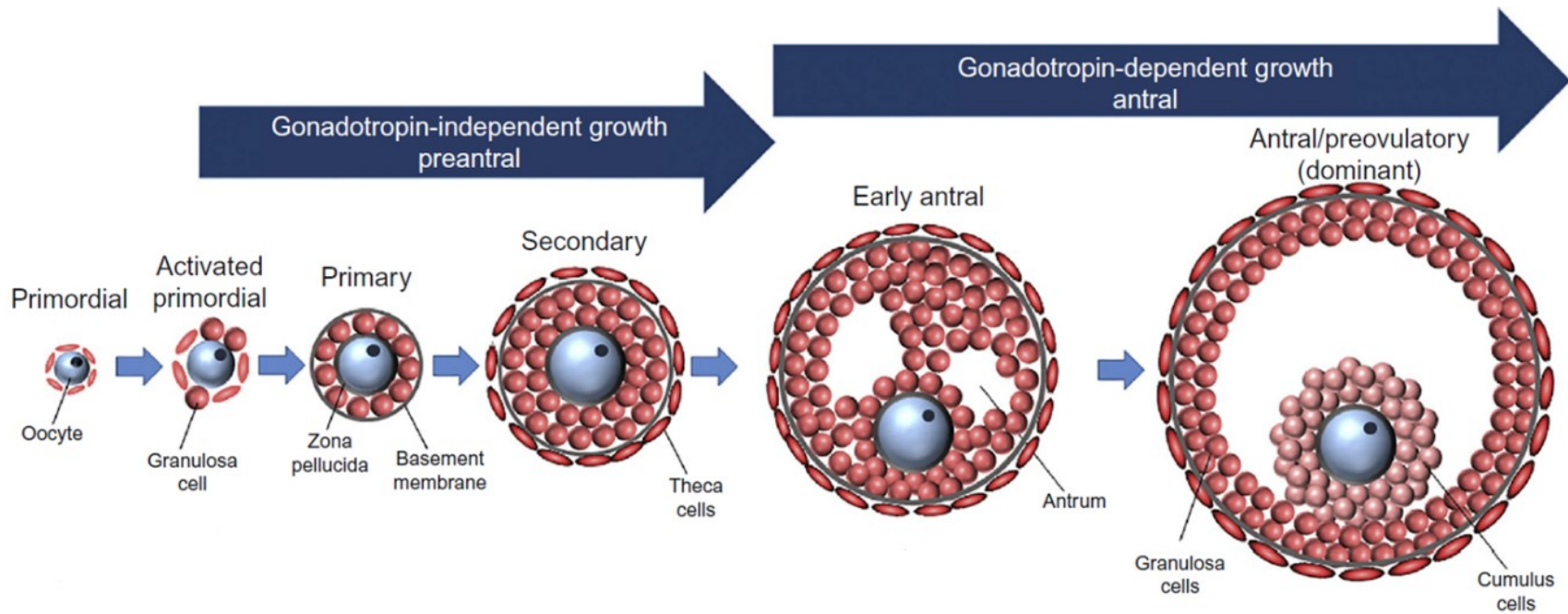
Figure 1.6: Folliculogenesis. The development of follicles from primordial to preovulatory stage is shown. See text for details. *(Reprinted from The Ovary, Findlay et al. 2019, with permission from Elsevier)*

Even at the early antral stage, many developing follicles undergo atresia. Only a small portion continue to grow and develop into follicles capable of ovulation (Hirshfield, 1991). Preovulatory follicles that contain mature oocytes are induced to rupture by a surge of LH, leading to the release of the oocyte-cumulus cell complex (ovulation). The granulosa and theca cells then transform into luteal cells, which produce estradiol and progesterone (reviewed in Stocco, Telleria, and Gibori 2007). This surge of LH also induces the oocyte to resume meiosis, proceeding to metaphase II and extruding the first polar body (Edwards, 1965).

The oocyte itself also undergoes dramatic changes during folliculogenesis. Oocytes synthesize and accumulate vast amounts of RNA and proteins that are necessary for the development of a viable embryo upon fertilization. In fact, mature mouse oocytes have been estimated to contain approximately 200 times the amount of RNA of an average somatic cell, the majority being rRNA (Wassarman and Kinloch, 1992). Although transcription occurs mostly in early stages and is later silenced (Pan et al., 2005), oocyte mRNA undergoes complex post-transcriptional regulation to ensure products are available when needed (reviewed in Sánchez and Smitz 2012). Overall, the accumulation of products necessary for early embryonic development as oocytes mature results in an approximately 100 fold increase in their volume by the time of ovulation (Sánchez and Smitz, 2012). Communication between granulosa cells and oocytes is essential to support follicle growth and the acquisition of both meiotic and developmental competence. The differentiation and expansion of cumulus cells is regulated largely by oocyte factors, and the metabolic activity of cumulus cells is critical to support oocyte growth (reviewed in Sánchez and Smitz 2012; Findlay et al. 2019).

1.3.3 Estrous cycle

The cyclic nature of the estrous cycle is due to changes in gonadotropin secretion by the pituitary gland, regulated by the hypothalamus (reviewed in Bronson, Dagg, and Snell 1966). The secretion of FSH promotes follicle growth, but the gonadal hormones produced by growing follicles act on the hypothalamus to suppress FSH release and

promote LH release. This triggers the final maturation of the follicle and ovulation. When mating does not occur, the gonadal hormones decrease to allow a new cycle to begin with increased FSH secretion. When mating does occur, a functional corpus luteum forms and prevents the initiation of a new cycle (Hilliard, 1973).

At its simplest, the cycle can be divided into 4 stages (Bronson et al., 1966). During proestrus, high estrogen levels cause growth in the uterus and vaginal epithelium. A subset of follicles grow rapidly to prepare for ovulation. In estrus, ovulation occurs and the female becomes receptive to mating. The uterus becomes maximally vascularized in preparation for pregnancy, and the outer epithelial layer of the vagina becomes cornified and sloughs off. Metestrus is largely catabolic, and newly formed corpus lutea are present. Finally, diestrus is a period of quiescence or slow growth before the beginning of the next cycle.

The average length of a cycle is 4-5 days in mice (Van Ebbenhorst Tengbergen, 1955), but they can vary considerably and have been observed as short as 2 days and as long as 28 days within one strain (Parkes, 1928). Cycle length can also be affected by strain, season, diet, and stress. When a group of females only are housed together, the Lee-Boot effect can cause prolonged diestrus (van der Lee and Boot, 1956). On the other hand, the introduction of a male can stimulate and normalize the estrus cycle in females, known as the Whitten effect (Whitten, 1957).

1.3.4 Implications of oogenesis for female fertility and reproduction in humans

The molecular events of oogenesis have important implications for female fertility. Two of the most impactful are premature ovarian insufficiency (also known as premature ovarian failure) and the high rates of aneuploidy that result from meiotic errors occurring during oogenesis. Both of these have an increasing effect on female fertility with age, and are therefore only becoming more problematic as women are becoming pregnant at a later age (Statistics Canada, n.d.). As males are able to constantly produce spermatozoa

from a renewing population of stem cells, they do not develop problems related to the long dictyate phase or a limited lifetime supply of gametes.

The rate of aneuploidy in human oocytes has been estimated as high as 30-70%, while the rate in sperm is approximately 1-4% (reviewed in Nagaoka, Hassold, and Hunt 2012). While many aneuploidies are lethal so early in development that they result in death before a pregnancy would be clinically detected, approximately 7-10% of clinically recognized pregnancies are affected (Hassold and Hunt, 2001). This rate strongly increases with age, such that women in their mid 40s have a ≥50% risk of ovulating an oocyte with aneuploidy (Pellestor et al., 2005). A similar age-associated increase has also been observed in mouse oocytes (Pan et al., 2008). The increased rate in females over males may reflect a difference in the "efficiency" of the spindle assembly checkpoint, allowing oocytes with meiotic nondisjunction to continue maturing when the same error would almost always halt spermatogenesis (LeMaire-Adkins et al., 1997; Vogt et al., 2008). Females may also be more prone to meiotic non-disjunction; the number and location of crossovers during meiosis and the structure of the synaptonemal complex both impact chromosome segregation, and both have been found to exhibit sexual dimorphisms (reviewed in Morelli and Cohen 2005). The long dictyate stage that oocytes experience is widely thought to play a role in the age-related increase, and may be related to a breakdown of the cohesion proteins responsible for holding together sister chromatids (Hodges et al., 2005). Deterioration of checkpoint function with age has also been suggested as a possible mechanism (Jones, 2008), although it seems unlikely to be the primary cause (Duncan et al., 2009). An alternative idea is that the highest quality oocytes are selected for activation first during folliculogenesis, leading to a slow decline of oocyte quality with age (reviewed in Findlay et al. 2019).

Premature ovarian insufficiency is defined as the depletion or arrest of ovarian follicles or absence of menarche before 40 years of age. It affects approximately 0.01% of women by the age of 20, 0.1% of women by the age of 30, and 1% of women by the age of 40 (Coulam et al., 1986). One possible cause is a deficiency in the number of primordial follicles that are originally formed. This can be caused by the generation of fewer

primordial germ cells, defects in meiosis causing early loss of oocytes, or abnormal breakdown of germ cell cysts (reviewed in Jagarlamudi et al. 2010). Activation of follicles at an elevated rate can also lead to rapid depletion of the ovarian reserve, as activation is irreversible and oocytes are not continually self-renewing like spermatogonia (Adhikari and Liu, 2010; Reddy et al., 2008). In fact, until recently it was generally accepted that oocyte stem cells do not exist in adult mice. However, there is now some evidence that adult mouse ovaries contain oocyte stem cells based on mathematical modeling, immunostaining of mitotic ovarian cells, and transplantation experiments (Johnson et al., 2004; Zhang et al., 2011). The existence of these cells remains somewhat controversial, but their function *in vivo* is even more highly debated and it is thought that they may only be activated through *in vitro* culture conditions (reviewed in Horan and Williams, 2017).

1.4 Fertilization

Even after spermatozoa undergo epididymal maturation, they are incapable of fertilizing an oocyte until they undergo a period of 'capacitation' in the female reproductive tract. Capacitation is required for (1) the hyperactivated motility of spermatozoa acquired in the oviduct and (2) for the spermatozoa to acquire the competence to undergo acrosomal exocytosis (reviewed in Buffone et al. 2012).

As spermatozoa make their way through the vagina, cervix, and uterus, they must avoid the female immune system and navigate a physically challenging path (reviewed in S. Suarez and Pacey 2006). The seminal fluid aids in protecting the sperm (Dostál et al., 1997), but it is thought that selection against less motile sperm occurs at this stage (Hanson and Overstreet, 1981; Katz et al., 1990). Passage of sperm into the oviduct occurs through the uterotubal junction, which only opens shortly after coitus (Suarez, 1987). The sperm then bind to the epithelium of the isthmus region, effectively creating a sperm storage reservoir which may be important for preventing polyspermy and timing sperm release with ovulation. The release of sperm from the epithelium likely involves both the shedding of proteins required for binding to the epithelium and the hyperactivation of

sperm at this time, providing the force necessary to break away (reviewed in Suarez 2008). Capacitation also causes several other molecular changes to the spermatozoa that allow them to recognize and bind to the zona pellucida, followed by the acrosome reaction necessary for penetrating the zona pellucida (reviewed in Reid et al. 2011).

To reach the oocyte, spermatozoa first need to navigate their way through the surrounding cumulus cells. This layer is comprised of approximately 5000 cells, and the sperm require both hyperactivated motility and the activity of hyaluronidase to make their way to the zona pellucida (Lin et al. 1994; reviewed in Primakoff and Myles 2002). Fertilization itself can be broken down into 4 main steps (Figure 1.7). First, sperm need to recognize and bind to the zona pellucida. The zona pellucida in mouse is composed of three glycoproteins, aptly named ZP1, ZP2, and ZP3. ZP3 appears to be the main receptor for sperm binding and is necessary for inducing the acrosome reaction (Arnoult et al., 1996; Bleil and Wassarman, 1980). The contents of the acrosome are released by exocytosis, and it is thought that the enzymatic activity of these contents allows the sperm to penetrate through the zona pellucida and reach the oocyte itself (reviewed in Ikawa et al. 2010). The sperm then binds to the oolemma (the plasma membrane of the oocyte) and undergoes cell-cell fusion. Only acrosome-reacted sperm are able to complete this final step. Many plasma membrane proteins have been identified in both sperm and oocytes that play a role in these two distinct processes (reviewed in Nixon, Aitken, and McLaughlin 2007; Florman and Fissore 2014).
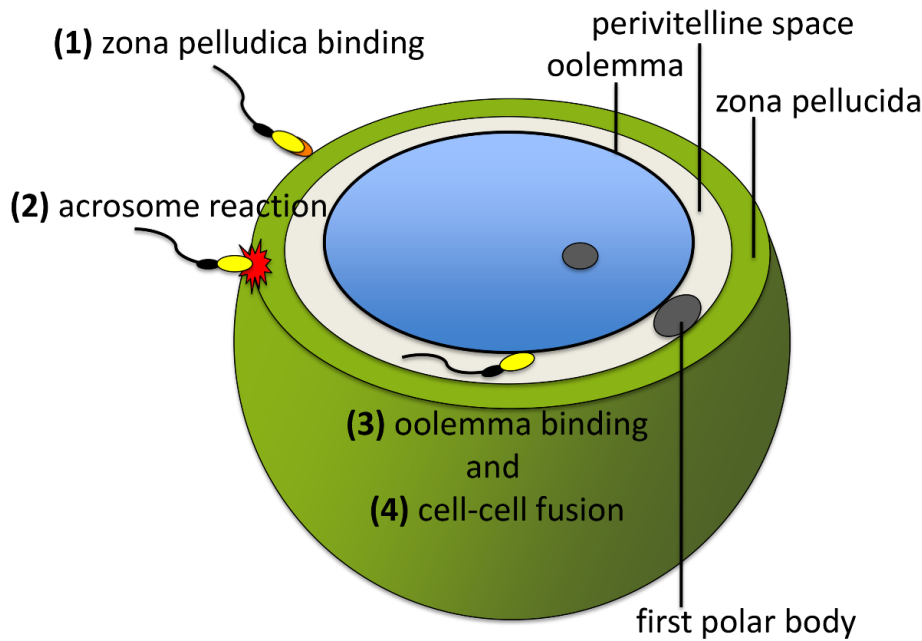
Figure 1.7: Fertilization. Four discrete phases of interaction between the fertilizing spermatozoan and the oocyte are necessary for successful fertilization. *(Figure modified with permission from Springer Nature Customer Service Centre GmbH: Springer Nature, Cellular and Molecular Life Sciences, Nixon et al., 2007)*

At a basic level, the fertilizing spermatozoon must deliver an intact genome and centrosome to the oocyte, and a factor that triggers the re-initiation of the cell cycle (Dale et al., 2010). This egg activation factor appears to be PLCζ, a sperm specific protein that is capable of triggering Ca^{2+} oscillations in the oocyte (Saunders et al., 2002; Yoon et al., 2008). These Ca^{2+} oscillations result in cortical granule exocytosis, leading to the cleavage of ZP2 and the prevention of polyspermy (Burkart et al., 2012). Ca^{2+} oscillations also trigger the resumption of meiosis, leading to the extrusion of a second polar body and formation of pronuclei (Ducibella et al., 2002; Nixon et al., 2002). Approximately 20 hours after fertilization, the pronuclei fuse and mitosis occurs for the first time (reviewed in Jukam et al. 2017). Fertilization also triggers the degradation of maternal transcripts, which is mostly complete by the 2-cell stage (Nothias et al., 1995). Although some embryonic transcripts are detected at the 1 cell stage, major transcription from the embryonic genome begins at the 2 cell stage (Flach et al., 1982).

1.5 Implantation and early embryonic development

By 3 days after fertilization, the zygote undergoes 5 rounds of cell division, resulting in a 32 cell embryo known as a blastocyst. At this stage, a fluid-filled cavity known as the blastocoel has formed, and two populations of cells become evident (reviewed in Fujimori 2010). The outer layer of cells is known as the trophectoderm, and will form extra-embryonic tissues including the placenta. The cells of the inner cell mass are pluripotent, and will mainly form the embryo itself. In the oviduct, both smooth muscle contractions and the directional beating of cilia are important for transporting the developing embryo and surrounding cumulus cells to the uterus as these cell divisions are occurring (Stewart and Behringer, 2012).

Approximately 4 days after fertilization (E4) in mice, the blastocyst hatches from the zona pellucida and begins to interact with the uterine lining for implantation. Implantation can be divided into three stages of interaction between the blastocyst and uterus: apposition, adhesion, and penetration (Enders and Schlafke, 1967). During apposition, the trophectoderm cells of the blastocyst become closely apposed to the luminal epithelium of the uterus. This is aided by uterine stromal edema and resorption of luminal secretions, which shrinks the lumen and brings the blastocyst in closer contact with the luminal epithelium (reviewed in H. Wang and Dey 2006). Attachment of the blastocyst requires many adhesion molecules, and is accompanied by increased vascular permeability in the uterus at the site of blastocyst adhesion (Psychoyos, 1986). For this reason, implantation sites can be visualized as early as E4.5 by the injection of a blue dye that concentrates in highly vascularized regions (Dey, 2006). Attachment is closely followed by penetration or invasion of the blastocyst through the luminal epithelium, facilitated by local epithelial apoptosis (Carson et al., 2000).

These processes require development of the blastocyst to be synchronized with receptivity of the uterus, which is controlled by ovarian steroid hormones (Figure 1.8) (reviewed in Carson et al. 2000; K. Y. Lee et al. 2007). Following ovulation, ovarian estrogen stimulates the proliferation of uterine epithelial cells. Stromal cell proliferation

is induced by progesterone produced by corpora lutea on day 3, and is further stimulated by an estrogen spike on day 4 which causes the uterus to become receptive to implantation. These steroid hormones work through inducing the expression of other signaling molecules including cytokines, growth factors, and homeobox transcription factors. The "implantation window" during which the uterus is receptive to implantation only lasts approximately 24 hours, after which the uterus enters a non-receptive or refractory period (reviewed in Namiki et al., 2018).

Embryonic implantation triggers the surrounding stromal cells to proliferate and differentiate into decidual cells, a process which is necessary for successful implantation (Ramathal et al., 2010). The primary decidual zone is formed by late E5, and is a small avascular zone closely surrounding the embryo (Figure 1.8) (Namiki et al., 2018). The larger, highly vascularized secondary decidual zone then forms and largely replaces the primary decidual zone by E8. Decidual cells in rodents are polyploid, enabling them to transcribe mRNA at an elevated rate and giving them a higher synthetic capacity to support embryo growth. Polyploidy is also thought to limit their lifespan to make room for the growing placenta and embryo throughout pregnancy (reviewed in Cha, Dey, and Lim 2014). In fact, it is the degradation of the avascular primary decidua that brings the trophoblast into contact with the maternal blood supply of the secondary decidual zone (Carson et al., 2000). The decidua is important in protecting the developing embryo from the mother's immunological response, and provides nutritional support during early pregnancy (reviewed in Cha, Dey, and Lim 2014). Decidualization is also critical for placental development, and forms part of the mature placenta (Woods et al., 2018).

While implantation and decidualization occur similarly between mice and humans, there are some key differences (reviewed in Gellersen and Brosens, 2014). The most notable is that while decidualization in mice is triggered by implantation, humans undergo spontaneous decidualization in every cycle. Because of this, they must also shed the decidualized endometrial layer in a cyclic manner, known as menstruation, which is normally not present in mice. Implantation in humans is also more invasive, and results in

deeper placentation. Polyploidy likely does not occur in human decidual tissue (Cha et al.,

2014b; Gellersen and Brosens, 2014).
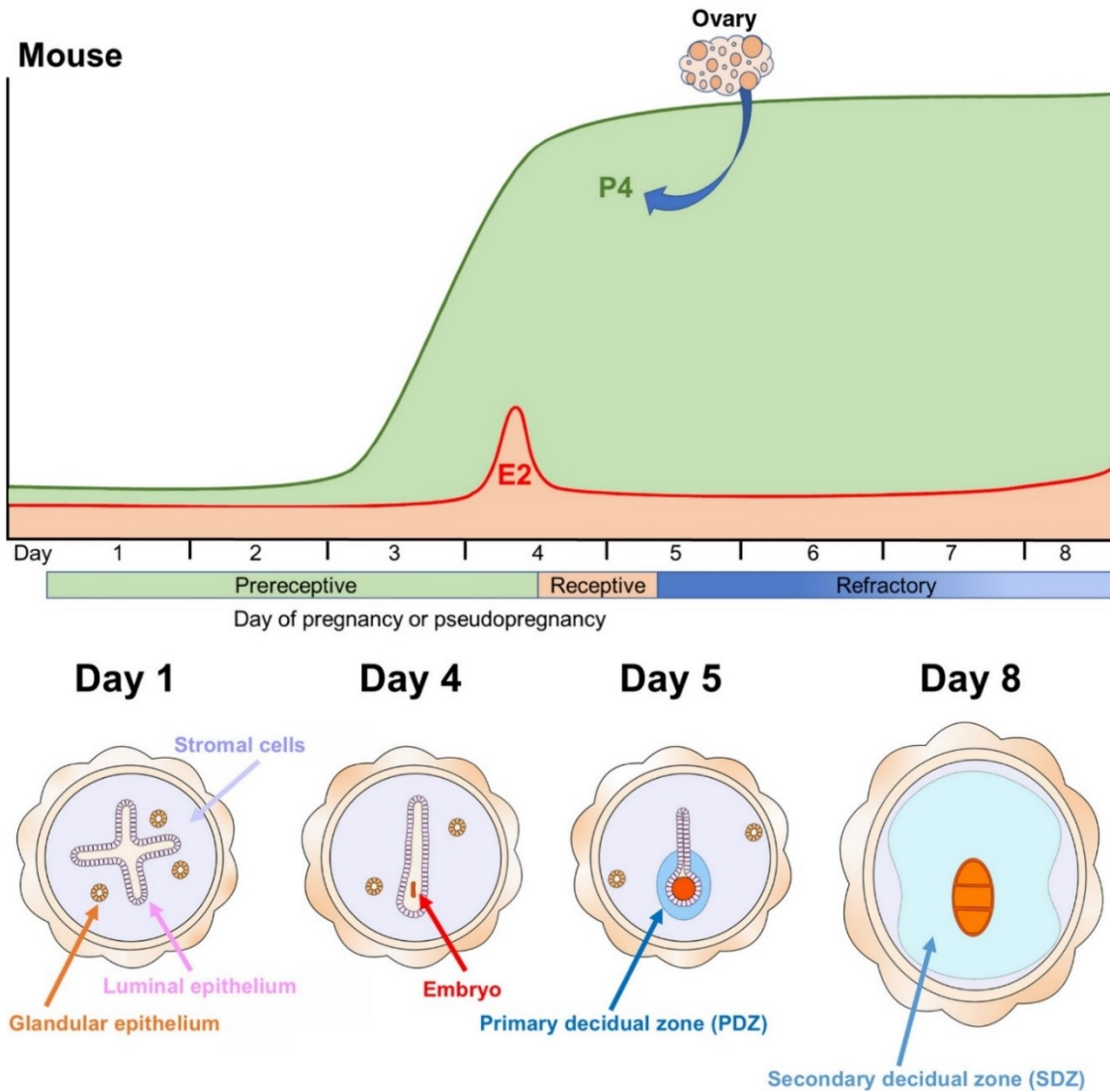
Figure 1.8: Hormonal and uterine changes during early pregnancy. Changes in progesterone (P4) and estrogen (estradiol, E2) levels control uterine receptivity. A spike in E2 on the fourth day stimulates the uterus to become receptive for implantation, and P4 is secreted from the newly formed corpus lutea. Morphological changes that occur during this time period are also shown, including the development of the primary and secondary decidual zone after implantation. *(Figure reused from Namiki et al., 2018 under the Creative Commons Attribution-NonCommercial-NoDerivs License).*

Placental function is critical for the remainder of the pregnancy, as it is required for providing the developing embryo with sufficient nutrients and oxygen, producing hormones, providing an immune-privileged environment, and anchoring the developing embryo to the uterine wall (reviewed in Woods et al., 2018). One critical aspect of placental development is labyrinth formation, the interface at which the bi-directional exchange of nutrients and gases occurs. In mice, the yolk sac is able to nutritionally support the developing embryo until this process occurs around E9.5-E10.5, after which the embryo is reliant on placental function for survival (Woods et al., 2018). The junctional zone is found between the labyrinth and the decidua, and provides endocrine support. As the decidua forms the maternal portion of the placenta, defects in decidualization can lead to shallow invasion and poor remodeling of maternal vasculature. For example, deletion of *Bmpr2* in the uterus results in a reduced decidualization response with impaired vascular development, leading to mid-gestational embryo loss associated with placental hemorrhaging (Nagashima et al., 2013). Evidence from several mouse mutants (reviewed in Wang and Dey, 2006) as well as human studies (Macklon et al., 2002; Mahendru et al., 2012) have indicated that late implantation can lead to poor fetal growth and development due to abnormal placenta development. Defects in placental function can lead not only to embryonic lethality, but also cardiovascular and brain developmental defects and premature birth (reviewed in Woods et al., 2018).

1.6 CECR2 and ATP-dependent chromatin remodeling

1.6.1 ATP-dependent chromatin remodeling overview

ATP-dependent chromatin remodelers are able to change the structure of chromatin by shifting, ejecting, or altering the histone composition of nucleosomes (reviewed in Clapier and Cairns, 2009). Through this action, they play important roles in DNA replication, recombination and repair, chromosome segregation, and gene regulation

(Clapier and Cairns, 2009). Different chromatin remodeling complexes are specialized in a different subset of these roles, but they can have multiple functions. There are four subfamilies of chromatin remodelers, which are based on the domain organization of their catalytic ATPases: inositol-requiring 80 (INO80), chromodomain, helicase, DNA binding (CHD), switching defective/sucrose nonfermenting (SWI/SNF), and imitation switch (ISWI) (Clapier et al., 2017). ISWI complexes, which are the focus of this study, have been mainly shown to function in nucleosome spacing both to repress and promote transcription (Clapier et al., 2017). Some ISWI complexes also have roles in DNA replication and repair (Erdel and Rippe, 2011). The catalytic ATPases these four subfamilies are based on are only one part of a sometimes large chromatin remodeling complex. Other proteins in the complex often have domains that target the complex through recognition of specific DNA sequence or structure, histone variants or modifications, or other DNA-bound proteins (Längst and Manelyte, 2015).

1.6.2 Cecr2 structure and molecular function

Cecr2 (Cat eye syndrome chromosome region, candidate 2) is named for its localization within the region on chromosome 22q11.2 that is duplicated in cat eye syndrome (Banting et al., 2005). CECR2 forms a complex with the ISWI ATP-dependent chromatin remodelers SNF2L (SMARCA1) or SNF2H (SMARCA5) as well as other proteins to form the CERF (CECR2-containing remodeling factor) chromatin remodeling complex (Banting et al., 2005; Niri, 2016; Oppikofer et al., 2017; Thompson et al., 2012). This complex has been shown to remodel chromatin *in vitro* in an ATP-dependent manner (Banting et al., 2005). CECR2 has several motifs and domains characteristic of ISWI-binding proteins (Figure 1.9 A), including a DDT domain which enables it to bind to ISWI proteins (Banting et al., 2005; Fyodorov and Kadonaga, 2002). It also has a bromodomain (Banting et al., 2005), a domain that has been shown to bind acetylated lysine residues on histone tails and likely helps to target chromatin remodeling activity (Längst and Manelyte, 2015). CECR2 contains an AT hook as well (Banting et al., 2005), which is associated with DNA binding (Aravind and Landsman, 1998).

ISWI chromatin remodeling complexes have been shown to function in the regulation of transcription as well as DNA replication and repair (Clapier et al., 2017; Erdel and Rippe, 2011). Transcriptional changes have been identified in *Cecr2* mutant embryos (Fairbridge et al., 2010; Terpstra, 2018), but it remains unclear whether or not these are due to the direct chromatin remodeling activity of CECR2. In HEK-293T cells, both transfection with isolated CECR2 bromodomain and siRNA knockdown of *Cecr2* resulted in a reduced number of γ-H2AX foci after gamma irradiation, indicating a role for *Cecr2* in the induction of DSB repair (Lee et al., 2012). However, we recently tested the role of *Cecr2* in DSB repair using primary cultures of mouse neurospheres null for *Cecr2* (*Cecr2$^{Del/Del}$*, see section 1.6.3) and found no defects in cell survival or growth and no decrease in the number of γ-H2AX foci after gamma irradiation (Elliott, Norton, et al., in revision). Therefore, the function of CECR2 may vary between cell types.

1.6.3 Cecr2 expression and mutant phenotypes

This and previous studies have utilized two mutant alleles of *Cecr2* to study its function in mice (Figure 1.9 A). The *Cecr2$^{Gt(pGT1)1Hemc}$* allele, hereafter referred to as *Cecr2^{GT}*, is an insertion of a β-galactosidase genetrap between exons 7 and 8 (Banting et al., 2005). This leads to the production of a CECR2:β-Gal fusion protein that can be used in combination with X-Gal staining to detect the localization of CECR2. *Cecr2$^{GT/GT}$* neurulating embryos have an approximately 14 fold reduction in normal *Cecr2* transcripts, indicating that some transcripts successfully splice around this insertion (Fairbridge et al., 2010). This leads to the production of a small amount of CECR2 protein in *Cecr2$^{GT/GT}$* animals (demonstrated in results Figure 2.1 D), making this allele hypomorphic. The *Cecr2$^{tm.1.1Hemc}$* allele, hereafter referred to as *Cecr2^{Del}*, is a deletion of the first exon and ~1 kb of upstream sequence (Fairbridge et al., 2010). This mutation is therefore a presumptive null, and leads to more severe phenotypes than the *Cecr2^{GT}* mutation.

The difference in deleteriousness between these two alleles can be seen in the penetrance of exencephaly observed for *Cecr2$^{GT/GT}$* and *Cecr2$^{Del/Del}$* embryos. Exencephaly, equivalent to human anencephaly, is a perinatal lethal birth defect that occurs when the

neural tube fails to close in the cranial region (Copp et al., 2003). While only 54% of BALB/c *Cecr2^{GT/GT}* embryos are exencephalic, the penetrance rises to 96% in *Cecr2^{Del/Del}* embryos of the same strain (Fairbridge et al., 2010; Leduc et al., 2017). The genetic background also affects the phenotype of *Cecr2* mutations: FVB/N *Cecr2^{GT/GT}* embryos do not develop exencephaly, and even *Cecr2^{Del/Del}* FVB/N embryos have a penetrance of only 12% (Leduc et al., 2017).
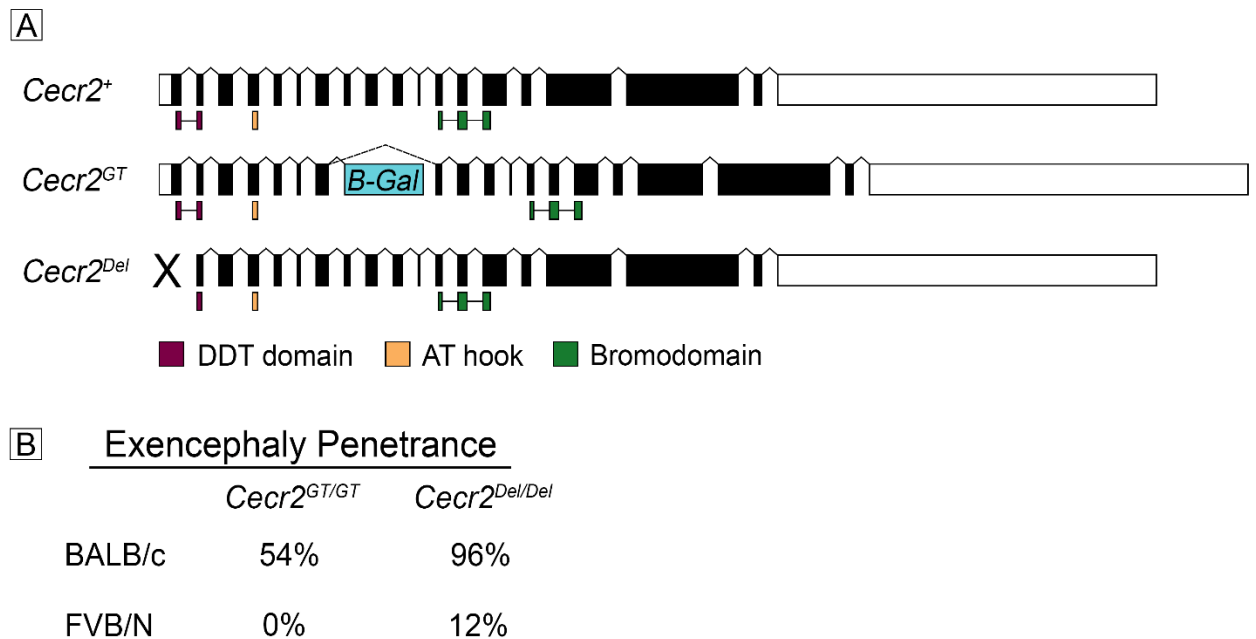
Figure 1.9: Mutant alleles of *Cecr2* and associated exencephaly penetrances. The three alleles of *Cecr2* used in this study are shown with the location of important motifs and domains. The *Cecr2^{GT}* allele has an insertion of β-Galactosidase between exons 7 and 8, leading to the production of a fusion protein. However, some transcripts splice around this insertion and produce full-length CECR2. The *Cecr2^{Del}* allele has a deletion of exon 1 and is a presumptive null due to abolished transcription. (B) The penetrance of exencephaly is affected by both the severity of *Cecr2* mutation and the mouse strain used. *(Figure created using penetrance information from Leduc et al., 2017).*

As might be expected given the phenotype of exencephaly, *Cecr2* is highly expressed during embryonic development of the nervous system (Banting et al., 2005). In fact, recent work has shown that *Cecr2* is highly expressed in early embryos, beginning at the

2-cell stage (Niri, Norton et al., in prep). Expression greatly diminishes with age, and by adulthood *Cecr2* is only found in a few tissues, including the testis. (Thompson et al., 2012). Within the testis, X-Gal staining shows *Cecr2* is expressed in the developing germline and is found in the gonocytes perinatally (Figure 1.10 A). In the adult, *Cecr2* staining is strongest in spermatogonia and early spermatocytes and decreases in more advanced cell types (Figure 1.10 A). As these results make use of the CECR2:β-Gal fusion protein, it is possible they do not accurately reflect the localization of native CECR2. While X-Gal staining shows that the *Cecr2* promoter is transcriptionally active, the translation and proteolytic stability of the CECR2:β-Gal fusion protein may differ from wild type CECR2. X-Gal staining in the female reproductive system at E18.5 shows that *Cecr2* is expressed in the ovary, oviduct, and uterus (Figure 1.11 A-B). Due to high endogenous background staining, the localization of *Cecr2* in the adult female reproductive system cannot be determined using this method.

While exencephaly is the most immediately obvious phenotype of *Cecr2* mutants, they also have other abnormalities. The inner ears of BALB/c *Cecr2* mutant embryos have misaligned stereocilia at E18.5 (Dawe et al., 2011), and a variety of kidney defects have been identified in adult FVB/N *Cecr2^{GT/GT}* mutants, a strain which does not show exencephaly (Fairbridge, 2013). The differing phenotypes observed between strains are likely due to mutations in modifier genes that differ between genetic backgrounds. For example, a region on chromosome 19 has been shown to be partially responsible for the difference in exencephaly penetrance between FVB/N and BALB/c embryos (Leduc et al., 2017). All of the data presented in this work was done using BALB/c mice except for Figure 2.1 C-D where FVB/N tissues were also used for western blot analysis. Adult BALB/c *Cecr2^{GT/GT}* mice (non-penetrant for exencephaly) appear normal, but male *Cecr2^{GT/GT}* mice are subfertile (Figure 1.10 B) (Thompson, Norton et al., 2012). *Cecr2^{GT/GT}* males also showed normal testis histology and normal sperm count, motility, and morphology. However, the age-dependent nature of *Cecr2* subfertility was not yet known when this study was done, because of this the males used for this analysis were old enough to have already recovered significantly (P128-423). Despite this, the number of

fertilized oocytes after *in vivo* matings was significantly lower for *Cecr2$^{GT/GT}$* males (Thompson, Norton et al., 2012). A preliminary unpublished analysis showed that *Cecr2$^{GT/GT}$* females also show subfertility (Figure 1.11 C) and that ovaries also appeared histologically normal, but no further information about their phenotype was known at the beginning of this study (unpublished work done by K.A. Norton as an undergraduate student).
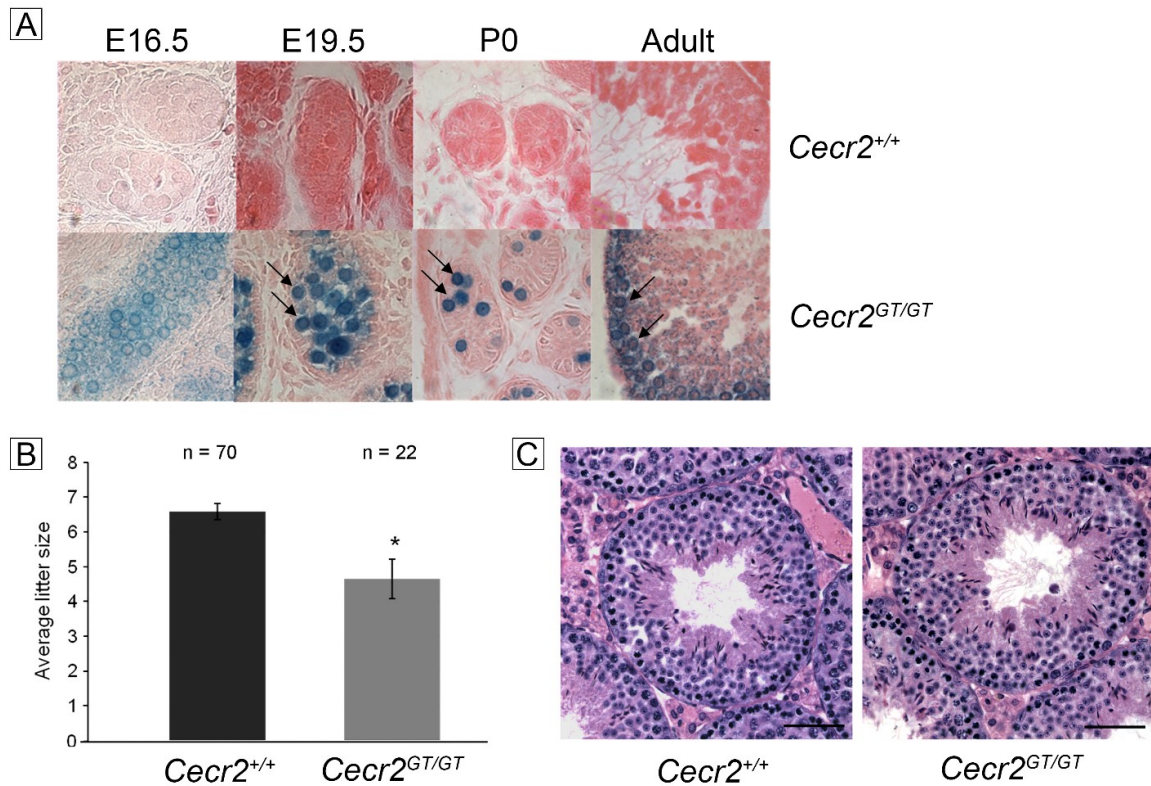
Figure 1.10: *Cecr2* testis localization and male subfertility phenotypes. X-Gal staining (A) with the *Cecr2^GT^* allele shows that *Cecr2* is localized to gonocytes during testis development and spermatogonia and spermatocytes in adults (arrows). Faint staining can also be seen in spermatids. Tissue from *Cecr2^+/+^* mice was used as a negative control. *Cecr2^GT/GT^* males are subfertile (B), siring smaller litters on average than *Cecr2^+/+^* males (*Cecr2^+/+^* n=70, *Cecr2^GT/GT^* n=22, p=0.022). Testis histology (C) of *Cecr2^GT/GT^* males appeared grossly normal. *(Adapted from Thompson et al., 2012.; B and C are work done by K.A. Norton as an undergraduate student)*
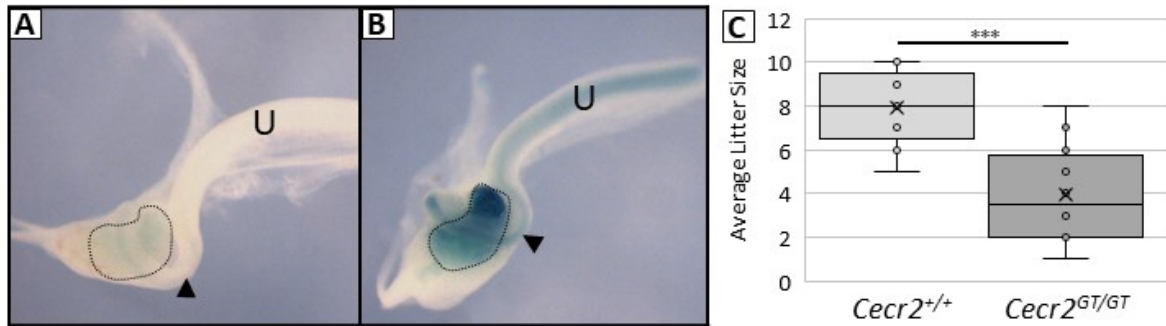
Figure 1.11: *Cecr2* localization in the female reproductive system and female subfertility. X-Gal staining of *Cecr2^{+/+}* (A) and *Cecr2^{GT/GT}* (B) female reproductive systems at E18.5 shows that *Cecr2* is expressed in the ovary (outlined by a dotted line), oviduct (arrow), and uterus (U). *Cecr2^{+/+}* tissues are used as a negative control and show faint background staining. *Cecr2^{GT/GT}* females are also subfertile (C), with approximately 50% smaller litter sizes than *Cecr2^{+/+}* dams when mated to *Cecr2^{+/+}* males. *(Adapted from Dawe, 2009 (A, B) and K. A. Norton, unpublished work from undergraduate research, now part of Norton et al., in prep, Chapter 3 (C)).*

1.6.4 Other chromatin remodelers in reproduction

Several chromatin remodeling complexes have been shown to play a role in spermatogenesis, at a variety of stages. BRG1, the catalytic subunit of the BAF (SWI/SNF) complex, is critical for normal synapsis and homologous recombination during meiosis I (Wang et al., 2012). Germline specific deletion of *Brg1* leads to pachytene arrest and apoptosis, likely due to the failure of MSCI (Wang et al., 2012). Similarly, INO80 is thought to remodel the chromatin structure to make it permissive for crossover formation, and a conditional knockout of INO80 results in defective DSB repair and synapsis (Serber et al., 2015). BAZ1A, the defining subunit of the ACF and CHRAC ISWI complexes, is also highly expressed in pachytene spermatocytes but is not required for DSB repair or synapsis (Dowdle et al., 2013). Instead, the decrease in sperm number and motility in mutants appear to be due to abnormal post-meiotic gene expression affecting spermiogenesis in a highly pleiotropic manner (Dowdle et al., 2013). *Chd5* is highly expressed post-meiotically, at step 7-8 of spermiogenesis, and is important in the exchange of histones for transition

proteins followed by protamines (Li et al., 2014). Without it, the condensation of chromatin is disturbed, leading to decreased sperm count and abnormal motility and morphology (Li et al., 2014). ATRX, an orphan remodeler not belonging to any of the four subfamilies (Clapier et al., 2017) binds to centromeric heterochromatin and repetitive sequences on the Y chromosome in spermatogonia (Baumann et al., 2008). There, it is hypothesized to be important for the transcriptional silencing of potentially deleterious repetitive elements (Baumann et al., 2008). Apart from ATRX, only BRG1 is detectable at a low level in spermatogonia (Wang et al., 2012). While it is possible that BRG1 has a function in spermatogonia in addition to its major role in spermatocytes, the significance of this expression is unknown. SNF2H has also been detected in spermatogonia as well as pachytene spermatocytes (Dowdle et al., 2013). While it forms a complex with BAZ1A in pachytene spermatocytes, BAZ1A is absent in spermatogonia, indicating that SNF2H may form a different complex in spermatogonia (Dowdle et al., 2013). Similarly, BAZ1B, which binds to SNF2H to form the WICH complex in somatic cells, is dispensable for SNF2H localization during spermatogenesis and for fertility (Broering et al., 2015).

There are fewer examples of chromatin remodelers in mammalian oogenesis, but a handful of remodelers have been identified as important. In contrast to BRG1's role in spermatocyte meiosis, it is not required for successful completion of oogenesis or fertilization but is required for subsequent zygotic genome activation (Bultman et al., 2006). ATRX in oocytes is required at the centromeric heterochromatin for proper chromosome alignment during meiosis II and maintenance of the meiotic spindle (De La Fuente et al., 2004), despite being almost completely absent in meiotic and post-meiotic male germ cells (Baumann et al., 2008). In the ISWI family of chromatin remodelers, both *Snf2h* and *Snf2l* are expressed in granulosa cells within the ovary (Lazzaro et al., 2006). Although female mice mutant for *Snf2l* do not have impaired fertility, (Pépin et al., 2013; Yip et al., 2012), they do have abnormal follicle maturation and decreased ovulated oocytes after superovulation (Pépin et al., 2013). This is likely due to a role for SNF2L in regulating gene expression in granulosa cells during folliculogenesis (Lazzaro et al., 2006; Pépin et al., 2013). The role of SNF2H in the ovary remains unknown.

1.7 Goals of this study

The overall aim of this study was to investigate the cause of subfertility in mice mutant for *Cecr2.* To accomplish this, the specific goals of this study were as follows, for both males and females:

1. Characterize the fertility of both *Cecr2*^{GT/GT} and compound heterozygote *Cecr2*^{GT/Del} mice with a more severe *Cecr2* deficiency
2. Determine in what biological process the defect causing subfertility occurs
3. Investigate the molecular mechanisms that cause these defects

The vast majority of work on male fertility was conducted using the compound heterozygote *Cecr2*^{GT/Del} mice, as their phenotypes should theoretically be more severe and thus easier to explore, yet they are frequent enough in *Cecr2*^{GT/+}x *Cecr2*^{Del/+} crosses to make experiments feasible. As *Cecr2* mutant females have a higher penetrance of exencephaly than males (Leduc, 2015) and many experiments involving mutant females required euthanasia, both *Cecr2*^{GT/GT} and *Cecr2*^{GT/Del} females were used to achieve these goals in regard to female fertility. This was, in the end, fortuitous, as the investigation of goal #2 separately in both *Cecr2*^{GT/GT} and *Cecr2*^{GT/Del} females proved informative.

Chapter 2 Subfertility in young male mice mutant for chromatin remodeler CECR2

A version of this chapter was submitted for publication in the journal Reproduction and is currently in the revision process. Authors: Norton, K.A., Niri, F., Humphreys, R., Weatherill, C., Duong, K. Nguyen, V.V., Kommadath, A. Stothard, P. and McDermid, H. E.

Dr. Farshad Niri generated the CECR2 antibody and did the western blots shown in Figure 2.1 B-C and Figure 2.2 O. Undergraduate student Ross Humphreys aided in collecting the testis weight data for Figure 2.3 F. Undergraduate students Ross Humphreys, Chelsey Weatherill, and Vivian V. Nguyen characterized histological abnormalities in the testis shown in Figure 2.5. Undergraduate student Kevin Duong assisted with RNA extractions and performed qPCR on a small portion of the genes. Drs. Arun Kommadath and Paul Stothard analyzed the RNA-seq data to generate the list of differentially expressed genes and the heat map shown in in Figure 2.8. Dr. Heather E. McDermid contributed to conceptualization of some experiments and to the histological analysis of embryonic testes shown in Figure 2.6. Kacie A. Norton conceptualized and designed the experiments, performed all experiments not mentioned above, supervised all undergraduates and wrote the first draft of the manuscript.

2.1 Introduction

The use of model organisms such as mice has proven invaluable in identifying the molecular factors involved in spermatogenesis. Despite this, the genetic causes of infertility remain poorly understood; in infertile men, the cause of abnormal spermatogenesis remains undetermined in approximately 72% of cases even after genetic testing (Tüttelmann et al., 2018).

Many genes identified as critical for spermatogenesis are specifically essential for meiosis (Matzuk and Lamb, 2002). Successful completion of meiosis requires intrinsically linked processes, including the induction of DNA double-strand breaks (DSBs), formation of crossovers, and synapsis of homologous chromosomes (Handel and Schimenti, 2010). At pachytene stage, any chromosome regions that remain unsynapsed undergo transcriptional silencing. Since the sex chromosomes in males have no homolog to fully pair with, they are obligatorily silenced, a process referred to as Meiotic Sex Chromosome Inactivation (MSCI) (Turner, 2007). As these processes are all connected, mutations affecting one often lead to phenotypes in other parts of meiosis. For example, reducing the number of induced DSBs leads to incomplete synapsis (Kauppi et al., 2013), and disrupting synapsis leads to aberrant recombination and failure of MSCI (de Vries et al., 2005). The failure of synapsis, DSB repair, or MSCI can trigger the pachytene checkpoint and lead to apoptosis, or abnormal spermatogenesis in cells which do not trigger apoptosis (Burgoyne et al., 2009).

Chromatin remodelers are known to play a role in spermatogenesis through control of DNA replication, repair, and transcriptional regulation. For example, CHD5 is critical during the exchange of histones for protamines through both facilitating the removal of histones and controlling the levels of transition proteins and protamines (Li et al., 2014). BRG1, a catalytic subunit of the BAF complex, is important for homologous recombination (Wang et al., 2012). BAZ1A, the defining subunit of the ACF and CHRAC ISWI complexes, regulates post-meiotic gene expression (Dowdle et al., 2013). CECR2 is a critical member of the CERF complex, an ISWI chromatin remodeling complex that has roles in male

fertility and neurulation (Thompson et al., 2012; Banting et al., 2005), but the specific mechanisms are unknown.

Here, we show that a large reduction in CECR2 levels leads to severe subfertility at sexual maturity that improves dramatically with age. We also demonstrate corresponding defects in early spermatogenesis, including histological abnormalities in the testis and incomplete synapsis of homologous chromosomes during meiosis. Further, we provide evidence of transcriptional changes in mutant testes that may explain some of these phenotypes.

2.2 Materials and Methods

2.2.1 Mice and Cecr2 mutations

Approval was obtained from the University of Alberta Animal Care and Use Committee for all experiments involving mice (AUP00000094). Mice were housed at 22±2°C with a 14 hour light/10 hour dark cycle and fed PicoLab Diet #5053 except for breeders and plugged females, who were fed higher fat PicoLab Diet #5058. This study utilizes two previously generated mutations in *Cecr2* (BALB/c background)*,* the hypomorphic *Cecr2*^{GT} allele (*Cecr2*$^{(pGT1)1Hemc}$) and the presumptive null *Cecr2*^{Del} deletion allele (*Cecr2*$^{tm1.1Hemc}$) , both of which result in the perinatal lethal neural tube defect exencephaly (Figure 2.1 A-B). Genotyping was done as previously described (Banting et al., 2005; Fairbridge et al., 2010).
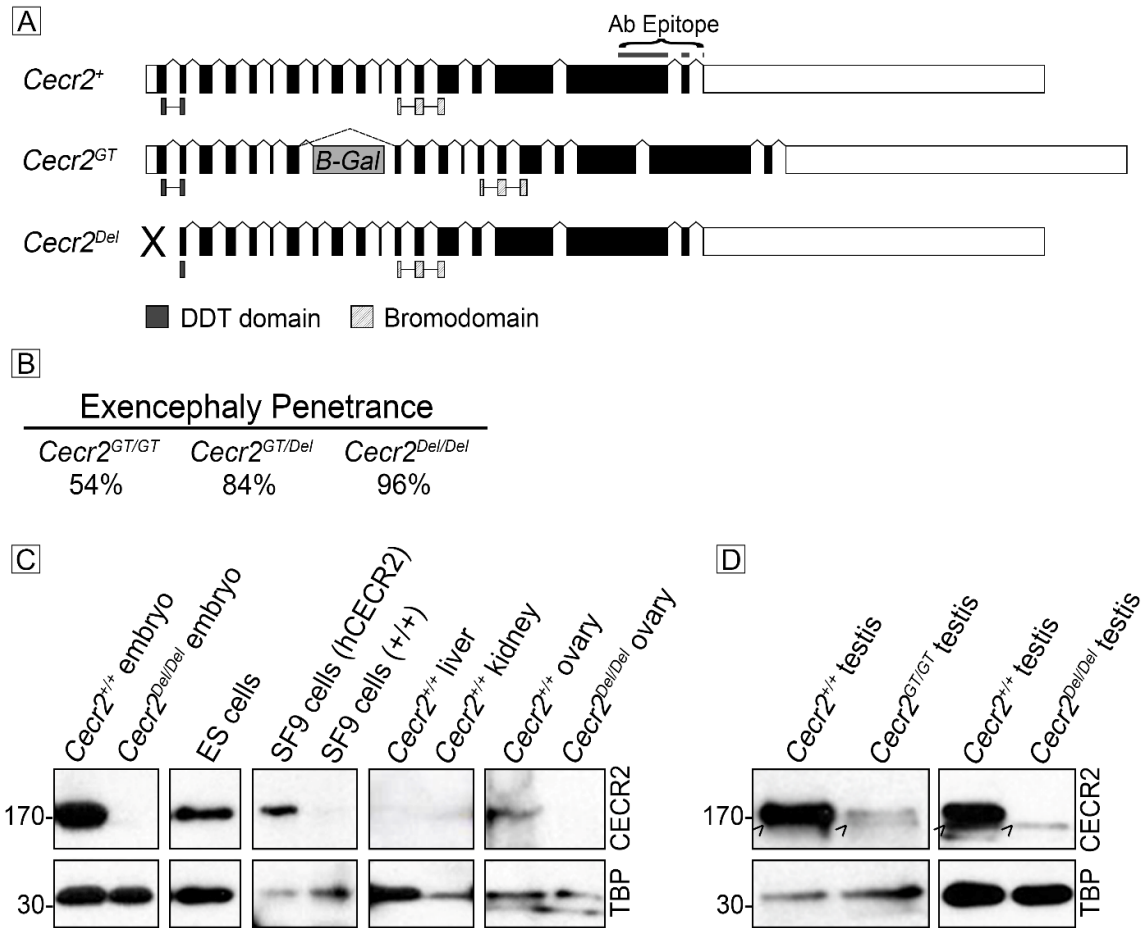
Figure 2.1: *Cecr2* alleles and antibody characterization: Mutant alleles of *Cecr2* have differing severities, as evidenced by the penetrance of exencephaly and the level of CECR2 protein they produce. Three alleles of *Cecr2* are used in this study (A). The wildtype *Cecr2* allele (*Cecr2⁺*) has 19 exons, with a DDT domain located in exons 1-2 and a bromodomain located in exons 12-14. The *Cecr2^GT^ (Cecr2^Gt(pGT1)1Hemc^)* genetrap allele has an insertion of β-Gal between exons 7 and 8; therefore, most transcripts lack exons 8-19 including the bromodomain. Some full-length transcript is still produced, presumably by splicing around the genetrap, thus making this allele a hypomorph. The *Cecr2^Del^ (Cecr2^tm.1.1Hemc^)* deletion allele is a deletion of exon 1 and ~1 kb upstream, and is a presumptive null allele. The difference in severity of these two mutations is reflected in the percentage of homozygous mutants that develop the perinatal lethal neural tube defect exencephaly (B). The production of compound heterozygous *Cecr2^GT/Del^* males (from the 16% non-exencephalic animals) allows the study of reproduction with the least amount of CECR2 present. (Modified from Leduc et al., 2017 with new data from this study). The epitope used to produce a polyclonal antibody against CECR2 in this study is shown above the *Cecr2⁺* allele. Western blots using wildtype and *Cecr2^Del/Del^* tissues demonstrate that this antibody is specific, as a band is visible at 170 kDa in wildtype

44

samples but not *Cecr2$^{Del/Del}$* samples (C). CECR2 expression can be seen in wildtype embryos and ES cells, but not in *Cecr2$^{Del/Del}$* embryos. The antibody also cross-reacts with human CECR2 in transfected SF9 cells. In adult mice, CECR2 is not detected in the liver or kidney, but is detected in the gonads. In the adult testis (D), it is clear that some CECR2 protein is detectable in *Cecr2$^{GT/GT}$* testes but not in *Cecr2$^{Del/Del}$* testes. A non-specific band of a lower molecular weight (~160 kDa) is present in all testis samples (indicated by >). The protein analysis of adult *Cecr2$^{Del/Del}$* gonads was possible by use of a second strain of mice (FVB/N) with a much lower penetrance of exencephaly (Leduc et al., 2017). TBP= TATA-Box Binding Protein, used as a loading control.

2.2.2 Antibody generation

A C-terminal fragment of *Cecr2* (Figure 2.1 A) was amplified using primers containing EcoRI and SalI restriction sites and a C-terminal His6 tag, ligated into the pET-21a expression vector (Novagen), and transformed into *E. coli* BL21 (DE3). The His6-tagged CECR2 polypeptide was purified using Ni-NTA Agarose (Qiagen), dialyzed against PBS, mixed 1:1 with complete Freund's adjuvant and 0.375 mg was injected into rabbits. Boosters were given at 3, 7, 11, and 15 weeks (0.375 mg in incomplete Freund's adjuvant), and CECR2-specific antibodies were purified from serum using SulfoLink Coupling Resin (Thermo Scientific). CECR2 antibody characterization is shown in Figure 2.1 C.

2.2.3 Cell culture

GC1 and GC2 cell lines (ATCC) were cultured in Dulbecco's Modified Eagle high glucose (Sigma) supplemented with 15% Fetal Bovine Serum (Life Technologies) and 100 Units/ml Penicillin-Streptomycin (Life Technologies). TT2 mouse ES cells were cultured as above, adding 2 mM L-glutamine (Life Technologies), 100 mM β-mercaptoethanol, 0.1 mM MEM non-essential amino acids solution (Life Technologies), and 1000 U/mL recombinant leukemia inhibitory factor (Sigma). Cells were grown on 100 mm Cell Culture Dishes (Thermo Scientific) coated with gelatin and incubated at 37°C in a 5% CO_2 atmosphere.

2.2.4 Western blotting

Cells and tissues were homogenized in lysis buffer (150 mM sodium chloride, 1.0% IGEPAL CA-630, 10% Glycerol, 2 mM EDTA, 20 mM Tris pH 8.0) supplemented with protease inhibitors, rocked for 30 min at 4°C, and cleared by centrifugation. Protein concentration measurement and western blotting were performed as previously described (Thompson et al., 2012) using our polyclonal anti-CECR2 antibody (1:50,000) and mouse monoclonal anti-TBP (1:5000, Abcam) followed by goat anti-rabbit IgG-HRP (Bio-Rad) and goat anti-mouse IgG-HRP (Sigma) secondary antibodies.

2.2.5 Fertility testing

Wildtype females were housed with males and monitored daily for post-copulatory plugs. Plugged females were separated until dissection at embryonic day 14.5-18.5 (E14.5-18.5). The number of live embryos was recorded. Females that were not pregnant upon dissection were recorded as zero.

2.2.6 Superovulation and antibody staining of oocytes

Wildtype females were superovulated as previously described (Thompson et al., 2012). The following morning, females were housed with males and monitored for a post-copulatory plug every 30 minutes. Successfully mated females were euthanized 5 hours post-mating, and their oocytes were isolated. The zona pellucida was removed using Tyrode's Solution (Sigma). Oocytes were fixed using 4% w/v formaldehyde in PBS for 15 minutes and permeabilized in 0.5% Triton-X in PBS for 10 minutes. After blocking in 10% goat serum (Sigma), the samples were incubated with 1:40 AlexaFluor488 phalloidin (Invitrogen) and 1:200 anti-acetylated tubulin antibody (T6793, Sigma) followed by 1:200 Cy3 goat anti-mouse secondary antibody (Jackson ImmunoResearch). Oocytes were mounted in PVA (Sigma) containing DAPI, and imaged with a Nikon Eclipse 80i confocal microscope.

2.2.7 Computer Assisted Sperm Analysis

Immediately after euthanasia, both vasa deferentia and cauda epididymides were dissected into prewarmed M2 medium (Sigma). Sperm were squeezed out of each vas deferens using fine forceps, and each epididymis was shredded using insulin needles. After incubation at 37°C, the sperm solution was diluted and sperm number and motility were assessed using the Hamilton Thorne MouseTraxx Sperm Analysis System Version 14.

2.2.8 Testis weights

After determining whole body weight, testes were dissected out and excess tissue was removed before weighing. The average of the testis weights was used to create a testis:bodyweight ratio.

2.2.9 Histology

Testes were fixed in Bouin's fixative (Sigma) for 20-24 hours. For all except E18.5 testes, the tunica albuginea was removed after 30-60 minutes to allow for better permeation of the fixative. Adult testes used for CECR2 immunofluorescence (Figure 2.2 G-N) were fixed in 4% formaldehyde instead, as Bouin's can disrupt antibody staining. Testes were processed through ethanol/toluene gradients for embedding in paraffin and sectioned at 5-7 µm. After hematoxylin and eosin (H&E) staining, samples were analyzed blind to the genotype to detect histological differences. Images were captured using SeBaView software (Laxco) and a SeBaCam5C digital camera with a Zeiss Axioscope.A1 microscope.

2.2.10 Immunostaining

Sections were deparaffinized then heated in antigen retrieval buffer (10 mM Tris Base, 1 mM EDTA, 0.05% Tween-20) to boiling 3 times over 30 minutes. Sections were blocked in 10% normal goat serum (Sigma) and 0.6% Triton-X (Sigma) in PBS for 1 hour before incubation with 1:10,000 anti-CECR2 in antibody dilution buffer (0.1% bovine serum albumin, 0.3% Triton-X in PBS) overnight at 4°C. After washing in PBS, sections were incubated with 1:200 AlexaFluor-488 goat anti-rabbit secondary antibody (Life

Technologies) for 2 hours at room temperature then 0.1% DAPI for 5 minutes. After washing, Fluoromount-G (Southern Biotech) was used for mounting and imaging was done as described for oocyte samples.

2.2.11 Testosterone ELISA

Serum samples were collected using tail bleeds and stored at -80°C. Serum testosterone levels were measured in duplicate for each mouse using a testosterone ELISA kit (ENZO) following the manufacturer's instructions, with a CV of <7%.

2.2.12 RNA-seq

Testes were isolated from 5 *Cecr2$^{+/+}$* and 5 *Cecr2$^{GT/Del}$* males at postnatal day 24 (P24), flash frozen in liquid nitrogen, and stored at -80°. RNA was extracted using the RNeasy Lipid Tissue MiniKit (Qiagen). RNA integrity was ≥9.3, measured using the Agilent 2100 Bioanalyzer. cDNA libraries were prepared for sequencing by Delta Genomics (Edmonton, Canada) using the TruSeq RNA Sample Prep Kit (Illumina). Sequencing was done by the McGill University and Génome Québec Innovation Centre on the Illumina HiSeq 4000 (paired-end sequencing; 100 bp reads). Read quality was assessed (using FastQC v0.11.5 software: http://www.bioinformatics.babraham.ac.uk/projects/fastqc/) prior to and after performing quality based read trimming and adapter removal using Trimmomatic (Bolger et al., 2014) with default settings. Reads that passed quality control were mapped to the mm9 (NCBI m37, GCA_000001635.18) mouse reference genome assembly using STAR v2.5.2b (Dobin et al., 2013). Gene expression metrics were generated using featureCounts v1.5.0-p3 (Liao et al., 2014) and Ensembl release 67 annotations (Zerbino et al., 2018). Genes expressed at very low levels in more than 5 samples were removed, where the expression threshold was determined based on the counts per million (CPM) mapped reads value corresponding to 5 reads in the sample with the lowest library size. The resulting expression dataset of 19395 genes was normalized using the TMM method in edgeR v3.18.1 (Robinson and Oshlack, 2010) and tested for differentially expressed genes between *Cecr2$^{GT/Del}$* and *Cecr2$^{+/+}$* using a generalized linear model with one factor,

treatment with 2 levels: mutant and wildtype. Multiple testing correction was conducted using a false discovery rate (FDR) calculation (Benjamini and Hochberg, 1995). Differentially expressed genes with a FDR <0.05 and a fold change of >1.5 determined based on a power analysis using R package RNASeqPower (Hart et al., 2013) were considered significant.

2.2.13 qPCR

RNA was extracted as above and cDNA was synthesized using the qScript cDNA SuperMix (Quanta Biosciences). qPCR was done on a minimum of 3 biological and 3 technical replicates using the QuantStudio 6 Flex Real-Time PCR System and software. The qPCR Mastermix (*Dynamite*) used is a proprietary mix (Molecular Biology Service Unit, Department of Biological Sciences, University of Alberta), containing Tris (pH 8.3), KCl, $MgCl_2$, Glycerol, Tween 20, DMSO, dNTPs, ROX as a normalizing dye, SYBR Green (Molecular Probes) as the detection dye, and an antibody-inhibited Taq polymerase. Samples were normalized to *Gapdh* as an endogenous control, and the ΔΔCT method was used for relative quantification. Primers are listed in Appendix A.

2.2.14 Immunofluorescence staining of spermatocyte chromosome spreads

Chromosome spreads were prepared and stained using a modified protocol originally provided by Hiroki Inoue (personal communication). Testes were minced in PBS and spermatogenic cells were dispersed by pipetting, then filtered through 40 μm nylon mesh (Fisherbrand) and isolated by centrifugation. Cells were resuspended and incubated in cold 0.5% w/v NaCl pH 8 before being dropped into fixative (2% w/v PFA, 0.03% w/v SDS, pH 8) on a microscope slide. After overnight incubation, slides were washed in 0.4% v/v Photo-Flo 200 (Kodak) pH 8, dried at room temperature, and stored at -80˚C. For immunostaining, slides were incubated in Tris-EDTA antigen retrieval buffer (see immunostaining) at 95˚C for 30 minutes, then with anti-SCP3 (1:1000, ab15093 Abcam) and anti-ATR (1:50, sc-515173 Santa Cruz Biotechnology) primary antibodies overnight at 4˚C. In the morning, slides were washed again in 0.4% Photo-Flo 200 followed by

incubation with AlexaFluor555 goat anti-rabbit antibody (Invitrogen) and AlexaFluor488 goat anti-mouse antibody (Invitrogen) at 1:200 and mounted in Fluoromount-G (Southern Biotech). Images were obtained using an inverted spinning-disk confocal microscope (Olympus IX81 with CSU10 Yokogawa head), using a 60X, NA 1.42, oil objective and an OCRA-R2 camera (Hamamatsu Photonics); camera and microscope were controlled by MetaMorph software (Molecular Devices).

2.2.15 Statistics

Results are expressed as mean ± S.E.M, and significance was evaluated using Student's t-test except where noted otherwise.

2.3 Results

2.3.1 CECR2 *is localized to gonocytes perinatally and spermatogonia in adults*

    To determine where CECR2 is found within the testis, we used antibody staining on testis sections from E18.5 embryos and adults. In E18.5 embryos, CECR2 immunostaining is localized to the gonocytes (prospermatogonia) in the middle of each seminiferous cord (Figure 2.2 A-C). In adult males, CECR2 immunostaining is seen in spermatogonia along the outer edge of each tubule (Figure 2.2 G-I). This was consistent at all adult ages examined, from sexual maturity (P42) to >P200 (data not shown). Localization to spermatogonia was confirmed by comparing CECR2 antibody immunostaining to H&E staining subsequently done on the same section (Figure 2.2 M-N). The histology, number of cells staining, and their presence at every stage of the cycle of the seminiferous epithelium is compatible with early spermatogonia, likely type A spermatogonia. No substantial staining was observed in more advanced germ cells, Sertoli cells, or interstitial cells. CECR2 localization to spermatogonia is supported by the absence of CECR2 in GC1 and GC2 cell lines, which are immortalized type B spermatogonia and spermatocytes, respectively (Figure 2.2 O). However, gene expression in these immortalized cell lines may not be representative of *in vivo* gene expression. Support from the literature for the expression of *Cecr2* in spermatogonia is seen in recent studies using RNA-seq to analyze the transcriptome of single cells during spermatogenesis (Green et al., 2018; Hermann et al., 2018), with the highest level of expression in Type A_1-A_4 spermatogonia that have committed to differentiation (Green et al., 2018). Testes of $Cecr2^{GT/Del}$ males showed no staining (Figure 2.2 D-F, J-L). $Cecr2^{GT/Del}$ mice combine a $Cecr2^{GT}$ hypomorphic allele and a $Cecr2^{Del}$ presumptive null allele (Figure 2.1 A). Only 16% (6/38 in an exencephaly penetrance analysis) of $Cecr2^{GT/Del}$ mice survive to reproductive age, while the other 84% (32/38) die perinatally of exencephaly. The lack of testis staining in these mice indicates that the level of CECR2 from one hypomorphic allele is below fluorescence detection.

DAPI   CECR2   MERGE

E18.5 Cecr2⁺/⁺

A   B   C

E18.5 Cecr2^GT/Del

D   E   F

Adult Cecr2⁺/⁺

G   H   I

Adult Cecr2^GT/Del

J   K   L

CECR2 + DAPI   H & E   Western blot

M   N   O

52
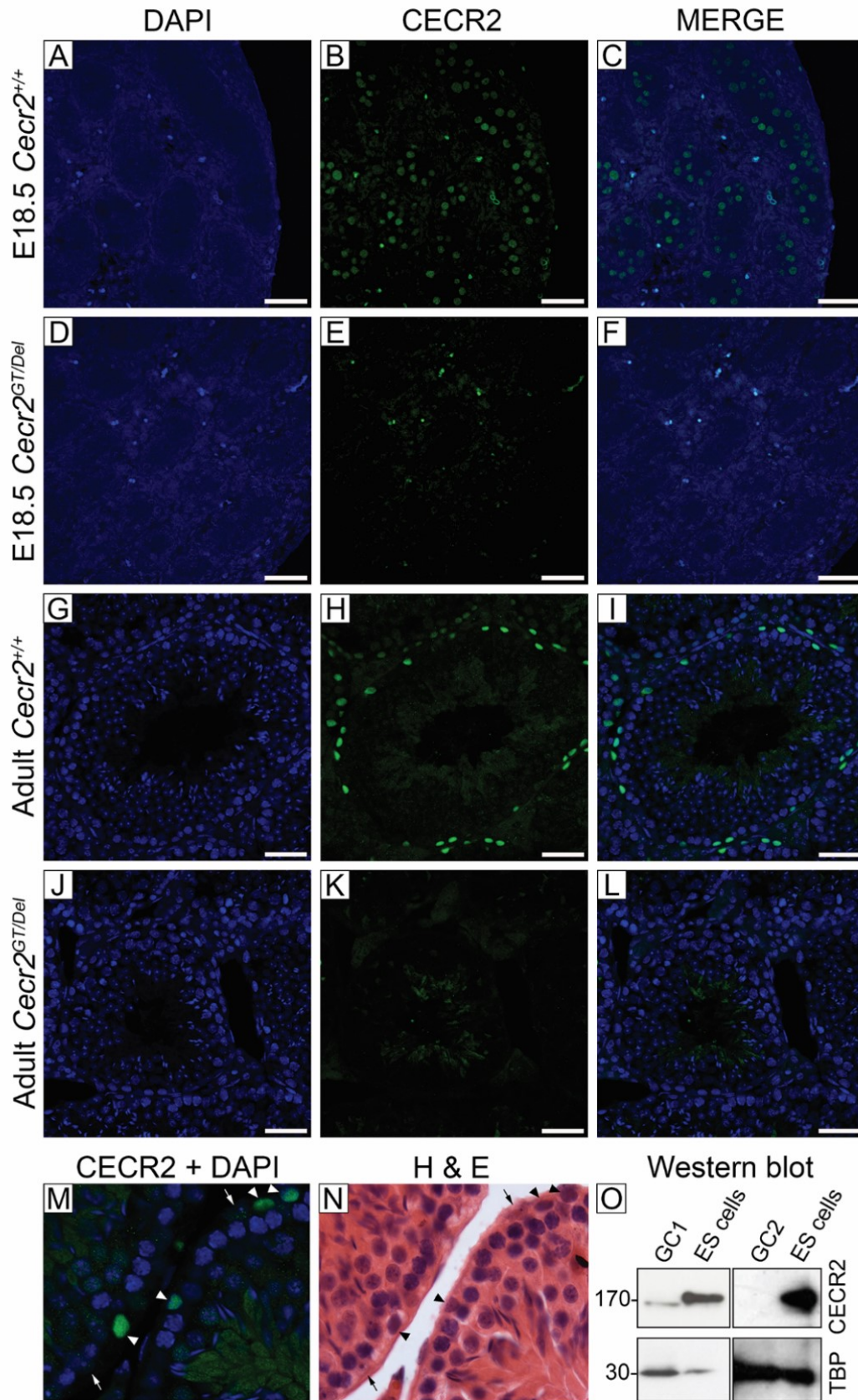
Figure 2.2: CECR2 is localized to gonocytes in E18.5 testes and spermatogonia in adults.
Immunofluorescence using CECR2 antibody shows staining in the gonocytes at E18.5 in
Cecr2^{+/+} testes (A-C). Staining in adult testes is observed only in cells localized to the outer
edge of the tubules but is present in all tubules, consistent with spermatogonia (G-I). Only
background staining is observed in E18.5 (D-F) and adult (J-L) *Cecr2*^{GT/Del} seminiferous
tubules, including non-specific staining in the lumen of all adult seminiferous tubules.
CECR2 antibody stained adult testis (M) subsequently stained with H&E (N) confirms
CECR2 immunofluorescence localization to spermatogonia (arrowheads) but not Sertoli
cells (arrows). Embryonic testes (A-F) were fixed in Bouin's, leading to cloudy DAPI
staining. The absence of CECR2 in western blots (O) on an immortalized mouse type B
spermatogonia cell line (GC1) and an immortalized spermatocyte cell line (GC2) also
support CECR2 localization to type A spermatogonia. The ~160 kDa non-specific band
observed in testis samples (see Figure 2.1 D) is also present in GC1 cells. ES cells (TT2)
were used as a positive control for CECR2. Scale bar= 50 μm.

2.3.2 Loss of CECR2 *results in subfertility that is most severe in young adults and*
improves with age

   To test the effect of severe CECR2 deficiency on fertility, *Cecr2*^{GT/Del} and wildtype

males were fertility tested at several ages. No difference was observed in mating behavior

between *Cecr2*^{+/+} males (25/49, 51%) and *Cecr2*^{GT/Del} males (36/67, 54%, Fisher's exact

test p>0.05) as measured by presence of a post-copulatory plug when mated to

superovulated females for 3 hours. Strikingly, *Cecr2*^{GT/Del} males sired very few pups when

mated at the start of sexual maturity, P42-60 (average of 0.6 pups per confirmed mating;

5.1 for wildtypes). However, fertility improved significantly with age (Figure 2.3 A). By

P81-100, *Cecr2*^{GT/Del} males sired an average of 3.1 pups (p=0.007 compared to *Cecr2*^{GT/Del}

P42-60). This is still significantly lower than wildtype males, with an average of 6.0 pups at

P81-101 (p=0.003). No further improvement was observed in older *Cecr2*^{GT/Del} males. The

average litter size of wildtype males did not significantly differ between ages.

   We previously reported that *Cecr2*^{GT/GT} males (homozygous for the hypomorphic

allele) sire ~31% smaller litters than wildtype (Thompson et al., 2012), however that study

combined males from P42-216. We reassessed this data based on age and added 21

wildtype and 10 *Cecr2*^{GT/GT} males (see Appendix C, Figure C.1). *Cecr2*^{GT/GT} males also sired

smaller litters at P42-60 (average of 1.9 pups) and later improved significantly but remained subfertile even at P121-251 (average of 3.8 pups compared to 6.0 for wildtype, p=0.005).

Although the $Cecr2^{Del}$ allele produces no detectable protein, the $Cecr2^{GT}$ allele produces some protein detectable by western blot due to transcripts splicing around the genetrap (Figure 2.1 D). Consequently, improvement with age could be due to upregulation of the $Cecr2^{GT}$ allele in older males to compensate for $Cecr2$ deficiency. We therefore used qPCR to measure $Cecr2$ levels in the testes at P24 and P103-104. Although we did observe a small increase with age in both genotypes, the levels in $Cecr2^{GT/Del}$ males did not increase in proportion to wildtype levels (54% increase in $Cecr2^{+/+}$, 26% increase in $Cecr2^{GT/Del}$, Figure 2.3 B). This suggests that an upregulation of $Cecr2$ from the hypomorphic allele in response to $Cecr2$ deficiency is not responsible for the phenotypic recovery with age.

2.3.3 Multiple fertility measures are reduced in young males and improve with age

Fertilization frequency was assessed by mating $Cecr2^{GT/Del}$ males with wildtype females and fluorescently detecting paternal DNA in the oocyte as evidence of successful fertilization (Figure 2.4). Only 2.8% of oocytes were fertilized *in vivo* by P42-60 $Cecr2^{GT/Del}$ males, whereas 52.9% were fertilized by wildtype males of the same age (p<0.0001, Figure 2.3 C). The fertilization frequency of $Cecr2^{GT/Del}$ males improved significantly by P61-80 (26.3% fertilized, p<0.0001) and was comparable to wildtype in P101-154 males (61.3% for $Cecr2^{GT/Del}$, 67.1% for wildtype, p>0.05).

Computer assisted sperm analysis was used to assess sperm number and motility of $Cecr2^{GT/Del}$ and wildtype males (Figure 2.3 D-E). $Cecr2^{GT/Del}$ males showed both lower sperm concentration and poor sperm motility compared to wildtype males. These defects were most severe in P42-60 males and improved with age, with comparable sperm concentration to wildtype in P101-160 males. $Cecr2^{GT/Del}$ sperm motility remained lower

than wildtype at P101-160 but significantly improved from P42-60 $Cecr2^{GT/Del}$ levels (p=0.003).

$Cecr2^{GT/Del}$ males also had smaller testes than wildtype males of the same age (Figure 2.3 F). Although no difference was observed between average $Cecr2^{+/+}$ and $Cecr2^{GT/Del}$ male bodyweight, the testis:bodyweight ratio was used to account for variation between mice. At P42, the average testis:bodyweight ratio of $Cecr2^{GT/Del}$ males was 56% of wild-type (p=3.3E-4). At P140-221, the $Cecr2^{GT/Del}$ ratio had increased to 82% of wild-type (p=1.1E-4). The $Cecr2^{GT/Del}$ testis:bodyweight ratio was significantly larger at P140-221 than P42 (p=2.5E-3). Similar results were obtained when testis weights were measured without accounting for bodyweight: At P42 $Cecr2^{+/+}$ testes weighed on average 76 mg while $Cecr2^{GT/Del}$ testes averaged 41 mg (54% of wild-type, p=1.7E-7), and at P140-221 $Cecr2^{+/+}$ testes weighed on average 95 mg while $Cecr2^{GT/Del}$ averaged 76 mg (79% of wildtype, p=4.3E-12).

Overall, all measures suggest moderate spermatogenesis defects at the onset of maturity and improvement with age.
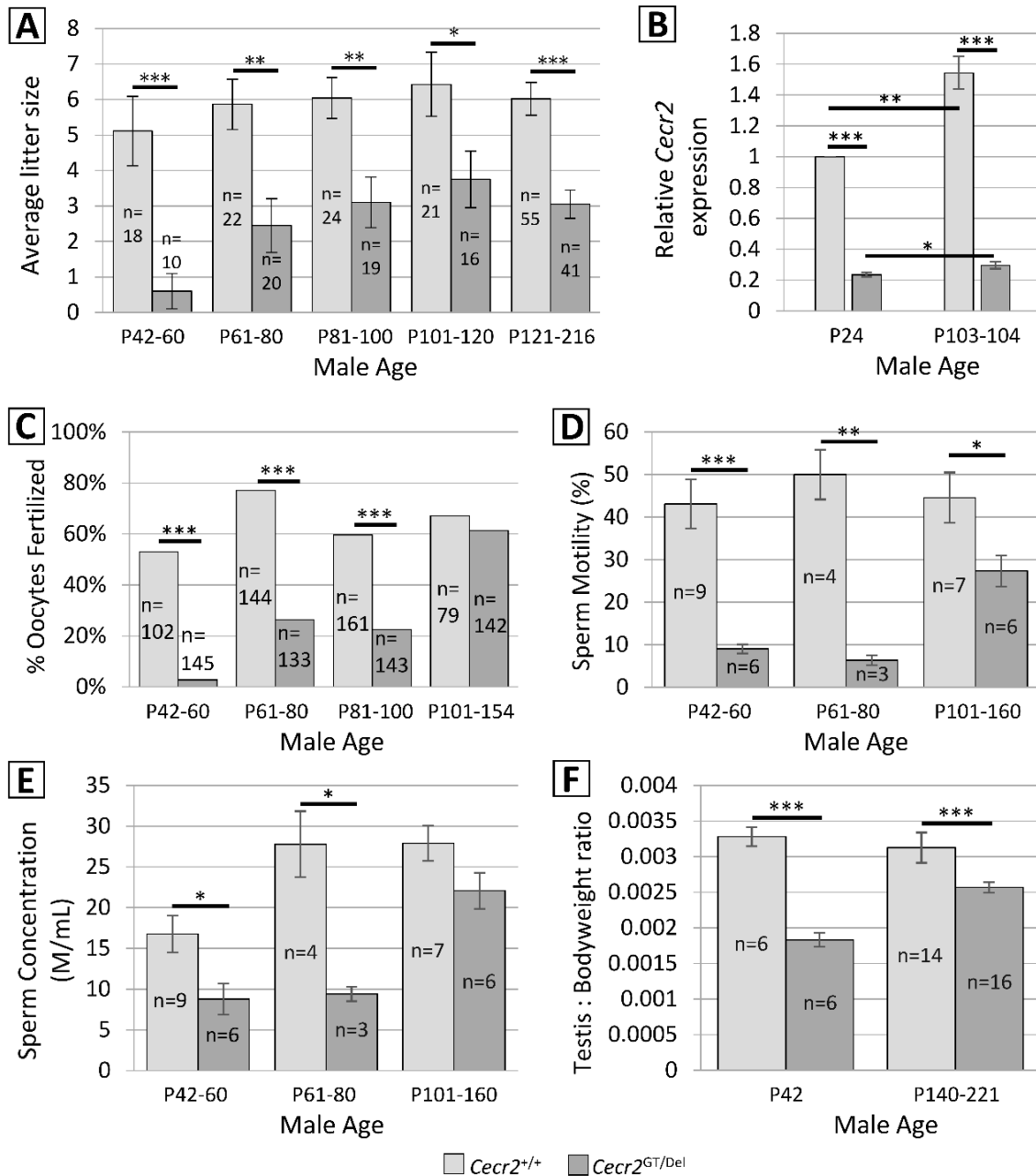
Figure 2.3: Age-dependent subfertility and spermatogenesis-related defects in Cecr2$^{GT/Del}$ testes. The average litter size (A) of Cecr2$^{GT/Del}$ and wildtype males at differing ages was determined by mating them with wildtype females (n=number of litters). Subfertility of Cecr2$^{GT/Del}$ males is most severe at the start of sexual maturity (P42-60 days), and while it improves over time, never reaches wildtype levels. qPCR was used to measure the level of Cecr2 expression in Cecr2$^{+/+}$ and Cecr2$^{GT/Del}$ testes at P24 and P103-104 (B). The Cecr2$^{+/+}$ level at P24 is set to 1 for relative quantification purposes. Primers past the genetrap were used to detect only transcripts that had spliced around it. Although an increase was observed for both genotypes, the relative expression of Cecr2

in *Cecr2$^{GT/Del}$* testes in comparison to wildtype does not increase (0.23:1 at P24, 0.19:1 at P103-104). The percentage of oocytes fertilized by *Cecr2$^{+/+}$* or *Cecr2$^{GT/Del}$* males (C) was determined by naturally mating them to superovulated *Cecr2$^{+/+}$* females. The oocytes were immunostained (see Supplementary Figure 1) to determine if fertilization had occurred (n=number of oocytes examined, obtained from 6-13 mating events per category). While < 3% oocytes were fertilized by P42-60 *Cecr2$^{GT/Del}$* males, the fertilization rate of *Cecr2$^{GT/Del}$* males improved with age. Computer assisted sperm analysis was used to assess sperm motility (D) and sperm concentration (E) in *Cecr2$^{+/+}$* and *Cecr2$^{GT/Del}$* males at three different ages (M/mL= millions per mL, n= number of males). Both measures mirrored the improvement in fertility over time seen in (A). The testis:bodyweight ratio (F) was measured for males at P42 and P140-221 (n=number of males). Although *Cecr2$^{GT/Del}$* males still had smaller testes at P140-221, they were closer to the size of wildtypes. Levels of significance: *** $P \leq 0.001$, ** $0.001 \leq P < 0.01$, * $0.01 \leq P < 0.05$, and no asterisk indicates a lack of significance ($P > 0.05$). Chi square test for independence was used for (C), all others are student's t-tests.
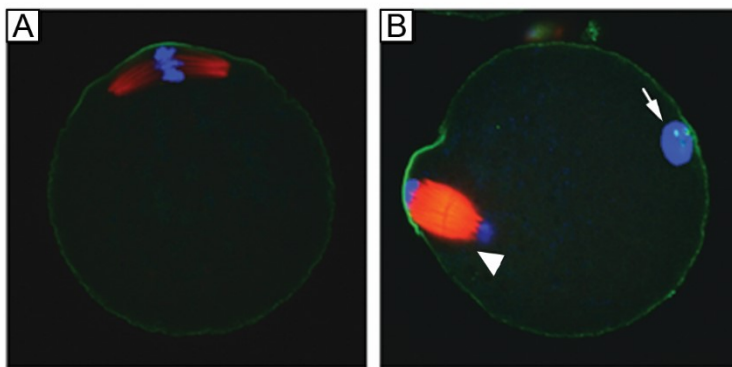
Figure 2.4: Example images obtained using immunofluorescence to test *in vivo* fertilization frequency. To test *in vivo* fertilization frequency, oocytes were dissected out 5 hours post-mating and stained with DAPI (blue), phalloidin (green), and α-tubulin (red). While the maternal chromosomes of unfertilized oocytes (A) were at metaphase, in fertilized oocytes (B) they could be seen at anaphase (arrowhead) and the paternal DNA was inside (arrow). We used this method instead of testing for the presence of pronuclei as CECR2 is a chromatin remodeler and could plausibly play a role in pronuclei formation.

2.3.4 Histological abnormalities of the testis are most severe in young adults and improve with age

Genotypically blinded wildtype and *Cecr2$^{GT/Del}$* P19 testes were indistinguishable (Figure 2.5 A-B), as were P7, P14, and P21 testes (data not shown). By P24, many seminiferous tubules in *Cecr2$^{GT/Del}$* testes showed abnormal spermatogenesis, with fewer advanced germ cells than wildtype and often unequal germ cell loss in different areas of the same tubule (Figure 2.5 C-D). In P42 testes these defects were even more pronounced (Figure 2.5 E-F), disrupting spermatogenesis in the majority of tubules; however, some seminiferous tubules successfully produced sperm (Figure 2.3 D-E). Seminiferous epithelium synchronization was frequently disturbed leading to non-uniform tubules, and many tubules were sparsely populated with germ cells. Spermatogenesis did not consistently halt at a specific cell type. In older *Cecr2$^{GT/Del}$* males, most seminiferous tubules appeared normal (Figure 2.5 G-H), and visibly atypical tubules were less drastically halted or asynchronized than those at P42.
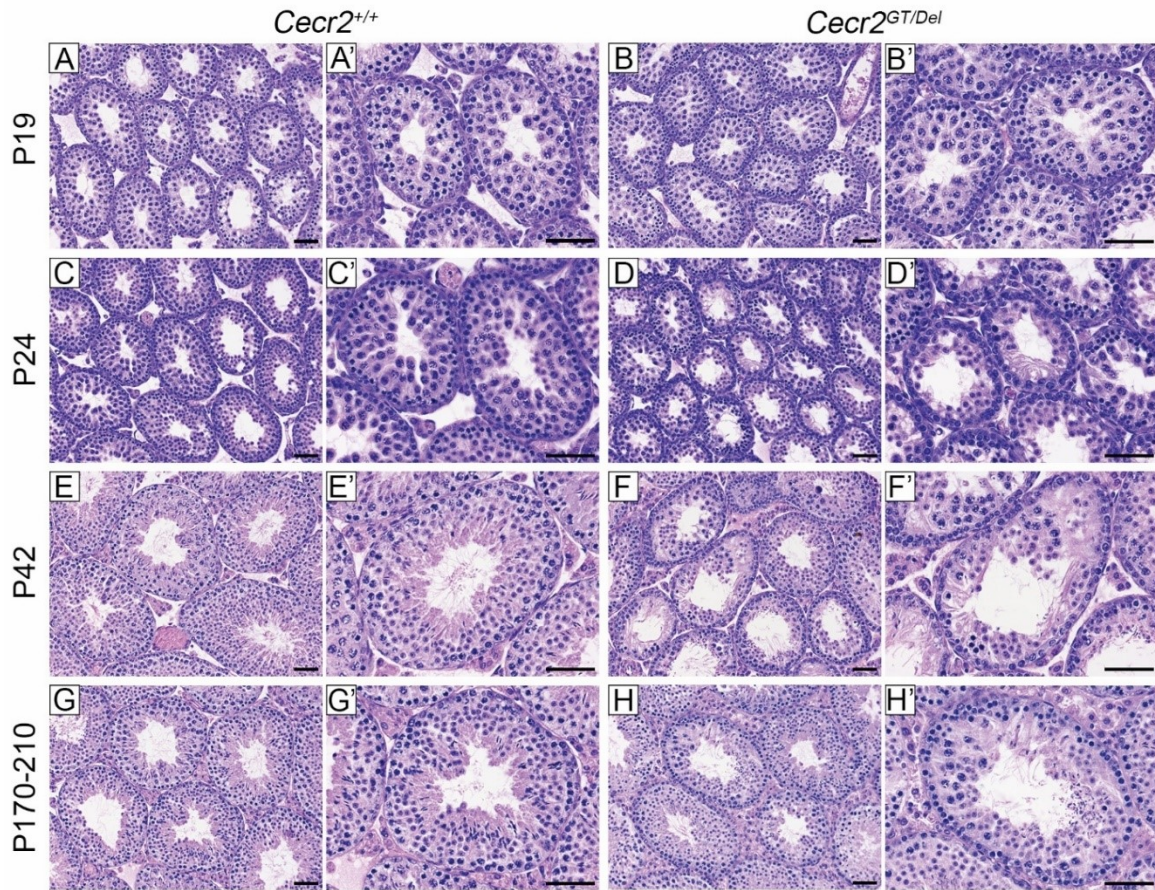
Figure 2.5: Histological abnormalities in *Cecr2^{GT/Del}* testes appear around P24, are moderate at maturity (P42), then improve with age. H&E stained *Cecr2^{+/+}* (A, C, E, G) and *Cecr2^{GT/Del}* (B, D, F, H) testes. No difference was observed between genotypes at P19 (A, B), but *Cecr2^{GT/Del}* testes could be clearly distinguished at P24 (C, D) by the presence of many tubules missing germ cells in portions of the tubule. More severe defects were observed at P42 (E, F), when most tubules exhibited an uneven lack of advanced germ cells or a disruption of the normal cell associations of the seminiferous epithelium. These defects were less pronounced by P170-210 (G, H). Magnified portions of each image are also shown (A'-H'). Scale bar= 50 μm.

As *Cecr2^{GT/Del}* males produce a small amount of CECR2 due to the hypomorphic *Cecr2^{GT}* allele (Figure 2.1 D, Figure 2.3 B), we also examined histology of *Cecr2^{Del/Del}* testes (complete CECR2 deficiency). As these mice die perinatally due to exencephaly, we could only assess E18.5 testes. Although the seminiferous cords appeared normal, *Cecr2^{Del/Del}* males had significantly fewer seminiferous cords than wildtype (Figure 2.6).
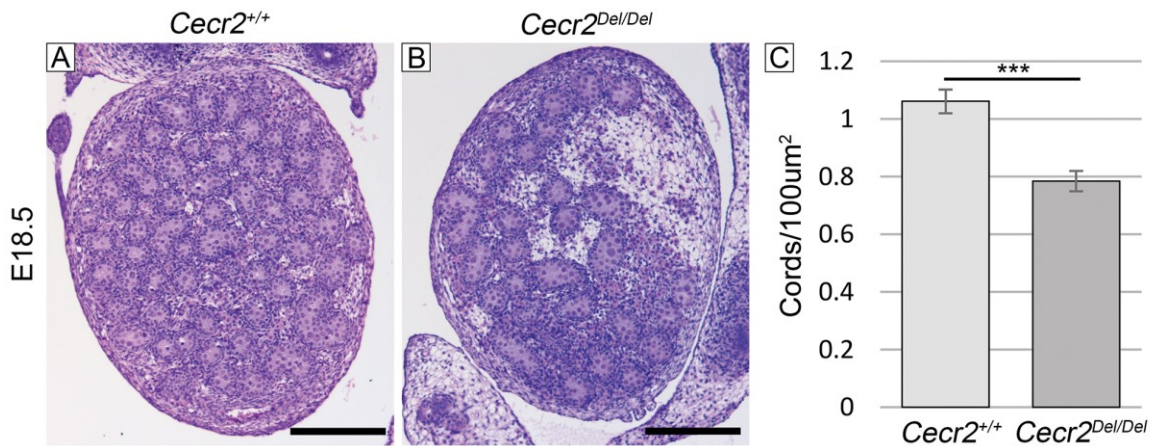
Figure 2.6: Histological defects in *Cecr2^{Del/Del}* embryonic testes. H&E stained E18.5 *Cecr2^{+/+}* (A) and *Cecr2^{Del/Del}* (B) testes. Areas with no seminiferous cords can be seen in the *Cecr2^{Del/Del}* testis. The number of cords per 100 μm^2 of testis section is quantified in (C). *Cecr2^{+/+}* n= 27 sections from 5 embryos, *Cecr2^{Del/Del}* n= 25 sections from 4 embryos. ***P<0.001, scale bar= 200 μm.

2.3.5 Testosterone levels are not affected by loss of CECR2

Testosterone is required for spermatogenesis (O'Donnell et al., 2006), and mouse mutants with lower serum testosterone levels can have decreased testis size and arrested spermatogenesis (Wang et al., 2009). We therefore measured serum testosterone levels in males when they have the most severe abnormalities in spermatogenesis (P42-60) (Figure 2.7). There was no significant difference in testosterone levels between *Cecr2$^{GT/Del}$* and wildtype males, indicating that testosterone is not contributing to the abnormal phenotype.
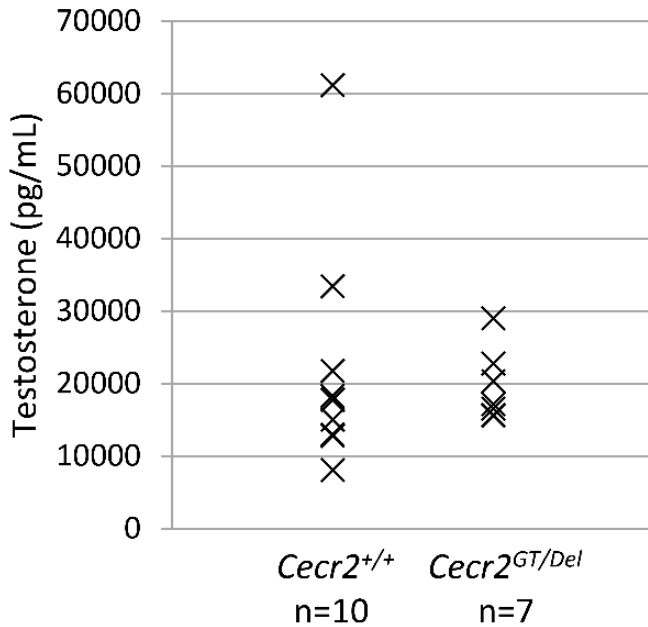
Figure 2.7: Testosterone levels are normal in *Cecr2$^{GT/Del}$* males. Testosterone levels were measured in serum from P42-60 males. No significant differences were observed between *Cecr2$^{+/+}$* and *Cecr2$^{GT/Del}$* males (Wilcoxon rank-sum test, p>0.05).

2.3.6 Differentially expressed genes in Cecr2$^{GT/Del}$ testes suggest a possible defect in MSCI

As *Cecr2* is a chromatin remodeler, it could cause the misregulation of genes critical for spermatogenesis. We therefore did an RNA-seq comparing the transcriptomes of *Cecr2$^{+/+}$* and *Cecr2$^{GT/Del}$* testes at P24, when the defect is first histologically evident. Sampling at P24 increases the likelihood of finding causative changes rather than secondary effects due to sustained abnormal spermatogenesis, although the presence of histological defects may still skew the results. RNA-seq analysis revealed 387 genes that were differentially expressed, 238 (61%) of which were expressed at a lower level in *Cecr2$^{GT/Del}$* testes and 149 (39%) of which were higher. If the majority of gene expression changes were due to fewer advanced germ cells in *Cecr2$^{GT/Del}$* testes, genes expressed in early and late cell types would be disproportionately found at higher and lower levels, respectively. However, an analysis assigning cell types to the differentially expressed genes based on a recent single cell transcriptome study (Hermann et al., 2018) did not show this trend. Of the 67 genes expressed in spermatogonia and primary spermatocytes, 10 were found at increased levels and 57 at decreased levels in *Cecr2$^{GT/Del}$* testes. Of the 35 genes expressed in post-meiotic cell types, 18 were found at increased levels and 17 at decreased levels in *Cecr2$^{GT/Del}$* testes. Therefore, the majority of the expression changes observed between *Cecr2$^{+/+}$* and *Cecr2$^{GT/Del}$* testes at P24 are unlikely to be simply due to the abnormal histological phenotype in *Cecr2$^{GT/Del}$* testes.

Strikingly, 18% of differentially expressed genes were on the sex chromosomes (66 on X, 2 on Y), representing a notable enrichment. Furthermore, differentially expressed sex chromosome genes exclusively had higher expression in *Cecr2$^{GT/Del}$* samples, representing 46% of all genes with a higher abundance (Figure 2.8 A). Visualization of the expression levels of all expressed genes in these samples revealed a general trend of higher gene expression in sex chromosomes across multiple *Cecr2$^{GT/Del}$* samples (Figure 2.8 B). This suggests that MSCI may not be occurring efficiently in *Cecr2$^{GT/Del}$* testes, leading to abnormally high transcription from the improperly silenced sex chromosomes. Several of the genes are known to be involved in MSCI, recombination or synapsis (see Table 2.1),

therefore their altered expression could lead to inefficient MSCI and the abnormally high

X chromosome transcript levels in *Cecr2*^{GT/Del} testes.
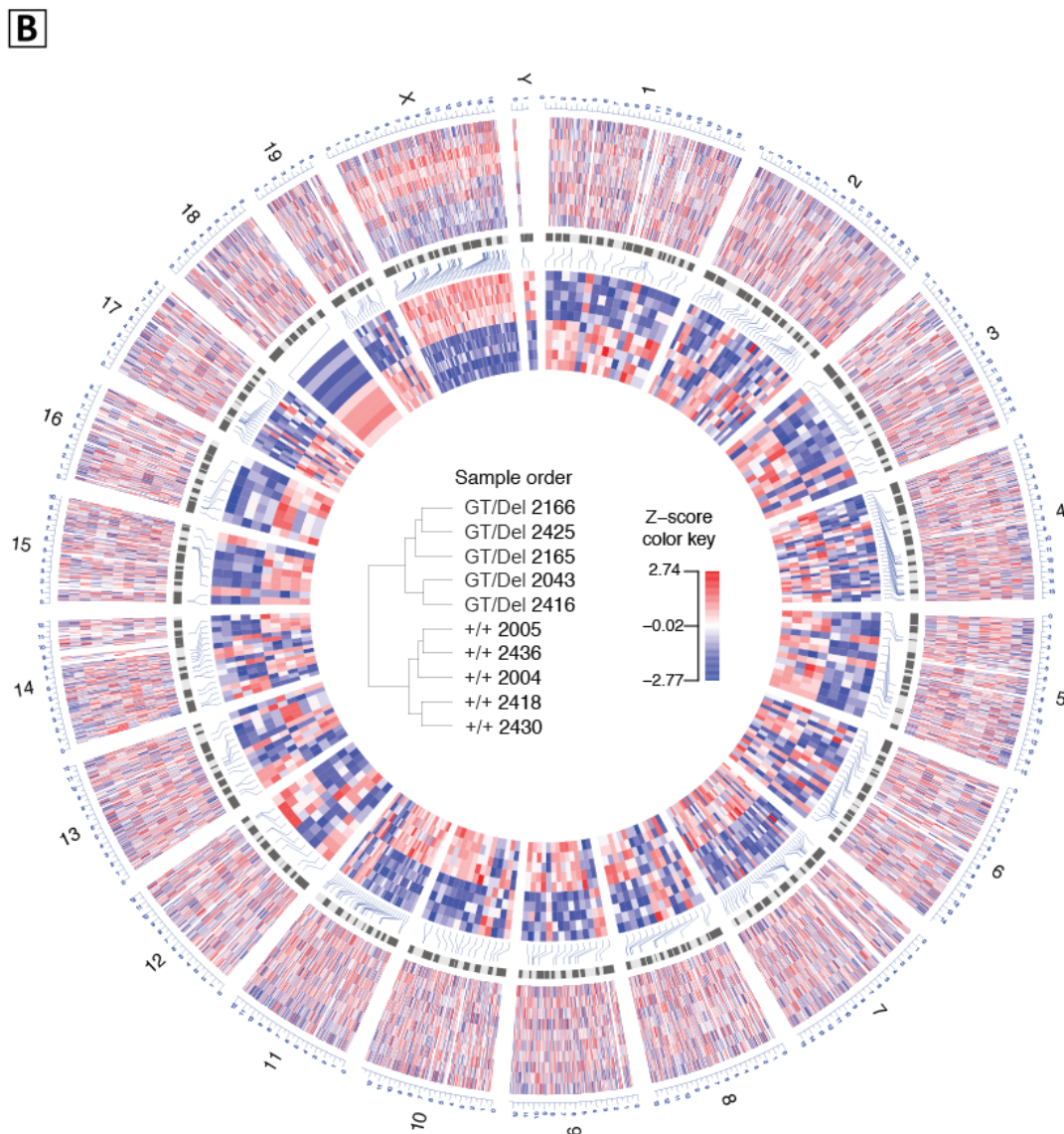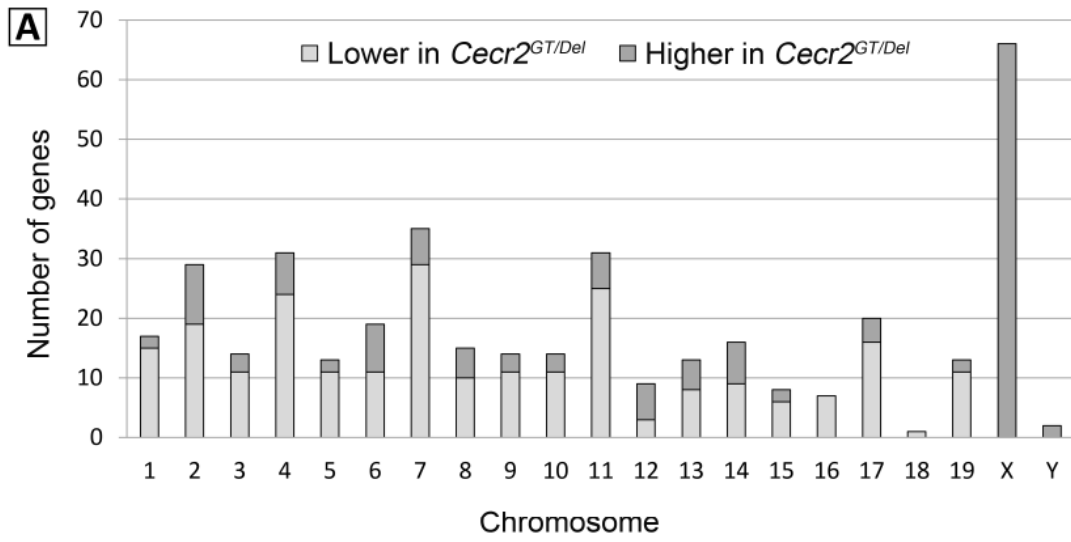
Figure 2.8: A disproportionately large number of sex chromosome genes are more highly expressed in _Cecr2^GT/Del_ testes than _Cecr2^+/+_ testes at P24 as determined by RNA-seq. The distribution of significantly differentially expressed genes across the chromosomes (A) reveals an enrichment in chromosome X. In addition, while the majority of autosomal genes are expressed at lower levels in _Cecr2^GT/Del_ testes, genes located on the sex chromosomes are exclusively higher. A circular heatmap (B) provides a visualization of the expression levels of differentially expressed genes in _Cecr2^GT/Del_ versus _Cecr2^+/+_ (inner ring) and that of all expressed genes (outer ring) in mice testes at P24. This reveals a general trend of higher gene expression from _Cecr2^GT/Del_ sex chromosomes across multiple _Cecr2^GT/Del_ samples, beyond what the differential expression analysis was able to detect within the statistical power constraints of the analysis. Circular tracks from outside to inside: genome positions by chromosomes (the scale multiplied by 10^8 gives the position in base pairs), a heatmap of all expressed genes (genome-wide gene expression), chromosomes with cytobands indicated, and a heatmap of differentially expressed genes in _Cecr2^GT/Del_ versus _Cecr2^+/+_ P24 testes with elbow connectors indicating the gene locations. The order of samples in the outer track is kept consistent to that of the inner track which is based on the order in the sample clustering dendrogram (plotted in the centre) observed when samples were hierarchically clustered using Z-score transformed expression values from differentially expressed genes. This plot was generated using R package OmicCircos v1.23.0 (Hu et al., 2014).

Based on known functions and/or expression data from previous literature, we tested the abnormal expression levels of 16 genes using qPCR, 6 of which are located on the X chromosome (Table 2.1). Of these, all except _Slx2_ were validated in P24 testes (Figure 2.9, Table 2.1). We also measured their relative expression levels in P103-104 testes to see if expression levels normalized. While 12/16 genes remained differentially expressed in the testes of older males, 11/16 were significantly closer to _Cecr2^+/+_ levels than at P24 (Figure 2.9), including all 8 expressed at lower levels in _Cecr2^GT/Del_ testes.

Table 2.1: Differentially expressed genes between wildtype and *Cecr2^GT/Del^* mouse testes at P24 and P103-104.

Gene	Chr.	RNA-seq FDR	RNA-seq FC	P24 qPCR FC	P103-104 qPCR FC	Relevant functions and features from literature	References
Fgr	4	2.0E-07	0.34	**0.27***	**0.73***	Highest expression in 2-3 week old testes, still moderately expressed in adult	(Goupil et al., 2011)
Hfm1	5	1.4E-08	0.59	**0.45***	**0.75***	Required for normal CO numbers and complete synapsis	(Guiraldelli et al., 2013)
Msh4	3	1.2E-15	0.51	**0.48***	**0.74***	Required for normal CO numbers and complete synapsis, mutations associated with spermatogenic failure in humans	(Kneitz et al., 2000; Snowden et al., 2004; Terribas et al., 2010)
Hormad2	11	1.6E-09	0.60	**0.46***	**0.83***	Required for ATR recruitment to unsynapsed axes and MSCI	(Fukuda et al., 2012; Kogo et al., 2012; Wojtasz et al., 2012)
Spata22	11	1.3E-06	0.61	**0.49***	**0.85***	Required for normal CO numbers and complete synapsis, forms a complex with MEIOB	(Hays et al., 2017; Salle et al., 2012; Xu et al., 2017)
Meiob	17	4.0E-11	0.61	**0.50***	**0.86**	Required for normal CO numbers and complete synapsis, mutations associated with spermatogenic failure in humans	(Gershoni et al., 2019; Luo et al., 2013; Souquet et al., 2013)
Ptchd3	11	1.3E-17	0.53	**0.57***	**0.74***	Testis specific *Ptchd*, predicted role in Hh signalling for sperm motility, not essential for spermatogenesis in humans	(Fan et al., 2007; Ghahramani Seno et al., 2011)
Cbs	17	3.2E-03	0.57	**0.53***	**1.30**	Generates H_2S, which is important for sperm motility. Associated with asthenospermia (poor sperm motility) in humans	(Li et al., 2015; Nuño-Ayala et al., 2012; Wang et al., 2018)
Glp1	9	9.5E-03	1.50	**1.34***	**1.31***	Expressed in Leydig cells, mutation leads to spermatogenic arrest	(Li et al., 2007)

						Description	References
Bmp7	2	5.7E-05	1.61	**1.39***	**0.80**	Expressed in spermatogonia and primary spermatocytes in immature testes, but spermatids in adults. Transient role in proliferation of germ cells in embryos, then in maintenance of spermatogenesis in adults	(Ciller et al., 2016; Ross et al., 2007; Zhao et al., 2001)
Tex11	X	2.2E-08	1.57	1.37*	1.34*	Expressed in spermatogonia, regulates recombination frequency and possibly proliferation of spermatogonia. Mutations cause azoospermia in humans	(Adelman and Petrini, 2008; Sha et al., 2018; Yang et al., 2015; Yatsenko et al., 2015; Yu et al., 2012)
Scml2	X	1.3E-10	1.58	1.41*	1.30*	Expressed in spermatogonia and early meiotic cells, plays a role in maintaining active histone modifications on sex chromosome genes needed in spermatids	(Adams et al., 2018; Hasegawa et al., 2015; Luo et al., 2015)
Taf7l	X	2.1E-14	1.58	1.31*	1.22*	Testis specific transcription factor required for the normal expression of postmeiotic genes. Necessary for normal sperm morphology and motility.	(Cheng et al., 2007; Zhou et al., 2013)
Slx2	X	5.2E-04	1.54	**1.26**	**0.96**	Expressed in primary spermatocytes and localizes to sex body	(Shi et al., 2013; Zhuang et al., 2016)
Rhox13	X	3.0E-08	1.78	1.72*	1.51*	Required for a histologically normal first wave of spermatogenesis, but not for normal adult spermatogenesis. No difference in litter sizes at any age.	(Busada et al., 2016; Geyer and Eddy, 2008)
Ccnb3	X	5.1E-21	2.52	**2.06***	**1.43***	Early meiotic cyclin normally downregulated at transition to pachytene. Continued expression causes aberrant spermatogenesis.	(Nguyen et al., 2002; Refik-Rogers et al., 2006)

FDR = False Discovery Rate adjusted significance, FC = Fold Change, where FC>1 indicates higher expression in *Cecr2*[GT/Del] testes, * indicates qPCR significance between wildtype and *Cecr2*[GT/Del] testes, bolded qPCR values indicate significance between P24 and P103-104, CO = crossover.
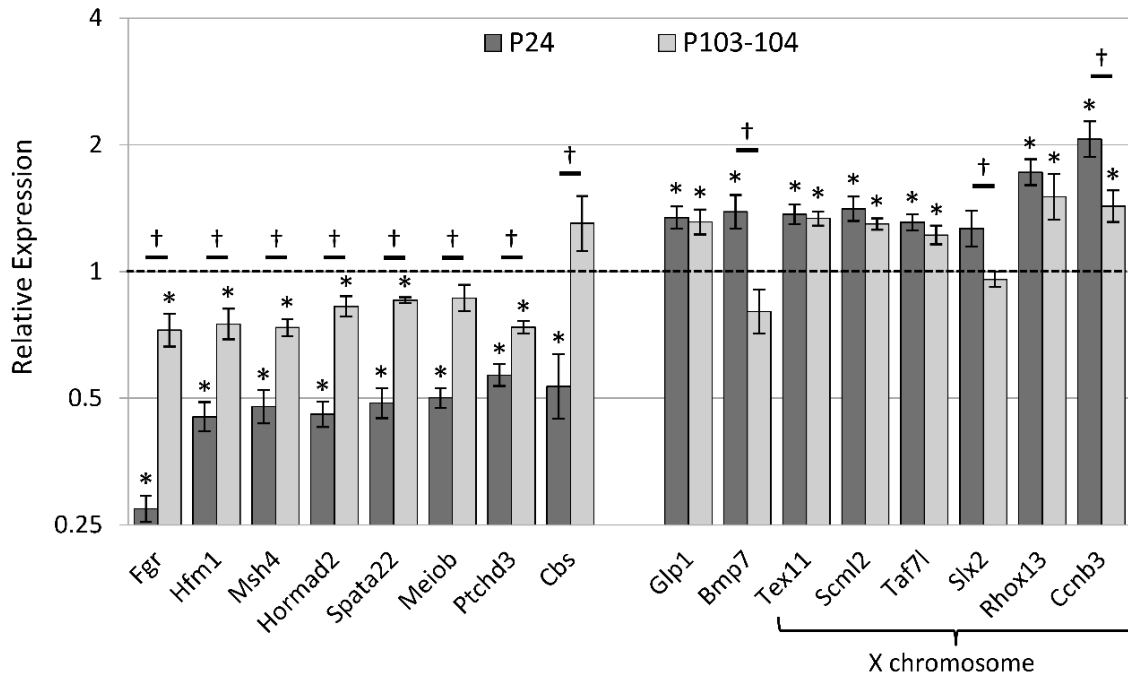
Figure 2.9: qPCR at P24 and P103-104 reveals several differentially expressed genes are expressed closer to wildtype levels in P103-104 *Cecr2^GT/Del* males. *Cecr2^GT/Del* expression levels are shown relative to *Cecr2^+/+* levels at the same age (set at 1). * indicates P<0.05 when comparing wildtype and *Cecr2^GT/Del* samples of the same age, † indicates P<0.05 when comparing the difference between wildtype and *Cecr2^GT/Del* samples at P24 and P103-104.

2.3.7 ATR staining reveals unsynapsed chromosomes in Cecr2$^{GT/Del}$ spermatocytes

To investigate the potential link to MSCI, we used pachytene spermatocyte spreads to look for abnormalities in ATR localization. ATR is recruited to unsynapsed axes at the zygotene/pachytene transition, and thus normally only sex chromosomes. ATR phosphorylates histone H2AX, leading to transcriptional silencing (Turner et al., 2004). Anti-SYCP3 staining was used to visualize synaptonemal complex assembly. Unexpectedly, we found that pachytene-like spermatocytes (spermatocytes with short, thick chromosomes characteristic of pachytene except for where they are unsynapsed) from P24 Cecr2$^{GT/Del}$ males were significantly more likely to have autosomal asynapsis (average of 22% vs 3% in Cecr2$^{+/+}$ samples, p=0.02, Figure 2.10), but P142-149 spermatocytes were comparable (average of 3% in both genotypes). The sex chromosomes were also unsynapsed at the pseudoautosomal region in some spermatocytes (Figure 2.10 D-F). However, multiple unsynapsed autosomes in a spread and the resulting absence of the sex body made it difficult to identify the sex chromosomes and whether they were synapsed or not. It is likely that many such spreads in the young Cecr2$^{GT/Del}$ males also contained unidentified unpaired sex chromosomes. Regardless, young Cecr2$^{GT/Del}$ males appear to have a general problem with chromosomal synapsis that may impact MSCI.
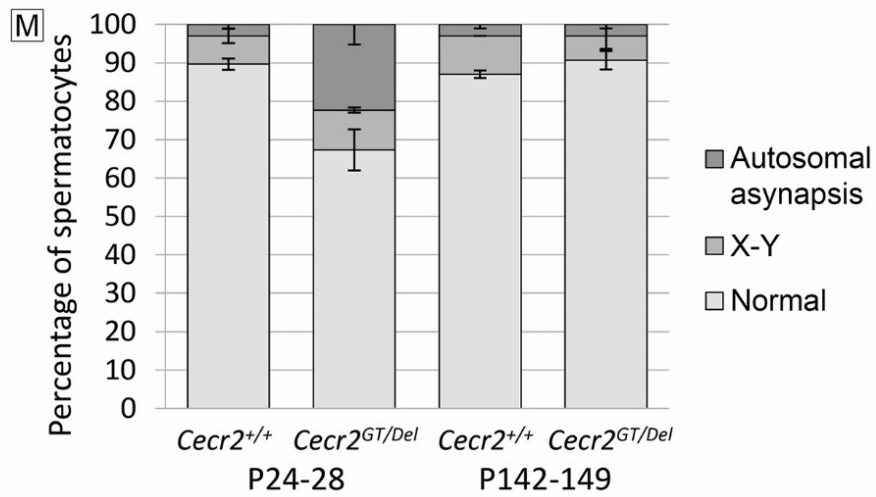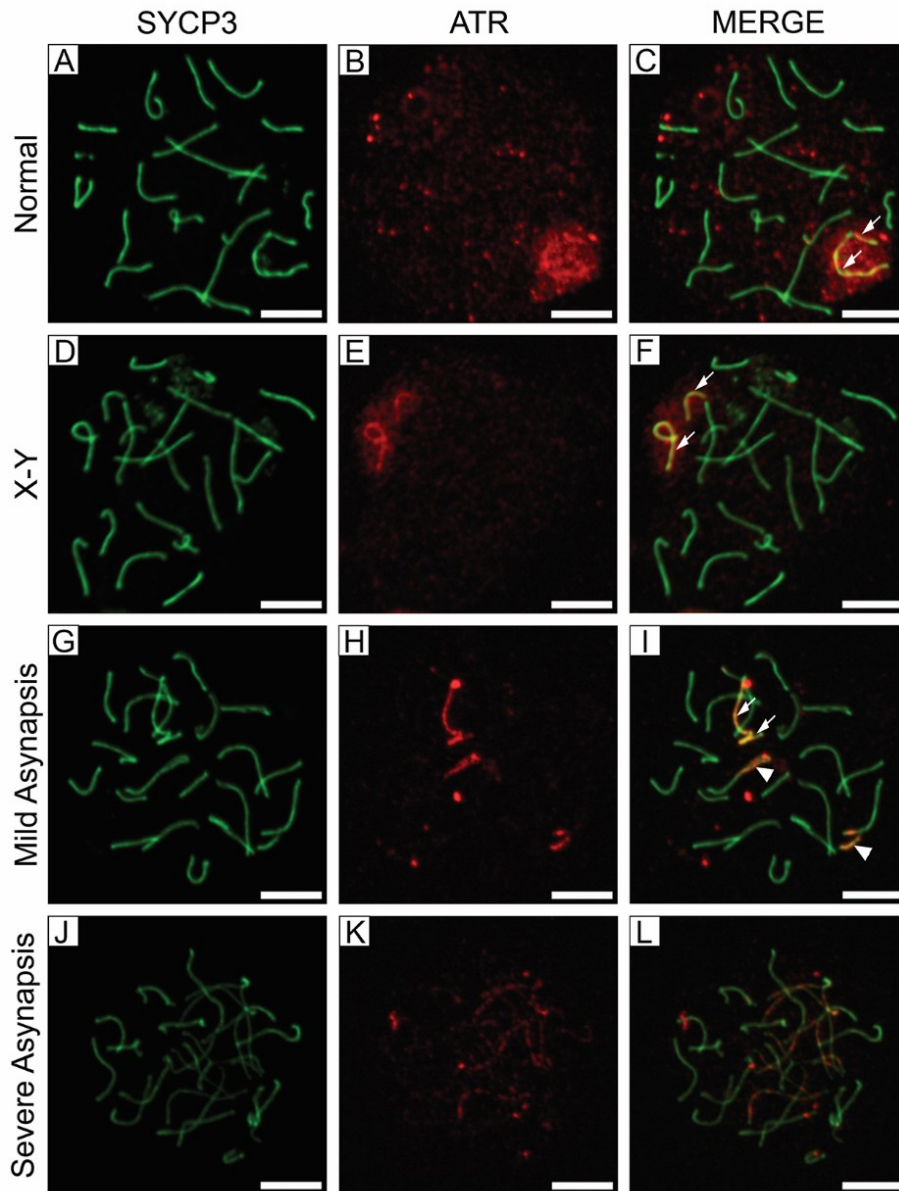
Figure 2.10: *Cecr2^{GT/Del}* spermatocytes show autosomal asynapsis. SYCP3 (green) antibody was used to visualize chromosome spreads from pachytene-like spermatocytes and ATR (red) antibody visualized asynapsis. In normal cells, (A, B, C), ATR mostly localizes to the sex body where the sex chromosomes reside. The sex chromosomes are synapsed only at the pseudoautosomal region. Spermatocytes with dissociated sex chromosomes, referred to as X-Y (D, E, F) were observed for both age points and genotypes at approximately the same rate. P24-28 *Cecr2^{GT/Del}* spermatocytes had a significantly higher prevalence of mild (G, H, I) or severe (J, K, L) autosomal asynapsis, which can be visualized by ATR staining to the unsynapsed regions. The number of each type of spermatocyte is quantified in (M), where all levels of autosomal asynapsis were included in the autosomal asynapsis category. Arrows indicate sex chromosomes, arrowheads indicate autosomal asynapsis in (I). Scale bar = 5 μm. n = 300 spermatocytes from 3 males except for P142-149 *Cecr2^{+/+}* where n = 200 spermatocytes from 2 males.

2.4 Discussion

2.4.1 Cecr2$^{GT/Del}$ males have a moderate defect in early spermatogenesis and milder defects as adults

We have shown that compound heterozygote Cecr2$^{GT/Del}$ males have the most severe fertility phenotypes just after sexual maturity and improve as they age. Both the average size of litter sired and the percentage of oocytes fertilized *in vivo* are close to zero in P42-60 males, and sperm concentration, sperm motility, and testis weight are also significantly decreased. All of these parameters show improvement with age. While some measures return to approximately wildtype levels in older Cecr2$^{GT/Del}$ males, they continue to sire significantly smaller litters with no further improvement after P100. A reexamination of the Cecr2$^{GT/GT}$ hypomorph mutants showed a similar pattern of subfertility. Cecr2$^{GT/GT}$ testis histology, sperm number, and sperm motility were reported as normal (Thompson et al., 2012), but this could be explained by their age (P128-243) combined with higher levels of CECR2 from two copies of the hypomorphic allele creating a milder phenotype.

Severe subfertility in young males just after sexual maturity and subsequent recovery is indicative of a defect during the first wave of spermatogenesis that begins shortly after birth (Geyer, 2017). This initial wave produces the first sperm available to adult males at sexual maturity, and establishes the basis for continuous spermatogenesis in adults. Male mice with a germ cell specific *Sox3* knockout have a strikingly similar phenotype to Cecr2$^{GT/Del}$ males. *Sox3* mutant newborn testes initially appear normal but they have a severe germ cell depletion by P20 which subsequently partially recovers in adults to ~80% of normal (Laronda and Jameson, 2011). As fertility was not tested in these animals, it is unknown whether the recovery in testis histology translates into increased litter size. *Sox3* mutants have a block at the point of spermatogonial differentiation, while Cecr2$^{GT/Del}$ males have a histologically abnormal phenotype later in the first wave.

It is unclear why the *Cecr2* and *Sox3* testis phenotypes disproportionately affect prepubertal spermatogenesis and recover as the males age. One intriguing possibility is that there are unique pathways or regulatory differences in spermatogenesis that differ between the first wave and steady-state adult spermatogenesis (Geyer, 2017; Laronda and Jameson, 2011). *Cecr2* may play a role specifically during prepubertal spermatogenesis that is no longer required in adults. Consequently, the disruption of prepubertal spermatogenesis, particularly the establishment of the spermatogenic wave and the stage-specific cell associations of the seminiferous epithelium, may lead to the milder but continued abnormal spermatogenesis we observe into adulthood. *Cecr2* may also be required for continuing adult spermatogenesis, since *Cecr2* expression and antibody staining remains in normal aging males. Interestingly, the decreased number of seminiferous cords observed in *Cecr2*$^{Del/Del}$ E18.5 testes completely lacking *Cecr2* suggests an earlier role for *Cecr2* during testis development, before we first observe abnormal spermatogenesis in *Cecr2*$^{GT/Del}$ testes with measurable CECR2 present at P24. While these *Cecr2*$^{Del/Del}$ embryos have exencephaly that could theoretically affect development of other organs, such embryos appear grossly normal outside of the brain. Improvement with age may also reflect increasing compensation over time by other genes or pathways (as suggested by Laronda and Jameson, 2011).

Furthermore, this compensation may be due to selective pressure acting on spermatogonial stem cells over time. Even in wild type testes, the fate of individual spermatogonial stem cells is highly variable over time due to apparently stochastic differences (Hara et al., 2014; Klein et al., 2010). Although spermatogonial stem cells are traditionally thought to produce one self-renewing and one differentiating daughter, they can also divide symmetrically to produce two self-renewing daughter cells or two differentiating daughter cells (reviewed in Yoshida, 2019). Over time, this can lead to descendants of a relatively small number of spermatogonial stem cells making up the stem cell population of the testis. When variation between spermatogonial stem cells provides a selective advantage, this clonal expansion can occur in a biased manner rather than stochastically. Supporting this, there is evidence that some de novo point mutations

are more commonly passed on from older fathers due to a colonization of the seminiferous tubules by mutant spermatogonia with a selective advantage (reviewed in Yamada et al., 2016). This is referred to as "selfish spermatogonial selection" (Goriely and Wilkie, 2012) and has been shown to occur with mutations in the receptor tyrosine kinase/RAS/MAPK signaling pathway. For example, gain-of-function mutations in FGFR2 result in enhanced fitness of spermatogonia stem cells and are associated with Apert syndrome (Martin et al., 2014). Therefore, it is possible that if cells predisposed to normal spermatogenesis in *Cecr2* mutant males also have a selective advantage towards clonal expansion, these cells promoting normal spermatogenesis would slowly take over the population of spermatogonial stem cells and lead to recovery with age. This theory is not mutually exclusive with the other ideas presented here. While any selective advantage does not appear to be due to increased levels of *Cecr2*, it could be, for example, that cells which better compensate for a lack of *Cecr2* with other genes or pathways have an advantage and increase in abundance with time. An analysis of spermatogenesis along the length of each tubule could help to determine whether clonal expansion of cells with a selective advantage is occurring, as this would lead to expanding patches of improved spermatogenesis rather than a random distribution.

As *Cecr2* is a chromatin remodeler, when and how it affects spermatogenesis may also involve misregulation of one or more genes. Although the phenotype of *Sox3* mutants closely resembles that of *Cecr2*$^{GT/Del}$ males, *Sox3* is not differentially expressed in P24 *Cecr2*$^{GT/Del}$ testes. However, *Rhox13*, loss of which results in a prepubertal defect in spermatogenesis in mice, is differentially expressed, and may contribute to the *Cecr2*$^{GT/Del}$ phenotype (see below).

2.4.2 Cecr2$^{GT/Del}$ pachytene-like spermatocytes show asynapsis

Our RNA-seq analysis showed clear increased expression of many genes on the sex chromosomes, leading us to hypothesize that MSCI may not be occurring efficiently.

When we used ATR to visualize asynapsis in pachytene spermatocytes, we observed not only unsynapsed sex chromosomes but also varying degrees of autosomal asynapsis in a significant number of $Cecr2^{GT/Del}$ spermatocytes. This provides a possible explanation for why transcripts of sex chromosome genes are abnormally abundant and may also explain how the loss of $Cecr2$ affects spermatogenesis. Meiotic silencing occurs in response to asynapsis, and autosomal asynapsis has been associated with the failure of MSCI (Ellnati et al., 2017; Homolka et al., 2012; Mahadevaiah et al., 2008; Turner, 2015; Xiong et al., 2017). One possible explanation for this is that autosomal asynapsis leads to key proteins being sequestered on asynapsed autosomes making them unavailable for MSCI (Mahadevaiah et al., 2008). Experiments have shown that increasing levels of autosomal asynapsis do not increase the overall levels of key proteins for silencing, ɣ-H2AX and BRCA1, but rather result in more fragmented localization across all unsynapsed chromosomes including the sex chromosomes (Mahadevaiah et al., 2008).This could lead to both ineffective MSCI and inappropriate autosomal meiotic silencing of unsynapsed chromatin. Widespread autosomal asynapsis triggers a checkpoint leading to apoptosis of pachytene spermatocytes (Burgoyne et al., 2009). However, limited autosomal asynapsis with aberrant expression from the X chromosome or lack of expression of a critical autosomal gene could lead to cell death later in spermatogenesis or the production of abnormal spermatids. As varying degrees of asynapsis were observed in $Cecr2^{GT/Del}$ spermatocytes, both of these scenarios could be occurring. This may explain some of the variability we observe in $Cecr2^{GT/Del}$ spermatogenesis, as spermatocytes would be affected at different stages depending on the degree of asynapsis in those cells. In addition, small regions of asynapsis would not have been detectable in our analysis, but could affect critical genes. This could produce an underestimation of the number of $Cecr2^{GT/Del}$ spermatocytes with asynapsis that could lead to abnormal sperm production, and be more consistent with the level of infertility we observe in young males.

2.4.3 Transcriptional changes in Cecr2$^{GT/Del}$ testes

To find differentially expressed genes that could shed light on the phenotypes we see, we used RNA-seq to compare Cecr2$^{GT/Del}$ and wildtype testes at the age we first observed defects (P24), to minimize secondary effects. As the RNA-seq analysis was done at a time when histological defects in the testis were beginning to appear, it is possible that expression changes are impacted by a change in the relative abundance of cell types in the Cecr2$^{GT/Del}$ testes (see Chapter 4 for further discussion). A precise quantification of round spermatids at P24 would help in determining the scope of this problem, and an analysis of the changes in gene expression by cell type would also be informative. RNA-seq analysis revealed 387 genes that were differentially expressed in Cecr2$^{GT/Del}$ testes, of which we further tested 16. The abnormal expression of all but Slx2 was validated. All 16 genes are involved in spermatogenesis. Additionally, 11/16 had not fully returned to wildtype levels by P103-104 (Fgr, Hfm1, Msh2, Hormad2, Spata22, Ptchd3 and Glp1), consistent with older males still showing subfertility.

Three of these 16 genes likely play a more important role in testes before sexual maturity than in adult spermatogenesis, possibly explaining why the defect is more severe in young males. Fgr, reduced to ~27% of wildtype levels in P24 Cecr2$^{GT/Del}$ testes, normally has highest expression levels in P14 and P21 testes and lower levels in adults (Goupil et al., 2011), suggesting an important role in prepubertal spermatogenesis. Similarly, Bmp7 is expressed in spermatogonia and spermatocytes before sexual maturity, but transitions to mid-late stage spermatids in adults (Zhao et al., 2001). Since CECR2 is found only in spermatogonia, it is possible that CECR2 only affects this early stage expression. This is supported by the qPCR analysis, which shows Bmp7 is significantly more highly expressed in Cecr2$^{GT/Del}$ testes at P24, but is not significantly different from wild-type at P103-104. Rhox13 is required for the first wave of spermatogenesis, and without it histological abnormalities occur in the seminiferous tubules (Busada et al., 2016). Despite the continued expression of Rhox13 into adulthood in wildtype testes, older Rhox13 KO mice have normal testis histology. Therefore, the overexpression of

Rhox13 in *Cecr2^GT/Del* testes at both P24 and P103-104 could disproportionately affect the first wave of spermatogenesis and contribute to the age-specific phenotype.

Six of the validated genes are associated with the intricately linked processes of homologous recombination, synapsis, or MSCI. Defects in any of these processes could lead to the autosomal asynapsis or abnormally high expression of sex chromosome genes that we observed. *Hfm1, Msh4, Spata22,* and *Meiob* are all required for normal crossover numbers and complete synapsis (Guiraldelli et al., 2013; Kneitz et al., 2000; Snowden et al., 2004; Salle et al., 2012; Luo et al., 2013). All of these genes were found at lower levels in P24 *Cecr2^GT/Del* testes, but significantly increased towards wildtype levels in P103-104 testes. *Tex11* regulates recombination frequency and therefore synapsis, and mutations in *Tex11* have been linked to infertility in humans (Adelman and Petrini, 2008; Yatsenko et al., 2015). *Hormad2* plays a more direct role in MSCI, as it is required for the recruitment of ATR to unsynapsed chromosomes (Kogo et al., 2012). A decrease in *Hormad2* could impair sex body formation and MSCI, elevating transcription from the sex chromosomes.

The remaining 6 RNA-seq genes we tested further all have proposed or confirmed functions in other parts of spermatogenesis. *Scml2*, more highly expressed in *Cecr2^GT/Del* testes, plays a role in regulating gene expression during spermatogenesis, including maintaining active histone modifications on sex chromosome genes required post-meiotically (Adams et al., 2018; Hasegawa et al., 2015). *Ptchd3* and *Cbs* are both predicted to be important for sperm motility (Fan et al., 2007; Wang et al., 2018), while mutations in *Glp1* lead to spermatogenic arrest (Li et al., 2007). *Taf7l* is required for the normal expression of postmeiotic genes (Zhou et al., 2013). *Ccnb3* is an early meiotic cyclin that is found at significantly higher levels in *Cecr2^GT/Del* testes. *Ccnb3* is normally downregulated at the zygotene to pachytene transition, and its continued expression leads to abnormal spermatogenesis (Refik-Rogers et al., 2006). The misregulation of any or all of these genes could contribute to the histological defects, lower sperm count, and lower sperm mobility we observe. Expression analysis of specific germ cell populations would help confirm that these expression changes are not due to a difference in the relative abundance of germ cell types in *Cecr2^GT/Del* testes.

2.4.4 Overall conclusions

Our results support a role for *Cecr2* in prepubertal spermatogenesis, possibly through an effect on chromosome synapsis. As a chromatin remodeling protein, CECR2 in spermatogonia could be directly affecting gene regulation, the effects of which aren't seen until later in meiosis when CECR2 is not present. CECR2 has also been suggested to have a role in DSB repair (Lee et al., 2012), which could affect chromosomal synapsis. However, no CECR2 is observed in spermatocytes, so a direct role for CECR2 binding to chromatin in homologous recombination is unlikely. In addition, our recent work in neurosphere primary cultures from mice does not support a role for CECR2 in DSB repair in these cells (Elliott, Norton, et al, in revision). Overall, loss of chromatin remodeling gene *Cecr2* is particularly detrimental to spermatogenesis in young males before sexual maturity and may also play a role in adult spermatogenesis.

Chapter 3 Subfertility in female mice mutant for chromatin remodeler *Cecr2*

A version of this chapter is in preparation for submission.

Authors: Norton, K.A., Weatherill, C.W., Williams, C.E., Duong, K. and McDermid, H.E.

Undergraduate student Chelsey Weatherill collected the ovary weight data mentioned in section 3.3.6 and the follicle counts shown in Figure 3.6 A. Graduate student Christine E. Williams did the X-Gal staining shown in Figure 3.2. Undergraduate student Kevin Duong assisted in the initial characterization of the histology of artificially decidualized uteri. Dr. Heather E. McDermid contributed to conceptualization of some experiments and did the uterine histology shown in Figure 3.8. Kacie A. Norton conceptualized and designed the experiments, performed all experiments not mentioned above, supervised both undergraduate students and wrote the first draft of the manuscript.

3.1 Introduction

It has been estimated that approximately 10% of women of reproductive age are infertile, and many genes have been identified that are critical for human female fertility (Yatsenko and Rajkovic, 2019). As a successful pregnancy requires both the production of a functional gamete and the ability to carry a pregnancy to term, defects in a wide variety of biological processes can result in female infertility. The use of animal models has aided in the identification of genes causing infertility in humans, including genes required for fetal ovarian development, folliculogenesis and oocyte maturation, early embryonic development, implantation, and growth of the fetus and placenta (Yatsenko and Rajkovic, 2019). While assisted reproductive technologies such as *in vitro* fertilization and embryo transfer techniques have aided many, ~50% of infertile couples are unable to have a child even with these technologies (Namiki et al., 2018). The failure of embryonic implantation remains a common problem, and is likely due to embryos being transferred to a non-receptive uterus (Wang and Dey, 2006). In fact, it has been estimated that approximately 60-75% of failed pregnancies in couples attempting to conceive naturally are due to failure around the time of implantation or shortly after (Cole, 2012; Koot et al., 2011; Wilcox et al., 1988). Implantation requires that the blastocyst becomes closely apposed to the luminal epithelium of the uterus, which is facilitated by uterine stromal edema (Wang and Dey, 2006). The blastocyst must then adhere and penetrate through the luminal epithelium with the aid of local epithelial apoptosis (Carson et al., 2000). Decidualization, the proliferation and differentiation of uterine stromal cells into large epithelioid decidual cells, is critical for both successful implantation and later placental development (Cha et al., 2014b). Decidualization in mice is triggered by implantation, and the decidua not only provides nutritional support and immunological support during early pregnancy but also forms part of the mature placenta (Woods et al., 2018).

Chromatin remodelers can have a wide variety of functions, including the regulation of transcription, DNA replication and repair, and chromosome segregation (Clapier and Cairns, 2009). For example, in oogenesis specifically, ATRX has been identified as critical for chromosome alignment and maintenance of the meiotic spindle during meiosis II (De

La Fuente et al., 2004). SNF2L/SMARCA1 is not necessary for normal fertility, but mutants have defects in follicle maturation and in their response to superovulation that are related to a role for SNF2L in gene regulation (Pépin et al., 2013). CECR2 is a chromatin remodeling protein that is thought to play a role in regulation of transcription (Fairbridge et al., 2010) as part of a large complex including SNF2L or SNF2H/SMARCA5, termed CERF (CECR2-containing remodeling factor) (Banting et al., 2005; Oppikofer et al., 2017; Thompson et al., 2012). The major abnormal phenotype observed in *Cecr2* mutants is the neural tube defect exencephaly, which is perinatally lethal (Banting et al., 2005). Most *Cecr2* mutant embryos are exencephalic, but individuals that are not appear to be healthy into adulthood. However, non-exencephalic males with mutations in *Cecr2* are severely subfertile at sexual maturity and improve with age (Norton et al., in revision (Chapter 2)). They also have corresponding defects in spermatogenesis including abnormal testis histology and decreased sperm count that improve with age. The abnormal expression levels of several genes, particularly in pre-pubertal testes, likely contributes to these phenotypes (Norton et al, in revision (Chapter 2)).

This study reveals that female mice with mutations in *Cecr2* are also subfertile and show mutation-dependent variation in phenotype. While oogenesis appears normal in mutant females, females with a severe deficiency of *Cecr2* appear to lose their embryos around the time of implantation and females with a less severe deficiency lose them several days later. Artificially induced decidualization revealed abnormal early loss of decidualized tissue in some mutant uteri, which may help explain both the loss of implantation sites and later embryonic death that we observe.

3.2 Materials and Methods

3.2.1 Mice

For all experiments involving mice, approval was obtained from the Animal Care and Use Committee of the University of Alberta (AUP 00000094). Mice were fed PicoLab Diet #5053 except after mating, when they were transferred to PicoLab Diet #5058. They were maintained at an ambient temperature of 22±2°C with a 14 hour light/10 hour dark cycle. Three different alleles of *Cecr2* were utilized in this study; the wild-type allele (*Cecr2*$^+$), a genetrap which partially disrupts *Cecr2* (*Cecr2*$^{Gt(pGT1)1Hemc}$ or *Cecr2*^{GT}), and a presumptive null deletion of the first exon (*Cecr2*$^{tm.1.1Hemc}$ or *Cecr2*^{Del}) that results in a more severe phenotype (Figure 3.1). Due to the high penetrance of exencephaly in *Cecr2*$^{Del/Del}$ embryos (96%), only *Cecr2*$^{GT/GT}$ (54% penetrance) and *Cecr2*$^{GT/Del}$ (84% penetrance) adult females were used in this study. Female *Cecr2* mutant embryos are even more likely to be exencephalic than males, leading to an even further reduced availability for study (1.39% or 13/937 live pups were *Cecr2*$^{GT/Del}$ females in an analysis from *Cecr2*$^{GT/+}$ x *Cecr2*$^{Del/+}$ crosses). A conditional knockout was not available to circumvent this at the time most of this work was completed. Genotyping was accomplished as previously described (Banting et al., 2005; Fairbridge et al., 2010).
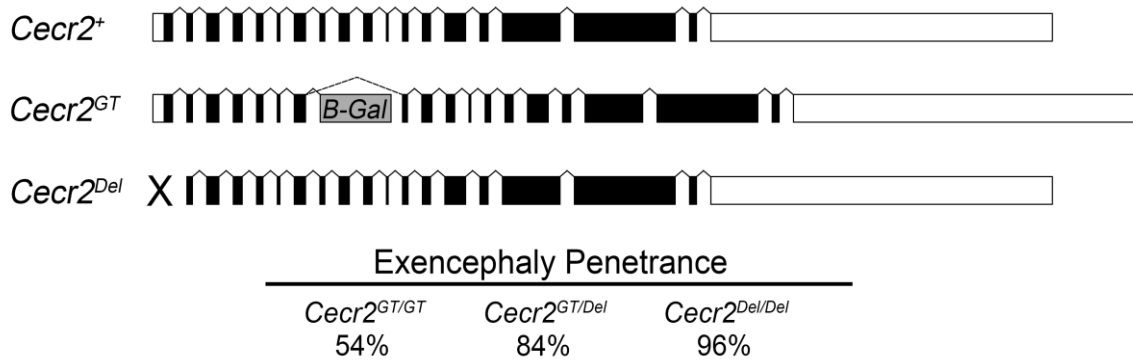
Figure 3.1: Mutations in _Cecr2_ used in this study. The wild-type _Cecr2_ allele (_Cecr2+_) has 19 exons. The _Cecr2GT_ (_Cecr2Gt(pGT1)1Hemc_) allele has an insertion of a β-Galactosidase genetrap between exons 7 and 8 and is hypomorphic, as some transcripts splice around the insertion. The _Cecr2Del_ (_Cecr2tm.1.1Hemc_) allele is a deletion of the first exon and approximately 1 kb of upstream sequence, and is a presumptive null. The differing severities of these two mutations is reflected in the percentage of embryos exhibiting the perinatal lethal neural tube defect exencephaly (Modified from Norton et al. in revision (Chapter 2)).

3.2.2 Histological Analysis

X-Gal staining was done on isolated female reproductive systems from _Cecr2GT/GT_ E18.5 embryos as previously described in Banting et al., 2005. Follicle counts were done on ovaries from adult females that were fixed for 3+ hours in 4% paraformaldehyde before being processed through ethanol/toluene gradients for embedding in paraffin wax. These samples were sectioned at 5 μm and stained using hematoxylin and eosin (H&E). The entire ovary was sectioned, and follicles were counted in every 7th section for comparison between samples. Antral follicles that were large enough to be present in more than one counted section were only counted once. Artificially decidualized uteri were fixed using neutral buffered formalin (0.4% w/v $NaH_2PO_4 \cdot H_2O$ (BDH), 0.65% w/v Na_2HPO_4 (BDH), 3.7% v/v formaldehyde (Fisher)), and histology was done as above. Sections were photographed using SeBaView software (Laxco) and a SeBaCam5C digital camera with a Zeiss Axioscope.A1 microscope.

3.2.3 Fertility Testing

$Cecr2^{GT/GT}$ and $Cecr2^{+/+}$ females were housed with $Cecr2^{+/+}$ males until visibly pregnant, then separated into individual cages to give birth. All mice were housed with higher fat PicoLab Diet #5058 during this time. The number of pups was recorded the day after birth, the pups were euthanized, and the female was placed back with a male for further mating. Each female had 3 litters except one $Cecr2^{GT/GT}$ female that only gave birth to one litter of 3 in the 3 month time period of the experiment. $Cecr2^{GT/Del}$ fertility testing was performed differently, as $Cecr2^{GT/Del}$ and $Cecr2^{+/+}$ females were housed individually with $Cecr2^{+/+}$ males and never separated to allow for better estimation of the frequency of litters. Pups were counted and euthanized the day following birth, and pups found dead were included.

Analysis of embryo numbers during development was accomplished by mating females with $Cecr2^{+/+}$ males and checking each day for the presence of a post-copulatory plug. Females were then euthanized at the desired developmental timepoint, and the number of live and resorbing embryos was recorded for each pregnancy.

3.2.4 Superovulation and oocyte analysis

Females were superovulated and oocytes were isolated as previously described (Thompson et al., 2012). The number of oocytes obtained from each female was recorded, and fertilization was scored by visualizing the maternal and paternal pronuclei using phase-contrast microscopy (Axioscop 2 mot plus microscope, Zeiss).

3.2.5 Chicago Sky Blue dye injections to visualize implantation sites

Females were injected with 100 µl of 1% Chicago Sky Blue 6B dye (Sigma) at embryonic day 5.5 (E5.5) as previously described (Dey, 2006). The number of implantation sites visible as blue bands was counted for each female. To exclude entirely failed matings, females with no implantation sites were not included in this analysis.

3.2.6 Measurement of blood in vaginal swabs

Vaginal swabs were performed on pregnant females at E9.5 and E10.5 and immediately swirled in 500 µl of water for one minute. A hemastix testing strip (Siemens) was dipped in the water sample, then the strip colour was photographed one minute later and compared to the provided chart. Based on the colour in comparison to the manufacturer provided chart, each sample was given a blood concentration score ranging from 0 (no blood detected) to 5 (high concentration of blood). The same females were tested for both developmental timepoints.

3.2.7 Oviduct cilia movement and bead transport assay

Immediately after euthanization, the infundibular region of the oviduct was opened longitudinally in PBS and laid lumen side up on a slide to examine cilia function (Shi et al., 2014). Fluorescent beads (Fluoresbrite Polychromatic Red 0.5 Micron Microspheres, Polysciences) were added to the oviducts in PBS, and samples were covered using coverslips supported with vacuum grease to avoid crushing them. Videos were obtained using a Zeiss Axioskop 2 mot plus DIC microscope with fluorescence using a Qimaging Retiga EXi camera and Q capture Plus imaging software. For each oviduct, 3-4 videos were taken of different areas of the sample, except for one sample which had 5 videos recorded. The approximate percentage of cilia that appeared to be beating in the correct orientation and speed was estimated for each video, blind to genotype. For each oviduct, the area with the most normal cilia was used for the analysis to eliminate areas with random damage caused during dissection and mounting. Fluorescent bead tracking was used to confirm that cilia were able to move beads in a directional manner, and was accomplished using a Manual Tracker plugin within Fiji image analysis software (Schindelin et al., 2012).

3.2.8 Artificial Decidualization

Vaginal swab cytology was used to determine when females were ready for mating (Byers et al., 2012) before housing them overnight with wild-type vasectomized males.

Females with post-copulatory plugs were separated and their vaginal swab cytology was re-examined 3 days later (day 3.5 of pseudopregnancy) to ensure they appeared pseudopregnant and had not resumed their estrous cycles. Between 11:00-13:00 h on the same day, females were anesthetized using isoflurane and 25 µl of sesame oil (Sigma) was injected just below the utero-tubal junction of one uterine horn (Deb et al., 2006). After surgery, females were housed on high fat PicoLab Diet #5058 for the desired number of days before euthanization by cervical dislocation for dissection.

3.2.9 Statistical Analysis

Significance was evaluated using Student's t-test. Data is represented as mean ±S.E.M. except where box and whisker plots are used to better represent the spread of the data and in Figure 3.4 D-E, where the blood rating is plotted against its frequency and therefore no mean is generated.

3.3 Results

3.3.1 Cecr2 is expressed in the female reproductive system

To see where *Cecr2* is localized within the female reproductive system, we used X-Gal staining on tissue from E18.5 embryos homozygous for the β-Gal genetrap (*Cecr2^{GT/GT}*). This staining revealed that *Cecr2* is expressed in the ovary, oviduct, and uterus (Figure 3.2). X-Gal staining and CECR2 antibody staining both had strong non-specific background in tissues from older females, preventing analysis after E18.5. However, a western blot for CECR2 has previously shown that CECR2 is found in the adult ovary (Norton et al., in revision (Chapter 2)), and X-Gal staining has shown that *Cecr2* is expressed in ovulated MII oocytes (Niri, Norton, et al., in prep). In addition, previous RNA-seq experiments have detected *Cecr2* in female primordial germ cells but not ovarian somatic cells at E13.5 and E16.5 (Guo et al., 2017) and in germinal vesicle and MII stage oocytes of adults (Sha et al., 2017; Stewart et al., 2015) (data accessed through the ReproGenomics Viewer; Darde et al., 2019, 2015).
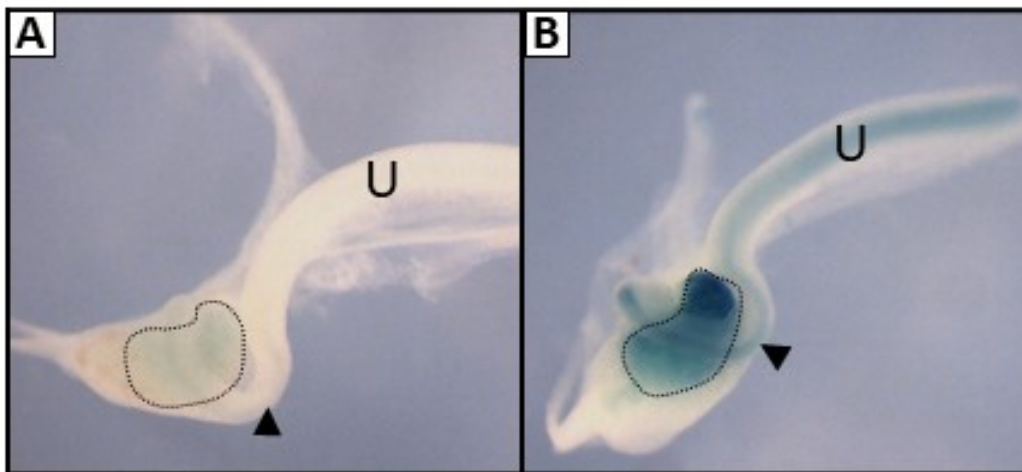
Figure 3.2: *Cecr2* is expressed in the ovary, oviduct, and uterus at E18.5. X-Gal staining of tissues from *Cecr2^{+/+}* (A) and *Cecr2^{GT/GT}* (B) E18.5 females reveals that *Cecr2* is expressed in the ovary (outlined), oviduct (arrowhead), and uterus (U). *Cecr2^{+/+}* tissues lacking the genetrap were used as a negative control and revealed low levels of endogenous staining in the ovary.

3.3.2 Cecr2$^{GT/GT}$ females have smaller litters

When mated with Cecr2$^{+/+}$ males, hypomorphic Cecr2$^{GT/GT}$ females have approximately 50% smaller litters than Cecr2$^{+/+}$ females (Figure 3.3 A; average of 7.9 pups per litter for Cecr2$^{+/+}$ females vs 3.9 for Cecr2$^{GT/GT}$ females, p=7.5E-5). The litter size of Cecr2$^{GT/GT}$ dams did not change significantly with age (average of 3.6 pups per litter before 135 days old (n=9) and 4.4 pups per litter after (n=7), p>0.05). The number of days before a post-copulatory plug was observed when a female was housed with a male in the implantation experiment below did not differ, indicating no change in mating behavior in Cecr2$^{GT/GT}$ females (average of 2.6 days for Cecr2$^{+/+}$ females vs 2.1 days for Cecr2$^{GT/GT}$ females, p>0.05).

3.3.3 Cecr2$^{GT/GT}$ embryo loss occurs after implantation

To determine the cause of subfertility in Cecr2$^{GT/GT}$ females, we checked for defects at several stages. First, we treated females with hormones to stimulate ovulation and mated them to Cecr2$^{+/+}$ males. The average number of oocytes ovulated did not differ between Cecr2$^{+/+}$ and Cecr2$^{GT/GT}$ females (Figure 3.3 B; average of 12.0 for Cecr2$^{+/+}$ females, 10.1 for Cecr2$^{GT/GT}$ females, p>0.05). The percentage of these oocytes that were fertilized *in vivo* was assessed by checking for the presence of pronuclei, and was also found not to differ (Figure 3.3 C, average of 62.5% for Cecr2$^{+/+}$ females, 65.4% for Cecr2$^{GT/GT}$ females, p>0.05). We next injected females with Chicago Sky Blue dye to visualize implantation sites at E5.5 after mating them to Cecr2$^{+/+}$ males (Figure 3.3 D-E). The number of implantation sites did not differ between Cecr2$^{+/+}$ and Cecr2$^{GT/GT}$ females (average of 8.4 for Cecr2$^{+/+}$ females, 7.3 for Cecr2$^{GT/GT}$ females, p>0.05), indicating that the decreased litter size we observed is due to embryo loss after E5.5.
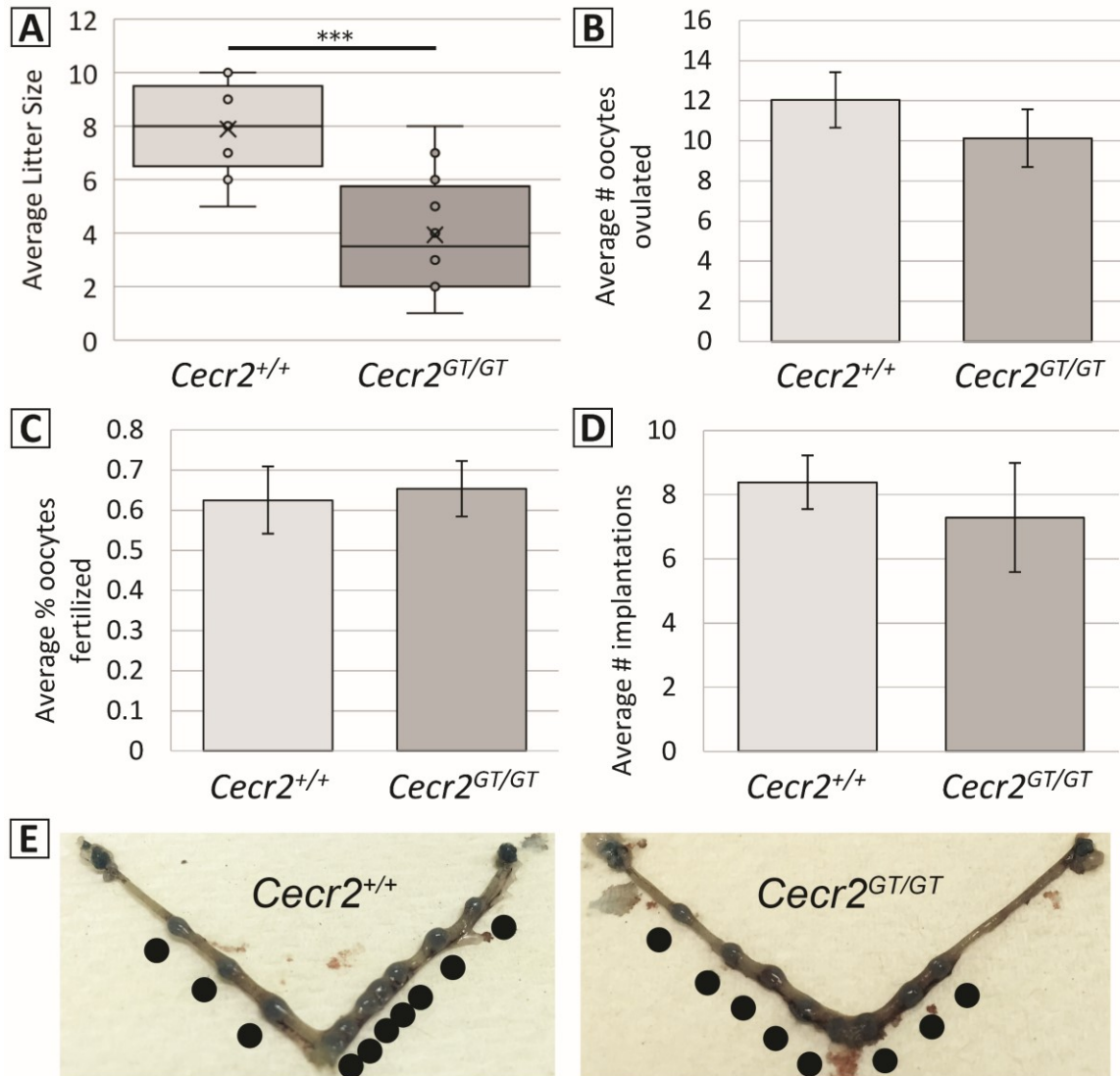
Figure 3.3: *Cecr2^{GT/GT}* females have smaller litters, but normal ovulation, fertilization, and implantation frequencies. *Cecr2^{GT/GT}* females have smaller litters than *Cecr2^{+/+}* females (A) X = mean, line = median, *Cecr2^{+/+}* n=9 litters from 3 females, *Cecr2^{GT/GT}* n=16 litters from 6 females, p=7.5E-5. No significant difference was seen in the number of oocytes ovulated after superovulation (B) n=26 *Cecr2^{+/+}* females, n=30 *Cecr2^{GT/GT}* females, p>0.05. When *Cecr2^{+/+}* or *Cecr2^{GT/GT}* females were mated to *Cecr2^{+/+}* males, no significant difference was seen in the percentage of oocytes that were fertilized *in vivo* (C) *Cecr2^{+/+}* n=178 oocytes from 15 females, *Cecr2^{GT/GT}* n=182 oocytes from 18 females, p>0.05. No significant difference was observed in the average number of implantation sites at E5.5 (D) *Cecr2^{+/+}* n=18 females, *Cecr2^{GT/GT}* n=7 females, p>0.05. Representative images of *Cecr2^{+/+}* and *Cecr2^{GT/GT}* uteri injected with dye to visualize implantation sites at E5.5 are shown (E).

3.3.4 Cecr2^{GT/GT} female embryo loss occurs around E10 and is associated with blood loss

To narrow down the developmental time at which embryo loss occurs in *Cecr2*$^{GT/GT}$ females, we checked for the presence of resorbing embryos in pregnant females late in gestation, at E15.5-18.5 (Figure 3.4 A). Approximately equal numbers of resorbing embryos were found in *Cecr2*$^{+/+}$ and *Cecr2*$^{GT/GT}$ females (average of 1.1 for *Cecr2*$^{+/+}$ females, 1.2 for *Cecr2*$^{GT/GT}$ females, p>0.05), but the number of live embryos was significantly decreased (average of 7.4 for *Cecr2*$^{+/+}$ females, 3.6 for *Cecr2*$^{GT/GT}$ females, p=0.001). This indicates that embryonic loss occurs early in gestation but after implantation.

We then did a more targeted analysis by dissecting pregnant females at E9.5 and E10.5 (Figure 3.4 B). While the number of live embryos did not significantly differ between *Cecr2*$^{+/+}$ and *Cecr2*$^{GT/GT}$ females at E9.5 (average of 7.5 for *Cecr2*$^{+/+}$ females, 5.9 for *Cecr2*$^{GT/GT}$ females, p>0.05), the number of live embryos appeared slightly lower in *Cecr2*$^{GT/GT}$ females. At E10.5, this difference had increased and *Cecr2*$^{GT/GT}$ females had significantly fewer live embryos (average of 7.9 for *Cecr2*$^{+/+}$ females, 3.3 for *Cecr2*$^{GT/GT}$ females, p=0.003). This is comparable to the total decrease in litter size observed (average of 7.9 pups per litter for *Cecr2*$^{+/+}$ females, 3.9 for *Cecr2*$^{GT/GT}$ females). The significant loss of embryos in *Cecr2*$^{GT/GT}$ females between E9.5 and E10.5 (p=0.02) was accompanied by increased blood detected in vaginal swabs using Hemastix blood test strips (Figure 3.4 C). While more blood was detected in *Cecr2*$^{GT/GT}$ female swabs than *Cecr2*$^{+/+}$ female swabs at both E9.5 (Figure 3.4 D, p=0.03) and E10.5 (Figure 3.4 E, p=7E-6), there was also a significant increase between these two developmental timepoints (p=0.04). Swabs from *Cecr2*$^{+/+}$ females never scored above a 3/5 on the scale, while *Cecr2*$^{GT/Del}$ females all scored 2 or more out of 5 at E10.5. Blood in many *Cecr2*$^{GT/Del}$ samples was also easily visible without the use of Hemastix test strips, as vaginal swabs with a high concentration were clearly discoloured with blood (Figure 3.4 C). Given that uterine bleeding has previously been associated with embryonic loss (Benson et al., 1996;

Monsivais et al., 2017), the presence of blood in vaginal swabs at E9.5 suggested that embryo loss had already begun and was complete by E10.5.
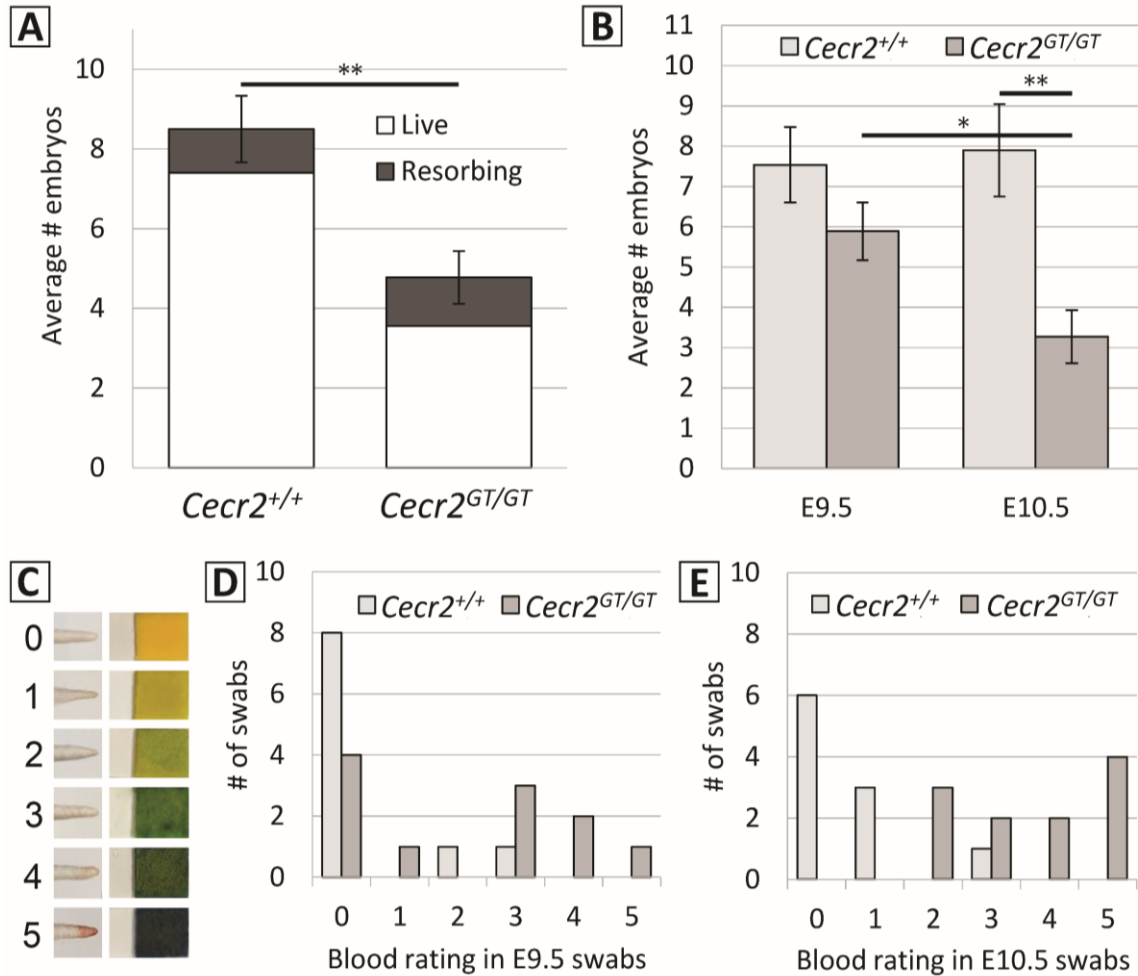
Figure 3.4: *Cecr2$^{GT/GT}$* **females have mid-gestational embryo loss accompanied by vaginal blood.** No increase was seen in the number of resorbing embryos to account for the decrease in live embryos in *Cecr2$^{GT/GT}$* females at E15.5-18.5 (A) *Cecr2$^{+/+}$* n=10 litters, *Cecr2$^{GT/GT}$* n=9 litters, p(live)=0.0015, p(resorbing)>0.05, p(total)=0.0029, error bars represent S.E.M. of total embryos. The average number of live embryos was not significantly different at E9.5 (p>0.05), but was significantly lower in *Cecr2$^{GT/GT}$* females at E10.5 (p=0.003) (B) *Cecr2$^{+/+}$* n=13 E9.5 litters, n=10 E10.5 litters; *Cecr2$^{GT/GT}$* n=9 E9.5 litters, n=11 E10.5 litters; p=0.02 when comparing *Cecr2$^{GT/GT}$* litters at E9.5 and E10.5. When Hemastix were used to detect blood in vaginal swabs based on a rating system (C) ranging from 0 (no blood detected) to 5 (high concentration of blood), E9.5 (D) *Cecr2$^{GT/GT}$* females had significantly higher levels of blood (*Cecr2$^{+/+}$* n=10 swabs, *Cecr2$^{GT/GT}$* n=11 swabs, p=0.03). The same was true at E10.5 (E) (*Cecr2$^{+/+}$* n=10 swabs, *Cecr2$^{GT/GT}$* n=11 swabs, p=7.5E-6), and even more blood was detected at E10.5 than at E9.5 in *Cecr2$^{GT/GT}$* females (p=0.04). Levels of significance: ***p<0.001, **0.001≤p< 0.01, *0.01≤p<0.05, and no asterisk indicates a lack of significance (p>0.05).

3.3.5 *Cecr2^{GT/Del} females are also subfertile*

We also fertility tested compound heterozygous *Cecr2^{GT/Del}* females that have a more severe deficiency in *Cecr2* (Figure 3.5). While the *Cecr2^{GT}* mutation still allows the production of some functional protein, the *Cecr2^{Del}* mutation produces no detectable CECR2, leading to a more severe phenotype in *Cecr2^{GT/Del}* mice than *Cecr2^{GT/GT}* mice (Norton et al, in revision (Chapter 2)). To allow for an analysis of how frequently *Cecr2^{GT/Del}* females become pregnant alongside data on litter size, these females were continuously housed with a *Cecr2^{+/+}* male for the duration of the experiment. *Cecr2^{GT/Del}* females had an average of 2.8 pups per litter in comparison to 5.9 pups per litter for *Cecr2^{+/+}* females (p=2.6E-4) and also had fewer litters, averaging one litter every 42.0 days in comparison to one litter every 23.6 days for *Cecr2^{+/+}* females (p=2.0E-3). No corresponding difference in mating behavior was observed: when females were assessed for post-copulatory plugs in a separate experiment, *Cecr2^{GT/Del}* females had mated after an average of 3.1 days compared to 2.6 days for *Cecr2^{+/+}* females (*Cecr2^{+/+}* n=18, *Cecr2^{GT/Del}* n=7, p>0.05). In addition, the age of *Cecr2^{GT/Del}* dams did not affect litter size in females tested up until 225 days of age: *Cecr2^{+/+}* females had an average of 6.2 pups per litter before the age of 135 days (n=13) and 5.6 pups per litter after (n=14), while *Cecr2^{GT/Del}* females had an average of 2.8 pups per litter both before (n=5) and after (n=11) 135 days of age (p>0.05).
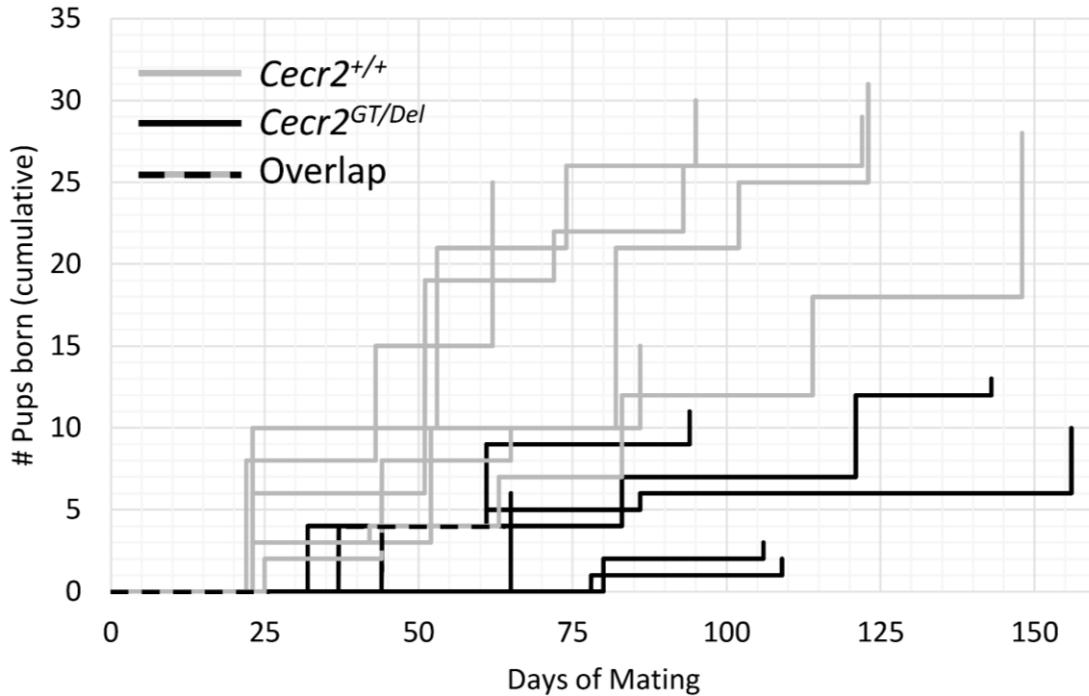
Cecr2+/+ #1		Cecr2+/+ #2		Cecr2+/+ #3		Cecr2+/+ #4		Cecr2+/+ #5		Cecr2+/+ #6	
DM	Pups	DM	Pups	DM	Pups	DM	Pups	DM	Pups	DM	Pups
23	3	23	10	25	2	22	8	23	6	23	3
42	1	53	11	44	6	43	7	51	13	52	7
63	3	74	5	65	2	62	10	72	3	82	11
83	5	95	4	86	5			93	4	102	4
114	6							122	3	123	6
148	10										

Cecr2GT/Del #1		Cecr2GT/Del #2		Cecr2GT/Del #3		Cecr2GT/Del #4		Cecr2GT/Del #5		Cecr2GT/Del #6	
DM	Pups	DM	Pups	DM	Pups	DM	Pups	DM	Pups	DM	Pups
44	4	78	1	32	4	37	4	80	2	65	6
83	3	109	1	61	5	61	1	106	1		
121	5			94	2	86	1				
143	1					156	4				

Figure 3.5: *Cecr2GT/Del* females have both smaller and fewer litters than normal. When *Cecr2GT/Del* females were housed with *Cecr2+/+* males and monitored each day for birth (A), they had fewer pups per litter than *Cecr2+/+* females, as indicated by the size of each vertical step (p=2.6E-4). They also had significantly increased time between their litters, as indicated by the size of each horizontal step (p=2.0E-3). All pups were culled after birth, and females were never separated from males to allow post-partum mating. *Cecr2+/+* n=27, *Cecr2GT/Del* n=16. The data for each litter represented in the graph is shown below (DM= Days of Mating).

94

3.3.6 Cecr2$^{GT/Del}$ females have normal follicle counts but fewer implantation sites at E5.5, indicating earlier loss than Cecr2$^{GT/GT}$ females

The ovarian histology of *Cecr2$^{GT/Del}$* females appeared grossly normal, and no difference was observed in ovary weight (average of 7.7 mg for 4 *Cecr2$^{+/+}$* ovaries, 8.5 mg for 6 *Cecr2$^{GT/Del}$* ovaries, p>0.05). We also counted primordial, primary, secondary, and antral follicles in the ovaries of *Cecr2$^{+/+}$* and *Cecr2$^{GT/Del}$* females. No significant difference in follicle numbers was observed (Figure 3.6 A), and there was no difference in the size of antral follicles (average of 197 µm for 115 *Cecr2$^{+/+}$* follicles, 208 µm for 172 *Cecr2$^{GT/Del}$* follicles). Thus, similar to *Cecr2$^{GT/GT}$* females, *Cecr2$^{GT/Del}$* females do not appear to have defects in oogenesis.

As we did above for *Cecr2$^{GT/GT}$* females, we injected pregnant females with Chicago Sky Blue dye at E5.5 to visualize implantation sites in the uterus (Figure 3.6 B-C). Unlike *Cecr2$^{GT/GT}$* females, *Cecr2$^{GT/Del}$* females had significantly fewer implantations at E5.5 than *Cecr2$^{+/+}$* females (average of 2.3 compared to 8.4 for *Cecr2$^{+/+}$* females, p=2.5E-6).
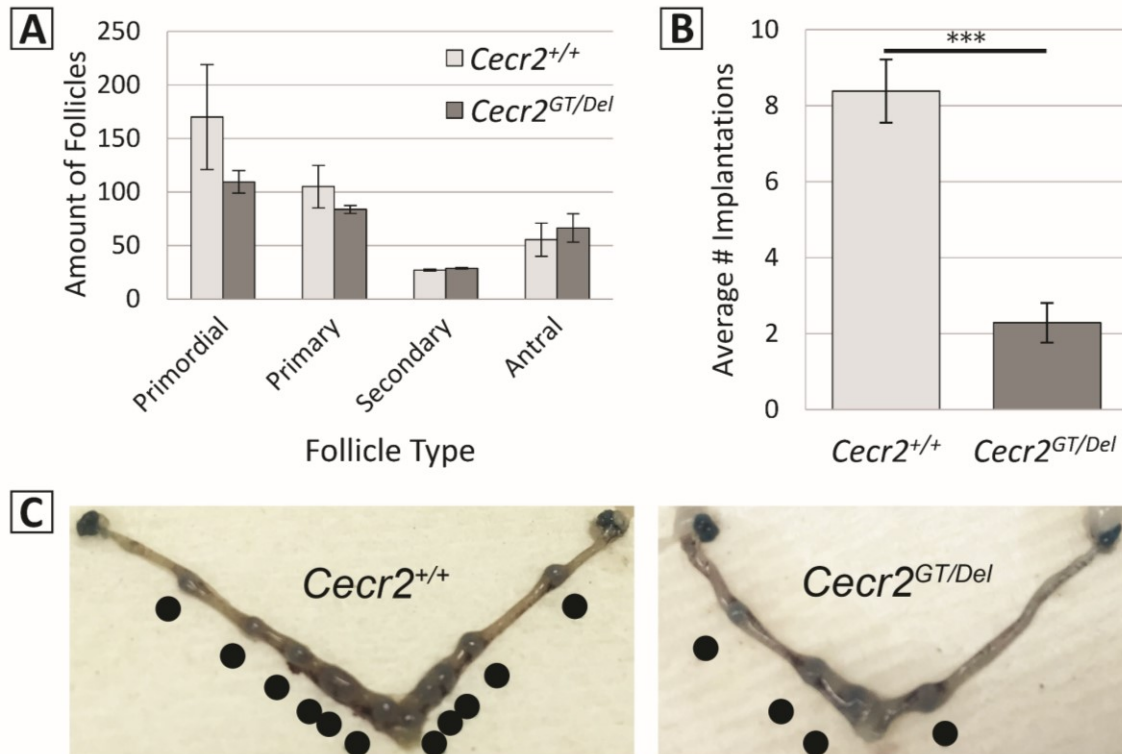
Figure 3.6: *Cecr2GT/Del* females have normal numbers of developing follicles, but have fewer implantation sites at E5.5. When the number of follicles was counted in histological sections from *Cecr2+/+* and *Cecr2GT/Del* ovaries (A), no significant differences in follicle numbers were detected (*Cecr2+/+* n=2 females, *Cecr2GT/Del* n=4 females, p>0.05 for all categories). The number of implantation sites at E5.5 (B) was significantly lower in *Cecr2GT/Del* females than in *Cecr2+/+* females (*Cecr2+/+* n=18, *Cecr2GT/Del* n=7, p=2.5E-6). Representative images of *Cecr2+/+* and *Cecr2GT/Del* uteri at E5.5 are shown (C). The results for A and B are expressed as the mean ± S.E.M. Levels of significance: ***p<0.001, no asterisk indicates a lack of significance (p>0.05).

3.3.7 Cilia function in Cecr2$^{GT/Del}$ oviducts is grossly normal

A previous analysis done on the inner ears of E18.5 embryos showed that both *Cecr2$^{GT/GT}$* and *Cecr2$^{Del/Del}$* embryos have misaligned stereocilia (Dawe et al., 2011). As fewer implantations are observed in *Cecr2$^{GT/Del}$* females at E5.5 despite normal ovarian histology, one possibility is that the coordination of ciliary movement in the oviduct is compromised (Shi et al., 2014). To assess this, the infundibular regions of *Cecr2$^{GT/Del}$* and *Cecr2$^{+/+}$* oviducts were opened longitudinally and broadly visually evaluated for frequency and orientation of cilia beating using 3 or more captured videos. With the exception of a single *Cecr2$^{GT/Del}$* outlier, all oviducts of both genotypes had at least one video where ≥80% of cilia were beating normally, and no difference was seen between genotypes (Figure 3.7 A; average of 97% normal for *Cecr2$^{+/+}$*, 87% normal for *Cecr2$^{GT/Del}$* including the outlier or 93% without it, p>0.05). A bead tracking analysis done on fluorescent beads propelled by oviduct cilia motion confirmed that both *Cecr2$^{GT/Del}$* and *Cecr2$^{+/+}$* oviduct cilia are capable of coordinated directional movement (Figure 3.7 B-C).
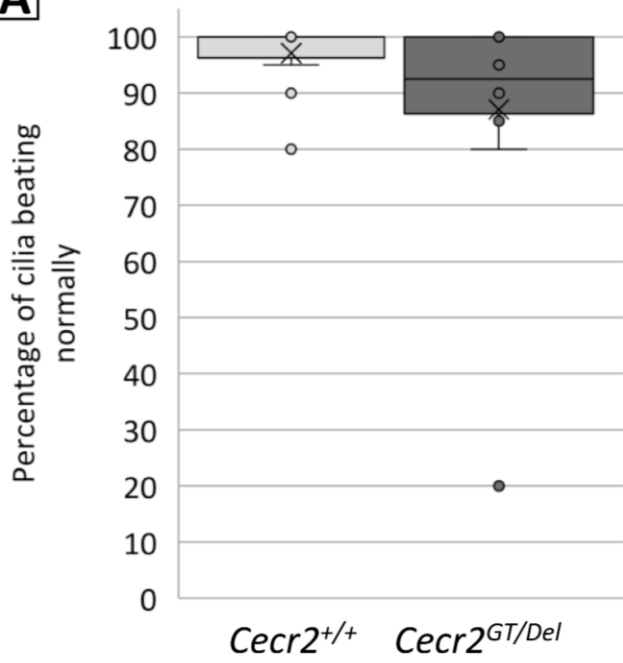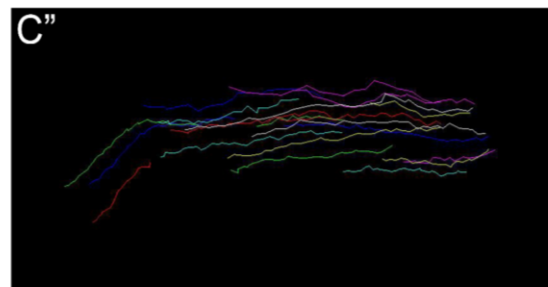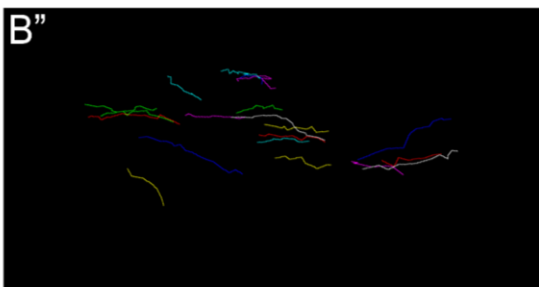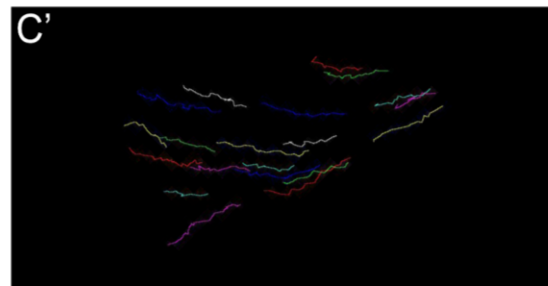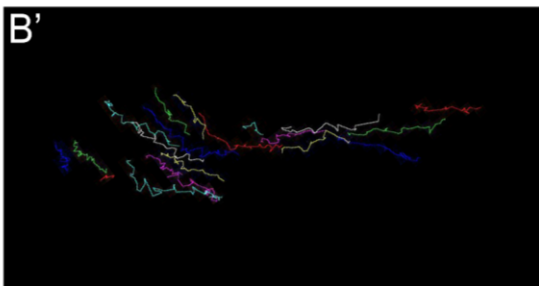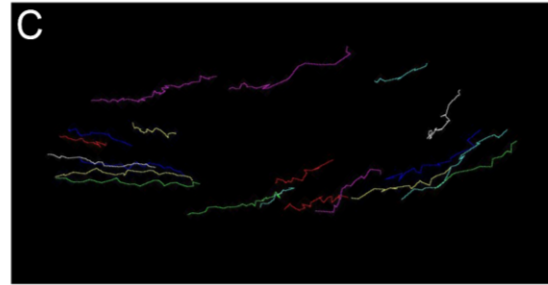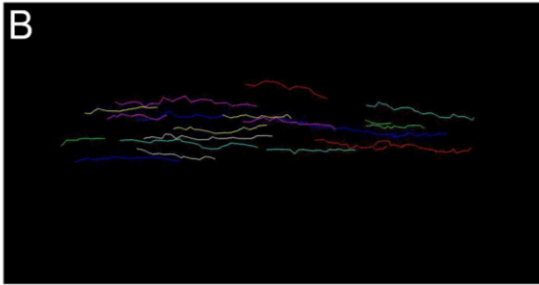
Figure 3.7: Cilia in *Cecr2^GT/Del* oviducts appear to function normally. Cilia of longitudinally opened oviducts were checked for grossly normal function. Based on the orientation and speed of their movement, the percentage of cilia beating normally was estimated (A). No difference was seen between *Cecr2^+/+* and *Cecr2^GT/Del* oviduct cilia (X= mean, line= median, n=12 females of each genotype, p>0.05). Tracking of fluorescent beads added to these oviduct samples was used to confirm the cilia could move beads in a directional manner. Three examples from *Cecr2^+/+* (B-B") and *Cecr2^GT/Del* (C-C") oviducts are shown, all oriented so that the direction of travel should be horizontal. Tracks from all samples showed a similar linear pattern, with no evidence of abnormal directional movement. The length of each track is not indicative of speed, as beads were able to move in the Z-plane and therefore were tracked for different lengths of time depending on when they were in focus.

3.3.8 Artificially stimulated decidualization initially appears normal, but decidual tissue is prematurely degraded in some Cecr2^GT/Del females

As *Cecr2^GT/Del* females have fewer implantations at E5.5 and *Cecr2^GT/GT* females lose embryos later in gestation, we hypothesized that decidualization of uterine tissue upon embryo implantation may be affected. To test this, we artificially stimulated decidualization of pseudopregnant *Cecr2^GT/Del* females by surgically injecting sesame oil 3.5 days after mating. Initially, decidualization appears normal in *Cecr2^GT/Del* females. While there is variation between samples of both genotypes, *Cecr2^GT/Del* and *Cecr2^+/+* uteri could not be distinguished ~48 hours post-surgery when photographs of sections were examined blind to the genotype (Figure 3.8 A-B). Approximately 72 hours after surgery, *Cecr2^+/+* samples had even more decidual tissue (Figure 3.8 C), whereas some *Cecr2^GT/Del* samples had already begun to shed this tissue. Of the 5 *Cecr2^GT/Del* uteri that were cut just below the junction of the two uterine horns to remove them from the female, a thick menstrual-like fluid immediately drained into the body cavity of 3 of the females (2 examples shown in Figure 3.8 D middle, right). These uteri then appeared outwardly similar to undecidualized samples, and H&E staining of sections revealed a large lumen with pronounced tissue loss. This tissue shedding did not occur in any of the 6 *Cecr2^+/+* uteri (3 examples shown in Figure 3.8).
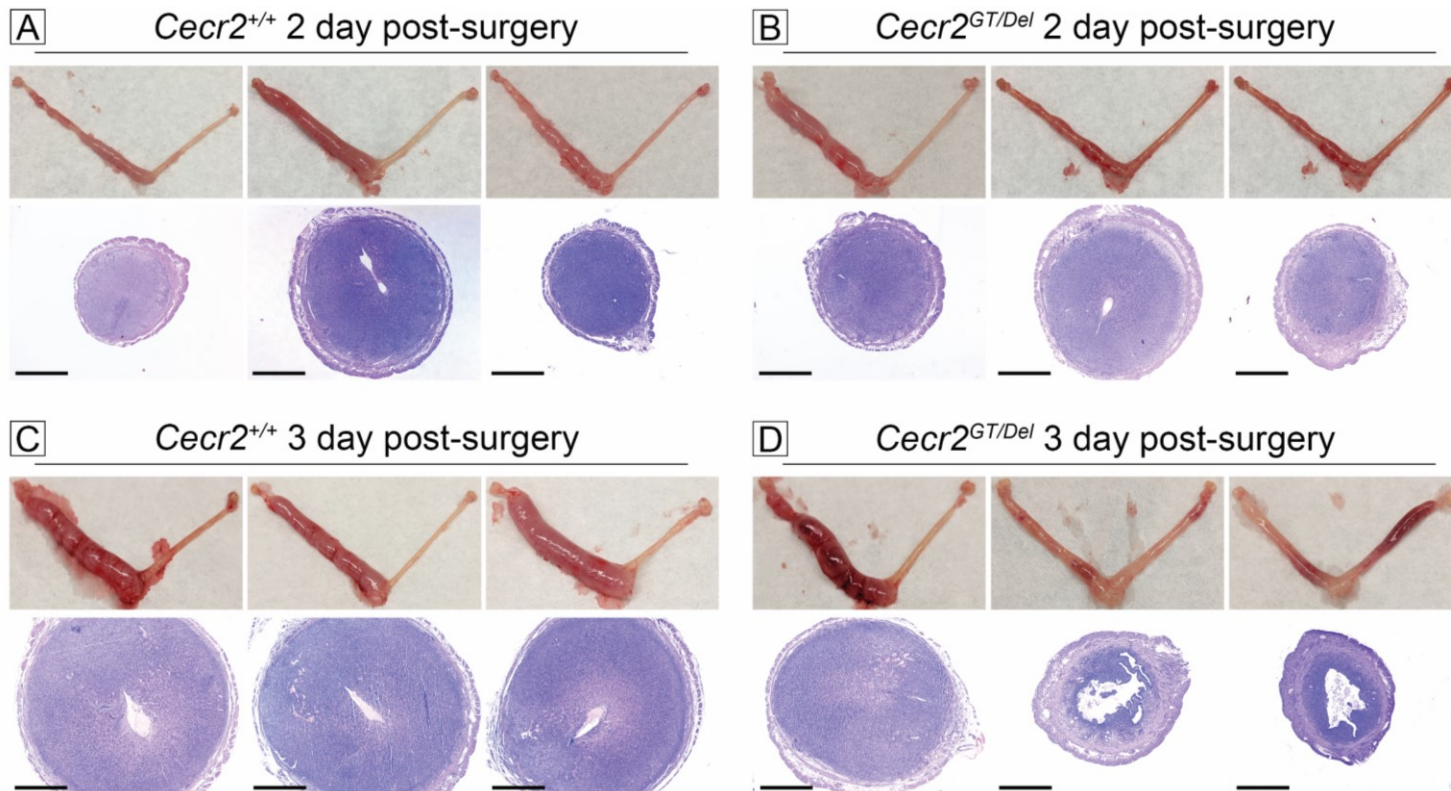
Figure 3.8: Decidualization is initially normal, but decidual tissue is prematurely lost in some *Cecr2^{GT/Del}* uteri. Decidualization was artificially stimulated in one uterine horn using a uterine injection of sesame oil in pseudopregnant females. A whole mount image of the uterus (top) is shown along with an H&E stained cross section (bottom) for each sample. The uterine horn that was injected is on the left, while the right horn was left untouched. Two days after the surgical injection, *Cecr2^{+/+}* (A) and *Cecr2^{GT/Del}* (B) showed approximately the same amount of decidualized tissue, although there was variation both between and within individual samples. Three days post-surgery, *Cecr2^{+/+}* uteri (C) consistently had greater decidual tissue than at 2 days post-surgery. Some *Cecr2^{GT/Del}* uteri appeared similar to *Cecr2^{+/+}* uteri (D, left), but others had degraded decidual tissue that was shed when the uterus was dissected from the body cavity (D, middle and right). This tissue loss was seen in 3/5 *Cecr2^{GT/Del}* uteri, but none of the 6 *Cecr2^{+/+}* uteri examined. Scale bar= 1 mm.

3.4 Discussion

3.4.1 Cecr2 mutant females are subfertile, and the severity of Cecr2 deficiency affects the phenotype

We have shown in this study that both $Cecr2^{GT/GT}$ and the more severe $Cecr2^{GT/Del}$ females are subfertile, with significantly smaller litters. The time between litters was not determined for $Cecr2^{GT/GT}$ females but was significantly increased for $Cecr2^{GT/Del}$ females, likely due to pregnancies that were entirely lost between the observed births. No defects were found in oogenesis or the fertilization of oocytes from $Cecr2^{GT/GT}$ females, and the number of implantation sites at E5.5 did not differ from $Cecr2^{+/+}$ females. However, $Cecr2^{GT/GT}$ females had significant embryo loss by E10.5, and this loss was accompanied by vaginal blood. They also had a trend towards fewer embryos at E9.5, indicating that embryo loss had probably already begun, but the difference was not large enough to be statistically significant. On the other hand, $Cecr2^{GT/Del}$ females have significantly fewer recognizable implantations at E5.5 despite no apparent defects in oogenesis or oviduct function. While it remains possible that embryonic death occurs before implantation in $Cecr2^{GT/Del}$ females, this is unlikely. Our previous work has shown that maternal Cecr2 is degraded upon fertilization and quickly replaced by zygotic Cecr2 (Niri, Norton et al., in prep). Therefore, the heterozygous embryos can quickly produce their own Cecr2 and embryonic loss is very unlikely to occur due to maternal effects in the embryo itself. In the future, reciprocal embryo transfer experiments could be used to confirm whether or not the defect is solely due to the maternal environment. In addition, we found a defect in artificially stimulated decidualization, making it more likely that the defect is due to the maternal environment at the time of implantation. The loss of decidual tissue we observed in artificially decidualized $Cecr2^{GT/Del}$ uteri 3 days after injection appears very similar to the tissue breakdown observed previously in artificially decidualized wild-type mice at a later stage (Rudolph et al., 2012). While our $Cecr2^{GT/Del}$ samples showed fluid/tissue loss upon dissection 3 days post-injection, the wild-type mice of Rudolph et al (2012) shed tissue through overt menstruation and resulted in very similar uterine

histology 6+ days after oil injection (Rudolph et al., 2012). These similarities indicate that the loss of decidual tissue we see is likely a normal response occurring prematurely in *Cecr2GT/Del* females. Although artificially decidualized tissue is not directly comparable to decidualized tissue at the site of embryo implantation, this defect may indicate abnormalities in decidualization that would also affect the quality of implantation.

3.4.2 Both Cecr2GT/GT and Cecr2GT/Del phenotypes may arise around the time of implantation due to defective decidualization

As *Cecr2* is expressed in the ovary, oviduct, and uterus during embryonic development, it is possible that the subfertility phenotype could arise from any of these tissues. However, the normal folliculogenesis and mid-gestational loss we observe combined with the defect in sustaining the decidualization reaction in *Cecr2GT/Del* females suggests that the uterus is likely the primary source of the defect. Other mouse mutants with defects in decidualization such as *Hoxa10* mutants (Lim et al., 1999) and uterine specific ablation of *Bmp2* (Lee et al., 2007b) give the phenotype of implantation failure, as decidualization is necessary for successful implantation. In cases where implantation does occur, the quality of implantation is also critical for the ongoing pregnancy (Cha and Dey, 2015). In fact, it has been suggested that many mutations causing embryonic lethality in early and mid-gestation are actually due to defects around the time of implantation (Cha et al., 2012; Wang and Dey, 2006). This is the case for mice with a deletion of *Bmp7* in the female reproductive tract, which have a ~50% reduction in pups per litter and have litters ~50% as frequently (Monsivais et al., 2017), similar to *Cecr2GT/Del* females. Although these *Bmp7* mutant dams have a normal number of implantation sites at E5.5, they have defects in decidualization leading to placental abnormalities, hemorrhagic sites, and ultimately embryonic loss around E8.5-E10.5 (Monsivais et al., 2017). A similar phenotype is observed in both a uterine knockout of *Wnt5a* (Cha et al., 2014a) and *Rbpj* (Zhang et al., 2014). Both have abnormalities around the time of implantation that do not prevent implantation but rather lead to significant (but not complete) loss later in gestation. Therefore, although we cannot rule out that *Cecr2* also plays a separate role in

maintaining pregnancy later in gestation, the mid-gestation embryonic loss we observe in *Cecr2^{GT/GT}* dams could be due to defects around the time of implantation and decidualization, and be a delayed effect of the same defect seen in *Cecr2^{GT/Del}* dams.

3.4.3 Female and male Cecr2 mutant subfertility appears to have different mechanistic origins

While male *Cecr2^{GT/Del}* mice have clear defects in spermatogenesis (Norton et al., in revision (Chapter 2)), we did not detect any abnormalities in *Cecr2* mutant oogenesis. In addition, male *Cecr2^{GT/Del}* mice appear to have chromosomal asynapsis during meiosis, but *Cecr2* mutant females do not have the phenotypes typically associated with chromosomal asynapsis. In such females, fertility often initially appears normal, but rapid depletion of oocytes due to associated defects in gene silencing or chromosomal pairing leads to premature ovarian insufficiency (Burgoyne et al., 2009). While *Cecr2* mutant females do not show the lower follicle numbers or tapering fertility that often accompanies asynapsis, they also do not show improvement with age as was seen in *Cecr2* mutant males. Therefore, whatever mechanism is responsible for partial recovery in males is not shared in mutant females.

3.4.4 Overall Conclusions

Together, our data suggests that loss of *Cecr2* affects decidualization and the establishment of a successful pregnancy. We hypothesize that in *Cecr2^{GT/Del}* females, which have a more severe deficiency in *Cecr2*, this defect affects implantation. In *Cecr2^{GT/GT}* females with a less severe deficiency, embryos are able to bypass the defect and implant, but perish later in gestation due to suboptimal conditions from a poorly established pregnancy. As *Cecr2* is a chromatin remodeler, these defects may result from the misregulated transcription of genes necessary for decidualization and implantation. It is also possible that *Cecr2*'s role in these phenotypes is less direct; although the phenotypes appear to be uterine in origin, they could result from a defect in another tissue. For example, premature breakdown of decidual tissue could be due to a

premature decrease in progesterone (Rudolph et al., 2012). Although no hormonal defects were observed in *Cecr2* mutant males (Norton et al., in revision (Chapter 2)), this possibility is worthy of further investigation. Overall, it is clear that chromatin remodeling gene *Cecr2* has a novel function in female reproduction and the severity of the mutant phenotype is dosage dependent.

Chapter 4 Discussion

4.1 *Cecr2* appears to have different functions in male and female reproduction

Many genes have been identified that affect the fertility of both sexes when mutated. Frequently, these genes play a role in processes with obvious parallels between the sexes such as the establishment and migration of primordial germ cells, meiosis, or the endocrine system (Matzuk and Lamb, 2002). However, there are some examples of genes that result in fertility defects in both sexes due to seemingly disparate biological defects. For example, males mutant for *Hoxa10* are infertile due to cryptorchidism, while females are subfertile due to defects in decidualization affecting implantation as described above (Lim et al., 1999; Satokata et al., 1995). Similarly, spermatogenesis in males lacking *Bsg* arrests at metaphase of meiosis I, while females are infertile due to defects in both fertilization and implantation (Igakura et al., 1998; Kuno et al., 1998).

Interestingly, mutations in *Cecr2* also appear to result in very different phenotypes in males and females, despite having an outwardly similar moderate reduction in the number of pups per litter. A potential defect in the endometrium affecting implantation and decidualization is unlikely to correspond to a similar defect in males at the molecular level. However, one might expect that the asynapsis of chromosomes during meiosis we observed in mutant males could also play a role in mutant female subfertility.

It has been observed that mutations in meiotic genes often have a greater impact on fertility in males than in females (Burgoyne et al., 2009; Hunt and Hassold, 2002). Several reasons for this have been suggested. First, there is evidence that the prophase I checkpoint is weaker in females than in males, allowing oocytes to "escape" where spermatocytes would undergo apoptosis (Hunt and Hassold, 2002; Turner, 2015). This has been demonstrated to be true for the spindle assembly checkpoint (LeMaire-Adkins et al., 1997), and recent evidence has suggested that the response to asynapsis during prophase I is also sexually dimorphic due to differences in MSUC (meiotic silencing of unsynapsed chromatin) (Cloutier et al., 2016). While the function of MSUC is unknown, it may act as a prophase I checkpoint by silencing essential genes on unsynapsed chromosomes and

leading to transcriptional starvation (Burgoyne et al., 2009). Meiotic silencing is less efficient in females than in males, resulting in higher transcription from asynapsed chromosomes in females (Cloutier et al., 2016). The efficiency of transcriptional silencing of asynapsed chromosomes during oogenesis appears to vary stochastically, creating different gene expression patterns between oocytes (Cloutier et al., 2016). Epigenetically, the heterochromatin marker H3K9me3 is associated with unsynapsed chromosomes in spermatocytes but not in the oocytes of XY sex-reversed female mice or XO oocytes (Cloutier et al., 2016; Taketo and Naumova, 2013). H3K27me3, which is also associated with facultative heterochromatin, localizes to the unsynapsed X chromosome in XY oocytes (Taketo and Naumova, 2013), yet is excluded from the sex body in spermatocytes (van der Heijden 2007). Differences such as these likely contribute to the less efficient transcriptional silencing observed in oocytes. Under the model that transcriptional silencing serves to eliminate cells with asynapsed chromosomes through transcriptional starvation, this "checkpoint" would be much more sensitive in males with efficient silencing.

It may also be that males are inherently more sensitive to asynapsis because moderate to high levels of asynapsis are thought to disrupt MSCI (Ellnati et al., 2017; Homolka et al., 2012, 2007; Mahadevaiah et al., 2008; Turner, 2015; Xiong et al., 2017). While MSCI does not occur in females under normal circumstances, it is essential in males to prevent the expression of toxic sex-linked genes including *Zfy2* on the Y chromosome (Royo et al., 2010). Some evidence for this comes from Haldane's rule: when one sex is observed to be sterile in hybrid species, it is almost always the heterogametic sex (Haldane, 1922). In addition, mutations that affect males more than females are frequently related to sex body formation (Kolas et al., 2005), and disruption of the silencing components themselves results in spermatocyte, but not oocyte, arrest (several examples reviewed in Turner, 2015). Therefore, if disruption of MSCI is the major cause of spermatocyte death in *Cecr2* mutant males, it is possible that similar asynapsis occurs in *Cecr2* mutant females without obvious repercussions.

Together, these sex differences in the consequences of asynapsis make it possible that the asynapsis phenotype observed in *Cecr2* mutant males is also present in *Cecr2* mutant females. However, a synapsis defect would not satisfactorily explain the phenotypes we observe in *Cecr2* mutant females. Moderate asynapsis during female meiosis could lead to the silencing of critical genes and meiotic arrest, but this would not result in the sustained subfertility with normal ovarian histology we observe. Due to oocyte selection during folliculogenesis, the loss of oocytes frequently results in approximately normal fertility but a shortened reproductive lifespan (Burgoyne et al., 2009). However, significant depletion of oocytes can usually be seen in ovarian histology just after birth (Burgoyne et al., 1985; Setterfield et al., 1988). In more severe cases, females are sterile with a severe depletion of follicles (Guiraldelli et al., 2013).

Despite these inconsistencies, it is theoretically possible that asynapsis could contribute to the embryonic loss we see in *Cecr2*$^{GT/GT}$ females. Synapsis is critical for the correct segregation of chromosomes during meiosis, therefore asynapsis can result in a higher risk of aneuploidy and embryonic death (Burgoyne et al., 2009; Yuan et al., 2002). However, this alone would not provide a satisfactory explanation for the much earlier loss of embryos seen in *Cecr2*$^{GT/Del}$ females and would not account for the premature loss of decidualized tissue observed in some *Cecr2*$^{GT/Del}$ females.

Nonetheless, it would be interesting to know whether *Cecr2*'s possible role in synapsis is truly sex specific. To test if asynapsis is occurring in *Cecr2* mutant females, chromosome spreads of oocyte nuclei from E17.5 ovaries could be fluorescently immunolabelled similarly to spermatocyte chromosome spreads (Bannister et al., 2007; Reinholdt et al., 2004). This would allow for the observation of oocytes at pachytene stage. If asynapsis was observed, this could be further investigated using markers for DSBs and recombination, as described below for spermatocytes. To assess chromosomal abnormalities, oocytes or 1-cell zygotes could be karyotyped (Yuan et al., 2002). These tests would reveal whether the role of *Cecr2* in synapsis is another way that synapsis is sexually dimorphic between males and females, or whether asynapsis occurs in both sexes with sexually dimorphic consequences.

4.2 Further investigation of *Cecr2* mutant male subfertility

This study has shown that *Cecr2^{GT/Del}* males are most severely subfertile just after sexual maturity but improve dramatically with age. The phenotypes that accompany this subfertility, including defects in spermatogenesis and expression level changes in several genes, also improved with age. Similar recovery in litter size with age has been observed previously for mouse mutants with hormonal defects (Acampora et al., 1998) and for genes that are specifically required during the first wave of spermatogenesis (Busada et al., 2016; Geyer, 2017; Laronda and Jameson, 2011). As *Cecr2* defects do not appear to be hormonal in nature, later recovery could indicate that *Cecr2* plays a more important role during initial testis development and/or the onset of spermatogenesis than in maintenance. However, as *Cecr2* continues to be expressed in spermatogonia in adults, it remains unclear whether it also plays a role in adult spermatogenesis. Spermatogenesis does not fully recover in older *Cecr2^{GT/Del}* males, but this could be due to the lasting effects of an abnormal first wave of spermatogenesis rather than an ongoing function of *Cecr2* in adult testis.

In this work the sub-type of spermatogonial cells expressing *Cecr2* was not identified. The use of markers in neonatal testes (P3-P4) for undifferentiated spermatogonia destined to become spermatogonial stem cells (GFRA1-positive) and differentiating spermatogonia (STRA8- and KIT-positive) (Busada and Geyer, 2015; Niedenberger et al., 2015) together with CECR2 antibody staining would help clarify which of these cell populations CECR2 is present in. These same markers can be used to label undifferentiated and differentiating type A spermatogonia in adult testes (Busada and Geyer, 2015; Niedenberger et al., 2015). If a change in CECR2 localization is observed (for example, localization to both undifferentiated and immediately differentiating spermatogonia neonatally but only undifferentiated spermatogonia in adults), it could shed light on a difference in the role of CECR2 between the first wave of spermatogenesis and steady-state adult spermatogenesis. In addition, the decreased number of seminiferous cords observed in E18.5 *Cecr2^{Del/Del}* testes suggest that *Cecr2* may be

important in the developing testis before spermatogenesis begins. This could be further investigated by creating a conditional knockout of *Cecr2* in primordial germ cells and then observing resulting adults, as discussed further below.

To differentiate between these early roles for *Cecr2* and a role for *Cecr2* in steady-state spermatogenesis, Ngn3/Cre mice (Yoshida et al., 2004) could be crossed to the recently created *Cecr2^{tm2a(EUCOMM)Hmgu}* mouse line, which has loxP sites flanking exon 4. *Ngn3* is not expressed in cells undergoing the very first wave of spermatogenesis, but is expressed starting at P3 in the undifferentiated spermatogonia that will then self-renew and establish ongoing adult spermatogenesis (Yoshida et al., 2006). Similarly, tamoxifen-inducible Ngn3/CreER^{TM} mice (Yoshida et al., 2006) could be used to knock out *Cecr2* expression in spermatogonia later in development, such as at sexual maturity after the first wave of spermatogenesis is complete.

If *Cecr2* does play an ongoing role in adults, it is possible that it performs the same function during the first wave as during adult spermatogenesis and this function is simply less important in adults. However, it is also possible that the function of CECR2 shifts with age, which could be related to a change in CERF complex composition. The CERF complex in testis is quite large (~2 MDa) (Niri, 2016), but its complete composition remains unknown. As *Cecr2* may play a role in gene regulation, it could be that (1) *Cecr2* is no longer required (or is less important) to regulate the expression of those genes in adulthood (2) those genes themselves play a different role in prepubertal spermatogenesis than adult spermatogenesis, or (3) a different subset of genes is misregulated in adults. Supporting (1), many of the genes that we chose to test at both P24 and P103-104 were expressed at closer to *Cecr2^{+/+}* levels in older testes.

It is also possible that the recovery we observe is due to compensation by another gene or pathway. The closest relatives of *Cecr2* are the BET subclass of bromodomain-containing proteins, *Brd2, Brd3, Brd4,* and *Brdt* (Zerbino et al., 2018). While *Brdt* is essential for spermatogenesis, it is expressed in mid-late spermatocytes and round spermatids, and functions in transcription and alternative splicing (Shang et al., 2007;

110

Berkovits et al., 2012). *Brd2* and *Brd4,* which are both expressed in spermatogonia, have been shown to regulate the expression of cell cycle genes in culture. However, as mutations in both are embryonic lethal, their role in spermatogenesis remains unknown (Berkovits et al., 2012).

As *Cecr2^Del/Del^* embryos almost all die perinatally from exencephaly, we were unable to assess the effect of a complete loss of CECR2 on reproduction. We did attempt grafting *Cecr2^Del/Del^* embryonic testes into *Cecr2^+/+^* host males as a method to study the histology of *Cecr2^Del/Del^* testes postnatally, but the results were uninterpretable. While *Cecr2^Del/Del^* and control *Cecr2^+/+^* embryonic testes did grow when transplanted both subcutaneously on the backs of hosts and within adult testes, the histology of controls was abnormal. While it is not unusual for only a portion of seminiferous tubules to appear normal in these experiments (Honaramooz et al., 2002; Takashima et al., 2015; Tang et al., 2012), the number of normal tubules in *Cecr2^+/+^* grafts was so low that the phenotype of *Cecr2^Del/Del^* testes could not be determined. The only clear change between these previous experiments and ours is that they used donor grafts from newborn mice, while we isolated them from E18.5 testes. In the future, the exencephaly phenotype could be circumvented by using tamoxifen inducible Oct4-MerCreMer mice, which express Cre recombinase in primordial germ cells when tamoxifen is injected at E9.5 (Greder et al., 2012), in combination with the floxed *Cecr2^tm2a(EUCOMM)Hmgu^* allele. Recent work in the McDermid lab has shown that the genetrap allele resulting from Cre-mediated excision of the floxed *Cecr2^tm2a(EUCOMM)Hmgu^* allele, *Cecr2^tm2b(EUCOMM)Hmgu^*, appears to be of equal severity to the *Cecr2^Del^* allele (Dicipulo, Norton et al., in prep). Therefore, this method would probably be an effective way to study a severe loss of CECR2 in germ cells.

The formation of DSBs and subsequent homologous strand invasion is critical for synapsis (Baudat et al., 2013; Turner, 2015). Therefore, it is possible that incomplete synapsis observed in *Cecr2^GT/Del^* spermatocytes is due to a DSB-related defect. As CECR2 is not detected in spermatocytes, it is highly unlikely that it would play a direct role in the induction or repair of DSBs. However, it remains possible that CECR2 could affect these processes through chromatin modifications made in spermatogonia or transcriptional

111

changes of a critical gene. An effective initial test of this hypothesis would be to stain spermatocytes for RAD51 foci. RAD51 marks sites of ongoing recombination (Ashley et al., 1995; Moens et al., 1997), and therefore can be used to determine if both the formation and resolution of these sites is normal (Guiraldelli et al., 2013). In normal cells, ~150 RAD51 foci are present at late zygotene, decreasing to ~30 by pachytene stage as DSB repair is completed (Guiraldelli et al., 2013). Therefore, a decrease in the number of foci at late zygotene could indicate that fewer DSBs are induced or strand invasion is not occurring (Romanienko and Camerini-Otero, 2000), while an elevated number at pachytene would suggest delayed or inefficient DSB repair (Guiraldelli et al., 2013). If a defect was identified, it could be further investigated using other markers such as MLH1, which marks crossovers and should have at least 1 focus per pair of homologous chromosomes (Baudat et al., 2013; Guiraldelli et al., 2013).

As the RNA-seq analysis in this study was done on whole testes, the gene expression changes we observed could be skewed by the wide array of cell types present in the samples. This may have caused a higher rate of false negatives due to differentially expressed transcripts being averaged out, particularly if they are differentially expressed in one cell type but not others. It could also lead to false positives, especially for genes expressed in cell types such as spermatids that would be found in decreased numbers in mutant testes. For this reason, and because *Cecr2* is expressed in spermatogonia, genes expressed in cell types early in spermatogenesis were preferentially chosen for further study. Many genes that are critical for meiosis are transcribed in spermatogonia and their translation is delayed (Busada and Geyer, 2015), providing one mechanism by which a lack of spermatogonial CECR2 could result in phenotypes in meiotic cell types. As only one timepoint could be analyzed using RNA-seq in this study, P24 (the earliest timepoint when histological defects were observed) was chosen to ensure that we did not assay before the lack of *Cecr2* had an effect on the testes. However, it is possible that an RNA-seq analysis of whole testes just prior to this could also reveal important changes in gene expression in mutant testes and avoid artifacts due to the mutant phenotype. This could also be avoided by doing RNA-seq on purified cell populations using fluorescence-

activated cell sorting (FACS) (Homolka et al., 2007) or STA-PUT velocity sedimentation (Han et al., 2001; Xiong et al., 2017). Likewise, these methods could be used in combination with qPCR to confirm the changes in gene expression identified in this study.

The exclusive increase in abundance of many sex-linked genes in *Cecr2* mutant testes could be due to a defect in MSCI. However, a decreased number of post-meiotic cells in mutant testes at P24 may have also skewed the results, as a decreased proportion of cells that have undergone MSCI could also lead to an apparent increase in the expression of sex-linked genes. The asynapsis that was observed during meiosis in the spermatocytes of young males suggests that the abnormally high abundance of sex chromosome transcripts may not be simply an artifact due to cell type. However, the presence of pachytene-like spermatocytes with asynapsed chromosomes could also be due to an increased arrest of mutant spermatocytes at late zygotene/early pachytene stage. As complete synapsis is a defining feature of pachytene stage, the presence of asynapsed chromosomes makes stage identification challenging. However, several other studies have observed pachytene-like spermatocytes with asynapsis that appear highly similar to *Cecr2*^{GT/Del} spermatocytes (Crichton et al., 2018; Mahadevaiah et al., 2008; Roig et al., 2010). Definitive identification of pachytene spermatocyte spreads to clarify this could be accomplished using an antibody against H1t, a marker that is not present in zygotene or early pachytene stage but appears at mid-pachytene stage (Pacheco et al., 2015). Confirmation that *Cecr2* mutant spermatocytes with asynapsis are in pachytene stage would support likely disruption of MSCI. MSCI failure could be further confirmed by checking for the absence of MSCI markers that normally strongly localize to the sex body during mid-late pachytene such as antibodies against SUMO-1 and XMR (Manterola et al., 2009; Page et al., 2012). The exclusion of RNA polymerase II from the sex body can also be measured using antibody staining of pachytene spermatocyte spreads (Page et al., 2012). In addition, the abnormal expression of specific sex chromosome genes known to be subject to MSCI such as *Scml2* can be visualized using RNA-FISH on pachytene spermatocyte spreads (Royo et al., 2013), or qPCR of purified pachytene spermatocytes (Xiong et al., 2017). A previous study of *Raptor* conditional knockout males, which have

impaired MSCI, identified global upregulation of expression from the sex chromosomes in an RNA-seq of whole testes at P18 (Xiong et al., 2017). Follow-up expression analysis of isolated pachytene spermatocytes showed the same results, but with more dramatic increased expression in mutant spermatocytes (Xiong et al., 2017).

As only a subset of genes were chosen for qPCR validation, there are also many more genes identified by RNA-seq that could be relevant to the *Cecr2* mutant phenotype. A full list of these genes is provided in Appendix B (Table B.4). Of particular interest are *Oct4* (*Pou5f1*), an autosomal gene expressed at approximately half of normal levels in *Cecr2*$^{GT/Del}$ testes, and *Fancb*, expressed at approximately twice the normal level in *Cecr2*$^{GT/Del}$ testes and located on the X chromosome. *Oct4* is a transcription factor expressed in primordial germ cells during embryogenesis, gonocytes in newborns and type A spermatogonia in adults (Pesce et al., 1998; Yeom et al., 1996). It is critical for both the survival of primordial germ cells (Kehler et al., 2004) and for the self-renewal of spermatogonia, and its downregulation is likely a trigger for spermatogonial differentiation (Dann et al., 2008). As CECR2 is also localized to gonocytes and spermatogonia, *Oct4* is an attractive candidate to potentially be a direct target of CECR2 chromatin remodeling. Downregulation of *Oct4* in the absence of CECR2 could plausibly contribute to the embryonic testis phenotypes seen in *Cecr2*$^{Del/Del}$ males and the disruption of prepubertal to adult *Cecr2*$^{GT/Del}$ spermatogenesis. Similarly, *Fancb* is involved in the maintenance of primordial germ cells and spermatogonia during embryogenesis and in adults, and also regulates H3K9 methylation of the sex chromosomes during meiosis but doesn't result in obvious MSCI defects (Kato et al., 2015). Since it is located on the X chromosome, it would be particularly useful to determine whether *Fancb* is also more highly expressed in pre-meiotic cells or its upregulation is simply due to failure of MSCI during meiosis. Overall, further investigation of differentially expressed genes in *Cecr2* mutant testes may reveal additional roles for *Cecr2* during spermatogenesis.

4.3 Further investigation of *Cecr2* mutant female subfertility

The results of this study show that the timing of embryo loss differs between *Cecr2*$^{GT/GT}$ and *Cecr2*$^{GT/Del}$ females. The number and appearance of implantation sites in *Cecr2*$^{GT/GT}$ females at E5.5 is grossly normal, but they lose a significant number of embryos around E9.5-10.5. In contrast, *Cecr2*$^{GT/Del}$ females have fewer implantation sites despite normal ovarian histology. They also showed a premature loss of decidualized tissue following artificially induced decidualization. Although *Cecr2*$^{GT/GT}$ and *Cecr2*$^{GT/Del}$ phenotypes seem distinct, they both may be related to a problem in decidualization, as discussed in section 3.4.2.

A number of experiments could be done to further investigate these phenotypes. While the decreased number of implantation sites in *Cecr2*$^{GT/Del}$ females is likely due to a failure of implantation, it is also possible that the embryos die in the preceding days. The presence of fully expanded blastocysts with no evidence of cellular death just before implantation could be confirmed by flushing the uterine lumen at E3.5. At E4.5, the attachment of embryos to the uterine epithelium could be assayed histologically (Lee et al., 2007b). This would help clarify the exact timing of the defect and whether decidualization is the most likely cause. The premature breakdown of decidualized endometrial tissue observed in artificially decidualized *Cecr2*$^{GT/Del}$ females could be due to a defect in the process of decidualization itself or a failure of the corpus lutea to produce sufficient progesterone (Rudolph et al., 2012). Serum progesterone levels could be measured using ELISA to see if progesterone levels fall more quickly after artificial decidualization in *Cecr2* mutant females than in *Cecr2*$^{+/+}$ females.

In *Cecr2*$^{GT/GT}$ dams, where embryos are lost much later, histology could be used to check for abnormalities in implantation or placentation. Immunostaining for markers specific to the embryo and different placental layers would be useful to aid in detecting abnormalities (Monsivais et al., 2017). It would be expected that if embryo death is occurring in some embryos due to placental defects by E10.5, the surviving pups could

also be adversely affected. Therefore, the incidence of preterm birth and birth weights of pups from *Cecr2* mutant and *Cecr2*$^{+/+}$ dams could be measured.

It has also been previously observed that a suboptimal maternal environment combined with mutant embryos can have a compounding negative effect: *Adm*$^{+/-}$ dams have defects in implantation, placentation, and fetal growth that contribute to defects later in embryogenesis in *Adm*$^{+/-}$ and *Adm*$^{-/-}$ embryos, including failure of neural tube closure and cardiovascular malformations (Li et al., 2008, 2006). This brings up the intriguing possibility that the phenotypes of *Cecr2* mutant embryos may be exacerbated by the maternal environment of their heterozygous mothers. There is evidence that CECR2 is dosage sensitive under some conditions: Heterozygous *Cecr2*$^{GT/+}$ embryos have a low (~3.5-4%) penetrance of exencephaly on mixed genetic backgrounds (Banting et al., 2005) and embryos heterozygous for the *Cecr2*$^{tm2b(EUCOMM)Hmgu}$ allele on a C57Bl/6 background exhibit coloboma and polydactyly at a lower rate than embryos homozygous for the same allele (Dicipulo, Norton et al., in prep). The impact of the maternal environment on embryonic *Cecr2* phenotypes could be tested using reciprocal embryo transfer experiments.

Although my results suggest that the defect lies in the uterus, it remains possible that the defect arises in the ovary, or in the case of a hormonal disruption, the pituitary. *Cecr2* is known to be expressed in the ovary, uterus, and brain during embryonic development, so these are all possibilities. To begin to narrow down these possibilities, it would be helpful to determine clearly whether the embryo itself or the maternal environment is causing embryonic loss. Although defective embryonic development due to a maternal effect is unlikely due to the quick degradation of maternal *Cecr2* and replacement with zygotic *Cecr2* upon fertilization (Niri, Norton et al, in prep), it is still possible that *Cecr2*'s activity during oogenesis could have an effect on embryogenesis. Reciprocal embryo transfer experiments between *Cecr2* mutant and *Cecr2*$^{+/+}$ dams would definitively reveal whether embryo death is due to the maternal environment. The use of Cre lines to create conditional knockouts as described in section 4.2 could also be helpful in determining which tissues CECR2 is required in for normal female reproduction. Depending on the

results of the above suggested experiments, there are several possibilities. For example, TNAP/Cre mice could be used to knockout *Cecr2* in primordial germ cells as described above for males (Kehler et al., 2004), or the Zp3/Cre line could be used to target *Cecr2* in oocytes beginning at the late primary follicle stage (Robker et al., 2014). The αGSU/Cre line could be used to knockout *Cecr2* in the anterior pituitary gland (Camacho-Hübner et al., 2000). Amhr2/Cre mice (targeting the uterine stroma and myometrium) PR/Cre mice (targeting the uterine stroma, myometrium, and epithelium) have both been previously used to study decidualization (Afshar et al., 2012; Zhang et al., 2012), but both can also target other relevant tissues so caution must be used when interpreting phenotypes (Daikoku et al., 2014).

With this information, it would then be possible to further investigate the relevant tissue(s), including potential molecular causes. In general, the use of an appropriate Cre mouse line to create a conditional knockout of *Cecr2* would be highly beneficial for any future studies. One of the major limitations of this study has been the difficulty in obtaining females with a severe *Cecr2* deficiency (*Cecr2*$^{GT/Del}$ females) due to their high penetrance of exencephaly. Targeting the knockout to specific tissues would greatly ease this problem and allow for the study of a severe *Cecr2* deficiency in reproductive tissue only without the inefficiency of losing the vast majority of female mutants at birth.

Given that *Cecr2* is a chromatin remodeler and the phenotype of *Cecr2* mutant females likely results from a uterine defect, it is possible that these defects are due to transcriptional misregulation in the mutant uterus during decidualization. Several genes identified as differentially expressed in *Cecr2* mutant testes are known to play critical roles in decidualization, making them intriguing targets for qPCR. Two of these, *Cbs* (Nuño-Ayala et al., 2012) and *Bmp7* (Monsivais et al., 2017), have already been tested by comparing artificially decidualized and control uterine samples from *Cecr2*$^{+/+}$ and *Cecr2*$^{GT/Del}$ females, but no differences were observed (results not shown). While more of these genes could be tested, it would clearly be more useful to sequence the transcriptome of the affected tissue in *Cecr2*$^{+/+}$ and *Cecr2* mutant females to identify genes that may be responsible for the phenotype. Based on what is currently known,

uterine tissue at the sites of implantation just starting to undergo decidualization at approximately E4.5 would be a good target, but the results of the above experiments would aid in confirming this.

4.4 Function of CECR2

Several experiments, including this work, have identified changes between the transcriptomes of *Cecr2*$^{+/+}$ and *Cecr2* mutant tissues. The first of these studies was a microarray done on whole embryos at the time of neurulation, which identified 114 misregulated genes (Fairbridge et al., 2010). In addition, a recent RNA-seq experiment specifically on the heads of neurulating embryos identified 143 differentially expressed genes (Terpstra, 2018). Of these 143 genes, four of them were also differentially regulated in the testes at P24 in this study: *Radil*, *A2m*, *Dlx1*, and *Prkaa2.* As none of these genes had functions with clear ties to the fertility phenotypes observed in *Cecr2* mutants, they were not further investigated. The small number of genes overlapping between these two RNA-seq experiments is not surprising, as they were done using RNA from two very different tissues and developmental timepoints.

Despite these experiments identifying transcriptional changes in *Cecr2* mutants, there is little evidence that CERF chromatin remodeling activity is directly responsible. Previous graduate student Dr. Farshad Niri used ChIP-seq to find possible sites of CERF chromatin remodeling activity by identifying overlapping binding sites of CECR2 and SNF2H (Niri, 2016). This was done on both ES cells and adult testis samples. Only one of the genes identified as differentially expressed in P24 testes in this study also had overlapping binding sites for CECR2 and SNF2H in adult testes: *Trp63*. The ChIP-seq analysis was done using a different strain of mice (FVB/N) that were ≥P42 rather than P24, which may contribute to the lack of overlap. However, the lack of overlap does suggest that if CECR2 is directly regulating the transcription of genes identified by RNA-seq in P24 testes it likely is not regulating those same genes in adult testes. If the function of CECR2 does change in this way between pre-pubertal and adult testes, this may contribute to the phenotypic

recovery we observe. However, it is also possible that the changes in transcript levels we observe in P24 testes are not due to the direct chromatin remodeling activity of the CERF complex in the promoter regions of affected genes, but rather are secondary effects. As CECR2 is localized to spermatogonia and many of the differentially expressed genes are expressed in later cell types, this is likely the case for a large portion of the genes.

As chromatin remodeling complexes can have many functions, it also remains possible that CECR2's role in spermatogenesis is related to a function other than gene regulation. As introduced in section 1.6.2, a role for CECR2 in DSB repair was identified in HEK-293T cells (Lee et al., 2012), but not in mouse neurospheres (Elliott, Norton, et al., in revision). A role for CECR2 in DSB repair during spermatogenesis has not yet been directly tested, but CECR2's absence in spermatocytes argues against a direct role for it in this process. However, it is possible that CECR2 chromatin remodeling in spermatogonia plays a role in making chromatin permissive for homologous recombination during meiosis or that it plays an indirect role through gene regulation. In addition, oocytes with abnormal DSB repair are usually eliminated shortly after birth (Di Giacomo et al., 2005; Li and Schimenti, 2007), arguing against a role for CECR2 in DSB repair during oogenesis. A very similar pattern was observed for BRG1, which plays a role in gene regulation in somatic cells (Chi, 2004). Studies in a somatic cell line showed that BRG1 also localizes to DSBs, and cells lacking BRG1 show a reduction in the number of γH2AX foci and increased susceptibility to irradiation (Lee et al., 2010; Park et al., 2006). During spermatogenesis, despite its expression in pachytene spermatocytes, BRG1 is not required for γH2AX formation (Wang et al., 2012).

4.5 Overall conclusions

The overall goal of this study was to identify the cause of subfertility in both male and female *Cecr2* mutant mice. While at the outset it seemed probable that the underlying cause would be the same in both sexes, the results presented here have suggested otherwise. Male *Cecr2* mutants have defects in spermatogenesis that are most severe just

after sexual maturity, indicating that CECR2 may be one of an emerging series of differences between prepubertal and steady-state adult spermatogenesis. Female *Cecr2* mutants have differing phenotypes depending on their level of *Cecr2*, with *Cecr2$^{GT/Del}$* dams showing fewer implantation sites at E5.5 whereas embryonic death occurs in *Cecr2$^{GT/GT}$* dams around E10, suggesting a role for *Cecr2* in early pregnancy. This study has therefore provided an additional example of how the same gene can function differently in fertility between the sexes. Several intriguing reproductive phenotypes have been identified in this study, providing the groundwork for future research. Due to its possible function in gene regulation, further investigation of fertility-related phenotypes in *Cecr2* mutant mice may also reveal new pathways and help elucidate how gene expression is orchestrated during these finely controlled processes.

Bibliography

Acampora, D., Mazan, S., Tuorto, F., Avantaggiato, V., Tremblay, J.J., Lazzaro, D., Di Carlo, A., Mariano, A., Macchia, P.E., Corte, G., Macchia, V., Drouin, J., Brûlet, P., Simeone, A., 1998. Transient dwarfism and hypogonadism in mice lacking Otx1 reveal prepubescent stage-specific control of pituitary levels of GH, FSH and LH. Development 125, 1229–1239.

Adams, S.R., Maezawa, S., Alavattam, K.G., Abe, H., Sakashita, A., Shroder, M., Broering, T.J., Sroga Rios, J., Thomas, M.A., Lin, X., Price, C.M., Barski, A., Andreassen, P.R., Namekawa, S.H., 2018. RNF8 and SCML2 cooperate to regulate ubiquitination and H3K27 acetylation for escape gene activation on the sex chromosomes. PLoS Genet. 14, e1007233. https://doi.org/10.1371/journal.pgen.1007233

Adelman, C.A., Petrini, J.H.J., 2008. ZIP4H (TEX11) deficiency in the mouse impairs meiotic double strand break repair and the regulation of crossing over. PLoS Genet. 4, e1000042. https://doi.org/10.1371/journal.pgen.1000042

Adhikari, D., Liu, K., 2010. mTOR signaling in the control of activation of primordial follicles. Cell Cycle 9, 1673–1674. https://doi.org/10.4161/cc.9.9.11626

Afshar, Y., Jeong, J.-W., Roqueiro, D., DeMayo, F., Lydon, J., Radtke, F., Radnor, R., Miele, L., Fazleabas, A., 2012. Notch1 mediates uterine stromal differentiation and is critical for complete decidualization in the mouse. FASEB J. Off. Publ. Fed. Am. Soc. Exp. Biol. 26, 282–294. https://doi.org/10.1096/fj.11-184663

Agarwal, A., Mulgund, A., Hamada, A., Chyatte, M.R., 2015. A unique view on male infertility around the globe. Reprod. Biol. Endocrinol. 13. https://doi.org/10.1186/s12958-015-0032-1

Aravind, L., Landsman, D., 1998. AT-hook motifs identified in a wide variety of DNA-binding proteins. Nucleic Acids Res. 26, 4413–4421. https://doi.org/10.1093/nar/26.19.4413

Arnoult, C., Zeng, Y., Florman, H.M., 1996. ZP3-dependent activation of sperm cation channels regulates acrosomal secretion during mammalian fertilization. J. Cell Biol.

134, 637–645. https://doi.org/10.1083/jcb.134.3.637

Ashley, T., Plug, A.W., Xu, J., Solari, A.J., Reddy, G., Golub, E.I., Ward, D.C., 1995. Dynamic changes in Rad51 distribution on chromatin during meiosis in male and female vertebrates. Chromosoma 104, 19–28. https://doi.org/10.1007/BF00352222

Baarends, W.M., Wassenaar, E., Van Der Laan, R., Hoogerbrugge, J., Sleddens-Linkels, E., Hoeijmakers, J.H.J., De Boer, P., Grootegoed, J.A., 2005. Silencing of Unpaired Chromatin and Histone H2A Ubiquitination in Mammalian Meiosis. Mol. Cell. Biol. 25, 1041–1053. https://doi.org/10.1128/MCB.25.3.1041-1053.2005

Baker, S.M., Plug, A.W., Prolla, T.A., Bronner, C.E., Harris, A.C., Yao, X., Christie, D., Monell, C., Amheim, N., Bradley, A., Ashley, T., Liskay, R.M., 1996. Involvement of mouse Mlh1 in DNA mismatch repair and meiotic crossing over. Nat. Genet. 13, 336–342.

Bannister, L.A., Pezza, R.J., Donaldson, J.R., De Rooij, D.G., Schimenti, K.J., Camerini-Otero, R.D., Schimenti, J.C., 2007. A dominant, recombination-defective allele of Dmc1 causing male-specific sterility. PLoS Biol. 5, 1016–1025. https://doi.org/10.1371/journal.pbio.0050105

Banting, G.S., Barak, O., Ames, T.M., Burnham, A.C., Kardel, M.D., Cooch, N.S., Davidson, C.E., Godbout, R., McDermid, H.E., Shiekhattar, R., 2005. CECR2, a protein involved in neurulation, forms a novel chromatin remodeling complex with SNF2L. Hum. Mol. Genet. 14, 513–524. https://doi.org/10.1093/hmg/ddi048

Baudat, F., Imai, Y., de Massy, B., 2013. Meiotic recombination in mammals: localization and regulation. https://doi.org/10.1038/nrg3573

Baumann, C., Schmidtmann, A., Muegge, K., De La Fuente, R., 2008. Association of ATRX with pericentric heterochromatin and the Y chromosome of neonatal mouse spermatogonia. BMC Mol. Biol. 9, 1–18. https://doi.org/10.1186/1471-2199-9-29

Bean, C.J., Schaner, C.E., Kelly, W.G., 2003. Meiotic pairing and imprinted X chromatin

assembly in Caenorhabditis elegans. Nat. Genet. 36. https://doi.org/10.1038/ng1283

Bellve, a R., Cavicchia, J.C., Millette, C.F., O'Brien, D.A., Bhatnagar, Y.M., Dym, M., 1977. Spermatogenic cells of the prepubertal mouse. Isolation and morphological characterization. J Cell Biol 74, 68–85. https://doi.org/10.1083/jcb.74.1.68

Benjamini, Y., Hochberg, Y., 1995. Controlling the False Discovery Rate: A Practical and Powerful Approach to Multiple Testing. J. R. Stat. Soc. Ser. B 57, 289–300. https://doi.org/10.1111/j.2517-6161.1995.tb02031.x

Benson, G. V., Lim, H., Paria, B.C., Satokata, I., Dey, S.K., Maas, R.L., 1996. Mechanisms of reduced fertility in Hoxa-10 mutant mice: Uterine homeosis and loss of maternal Hoxa-10 expression. Development 122, 2687–2696.

Berkovits, B.D., Wang, L., Guarnieri, P., Wolgemuth, D.J., 2012. The testis-specific double bromodomain-containing protein BRDT forms a complex with multiple spliceosome components and is required for mRNA splicing and 30-UTR truncation in round spermatids. Nucleic Acids Res. 40, 7162–7175. https://doi.org/10.1093/nar/gks342

Bleil, J.D., Wassarman, P.M., 1980. Mammalian sperm-egg interaction: Identification of a glycoprotein in mouse egg zonae pellucidae possessing receptor activity for sperm. Cell 20, 873–882. https://doi.org/10.1016/0092-8674(80)90334-7

Bolger, A.M., Lohse, M., Usadel, B., 2014. Trimmomatic: A flexible trimmer for Illumina sequence data. Bioinformatics 30, 2114–2120. https://doi.org/10.1093/bioinformatics/btu170

Borg, C.L., Wolski, K.M., Gibbs, G.M., O'Bryan, M.K., 2009. Phenotyping male infertility in the mouse: How to get the most out of a "non-performer." Hum. Reprod. Update 16, 205–224. https://doi.org/10.1093/humupd/dmp032

Borum, K., 1966. Oogenesis in the mouse. A study of the origin of the mature ova. Exp. Cell Res. 45, 39–47. https://doi.org/10.1016/0014-4827(67)90110-3

Braun, R.E., 1998. Post-transcriptional control of gene expression during

spermatogenesis. Semin. Cell Dev. Biol. 9, 483–489.
https://doi.org/10.1006/scdb.1998.0226

Broering, T.J., Wang, Y.L., Pandey, R.N., Hegde, R.S., Wang, S.C., Namekawa, S.H., 2015.
BAZ1B is dispensable for H2AX phosphorylation on Tyrosine 142 during
spermatogenesis. Biol. Open 4, 873–884. https://doi.org/10.1242/bio.011734

Bronson, F.H., Dagg, C.P., Snell, G.D., 1966. Reproduction, in: Green, E.L. (Ed.), Biology of
the Laboratory Mouse. Dover Publications Inc., New York.

Brown, M.S., Bishop, D.K., 2015. DNA strand exchange and RecA homologs in meiosis.
Cold Spring Harb. Perspect. Biol. 7. https://doi.org/10.1101/cshperspect.a016659

Buffone, M.G., Ijiri, T.W., Cao, W., Merdiushev, T., Aghajanian, H.K., 2012. Heads or Tails ?
Structural Events and Molecular Mechanisms That Promote Mammalian Sperm
Acrosomal Exocytosis and Motility. Mol. Reprod. Dev. 79, 4–18.
https://doi.org/10.1002/mrd.21393

Bultman, S.J., Gebuhr, T.C., Pan, H., Svoboda, P., Schultz, R.M., Magnuson, T., 2006.
Maternal BRG1 regulates zygotic genome activation in the mouse. Genes Dev. 20,
1744–1754. https://doi.org/10.1101/gad.1435106

Burgoyne, P.S., Mahadevaiah, S., Mittwoch, U., 1985. A reciprocal autosomal
translocation which causes male sterility in the mouse also impairs oogenesis. J.
Reprod. Fertil. 75, 647–652.

Burgoyne, P.S., Mahadevaiah, S.K., Turner, J.M.A., 2009. The consequences of asynapsis
for mammalian meiosis. Nat. Rev. Genet. 10, 207–216.
https://doi.org/10.1038/nrg1639

Burkart, A.D., Xiong, B., Baibakov, B., Jiménez-Movilla, M., Dean, J., 2012. Ovastacin, a
cortical granule protease, cleaves ZP2 in the zona pellucida to prevent polyspermy. J.
Cell Biol. 197, 37–44. https://doi.org/10.1083/jcb.201112094

Burns, K.H., Yan, C., Kumar, T.R., Matzuk, M.M., 2001. Analysis of ovarian gene expression

in follicle-stimulating hormone β knockout mice. Endocrinology 142, 2742–2751. https://doi.org/10.1210/endo.142.7.8279

Busada, J.T., Geyer, C.B., 2015. The Role of Retinoic Acid (RA) in Spermatogonial Differentiation. Biol. Reprod. 94, 1–10. https://doi.org/10.1095/biolreprod.115.135145

Busada, J.T., Velte, E.K., Serra, N., Cook, K., Niedenberger, B.A., Willis, W.D., Goulding, E.H., Eddy, E.M., Geyer, C.B., 2016. Rhox13 is required for a quantitatively normal first wave of spermatogenesis in mice. Reproduction 152, 379–388. https://doi.org/10.1530/REP-16-0268

Busso, D., Cohen, D.J., Maldera, J.A., Dematteis, A., Cuasnicu, P.S., 2007. A Novel Function for CRISP1 in Rodent Fertilization: Involvement in Sperm-Zona Pellucida Interaction1. Biol. Reprod. 77, 848–854. https://doi.org/10.1095/biolreprod.107.061788

Byers, S.L., Wiles, M. V, Dunn, S.L., Taft, R.A., 2012. Mouse estrous cycle identification tool and images. PLoS One 7, 35538. https://doi.org/10.1371/journal.pone.0035538

Camacho-Hübner, A., Rossier, A., Beermann, F., 2000. Cre-mediated recombination in the pituitary gland. Genesis 28, 167–174. https://doi.org/10.1002/1526-968X(200011/12)28:3/4<167::AID-GENE120>3.0.CO;2-N

Cannarella, R., Condorelli, R.A., Duca, Y., La Vignera, S., Calogero, A.E., 2019. New insights into the genetics of spermatogenic failure: a review of the literature. Hum. Genet. 138, 125–140. https://doi.org/10.1007/s00439-019-01974-1

Carson, D.D., Bagchi, I., Dey, S.K., Enders, A.C., Fazleabas, A.T., Lessey, B.A., Yoshinaga, K., 2000. Embryo Implantation. Dev. Biol. 223, 217–237. https://doi.org/:10.1006/dbio.2000.9767

Cha, J., Bartos, A., Park, C., Sun, X., Li, Y., Cha, S.W., Ajima, R., Ho, H.Y.H., Yamaguchi, T.P., Dey, S.K., 2014a. Appropriate crypt formation in the uterus for embryo homing and implantation requires Wnt5a-ROR signaling. Cell Rep. 8, 382–392.

https://doi.org/10.1038/jid.2014.371

Cha, J., Dey, S.K., Lim, H., 2014b. Embryo Implantation, in: Lim, H. (Jade) (Ed.), Knobil and Neill's Physiology of Reproduction. Elsevier, pp. 1697–1739. https://doi.org/10.1016/B978-0-12-397175-3.00038-7

Cha, J., Sun, X., Dey, S.K., 2012. Mechanisms of implantation: Strategies for successful pregnancy. Nat. Med. 18, 1754–1767. https://doi.org/10.1038/nm.3012

Cha, J.M., Dey, S.K., 2015. Reflections on Rodent Implantation, in: Geisert, R.D., Bazer, F.W. (Eds.), Regulation of Implantation and Establishment of Pregnancy in Mammals: Tribute to 45 Year Anniversary of Roger V. Short's ``Maternal Recognition of Pregnancy''. Springer International Publishing, Cham, pp. 69–85. https://doi.org/10.1007/978-3-319-15856-3_5

Cheng, Y., Buffone, M.G., Kouadio, M., Goodheart, M., Page, D.C., Gerton, G.L., Davidson, I., Wang, P.J., 2007. Abnormal Sperm in Mice Lacking the Taf7l Gene. Mol. Cell. Biol. 27, 2582–2589. https://doi.org/10.1128/MCB.01722-06

Chi, T., 2004. A BAF-centred view of the immune system. Nat. Rev. Immunol. 4, 965–977. https://doi.org/10.1038/nri1501

Ciller, I.M., Palanisamy, S.K.A., Ciller, U.A., Farlane, J.R.M.C., 2016. Postnatal Expression of Bone Morphogenetic Proteins and Their Receptors in the Mouse Testis. Physiol. Reseach 65, 673–682.

Clapier, C.R., Cairns, B.R., 2009. The Biology of Chromatin Remodeling Complexes. Annu. Rev. Biochem. 78, 273–304. https://doi.org/10.1146/annurev.biochem.77.062706.153223

Clapier, C.R., Iwasa, J., Cairns, B.R., Peterson, C.L., 2017. Mechanisms of action and regulation of ATP-dependent chromatin-remodelling complexes. Nat. Rev. Mol. Cell Biol. 18, 407–422. https://doi.org/10.1038/nrm.2017.26

Cloutier, J.M., Mahadevaiah, S.K., Ellnati, E., Tóth, A., Turner, J., 2016. Mammalian

meiotic silencing exhibits sexually dimorphic features. Chromosoma 125, 215–226. https://doi.org/10.1007/s00412-015-0568-z

Cole, L.A., 2012. Hyperglycosylated hCG and pregnancy failures. J. Reprod. Immunol. 93, 119–122. https://doi.org/10.1016/j.jri.2012.01.001

Copp, A.J., Greene, N.D.E., Murdoch, J.N., 2003. The genetic basis of mammalian neurulation. Nat. Rev. Genet. 4, 784–793. https://doi.org/10.1038/nrg1181

Coulam, C.B., Adamson, S.C., Annegers, J.F., 1986. Incidence of premature ovarian failure. Obstet. Gynecol. 67, 604–606.

Crichton, J.H., Read, D., Adams, I.R., 2018. Defects in meiotic recombination delay progression through pachytene in Tex19.1 –/– mouse spermatocytes. Chromosoma 127, 437–459. https://doi.org/10.1007/s00412-018-0674-9

Daikoku, T., Ogawa, Y., Terakawa, J., Ogawa, A., DeFalco, T., Dey, S.K., 2014. Lactoferrin-iCre: A new mouse line to study uterine epithelial gene function. Endocrinology 155, 2718–2724. https://doi.org/10.1210/en.2014-1265

Dale, B., Wilding, M., Coppola, G., Tosti, E., 2010. How do spermatozoa activate oocytes? Reprod. Biomed. Online 21, 1–3. https://doi.org/10.1016/j.rbmo.2010.02.015

Dann, C.T., Alvarado, A.L., Molyneux, L.A., Denard, B.S., Garbers, D.L., Porteus, M.H., 2008. Spermatogonial Stem Cell Self-Renewal Requires OCT4, a Factor Downregulated During Retinoic Acid-Induced Differentiation. Stem Cells 26, 2928–2937. https://doi.org/10.1634/stemcells.2008-0134

Darde, T.A., Lecluze, E., Lardenois, A., Stévant, I., Alary, N., Tüttelmann, F., Collin, O., Nef, S., Jégou, B., Rolland, A.D., Chalmel, F., 2019. The ReproGenomics Viewer: a multi-omics and cross-species resource compatible with single-cell studies for the reproductive science community. Bioinformatics 35, 3133–3139. https://doi.org/10.1093/bioinformatics/btz047

Darde, T.A., Sallou, O., Becker, E., Evrard, B., Monjeaud, C., Le Bras, Y., Jégou, B., Collin,

O., Rolland, A.D., Chalmel, F., 2015. The ReproGenomics Viewer: An integrative cross-species toolbox for the reproductive science community. Nucleic Acids Res. 43, W109–W116. https://doi.org/10.1093/nar/gkv345

Dawe, C.E., 2009. A Combination of Neural Tube Defects, Open Eyelids, and Inner Ear Defects Suggests a Role for Cecr2 in Regulation of the Planar Cell Polarity Pathway. University of Alberta.

Dawe, C.E., Kooistra, M.K., Fairbridge, N.A., Pisio, A.C., McDermid, H.E., 2011. Role of chromatin remodeling gene Cecr2 in neurulation and inner ear development. Dev. Dyn. 240, 372–383. https://doi.org/10.1002/dvdy.22547

De La Fuente, R., Viveiros, M.M., Wigglesworth, K., Eppig, J.J., 2004. ATRX, a member of the SNF2 family of helicase/ATPases, is required for chromosome alignment and meiotic spindle organization in metaphase II stage mouse oocytes. Dev. Biol. 272, 1–14. https://doi.org/10.1016/j.ydbio.2003.12.012

de Rooij, D.G., 2017. The nature and dynamics of spermatogonial stem cells. Development 144, 3022–3030. https://doi.org/10.1242/dev.146571

de Vries, F.A.T., de Boer, E., Van Den Bosch, M., Baarends, W.M., Ooms, M., Yuan, L., Liu, J.G., Van Zeeland, A.A., Heyting, C., Pastink, A., 2005. Mouse Sycp1 functions in synaptonemal complex assembly, meiotic recombination, and XY body formation. Genes Dev. 19, 1376–1389. https://doi.org/10.1101/gad.329705

Deb, K., Reese, J., Paria, B.C., 2006. Methodologies to study implantation in mice. Methods Mol. Med. 121, 9–34. https://doi.org/10.1385/1-59259-983-4:007

Dey, S.K., 2006. Visualizing Early Embryo Implantation Sites by Dye Injection. Cold Spring Harb. Protoc. 2006, pdb.prot4361. https://doi.org/10.1101/pdb.prot4361

Di Giacomo, M., Barchi, M., Baudat, F., Edelmann, W., Keeney, S., Jasin, M., 2005. Distinct DNA-damage-dependent and -independent responses drive the loss of oocytes in recombination-defective mouse mutants. PNAS 102, 737–742.

Dobin, A., Davis, C.A., Schlesinger, F., Drenkow, J., Zaleski, C., Jha, S., Batut, P., Chaisson, M., Gingeras, T.R., 2013. STAR: Ultrafast universal RNA-seq aligner. Bioinformatics 29, 15–21. https://doi.org/10.1093/bioinformatics/bts635

Dostál, J., Veselský, L., Marounek, M., Železná, B., Jonáková, V., 1997. Inhibition of bacterial and boar epididymal sperm immunogenicity by boar seminal immunosuppressive component in mice. Reproduction 111, 135–141. https://doi.org/10.1530/jrf.0.1110135

Dowdle, J.A., Mehta, M., Kass, E.M., Vuong, B.Q., Inagaki, A., Egli, D., Jasin, M., Keeney, S., 2013. Mouse BAZ1A (ACF1) Is Dispensable for Double-Strand Break Repair but Is Essential for Averting Improper Gene Expression during Spermatogenesis. PLoS Genet. 9, e1003945. https://doi.org/10.1371/journal.pgen.1003945

Ducibella, T., Huneau, D., Angelichio, E., Xu, Z., Schultz, R.M., Kopf, G.S., Fissore, R., Madoux, S., Ozil, J.P., 2002. Egg-to-embryo transition is driven by differential responses to Ca2+oscillation number. Dev. Biol. 250, 280–291. https://doi.org/10.1016/S0012-1606(02)90788-8

Duncan, F.E., Chiang, T., Schultz, R.M., Lampson, M.A., 2009. Evidence That a Defective Spindle Assembly Checkpoint Is Not the Primary Cause of Maternal Age-Associated Aneuploidy in Mouse Eggs1. Biol. Reprod. 81, 768–776. https://doi.org/10.1095/biolreprod.109.077909

Durlinger, A.L., Kramer, P., Karels, B., de Jong, F.H., Uilenbroek, J.T., Grootegoed, J.A., Themmen, A.P., 1999. Control of Primordial Follicle Recruitment by Anti-Mullerian Hormone in the Mouse Ovary. Endocrinology 140, 5789–5796. https://doi.org/10.1210/en.140.12.5789

Edwards, R.G., 1965. Maturation in vitro of mouse, sheep, cow, pig, rhesus monkey and human ovarian oocytes. Nature 208, 349–351.

Ellnati, E., Russell, H.R., Ojarikre, O.A., Sangrithi, M., Hirota, T., De Rooij, D.G., McKinnon, P.J., Turner, J.M.A., 2017. DNA damage response protein TOPBP1 regulates X

chromosome silencing in the mammalian germ line. Proc. Natl. Acad. Sci. U. S. A. 114, 12536–12541. https://doi.org/10.1073/pnas.1712530114

Enders, A.C., Schlafke, S., 1967. A morphological analysis of the early implantation stages in the rat. Am. J. Anat. 120, 185–225. https://doi.org/10.1002/aja.1001200202

Erdel, F., Rippe, K., 2011. Chromatin remodelling in mammalian cells by ISWI-type complexes - Where, when and why? FEBS J. 278, 3608–3618. https://doi.org/10.1111/j.1742-4658.2011.08282.x

Ernst, C., Eling, N., Martinez-Jimenez, C.P., Marioni, J.C., Odom, D.T., 2019. Staged developmental mapping and X chromosome transcriptional dynamics during mouse spermatogenesis. Nat. Commun. 10. https://doi.org/10.1038/s41467-019-09182-1

Fairbridge, N.A., 2013. Molecular and phenotypic characterization of Cecr2 mouse models: implications for the role of mesenchymal/epithelial regulation in neural tube and renal development. University of Alberta.

Fairbridge, N.A., Dawe, C.E., Niri, F.H., Kooistra, M.K., King-Jones, K., McDermid, H.E., 2010. Cecr2 mutations causing exencephaly trigger misregulation of mesenchymal/ectodermal transcription factors. Birth Defects Res. Part A - Clin. Mol. Teratol. 88, 619–625. https://doi.org/10.1002/bdra.20695

Fan, J., Akabane, H., Zheng, X., Zhou, X., Zhang, L., Liu, Q., Zhang, Y.L., Yang, J., Zhu, G.Z., 2007. Male germ cell-specific expression of a novel Patched-domain containing gene Ptchd3. Biochem. Biophys. Res. Commun. 363, 757–761. https://doi.org/10.1016/j.bbrc.2007.09.047

Findlay, J.K., Dunning, K.R., Gilchrist, R.B., Hutt, K.J., Russell, D.L., Walters, K.A., 2019. Follicle Selection in Mammalian Ovaries, in: The Ovary. pp. 3–21. https://doi.org/10.1016/b978-0-12-813209-8.00001-7

Flach, G., Johnson, M.H., Braude, P.R., Taylor, R.A., Bolton, V.N., 1982. The transition from maternal to embryonic control in the 2-cell mouse embryo. EMBO J. 1, 681–686.

https://doi.org/10.1002/j.1460-2075.1982.tb01230.x

Florman, H.M., Fissore, R.A., 2014. Fertilization in Mammals, in: Knobil and Neill's Physiology of Reproduction. Elsevier, pp. 149–196. https://doi.org/10.1016/B978-0-12-397175-3.00004-1

Fujimori, T., 2010. Preimplantation development of mouse: A view from cellular behavior. Dev. Growth Differ. 52, 253–262. https://doi.org/10.1111/j.1440-169X.2010.01172.x

Fukuda, T., Pratto, F., Schimenti, J.C., Turner, J.M.A., Camerini-Otero, R.D., Höög, C., 2012. Phosphorylation of chromosome core components may serve as axis marks for the status of chromosomal events during mammalian meiosis. PLoS Genet. 8. https://doi.org/10.1371/journal.pgen.1002485

Furnes, B., Schimenti, J., 2007. Fast forward to new genes in mammalian reproduction. J. Physiol. 578, 25–32. https://doi.org/10.1113/jphysiol.2006.119164

Fyodorov, D. V., Kadonaga, J.T., 2002. Binding of Acf1 to DNA Involves a WAC Motif and Is Important for ACF-Mediated Chromatin Assembly. Mol. Cell. Biol. 22, 6344–6353. https://doi.org/10.1128/mcb.22.18.6344-6353.2002

Gellersen, B., Brosens, J.J., 2014. Cyclic decidualization of the human endometrium in reproductive health and failure. Endocr. Rev. 35, 851–905. https://doi.org/10.1210/er.2014-1045

Gershoni, M., Hauser, R., Barda, S., Lehavi, O., Arama, E., Pietrokovski, S., Kleiman, S.E., 2019. A new MEIOB mutation is a recurrent cause for azoospermia and testicular meiotic arrest. Hum. Reprod. https://doi.org/10.1093/humrep/dez016

Gervasi, M.G., Visconti, P.E., 2017. Molecular changes and signaling events occurring in spermatozoa during epididymal maturation. Andrology 5, 204–218. https://doi.org/10.1111/andr.12320

Geyer, C.B., 2017. Setting the Stage: The First Round of Spermatogenesis, in: The Biology of Mammalian Spermatogonia. Springer New York, New York, NY, pp. 39–63.

https://doi.org/10.1007/978-1-4939-7505-1_3

Geyer, C.B., Eddy, E.M., 2008. Identification and characterization of Rhox13, a novel X-linked mouse homeobox gene. Gene 423, 194–200. https://doi.org/10.1016/j.gene.2008.06.031

Ghahramani Seno, M.M., Kwan, B.Y., Lee-Ng, K.K.M., Moessner, R., Lionel, A.C., Marshall, C.R., Scherer, S.W., 2011. Human PTCHD3 nulls: Rare copy number and sequence variants suggest a non-essential gene. BMC Med. Genet. 12. https://doi.org/10.1186/1471-2350-12-45

Ginsburg, M., Snow, M.H.L., Mclaren, A., 1990. Primordial germ cells in the mouse embryo during gastrulation. Development 110, 521–528.

Goriely, A., Wilkie, A.O.M., 2012. Paternal age effect mutations and selfish spermatogonial selection: Causes and consequences for human disease. Am. J. Hum. Genet. 90, 175–200. https://doi.org/10.1016/j.ajhg.2011.12.017

Goupil, S., La Salle, S., Trasler, J.M., Bordeleau, L.-J., Leclerc, P., 2011. Developmental expression of SRC-related tyrosine kinases in the mouse testis. J. Androl. 32, 95–110. https://doi.org/10.2164/jandrol.110.010462

Greder, L. V., Gupta, S., Li, S., Abedin, M.J., Sajini, A., Segal, Y., Slack, J.M.W., Dutton, J.R., 2012. Brief report: Analysis of endogenous Oct4 activation during induced pluripotent stem cell reprogramming using an inducible Oct4 lineage label. Stem Cells 30, 2596–2601. https://doi.org/10.1002/stem.1216

Green, C.D., Ma, Q., Manske, G.L., Niederriter, A., Li, J.Z., Correspondence, S.H., 2018. A Comprehensive Roadmap of Murine Spermatogenesis Defined by Single-Cell RNA-Seq Data Resources GSE112393 Green et al. Dev. Cell 46, 651–667. https://doi.org/10.1016/j.devcel.2018.07.025

Guillon, H., Baudat, F., Grey, C., Liskay, R.M., De Massy, B., 2005. Crossover and noncrossover pathways in mouse meiosis. Mol. Cell 20, 563–573.

https://doi.org/10.1016/j.molcel.2005.09.021

Guiraldelli, M.F., Eyster, C., Wilkerson, J.L., Dresser, M.E., Pezza, R.J., 2013. Mouse HFM1/Mer3 Is Required for Crossover Formation and Complete Synapsis of Homologous Chromosomes during Meiosis. PLoS Genet. 9, e1003383. https://doi.org/10.1371/journal.pgen.1003383

Guo, H., Hu, B., Yan, L., Yong, J., Wu, Y., Gao, Y., Guo, F., Hou, Y., Fan, X., Dong, J., Wang, X., Zhu, X., Yan, J., Wei, Y., Jin, H., Zhang, W., Wen, L., Tang, F., Qiao, J., 2017. DNA methylation and chromatin accessibility profiling of mouse and human fetal germ cells. Cell Res. 27, 165–183. https://doi.org/10.1038/cr.2016.128

Haldane, J.B.S., 1922. Sex ratio and unisexual sterility in hybrid animals. J. Genet. 12, 101–109. https://doi.org/10.1007/BF02983075

Han, S., Zhou, L., Upadhyaya, A., Hyun Lee, S., Parker, K.L., DeJong, J., 2001. TFIIAα/β-Like Factor Is Encoded by a Germ Cell-Specific Gene Whose Expression Is Up-Regulated with Other General Transcription Factors During Spermatogenesis in the Mouse1. Biol. Reprod. 64, 507–517. https://doi.org/10.1095/biolreprod64.2.507

Handel, M.A., Schimenti, J.C., 2010. Genetics of mammalian meiosis: Regulation, dynamics and impact on fertility. Nat. Rev. Genet. 11, 124–136. https://doi.org/10.1038/nrg2723

Hanson, F.W., Overstreet, J.W., 1981. The interaction of human spermatozoa with cervical mucus in vivo. Am. J. Obstet. Gynecol. 140, 173–178. https://doi.org/10.1016/0002-9378(81)90105-8

Hara, K., Nakagawa, T., Enomoto, H., Suzuki, M., Yamamoto, M., Simons, B.D., Yoshida, S., 2014. Mouse spermatogenic stem cells continually interconvert between equipotent singly isolated and syncytial states. Cell Stem Cell 14, 658–672. https://doi.org/10.1016/j.stem.2014.01.019

Hart, S.N., Therneau, T.M., Zhang, Y., Poland, G.A., Kocher, J.P., 2013. Calculating sample

size estimates for RNA sequencing data. J. Comput. Biol. 20, 970–978. https://doi.org/10.1089/cmb.2012.0283

Hasegawa, K., Sin, H.S., Maezawa, S., Broering, T.J., Kartashov, A. V., Alavattam, K.G., Ichijima, Y., Zhang, F., Bacon, W.C., Greis, K.D., Andreassen, P.R., Barski, A., Namekawa, S.H., 2015. SCML2 Establishes the Male Germline Epigenome through Regulation of Histone H2A Ubiquitination. Dev. Cell 32, 574–588. https://doi.org/10.1016/j.devcel.2015.01.014

Hassold, T., Hunt, P., 2001. To err (meiotically) is human: the genesis of human aneuploidy. Nat. Rev. Genet. 2, 280–91.

Hays, E., Majchrzak, N., Daniel, V., Ferguson, Z., Brown, S., Hathorne, K., La Salle, S., 2017. Spermatogenesis associated 22 is required for DNA repair and synapsis of homologous chromosomes in mouse germ cells. Andrology 5, 299–312. https://doi.org/10.1111/andr.12315

Hermann, B.P., Cheng, K., Singh, A., Roa-De La Cruz, L., Mutoji, K.N., Chen, I.C., Gildersleeve, H., Lehle, J.D., Mayo, M., Westernströer, B., Law, N.C., Oatley, M.J., Velte, E.K., Niedenberger, B.A., Fritze, D., Silber, S., Geyer, C.B., Oatley, J.M., McCarrey, J.R., 2018. The Mammalian Spermatogenesis Single-Cell Transcriptome, from Spermatogonial Stem Cells to Spermatids. Cell Rep. 25, 1650-1667.e8. https://doi.org/10.1016/j.celrep.2018.10.026

Hilliard, J., 1973. Corpus Luteum Function in Guinea Pigs, Hamsters, Rats, Mice and Rabbits. Biol. Reprod. 8, 203–221. https://doi.org/10.1093/biolreprod/8.2.203

Hillier, S.G., Whitelaw, P.F., Smyth, C.D., 1994. Follicular oestrogen synthesis: the "two-cell, two-gonadotrophin" model revisited. Mol. Cell. Endocrinol. 100, 51–54. https://doi.org/10.1016/0303-7207(94)90278-X

Hirshfield, A.N., 1991. Development of Follicles in the Mammalian Ovary. Int. Rev. Cytol. 124, 43–101.

Hodges, C.A., Revenkova, E., Jessberger, R., Hassold, T.J., Hunt, P.A., 2005. SMC1B-deficient female mice provide evidence that cohesins are a missing link in age-related nondisjunction. Nat. Genet. 37, 1351–1355. https://doi.org/10.1038/ng1672

Homolka, D., Ivanek, R., Capkova, J., Jansa, P., Forejt, J., 2007. Chromosomal rearrangement interferes with meiotic X chromosome inactivation. Genome Res. 17, 1431–1437. https://doi.org/10.1101/gr.6520107

Homolka, D., Jansa, P., Forejt, J., 2012. Genetically enhanced asynapsis of autosomal chromatin promotes transcriptional dysregulation and meiotic failure. Chromosoma 121, 91–104. https://doi.org/10.1007/s00412-011-0346-5

Honaramooz, A., Snedaker, A., Boiani, M., Schöler, H., Dobrinski, I., Schlatt, S., 2002. Sperm from neonatal mammalia testes grafted in mice. Nature 418, 778–781. https://doi.org/10.1038/nature00918

Horan, C.J., Williams, S.A., 2017. Oocyte stem cells: fact or fantasy? Reproduction 154, R23–R35. https://doi.org/10.1530/rep-17-0008

Hu, Y., Yan, C., Hsu, C.H., Chen, Q.R., Niu, K., Komatsoulis, G.A., Meerzaman, D., 2014. Omiccircos: A simple-to-use R package for the circular visualization of multidimensional Omics data. Cancer Inform. 13, 13–20. https://doi.org/10.4137/CIN.S13495

Huang, D.W., Sherman, B.T., Lempicki, R.A., 2009a. Systematic and integrative analysis of large gene lists using DAVID bioinformatics resources. Nat. Protoc. 4, 44–57. https://doi.org/10.1038/nprot.2008.211

Huang, D.W., Sherman, B.T., Lempicki, R.A., 2009b. Bioinformatics enrichment tools: paths toward the comprehensive functional analysis of large gene lists. Nucleic Acids Res. 37, 1–13. https://doi.org/10.1093/nar/gkn923

Hunt, P.A., Hassold, T.J., 2002. Sex matters in meiosis. Science 296, 2181–2183. https://doi.org/10.1126/science.1071907

Ichijima, Y., Ichijima, M., Lou, Z., Camerini-otero, R.D., Chen, J., Andreassen, P.R., Namekawa, S.H., 2011. MDC1 directs chromosome-wide silencing of the sex chromosomes in male germ cells. Genes Dev. 25, 959–971. https://doi.org/10.1101/gad.2030811.activation

Igakura, T., Kadomatsu, K., Kaname, T., Muramatsu, H., Fan, Q.W., Miyauchi, T., Toyama, Y., Kuno, N., Yuasa, S., Takahashi, M., Senda, T., Taguchi, O., Yamamura, K.I., Arimura, K., Muramatsu, T., 1998. A null mutation in basigin, an immunoglobulin superfamily member, indicates its important roles in peri-implantation development and spermatogenesis. Dev. Biol. 194, 152–165. https://doi.org/10.1006/dbio.1997.8819

Ikawa, M., Benham, A.M., Okabe, M., Ikawa, M., Inoue, N., Benham, A.M., Okabe, M., 2010. Fertilization: a sperm's journey to and interaction with the oocyte. J. Clin. Invest. 120, 984–994. https://doi.org/10.1172/JCI41585.984

Inagaki, A., Sleddens-Linkels, E., Wassenaar, E., Ooms, M., van Cappellen, W.A., Hoeijmakers, J.H.J., Seibler, J., Vogt, T.F., Shin, M.K., Grootegoed, J.A., Baarends, W.M., 2011. Meiotic functions of RAD18. J. Cell Sci. 124, 2837–2850. https://doi.org/10.1242/jcs.081968

Jagarlamudi, K., Reddy, P., Adhikari, D., Liu, K., 2010. Genetically modified mouse models for premature ovarian failure (POF). Mol. Cell. Endocrinol. 315, 1–10. https://doi.org/10.1016/j.mce.2009.07.016

Jamsai, D., O'Bryan, M.K., 2011. Mouse models in male fertility research. Asian J. Androl. 13, 139–151. https://doi.org/10.1038/aja.2010.101

Johnson, J., Canning, J., Kaneko, T., Pru, J.K., Tilly, J.L., 2004. Germline stem cells and follicular renewal in the postnatal mammalian ovary. Nature 430, 1062. https://doi.org/10.1038/nature02868

Jones, K.T., 2008. Meiosis in oocytes: Predisposition to aneuploidy and its increased incidence with age. Hum. Reprod. Update 14, 143–158.

https://doi.org/10.1093/humupd/dmm043

Jukam, D., Shariati, S.A.M., Skotheim, J.M., 2017. Zygotic Genome Activation in
Vertebrates. Dev. Cell 42, 316–332. https://doi.org/10.1016/j.devcel.2017.07.026

Kato, Y., Alavattam, K.G., Sin, H.S., Meetei, A.R., Pang, Q., Andreassen, P.R., Namekawa,
S.H., 2015. FANCB is essential in the male germline and regulates H3K9 methylation
on the sex chromosomes during meiosis. Hum. Mol. Genet. 24, 5234–5249.
https://doi.org/10.1093/hmg/ddv244

Katz, D.F., Morales, P., Samuels, S.J., Overstreet, J.W., 1990. Mechanisms of filtration of
morphologically abnormal human sperm by cervical mucus. Fertil. Steril. 54, 513–
516. https://doi.org/10.1016/s0015-0282(16)53772-8

Kauppi, L., Barchi, M., Baudat, F., Romanienko, P.J., Keeney, S., Jasin, M., 2011. Distinct
properties of the XY pseudoautosomal region crucial for male meiosis. Science 331,
916–920. https://doi.org/10.1126/science.1195774

Kauppi, L., Barchi, M., Lange, J., Baudat, F., Jasin, M., Keeney, S., 2013. Numerical
constraints and feedback control of double-strand breaks in mouse meiosis. Genes
Dev. 27, 873–886. https://doi.org/10.1101/gad.213652.113

Keeney, S., Giroux, C.N., Kleckner, N., 1997. Meiosis-specific DNA double-strand breaks
are catalyzed by Spo11, a member of a widely conserved protein family. Cell 88,
375–384. https://doi.org/10.1016/S0092-8674(00)81876-0

Kehler, J., Tolkunova, E., Koschorz, B., Pesce, M., Gentile, L., Boiani, M., Lomelí, H., Nagy,
A., McLaughlin, K.J., Schöler, H.R., Tomilin, A., 2004. Oct4 is required for primordial
germ cell survival. EMBO Rep. 5, 1078–1083.
https://doi.org/10.1038/sj.embor.7400279

Kierszenbaum, A.L., 2001. Apoptosis during spermatogenesis: The thrill of being alive.
Mol. Reprod. Dev. 58, 1–3. https://doi.org/10.1002/1098-2795(200101)58:1<1::AID-
MRD1>3.0.CO;2-0

Klein, A.M., Nakagawa, T., Ichikawa, R., Yoshida, S., Simons, B.D., 2010. Mouse germ line stem cells undergo rapid and stochastic turnover. Cell Stem Cell 7, 214–224. https://doi.org/10.1016/j.stem.2010.05.017

Kneitz, B., Cohen, P.E., Avdievich, E., Zhu, L., Kane, M.F., Hou, H., Kolodner, R.D., Kucherlapati, R., Pollard, J.W., Edelmann, W., 2000. MutS homolog 4 localization to meiotic chromosomes is required for chromosome pairing during meiosis in male and female mice. Genes Dev. 14, 1085–1097. https://doi.org/10.1101/gad.14.9.1085

Kogo, H., Tsutsumi, M., Inagaki, H., Ohye, T., Kiyonari, H., Kurahashi, H., 2012. HORMAD2 is essential for synapsis surveillance during meiotic prophase via the recruitment of ATR activity. Genes to Cells 17, 897–912. https://doi.org/10.1111/gtc.12005

Kol, S., Adashi, E.Y., 1995. Intraovarian factors regulating ovarian function. Curr. Opin. Obstet. Gynecol. 7, 209–213.

Kolas, N.K., Marcon, E., Crackower, M.A., Höög, C., Penninger, J.M., Spyropoulos, B., Moens, P.B., 2005. Mutant meiotic chromosome core components in mice can cause apparent sexual dimorphic endpoints at prophase or X-Y defective male-specific sterility. Chromosoma 114, 92–102. https://doi.org/10.1007/s00412-005-0334-8

Koopman, P., Gubbay, J., Vivian, N., Goodfellow, P., Lovell-Badge, R., 1991. Male development of chromosomally female mice transgenic for Sry. Lett. to Nat. 353, 737–740.

Koot, Y.E.M., Boomsma, C.M., Eijkemans, M.J.C., Lentjes, E.G.W., MacKlon, N.S., 2011. Recurrent pre-clinical pregnancy loss is unlikely to be a "cause" of unexplained infertility. Hum. Reprod. 26, 2636–2641. https://doi.org/10.1093/humrep/der217

Kramer, J.M., Erickson, R.P., 1981. Developmental program of PGK-1 and PGK-2 isozymes in spermatogenic cells of the mouse: Specific activities and rates of synthesis. Dev. Biol. 87, 37–45. https://doi.org/10.1016/0012-1606(81)90058-0

Kuno, N., Kadomatsu, K., Fan, Q.W., Hagihara, M., Senda, T., Mizutani, S., Muramatsu, T.,

1998. Female sterility in mice lacking the basigin gene, which encodes a transmembrane glycoprotein belonging to the immunoglobulin superfamily. FEBS Lett. 425, 191–194. https://doi.org/10.1016/S0014-5793(98)00213-0

Lakoski, K.A., Carron, C.P., Cabot, C.L., Saling, P.M., 1988. Epididymal Maturation and the Acrosome Reaction in Mouse Sperm: Response to Zona Pellucida Develops Coincident with Modification of M42 Antigen1. Biol. Reprod. 38, 221–233. https://doi.org/10.1095/biolreprod38.1.221

Längst, G., Manelyte, L., 2015. Chromatin remodelers: From function to dysfunction. Genes (Basel). 6, 299–324. https://doi.org/10.3390/genes6020299

Laronda, M.M., Jameson, J.L., 2011. Sox3 functions in a cell-autonomous manner to regulate spermatogonial differentiation in mice. Endocrinology 152, 1606–1615. https://doi.org/10.1210/en.2010-1249

Lazzaro, M. a, Pépin, D., Pescador, N., Murphy, B.D., Vanderhyden, B.C., Picketts, D.J., 2006. The imitation switch protein SNF2L regulates steroidogenic acute regulatory protein expression during terminal differentiation of ovarian granulosa cells. Mol. Endocrinol. 20, 2406–17. https://doi.org/10.1210/me.2005-0213

Leduc, R.Y.M., 2015. Role of Cecr2 and Candidate Modifier Genes of Cecr2 in the Neural Tube Defect Exencephaly. University of Alberta.

Leduc, R.Y.M., Singh, P., McDermid, H.E., 2017. Genetic backgrounds and modifier genes of NTD mouse models: An opportunity for greater understanding of the multifactorial etiology of neural tube defects. Birth Defects Res. 109, 140–152. https://doi.org/10.1002/bdra.23554

Lee, H.S., Park, J.H., Kim, S.J., Kwon, S.J., Kwon, J., 2010. A cooperative activation loop among SWI/SNF, γ-H2AX and H3 acetylation for DNA double-strand break repair. EMBO J. 29, 1434–1445. https://doi.org/10.1038/emboj.2010.27

Lee, K.Y., Jeong, J.W., Tsai, S.Y., Lydon, J.P., DeMayo, F.J., 2007a. Mouse models of

implantation. Trends Endocrinol. Metab. 18, 234–239.
https://doi.org/10.1016/j.tem.2007.06.002

Lee, K.Y., Jeong, J.W., Wang, J., Ma, L., Martin, J.F., Tsai, S.Y., Lydon, J.P., DeMayo, F.J.,
2007b. Bmp2 Is Critical for the Murine Uterine Decidual Response. Mol. Cell. Biol. 27,
5468–5478. https://doi.org/10.1128/mcb.00342-07

Lee, S.K., Park, E.J., Lee, H.S., Lee, Y.S., Kwon, J., 2012. Genome-wide screen of human
bromodomain-containing proteins identifies Cecr2 as a novel DNA damage response
protein. Mol. Cells 34, 85–91. https://doi.org/10.1007/s10059-012-0112-4

LeMaire-Adkins, R., Radke, K., Hunt, P.A., 1997. Lack of Checkpoint Control at the
Metaphase/Anaphase Transition: A Mechanism of Meiotic Nondisjunction in
Mammalian Females. J. Cell Biol. 139, 1611–1619.
https://doi.org/10.1083/JCB.139.7.1611

Lessard, C., Lothrop, H., Schimenti, J.C., Handel, M.A., 2007. Mutagenesis-generated
mouse models of human infertility with abnormal sperm. Hum. Reprod. 22, 159–
166. https://doi.org/10.1093/humrep/del322

Li, G., Xie, Z.Z., Chua, J.M.W., Wong, P.C., Bian, J., 2015. Hydrogen sulfide protects
testicular germ cells against heat-induced injury. Nitric Oxide - Biol. Chem. 46, 165–
171. https://doi.org/10.1016/j.niox.2014.10.005

Li, M., Wu, Y., Caron, K.M., 2008. Haploinsufficiency for Adrenomedullin Reduces
Pinopodes and Diminishes Uterine Receptivity in Mice1. Biol. Reprod. 79, 1169–
1175. https://doi.org/10.1095/biolreprod.108.069336

Li, M., Yee, D., Magnuson, T.R., Smithies, O., Caron, K.M., 2006. Reduced maternal
expression of adrenomedullin disrupts fertility, placentation, and fetal growth in
mice. J. Clin. Invest. 116, 2653–2662. https://doi.org/10.1172/JCI28462

Li, S., Lu, M.M., Zhou, D., Hammes, S.R., Morrisey, E.E., 2007. GLP-1: A novel zinc finger
protein required in somatic cells of the gonad for germ cell development. Dev. Biol.

301, 106–116. https://doi.org/10.1016/j.ydbio.2006.07.048

Li, W., Wu, J., Kim, S.Y., Zhao, M., Hearn, S.A., Zhang, M.Q., Meistrich, M.L., Mills, A.A., 2014. Chd5 orchestrates chromatin remodelling during sperm development. Nat. Commun. 5:3812. https://doi.org/10.1038/ncomms4812

Li, X., Schimenti, J.C., 2007. Mouse pachytene checkpoint 2 (Trip13) is required for completing meiotic recombination but not synapsis. PLoS Genet. 3, 1365–1376. https://doi.org/10.1371/journal.pgen.0030130

Liao, Y., Smyth, G.K., Shi, W., 2014. FeatureCounts: An efficient general purpose program for assigning sequence reads to genomic features. Bioinformatics 30, 923–930. https://doi.org/10.1093/bioinformatics/btt656

Lim, H., Ma, L., Ma, W.G., Maas, R.L., Dey, S.K., 1999. Hoxa-10 regulates uterine stromal cell responsiveness to progesterone during implantation and decidualization in the mouse. Mol. Endocrinol. 13, 1005–1017. https://doi.org/10.1210/mend.13.6.0284

Lin, Y., Mahan, K., Lathrop, W.F., Myles, D.G., Primakoff, P., 1994. A hyaluronidase activity of the sperm plasma membrane protein PH-20 enables sperm to penetrate the cumulus cell layer surrounding the egg. J. Cell Biol. 125, 1157–1163. https://doi.org/10.1083/jcb.125.5.1157

Lipkin, S.M., Moens, P.B., Wang, V., Lenzi, M., Shanmugarajah, D., Gilgeous, A., Thomas, J., Cheng, J., Touchman, J.W., Green, E.D., Schwartzberg, P., Collins, F.S., Cohen, P.E., 2002. Meiotic arrest and aneuploidy in MLH3-deficient mice. Nat. Genet. 31, 385–390. https://doi.org/10.1038/ng931

Lopez, M., 2012. A Quick, No Frills Approach to Mouse Genotyping. Bio protoc. 2, 1–6. https://doi.org/10.21769/bioprotoc.244

Lubahn, D.B., Moyer, J.S., Golding, T.S., Couse, J.F., Korach, K.S., Smithies, O., 1993. Alteration of reproductive function but not prenatal sexual development after insertional disruption of the mouse estrogen receptor gene. Proc. Natl. Acad. Sci. U.

S. A. 90, 11162–11166.

Luo, M., Yang, F., Leu, N.A., Landaiche, J., Handel, M.A., Benavente, R., La Salle, S., Wang, P.J., 2013. MEIOB exhibits single-stranded DNA-binding and exonuclease activities and is essential for meiotic recombination. Nat. Commun. 4, 2788. https://doi.org/10.1038/ncomms3788

Luo, M., Zhou, J., Leu, N.A., Abreu, C.M., Wang, J., Anguera, M.C., de Rooij, D.G., Jasin, M., Wang, P.J., 2015. Polycomb Protein SCML2 Associates with USP7 and Counteracts Histone H2A Ubiquitination in the XY Chromatin during Male Meiosis. PLoS Genet. 11, 1004954. https://doi.org/10.1371/journal.pgen.1004954

Ma, X., Dong, Y., Matzuk, M.M., Kumar, T.R., 2004. Targeted disruption of luteinizing hormone -subunit leads to hypogonadism, defects in gonadal steroidogenesis, and infertility. Proc. Natl. Acad. Sci. 101, 17294–17299. https://doi.org/10.1073/pnas.0404743101

Macklon, N.S., Geraedts, J.P.M., Fauser, B.C.J.M., 2002. Conception to ongoing pregnancy: The "black box" of early pregnancy loss. Hum. Reprod. Update 8, 333–343. https://doi.org/10.1093/humupd/8.4.333

Mahadevaiah, S.K., Bourc'his, D., De Rooij, D.G., Bestor, T.H., Turner, J.M.A., Burgoyne, P.S., 2008. Extensive meiotic asynapsis in mice antagonises meiotic silencing of unsynapsed chromatin and consequently disrupts meiotic sex chromosome inactivation. J. Cell Biol. 182, 263–276. https://doi.org/10.1083/jcb.200710195

Mahendru, A.A., Daemen, A., Everett, T.R., Wilkinson, I.B., McEniery, C.M., Abdallah, Y., Timmerman, D., Bourne, T., Lees, C.C., 2012. Impact of ovulation and implantation timing on first-trimester crown-rump length and gestational age. Ultrasound Obstet. Gynecol. 40, 630–635. https://doi.org/10.1002/uog.12277

Mäkelä, J., Hobbs, R.M., 2019. Molecular regulation of spermatogonial stem cell renewal and differentiation. Reproduction 158, R169–R187. https://doi.org/10.1530/rep-18-0476

Manterola, M., Page, J., Vasco, C., Berríos, S., Parra, M.T., Viera, A., Rufas, J.S., Zuccotti, M., Garagna, S., Fernández-Donoso, R., 2009. A high incidence of meiotic silencing of unsynapsed chromatin is not associated with substantial pachytene loss in heterozygous male mice carrying multiple simple Robertsonian translocations. PLoS Genet. 5, e1000625. https://doi.org/10.1371/journal.pgen.1000625

Martin, L.A., Assif, N., Gilbert, M., Wijewarnasuriya, D., Seandel, M., 2014. Enhanced fitness of adult spermatogonial stem cells bearing a paternal age-associated FGFR2 mutation. Stem Cell Reports 3, 219–226. https://doi.org/10.1016/j.stemcr.2014.06.007

Matzuk, M.M., Lamb, D.J., 2002. Genetic dissection of mamalian fertility pathways. Nat. Cell Biol. 4, S41–S49. https://doi.org/https://doi.org/10.1038/ncb-nm-fertilityS41

Moens, P.B., Chen, D.J., Shen, Z., Kolas, N., Tarsounas, M., Heng, H.H.Q., Spyropoulos, B., 1997. Rad51 immunocytology in rat and mouse spermatocytes and oocytes. Chromosoma 106, 207–215. https://doi.org/10.1007/s004120050241

Molyneaux, K.A., Stallock, J., Schaible, K., Wylie, C., 2001. Time-lapse analysis of living mouse germ cell migration. Dev. Biol. 240, 488–498. https://doi.org/10.1006/dbio.2001.0436

Monsivais, D., Clementi, C., Peng, J., Fullerton, P.T., Prunskaite-Hyyryläinen, R., Vainio, S.J., Matzuk, M.M., 2017. BMP7 induces uterine receptivity and blastocyst attachment. Endocrinology 158, 979–992. https://doi.org/10.1210/en.2016-1629

Morelli, M.A., Cohen, P.E., 2005. Not all germ cells are created equal: Aspects of sexual dimorphism in mammalian meiosis. Reproduction 130, 761–781. https://doi.org/10.1530/rep.1.00865

Mori, C., Nakamura, N., Dix, D.J., Fujioka, M., Nakagawa, S., Shiota, K., Eddy, E.M., 1997. Morphological analysis of germ cell apoptosis during postnatal testis development in normal and Hsp70-2 knockout mice. Dev. Dyn. 208, 125–136. https://doi.org/10.1002/(SICI)1097-0177(199701)208:1<125::AID-AJA12>3.0.CO;2-5

Nagaoka, S.I., Hassold, T.J., Hunt, P.A., 2012. Human aneuploidy: Mechanisms and new insights into an age-old problem. Nat. Rev. Genet. 13, 493–504. https://doi.org/10.1038/nrg3245

Nagashima, T., Li, Q., Clementi, C., Lydon, J.P., DeMayo, F.J., Matzuk, M.M., 2013. BMPR2 is required for postimplantation uterine function and pregnancy maintenance. J. Clin. Invest. 123, 2539–2550. https://doi.org/10.1172/JCI65710

Namiki, T., Ito, J., Kashiwazaki, N., 2018. Molecular mechanisms of embryonic implantation in mammals: Lessons from the gene manipulation of mice. Reprod. Med. Biol. 17, 331–342. https://doi.org/10.1002/rmb2.12103

Nguyen, T.B., Manova, K., Capodieci, P., Lindon, C., Bottega, S., Wang, X.Y., Refik-Rogers, J., Pines, J., Wolgemuth, D.J., Koff, A., 2002. Characterization and expression of mammalian cyclin B3, a prepachytene meiotic cyclin. J. Biol. Chem. 277, 41960–41969. https://doi.org/10.1074/jbc.M203951200

Niedenberger, B.A., Busada, J.T., Geyer, C.B., 2015. Marker expression reveals heterogeneity of spermatogonia in the neonatal mouse testis. Reproduction 149, 329–338. https://doi.org/10.1530/REP-14-0653

Niri, F.H., 2016. Identification of CECR2 containing chromatin-remodeling complexes and their chromatin-binding sites in mice. University of Alberta.

Nixon, B., Aitken, R.J., McLaughlin, E.A., 2007. New insights into the molecular mechanisms of sperm-egg interaction. Cell. Mol. Life Sci. 64, 1805–1823. https://doi.org/10.1007/s00018-007-6552-x

Nixon, V.L., Levasseur, M., McDougall, A., Jones, K.T., 2002. Ca2+ oscillations promote APC/C-dependent cyclin B1 degradation during metaphase arrest and completion of meiosis in fertilizing mouse eggs. Curr. Biol. 12, 746–750. https://doi.org/10.1016/S0960-9822(02)00811-4

Noguchi, T., Stevens, L.C., 1982. Primordial germ cell proliferation in fetal testes in mouse

strains with high and low incidences of congenital testicular teratomas. J. Natl. Cancer Inst. 69, 907–13.

Nothias, J., Majumder, S., Kaneko, K., DePamphilis, M., 1995. Regulation of gene expression at the beginning of mammalian development. J. Biol. Chem. 270, 22077–22080. https://doi.org/10.1002/(SICI)1520-6408(1998)22:1<43::AID-DVG5>3.0.CO;2-7

Nuño-Ayala, M., Guillén, N., Arnal, C., Lou-Bonafonte, J.M., de Martino, A., García-de-Jalón, J.-A., Gascón, S., Osaba, L., Osada, J., Navarro, M.-A., 2012. Cystathionine β-synthase deficiency causes infertility by impairing decidualization and gene expression networks in uterus implantation sites. Physiol. Genomics 44, 702–716. https://doi.org/10.1152/physiolgenomics.00189.2010

O'Donnell, L., Meachem, S., Stanton, P., McLachlan, R., 2006. Endocrine Regulation of Spermatogenesis in Mammals, in: Neill, J. (Ed.), Knobil and Neill's Physiology of Reproduction. pp. 1017–1069. https://doi.org/10.1201/b18900-5

Oakberg, E.F., 1956. Duration of spermatogenesis in the mouse and timing of stages of the cycle of the seminiferous epithelium. Am. J. Anat. 99, 507–516. https://doi.org/10.1002/aja.1000990307

Oppikofer, M., Bai, T., Gan, Y., Haley, B., Liu, P., Sandoval, W., Ciferri, C., Cochran, A.G., 2017. Expansion of the ISWI chromatin remodeler family with new active complexes. EMBO Rep. 18, 1697–1706. https://doi.org/10.15252/embr.201744011

Pacheco, S., Marcet-Ortega, M., Lange, J., Jasin, M., Keeney, S., Roig, I., 2015. The ATM Signaling Cascade Promotes Recombination-Dependent Pachytene Arrest in Mouse Spermatocytes. PLoS Genet. 11, e1005017. https://doi.org/10.1371/journal.pgen.1005017

Page, J., De La Fuente, R., Manterola, M., Parra, M.T., Viera, A., Berríos, S., Fernández-Donoso, R., Rufas, J.S., 2012. Inactivation or non-reactivation: What accounts better for the silence of sex chromosomes during mammalian male meiosis? Chromosoma

121, 307–326. https://doi.org/10.1007/s00412-012-0364-y

Page, S.L., Hawley, R.S., 2004. The genetics and molecular biology of the synaptonemal complex. Annu. Rev. Cell Dev. Biol. 20, 525–558. https://doi.org/10.1146/annurev.cellbio.19.111301.155141

Pan, H., Ma, P., Zhu, W., Schultz, R.M., 2008. Age-associated increase in aneuploidy and changes in gene expression in mouse eggs. Dev. Biol. 316, 397–407. https://doi.org/10.1016/j.ydbio.2008.01.048

Pan, H., O'Brien, M.J., Wigglesworth, K., Eppig, J.J., Schultz, R.M., 2005. Transcript profiling during mouse oocyte development and the effect of gonadotropin priming and development in vitro. Dev. Biol. 286, 493–506. https://doi.org/10.1016/j.ydbio.2005.08.023

Park, J.H., Park, E.J., Lee, H.S., Kim, S.J., Hur, S.K., Imbalzano, A.N., Kwon, J., 2006. Mammalian SWI/SNF complexes facilitate DNA double-strand break repair by promoting γ-H2AX induction. EMBO J. 25, 3986–3997. https://doi.org/10.1038/sj.emboj.7601291

Parkes, A.S., 1928. The Length of the Oestrous Cycle in the Unmated Normal Mouse: Records of One Thousand Cycles. J. Exp. Biol. 5, 371–377.

Pellestor, F., Anahory, T., Hamamah, S., 2005. Effect of maternal age on the frequency of cytogenetic abnormalities in human oocytes. Cytogenet. Genome Res. 111, 206–212.

Pépin, D., Paradis, F., Perez-Iratxeta, C., Picketts, D.J., Vanderhyden, B.C., 2013. The imitation switch ATPase Snf2l is required for superovulation and regulates Fgl2 in differentiating mouse granulosa cells. Biol. Reprod. 88, 142, 1–9. https://doi.org/10.1095/biolreprod.112.105742

Pepling, M.E., 2006. From primordial germ cell to primordial follicle: Mammalian female germ cell development. Genesis 44, 622–632. https://doi.org/10.1002/dvg.20258

Pepling, M.E., Spradling, A.C., 2001. Mouse ovarian germ cell cysts undergo programmed

breakdown to form primordial follicles. Dev. Biol. 234, 339–351.
https://doi.org/10.1006/dbio.2001.0269

Pesce, M., Wang, X., Wolgemuth, D.J., Schöler, H.R., 1998. Differential expression of the
Oct-4 transcription factor during mouse germ cell differentiation. Mech. Dev. 71, 89–
98. https://doi.org/10.1016/S0925-4773(98)00002-1

Plug, A.W., Xu, J., Reddy, G., Golub, E.I., Ashley, T., 1996. Presynaptic association of Rad51
protein with selected sites in meiotic chromatin. Proc. Natl. Acad. Sci. 93, 5920–
5924. https://doi.org/10.1073/pnas.93.12.5920

Primakoff, P., Myles, D.G., 2002. Penetration, adhesion, and fusion in mammalian sperm-
egg interaction. Science 296, 2183–2185. https://doi.org/10.1126/science.1072029

Psychoyos, A., 1986. Uterine Receptivity for Nidation. Ann. N. Y. Acad. Sci. 476, 36–42.
https://doi.org/10.1111/j.1749-6632.1986.tb20920.x

Ramathal, C.Y., Bagchi, I.C., Taylor, R.N., Bagchi, M.K., 2010. Endometrial decidualization:
Of mice and men. Semin. Reprod. Med. 28, 17–26. https://doi.org/10.1055/s-0029-
1242989

Reddy, P., Liu, L., Adhikari, D., Jagarlamudi, K., Rajareddy, S., Shen, Y., Du, C., Tang, W.,
Hämäläinen, T., Peng, S.L., Lan, Z.-J., Cooney, A.J., Huhtaniemi, I., Liu, K., 2008.
Oocyte-Specific Deletion of Pten Causes Premature Activation of the Primordial
Follicle Pool. Science 319, 611–613. https://doi.org/10.1126/science.1152257

Refik-Rogers, J., Manova, K., Koff, A., 2006. Misexpression of cyclin B3 leads to aberrant
spermatogenesis. Cell Cycle 5, 1966–1973. https://doi.org/10.4161/cc.5.17.3137

Reid, A.T., Redgrove, K., Aitken, R.J., Nixon, B., 2011. Cellular mechanisms regulating
sperm-zona pellucida interaction. Asian J. Androl. 13, 88–96.
https://doi.org/10.1038/aja.2010.74

Reinholdt, L., Ashley, T., Schimenti, J., Shima, N., 2004. Forward Genetic Screens for
Meiotic and Mitotic Recombination-Defective Mutants in Mice, in: Waldman, A.S.

(Ed.), Genetic Recombination: Reviews and Protocols. Humana Press, Totowa, NJ, pp. 87–107. https://doi.org/10.1385/1-59259-761-0:087

Rice, W.R., 1984. Sex Chromosomes and the Evolution of Sexual Dimorphism. Evolution (N. Y). 38, 735–742. https://doi.org/doi:10.1111/j.1558-5646.1984.tb00346.x

Robinson, M.D., Oshlack, A., 2010. A scaling normalization method for differential expression analysis of RNA-seq data. Genome Biol. 11, R25. https://doi.org/10.1186/gb-2010-11-3-r25

Robker, R.L., Watson, L.N., Robertson, S.A., Dunning, K.R., McLaughlin, E.A., Russell, D.L., 2014. Identification of sites of STAT3 action in the female reproductive tract through conditional gene deletion. PLoS One 9, 1–9. https://doi.org/10.1371/journal.pone.0101182

Rochwerger, L., Cohen, D.J., Cuasnicú, P.S., 1992. Mammalian sperm-egg fusion: The rat egg has complementary sites for a sperm protein that mediates gamete fusion. Dev. Biol. 153, 83–90. https://doi.org/10.1016/0012-1606(92)90093-V

Rodriguez, I., Ody, C., Araki, K., Garcia, I., Vassalli, P., 1997. An early and massive wave of germinal cell apoptosis is required for the development of functional spermatogenesis. EMBO J. 16, 2262–2270. https://doi.org/10.1093/emboj/16.9.2262

Roig, I., Dowdle, J.A., Toth, A., De Rooij, D.G., Jasin, M., 2010. Mouse TRIP13/PCH2 Is Required for Recombination and Normal Higher-Order Chromosome Structure during Meiosis. PLoS Genet 6, 1001062. https://doi.org/10.1371/journal.pgen.1001062

Romanienko, P.J., Camerini-Otero, R.D., 2000. The mouse Spo11 gene is required for meiotic chromosome synapsis. Mol. Cell 6, 975–987. https://doi.org/10.1016/S1097-2765(00)00097-6

Romano, F., Tripiciano, A., Muciaccia, B., De Cesaris, P., Ziparo, E., Palombi, F., Filippini, A.,

2005. The contractile phenotype of peritubular smooth muscle cells is locally controlled: Possible implications in male fertility. Contraception 72, 294–297. https://doi.org/10.1016/j.contraception.2005.03.009

Ross, A., Munger, S., Capel, B., 2007. Bmp7 regulates germ cell proliferation in mouse fetal gonads. Sex. Dev. 1, 127–137. https://doi.org/10.1159/000100034

Royo, H., Polikiewicz, G., Mahadevaiah, S.K., Prosser, H., Mitchell, M., Bradley, A., De Rooij, D.G., Burgoyne, P.S., Turner, J.M.A., 2010. Evidence that Meiotic Sex Chromosome Inactivation Is Essential for Male Fertility. Curr. Biol. 20, 2117–2123. https://doi.org/10.1016/j.cub.2010.11.010

Royo, H., Prosser, H., Ruzankina, Y., Mahadevaiah, S.K., Cloutier, J.M., Baumann, M., Fukuda, T., Höög, C., Tóth, A., de Rooij, D.G., Bradley, A., Brown, E.J., Turner, J.M.A., 2013. ATR acts stage specifically to regulate multiple aspects of mammalian meiotic silencing. Genes Dev. 27, 1484–1494. https://doi.org/10.1101/gad.219477.113

Rudolph, M., Döcke, W.D., Müller, A., Menning, A., Röse, L., Zollner, T.M., Gashaw, I., 2012. Induction of Overt menstruation in intact mice. PLoS One 7, 32922. https://doi.org/10.1371/journal.pone.0032922

Russell, L.D., Chiarini-Garcia, H., Korsmeyer, S.J., Knudson, C.M., 2002. Bax-Dependent Spermatogonia Apoptosis Is Required for Testicular Development and Spermatogenesis. Biol. Reprod. 66, 950–958. https://doi.org/10.1095/biolreprod66.4.950

Russell, L.D., Ettlin, R.A., Sinka Hikim, A.P., Clegg, E.D., 1990. Histological and histopathological evaluation of the testis. Cache River Press.

Salle, S. La, Palmer, K., O'brien, M., Schimenti, J.C., Eppig, J., Handel, M.A., 2012. Spata22, a Novel Vertebrate-Specific Gene, Is Required for Meiotic Progress in Mouse Germ Cells. Biol. Reprod. 86, 1–12. https://doi.org/10.1095/biolreprod.111.095752

Sánchez, F., Smitz, J., 2012. Molecular control of oogenesis. Biochim. Biophys. Acta - Mol.

Basis Dis. 1822, 1896–1912. https://doi.org/10.1016/j.bbadis.2012.05.013

Sassone, C.P., 2002. Unique chromatin remodeling and transcriptional regulation in spermatogenesis. Science (80-.). 296, 2176–2178.

Satokata, I., Benson, G., Maas, R., 1995. Hoxa10-deficient mice. Lett. to Nat. 374, 460–463.

Saunders, C.M., Larman, M.G., Parrington, J., Cox, L.J., Royse, J., Blayney, L.M., Swann, K., Lai, F.A., 2002. PLC zeta: a sperm-specific trigger of Ca(2+) oscillations in eggs and embryo development. Development 129, 3533–3544.

Schindelin, J., Arganda-Carreras, I., Frise, E., Kaynig, V., Longair, M., Pietzsch, T., Preibisch, S., Rueden, C., Saalfeld, S., Schmid, B., Tinevez, J.Y., White, D.J., Hartenstein, V., Eliceiri, K., Tomancak, P., Cardona, A., 2012. Fiji: An open-source platform for biological-image analysis. Nat. Methods 9, 676–682. https://doi.org/10.1038/nmeth.2019

Schultz, N., Hamra, F.K., Garbers, D.L., 2003. A multitude of genes expressed solely in meiotic or postmeiotic spermatogenic cells offers a myriad of contraceptive targets. Proc. Natl. Acad. Sci. 100, 12201–12206. https://doi.org/10.1073/pnas.1635054100

Serber, D.W., Runge, J.S., Menon, D.U., Magnuson, T., 2015. The Mouse INO80 Chromatin-Remodeling Complex Is an Essential Meiotic Factor for Spermatogenesis1. Biol. Reprod. 94, 1–9. https://doi.org/10.1095/biolreprod.115.135533

Setterfield, L., Mahadevaiah, S., Mittwoch, U., 1988. Chromosome pairing and germ cell loss in male and female mice carrying a reciprocal translocation. J. Reprod. Fertil. 82, 369–379.

Sha, Q.Q., Dai, X.X., Dang, Y., Tang, F., Liu, J., Zhang, Y.L., Fan, H.Y., 2017. A MAPK cascade couples maternal mRNA translation and degradation to meiotic cell cycle progression in mouse oocytes. Development 144, 452–463.

https://doi.org/10.1242/dev.144410

Sha, Y., Zheng, L., Ji, Z., Mei, L., Ding, L., Lin, S., Wang, X., Yang, X., Li, P., 2018. A novel TEX11 mutation induces azoospermia: A case report of infertile brothers and literature review. BMC Med. Genet. 19, 63: 1–7. https://doi.org/10.1186/s12881-018-0570-4

Shang, E., Nickerson, H.D., Wen, D., Wang, X., Wolgemuth, D.J., 2007. The first bromodomain of Brdt, a testis-specific member of the BET sub-family of double-bromodomain-containing proteins, is essential for male germ cell differentiation. Development 134, 3507–3515. https://doi.org/10.1242/dev.004481

Shi, D., Komatsu, K., Hirao, M., Toyooka, Y., Koyama, H., Tissir, F., Goffinet, A.M., Uemura, T., Fujimori, T., 2014. Celsr1 is required for the generation of polarity at multiple levels of the mouse oviduct. Development 141, 4558–4568. https://doi.org/10.1242/dev.115659

Shi, Y.-Q., Zhuang, X.-J., Xu, B., Hua, J., Liao, S.-Y., Shi, Q., Cooke, H.J., Chunsheng, H., 2013. SYCP3-like X-linked 2 is expressed in meiotic germ cells and interacts with synaptonemal complex central element protein 2 and histone acetyltransferase TIP60. Gene 527, 352–359. https://doi.org/https://doi.org/10.1016/j.gene.2013.06.033

Shiu, P.K.T., Raju, N.B., 2001. Meiotic Silencing by Unpaired DNA. Cell 107, 905–916. https://doi.org/https://doi.org/10.1016/s0092-8674(01)00609-2

Sin, H.S., Namekawa, S.H., 2013. The great escape: Active genes on inactive sex chromosomes and their evolutionary implications. Epigenetics 8, 887–892. https://doi.org/10.4161/epi.25672

Skinner, M.K., Fritz, I.B., 1985. Testicular peritubular cells secrete a protein under androgen control that modulates Sertoli cell functions. Proc. Natl. Acad. Sci. 82, 114–118. https://doi.org/10.1073/pnas.82.1.114

Skinner, M.K., Tung, P.S., Fritz, I.B., 1985. Cooperativity between sertoli cells and testicular peritubular cells in the production and deposition of extracellular matrix components. J. Cell Biol. 100, 1941–1947. https://doi.org/10.1083/jcb.100.6.1941

Snowden, T., Acharya, S., Butz, C., Berardini, M., Fishel, R., 2004. hMSH4-hMSH5 recognizes holliday junctions and forms a meiosis-specific sliding clamp that embraces homologous chromosomes. Mol. Cell 15, 437–451. https://doi.org/10.1016/j.molcel.2004.06.040

Souquet, B., Abby, E., Hervé, R., Finsterbusch, F., Tourpin, S., Le Bouffant, R., Duquenne, C., Messiaen, S., Martini, E., Bernardino-Sgherri, J., Toth, A., Habert, R., Livera, G., 2013. MEIOB Targets Single-Strand DNA and Is Necessary for Meiotic Recombination. PLoS Genet. 9. https://doi.org/10.1371/journal.pgen.1003784

Statistics Canada, n.d. Table 13-10-0416-01 Live births, by age of mother [WWW Document]. Accessed on: 2019-07-17. https://doi.org/https://doi.org/10.25318/1310041601-eng

Stewart, C.A., Behringer, R.R., 2012. Mouse oviduct development. Results Probl. Cell Differ. 55, 247–262. https://doi.org/10.1007/978-3-642-30406-4_14

Stewart, K.R., Veselovska, L., Kim, J., Huang, J., Saadeh, H., Tomizawa, S.I., Smallwood, S.A., Chen, T., Kelsey, G., 2015. Dynamic changes in histone modifications precede de novo DNA methylation in oocytes. Genes Dev. 29, 2449–2462. https://doi.org/10.1101/gad.271353.115

Stocco, C., Telleria, C., Gibori, G., 2007. The molecular control of corpus luteum formation, function, and regression. Endocr. Rev. 28, 117–149. https://doi.org/10.1210/er.2006-0022

Suarez, S., Pacey, A., 2006. Sperm transport in the female reproductive tract. Hum. Reprod. Update 12, 23–37. https://doi.org/10.1093/humupd/dmi047

Suarez, S.S., 2008. Regulation of sperm storage and movement in the mammalian oviduct.

Int. J. Dev. Biol. 52, 455–462. https://doi.org/10.1387/ijdb.072527ss

Suarez, S.S., 1987. Sperm Transport and Motility in the Mouse Oviduct: Observations in Situ. Biol. Reprod. 36, 203–210. https://doi.org/10.1095/biolreprod36.1.203

Takashima, S., Kanatsu-Shinohara, M., Tanaka, T., Morimoto, H., Inoue, K., Ogonuki, N., Jijiwa, M., Takahashi, M., Ogura, A., Shinohara, T., 2015. Functional differences between GDNF-dependent and FGF2-dependent mouse spermatogonial stem cell self-renewal. Stem Cell Reports 4, 489–502. https://doi.org/10.1016/j.stemcr.2015.01.010

Taketo, T., Naumova, A.K., 2013. Oocyte heterogeneity with respect to the meiotic silencing of unsynapsed X chromosomes in the XY female mouse. Chromosoma 122, 337–349. https://doi.org/10.1007/s00412-013-0415-z

Tang, L., Rodriguez-Sosa, J.R., Dobrinski, I., 2012. Germ cell transplantation and testis tissue xenografting in mice. J. Vis. Exp. https://doi.org/10.3791/3545

Terpstra, A.N., 2018. The role of the CECR2 chromatin remodeling complex in mouse developmental gene regulation. University of Alberta.

Terribas, E., Bonache, S., Garcia-arevalo, M., Sanchez, J., Franco, E., Bassas, L., Larriba, S., 2010. Changes in the Expression Profile of the Meiosis-Involved Mismatch Repair Genes in Impaired Human Spermatogenesis. J. Androl. 31, 346–357. https://doi.org/10.2164/jandrol.109.008805

Thompson, P.J., Norton, K.A., Niri, F.H., Dawe, C.E., McDermid, H.E., 2012. CECR2 is involved in spermatogenesis and forms a complex with SNF2H in the testis. J. Mol. Biol. 415, 793–806. https://doi.org/10.1016/j.jmb.2011.11.041

Tilly, J.L., 2001. Commuting the death sentence: How oocytes strive to survive. Nat. Rev. Mol. Cell Biol. 2, 838–848. https://doi.org/10.1038/35099086

Timmons, P.M., Rigby, P.W.J., Poirier, F., 2002. The murine seminiferous epithelial cycle is pre-figured in the Sertoli cells of the embryonic testis. Development 129, 635–47.

Tingen, C.M., Bristol-Gould, S.K., Kiesewetter, S.E., Wellington, J.T., Shea, L., Woodruff, T.K., 2009. Prepubertal Primordial Follicle Loss in Mice Is Not Due to Classical Apoptotic Pathways1. Biol. Reprod. 81, 16–25. https://doi.org/10.1095/biolreprod.108.074898

Toshimori, K., Eddy, E.M., 2014. The Spermatozoon, in: Knobil and Neill's Physiology of Reproduction. Elsevier, pp. 99–148. https://doi.org/10.1016/B978-0-12-397175-3.00003-X

Turner, J.M.A., 2015. Meiotic Silencing in Mammals. Annu. Rev. Genet. 49, 395–412. https://doi.org/10.1146/annurev-genet-112414-055145

Turner, J.M.A., 2007. Meiotic sex chromosome inactivation. Development 134, 1823–1831. https://doi.org/10.1242/dev.000018

Turner, J.M.A., Aprelikova, O., Xu, X., Wang, R., Kim, S., Chandramouli, G.V.R., Barrett, J.C., Burgoyne, P.S., Deng, C.-X., 2004. BRCA1, Histone H2AX Phosphorylation, and Male Meiotic Sex Chromosome Inactivation. Curr. Biol. 14, 2135–2142. https://doi.org/10.1016/j

Turner, J.M.A., Mahadevaiah, S.K., Fernandez-Capetillo, O., Nussenzweig, A., Xu, X., Deng, C.X., Burgoyne, P.S., 2005. Silencing of unsynapsed meiotic chromosomes in the mouse. Nat. Genet. 37, 41–47. https://doi.org/10.1038/ng1484

Tüttelmann, F., Ruckert, C., Röpke, A., 2018. Disorders of spermatogenesis. Medizinische Genet. 30, 12–20. https://doi.org/10.1007/s11825-018-0181-7

van der Lee, S., Boot, L.M., 1956. Spontaneous pseudopregnancy in mice. II. Acta Physiol. Pharmacol. Neerl. 5, 213–215.

Van Ebbenhorst Tengbergen, W.J., 1955. The morphology of the mouse anterior pituitary during the oestrous cycle. Acta Endocrinol. (Copenh). 18, 213–218. https://doi.org/10.1530/acta.0.0180213

Vander Borght, M., Wyns, C., 2018. Fertility and infertility: Definition and epidemiology.

Clin. Biochem. 62, 2–10. https://doi.org/10.1016/j.clinbiochem.2018.03.012

Visconti, P.E., Bailey, J.L., Moore, G.D., Pan, D., Olds-Clarke, P., Kopf, G.S., 1995. Capacitation of mouse spermatozoa. Development 121, 1129–1137.

Vogt, E., Kirsch-Volders, M., Parry, J., Eichenlaub-Ritter, U., 2008. Spindle formation, chromosome segregation and the spindle checkpoint in mammalian oocytes and susceptibility to meiotic error. Mutat. Res. 651, 14–29. https://doi.org/10.1016/j.mrgentox.2007.10.015

Wang, H., Dey, S.K., 2006. Roadmap to embryo implantation: Clues from mouse models. Nat. Rev. Genet. 7, 185–199. https://doi.org/10.1038/nrg1808

Wang, J., Gu, H., Lin, H., Chi, T., 2012. Essential Roles of the Chromatin Remodeling Factor Brg1 in Spermatogenesis in Mice. Biol. Reprod. 86, 186–187. https://doi.org/10.1095/biolreprod.111.097097

Wang, J., Wang, W., Li, S., Han, Y., Zhang, P., Meng, G., Xiao, Y., Xie, L., Wang, X., Sha, J., Chen, Q., Moore, P.K., Wang, R., Xiang, W., Ji, Y., 2018. Hydrogen Sulfide As a Potential Target in Preventing Spermatogenic Failure and Testicular Dysfunction. Antioxidants Redox Signal. 28, 1447–1462. https://doi.org/10.1089/ars.2016.6968

Wang, R.S., Yeh, S., Tzeng, C.R., Chang, C., 2009. Androgen receptor roles in spermatogenesis and fertility: Lessons from testicular cell-specific androgen receptor knockout mice. Endocr. Rev. 30, 119–132. https://doi.org/10.1210/er.2008-0025

Ward, J.O., Reinholdt, L.G., Hartford, S.A., Wilson, L.A., Munroe, R.J., Schimenti, K.J., Libby, B.J., O'Brien, M., Pendola, J.K., Eppig, J., Schimenti, J.C., O'Brien, M., Pendola, J.K., Eppig, J., Schimenti, J.C., 2003. Toward the Genetics of Mammalian Reproduction: Induction and Mapping of Gametogenesis Mutants in Mice. Biol. Reprod. 69, 1615–1625. https://doi.org/10.1095/biolreprod.103.019877

Wassarman, P.M., Kinloch, R.A., 1992. Gene expression during oogenesis in mice. Mutat. Res. Genet. Toxicol. 296, 3–15. https://doi.org/10.1016/0165-1110(92)90028-8

Welsh, M., Moffat, L., Belling, K., de França, L.R., Segatelli, T.M., Saunders, P.T.K., Sharpe, R.M., Smith, L.B., 2012. Androgen receptor signalling in peritubular myoid cells is essential for normal differentiation and function of adult Leydig cells. Int. J. Androl. 35, 25–40. https://doi.org/10.1111/j.1365-2605.2011.01150.x

Whitten, M.K., 1957. Effect of exteroceptive factors on the oestrous cycle of mice. Nature 180, 1436.

Wilcox, A., Weinberg, C., O'Connor, J., Baird, D., Schlatterer, J., Canfield, R., Armstrong, E., Nisula, B., 1988. Incidence of early loss of pregnancy. N. Engl. J. Med. 319, 189–194. https://doi.org/https://doi.org/10.1056/NEJM198807283190401

Wojtasz, L., Cloutier, J.M., Baumann, M., Daniel, K., Varga, J., Fu, J., Anastassiadis, K., Francis Stewart, A., Reményi, A., Turner, J.M.A., Tóth, A., 2012. Meiotic DNA double-strand breaks and chromosome asynapsis in mice are monitored by distinct HORMAD2-independent and -dependent mechanisms. Genes Dev. 26, 958–973. https://doi.org/10.1101/gad.187559.112

Woods, L., Perez-Garcia, V., Hemberger, M., 2018. Regulation of Placental Development and Its Impact on Fetal Growth—New Insights From Mouse Models. Front. Endocrinol. (Lausanne). 9, 1–18. https://doi.org/10.3389/fendo.2018.00570

Xiong, M., Zhu, Z., Tian, S., Zhu, R., Bai, S., Fu, K., Davis, J.G., Sun, Z., Baur, J.A., Zheng, K., Ye, L., 2017. Conditional ablation of Raptor in the male germline causes infertility due to meiotic arrest and impaired inactivation of sex chromosomes. FASEB J. 31, 3934–3949. https://doi.org/10.1096/fj.201700251R

Xu, Y., Greenberg, R.A., Schonbrunn, E., Jeremy Wang, P., 2017. Meiosis-specific proteins MEIOB and SPATA22 cooperatively associate with the single-stranded DNA-binding replication protein A complex and DNA double-strand breaks. Biol. Reprod. 96, 1096–1104. https://doi.org/10.1093/biolre/iox040

Yamada, M., De Chiara, L., Seandel, M., 2016. Spermatogonial stem cells: Implications for genetic disorders and prevention. Stem Cells Dev. 25, 1483–1494.

https://doi.org/10.1089/scd.2016.0210

Yang, F., Silber, S., Leu, N.A., Oates, R.D., Marszalek, J.D., Skaletsky, H., Brown, L.G., Rozen, S., Page, D.C., Wang, P.J., 2015. TEX11 is mutated in infertile men with azoospermia and regulates genome-wide recombination rates in mouse. EMBO Mol. Med. 7, 1198–1210. https://doi.org/10.15252/emmm.201404967

Yatsenko, A., Georgiadis, A., Ropke, A., Berman, A., Jaffe, T., Olszewska, M., Westernstroer, B., Sanfilippo, J., Kurpisz, M., Rajkovic, A., Yatsenko, S., Kliesch, S., Schlatt, S., Tuttelmann, F., 2015. X-Linked TEX11 Mutations, Meiotic Arrest and Azoospermia in Infertile Men. J. Urol. Surg. 2, 162–162. https://doi.org/10.4274/jus.2015.03.006

Yatsenko, S.A., Rajkovic, A., 2019. Genetics of human female infertility. Biol. Reprod. 101, 549–566. https://doi.org/10.1093/biolre/ioz084

Yeom, Y.I.I., Fuhrmann, G., Ovitt, C.E., Brehm, A., Ohbo, K., Gross, M., Hübner, K., Schöler, H.R., 1996. Germline regulatory element of Oct-4 specific for the totipotent cycle of embryonal cells. Development 122, 881–894.

Yip, D.J., Corcoran, C.P., Alvarez-Saavedra, M., DeMaria, A., Rennick, S., Mears, A.J., Rudnicki, M.A., Messier, C., Picketts, D.J., 2012. Snf2l Regulates Foxg1-Dependent Progenitor Cell Expansion in the Developing Brain. Dev. Cell 22, 871–878. https://doi.org/10.1016/j.devcel.2012.01.020

Yoon, S.-Y., Jellerette, T., Salicioni, A.M., Lee, H.C., Yoo, M., Coward, K., Parrington, J., Grow, D., Cibelli, J.B., Visconti, P.E., Mager, J., Fissore, R.A., 2008. Human sperm devoid of PLC, zeta 1 fail to induce Ca2+ release and are unable to initiate the first step of embryo development. J. Clin. Invest. 118, 3671–3681. https://doi.org/10.1172/JCI36942.the

Yoshida, S., 2019. Heterogeneous, dynamic, and stochastic nature of mammalian spermatogenic stem cells, 1st ed, Current Topics in Developmental Biology. Elsevier Inc. https://doi.org/10.1016/bs.ctdb.2019.04.008

Yoshida, S., Sukeno, M., Nakagawa, T., Ohbo, K., Nagamatsu, G., Suda, T., Nabeshima, Y., 2006. The first round of mouse spermatogenesis is a distinctive program that lacks the self-renewing spermatogonia stage. Development 133, 1495–1505. https://doi.org/10.1242/dev.02316

Yoshida, S., Takakura, A., Ohbo, K., Abe, K., Wakabayashi, J., Yamamoto, M., Suda, T., Nabeshima, Y.I., 2004. Neurogenin3 delineates the earliest stages of spermatogenesis in the mouse testis. Dev. Biol. 269, 447–458. https://doi.org/10.1016/j.ydbio.2004.01.036

Yu, Y.-H., Siao, F.-P., Hsu, L.C.-L., Yen, P.H., 2012. TEX11 Modulates Germ Cell Proliferation by Competing with Estrogen Receptor β for the Binding to HPIP. Mol. Endocrinol. 26, 630–642. https://doi.org/10.1210/me.2011-1263

Yuan, L., Liu, J.G., Hoja, M.R., Wilbertz, J., Nordqvist, K., Höög, C., 2002. Female germ cell aneuploidy and embryo death in mice lacking the meiosis-specific protein SCP3. Science 296, 1115–1118. https://doi.org/10.1126/science.1070594

Zerbino, D.R., Achuthan, P., Akanni, W., Ridwan Amode, M., Barrell, D., Bhai, J., Billis, K., Cummins, C., Gall, A., García, C., Gir´girón, G., Gil, L., Gordon, L., Haggerty, L., Haskell, E., Hourlier, T., Izuogu, O.G., Janacek, S.H., Juettemann, T., Kiang To, J., Laird, M.R., Lavidas, I., Liu, Z., Loveland, J.E., Maurel, T., Mclaren, W., Moore, B., Mudge, J., Murphy, D.N., Newman, V., Nuhn, M., Ogeh, D., Ong, C.K., Parker, A., Patricio, M., Riat, H.S., Schuilenburg, H., Sheppard, D., Sparrow, H., Taylor, K., Thormann, A., Vullo, A., Walts, B., Zadissa, A., Frankish, A., Hunt, S.E., Kostadima, M., Langridge, N., Martin, F.J., Muffato, M., Perry, E., Ruffier, M., Staines, D.M., Trevanion, S.J., Aken, B.L., Cunningham, F., Yates, A., Flicek, P., 2018. Ensembl 2018. Nucleic Acids Res. 46, D754–D761. https://doi.org/10.1093/nar/gkx1098

Zhang, Ling, Patterson, A.L., Zhang, Lihua, Teixeira, J.M., Pru, J.K., 2012. Endometrial stromal beta-catenin is required for steroid-dependent mesenchymal-epithelial cross talk and decidualization. Reprod. Biol. Endocrinol. 10, 1–13. https://doi.org/10.1186/1477-7827-10-75

Zhang, S., Kong, S., Wang, B., Cheng, X., Chen, Y., Wu, W., Wang, Q., Shi, J., Zhang, Y., Wang, S., Lu, J., Lydon, J.P., DeMayo, F., Pear, W.S., Han, H., Lin, H., Li, L., Wang, Hongmei, Wang, Y.L., Li, B., Chen, Q., Duan, E., Wang, Haibin, 2014. Uterine Rbpj is required for embryonic-uterine orientation and decidual remodeling via Notch pathway-independent and -dependent mechanisms. Cell Res. 24, 925–942. https://doi.org/10.1038/cr.2014.82

Zhang, Y., Yang, Z., Yang, Y., Wang, S., Shi, L., Xie, W., Sun, K., Zou, K., Wang, L., Xiong, J., Xiang, J., Wu, J., 2011. Production of transgenic mice by random recombination of targeted genes in female germline stem cells. J. Mol. Cell Biol. 3, 132–141. https://doi.org/10.1093/jmcb/mjq043

Zhao, G.-Q., Garbers, D.L., 2002. Male Germ Specification. Dev. Cell 2, 537–547.

Zhao, G.Q., Chen, Y.X., Liu, X.M., Xu, Z., Qi, X., 2001. Mutation in Bmp7 exacerbates the phenotype of Bmp8a mutants in spermatogenesis and epididymis. Dev. Biol. 240, 212–222. https://doi.org/10.1006/dbio.2001.0448

Zhou, H., Grubisic, I., Zheng, K., He, Y., Wang, P.J., Kaplan, T., Tjian, R., 2013. Taf7l cooperates with Trf2 to regulate spermiogenesis. Proc. Natl. Acad. Sci. 110, 16886–16891. https://doi.org/10.1073/pnas.1317034110

Zhuang, X.J., Tang, W.H., Feng, X., Liu, C.Y., Zhu, J.L., Yan, J., Liu, D.F., Liu, P., Qiao, J., 2016. Trim27 interacts with Slx2, is associated with meiotic processes during spermatogenesis. Cell Cycle 15, 2576–2584. https://doi.org/10.1080/15384101.2016.1174796

Appendices

Appendix A: Primers

Table A.1: Primers used for genotyping

Name	Oligonucleotide sequence 5'-3'	Purpose
IngeniousLox1	TTAGAATAGGTGAGGGAGGAG	*Cecr2^{Del}* genotyping
Ingenious SDL2	GTAGCGCCTATTTGTAATGGTCA	*Cecr2^{Del}* genotyping
LoxCECR2_DEL3R	AATGGTGGCGAAATCAACTC	*Cecr2^{Del}* genotyping
SRY FOR	GAGAGCATGGAGGGGCAT	SRY genotyping
SRY REV	CCACTCCTCTGTGACACT	SRY genotyping
Mmu Intron7 F4	CCCCATTTATTTGCTTGAGCTG	*Cecr2^{GT}* genotyping
Mmu Intron7 R4	CACGAACAATGGAAGGAATGA	*Cecr2^{GT}* genotyping
pGT1R4	ACGCCATACAGTCCTCTTCACATC	*Cecr2^{GT}* genotyping
Ex4genoF	TGTCTGGTTGATCTGGTTGGAA	*Cecr2^{Ex4}* genotyping
Ex4genoNormR	CAGGCAGATGAAATTCAGAGAGG	*Cecr2^{Ex4}* genotyping
Ex4genoMutR	TTGGGCAAGAACATAAAGTGACC	*Cecr2^{Ex4}* genotyping

Table A.2: Primers used for qPCR

Name	Oligonucleotide sequence 5'-3'	Purpose
Fgr FOR	CCCTCTTTGGCAGATTCAC	*Fgr* qPCR
Fgr REV	TTCATACCTGGGTAGGGAAC	*Fgr* qPCR
Hfm1 FOR	GGGAAATGAAGTCTGGGATG	*Hfm1* qPCR
Hfm1 REV	GAGTGTCTCCAAATCCTGATG	*Hfm1* qPCR
Msh4 FOR	ATAACCAGGACTACAGGAGTAA	*Msh4* qPCR
Msh4 REV	CTGATCGTCTCCACATCAAC	*Msh4* qPCR
Hormad2 FOR	GGCAGTCAAGTCCAAAGAA	*Hormad2* qPCR
Hormad2 REV	GGAATGAAGACTGTCACTGG	*Hormad2* qPCR
Spata22 FOR	AACAGTGAATACAGGGCAAATA	*Spata22* qPCR
Spata22 REV	CAGGCACTTTGGCTTCTT	*Spata22* qPCR
Meiob FOR	CTTTGGGCTGCACGATAA	*Meiob* qPCR
Meiob REV	CCCTTGCTCTGTGTGATAAA	*Meiob* qPCR
Ptchd3 FOR	GCATGGCTGACTCACTTT	*Ptchd3* qPCR
Ptchd3 REV	AGTAGACCACCTCTATCTCTTC	*Ptchd3* qPCR
Cbs FOR	GAAGTCTGCAAAGTCCTCTAC	*Cbs* qPCR
Cbs REV	TGGTCTCGTGATTGGATCT	*Cbs* qPCR
Glp1 FOR	GCGAATGGGTATTGAGAAGG	*Glp1* qPCR
Glp1 REV	TCTTCCAGGCAAGCTGTA	*Glp1* qPCR
Bmp7 FOR	CAGACACTGGTTCACTTCATC	*Bmp7* qPCR
Bmp7 REV	TAGAGCTGTCGTCGAAGTAG	*Bmp7* qPCR
Tex11 FOR	AAAGTGTCTCATGCGGATTAT	*Tex11* qPCR
Tex11 REV	CAGGAGTGCTGTATTCAAGTAG	*Tex11* qPCR
Scml2 FOR	AAGCAATGCCAGCTCTTT	*Scml2* qPCR
Scml2 REV	GAGGTAGAAGACTTTGGTTGTT	*Scml2* qPCR
Taf7l FOR	GGATGTTTCTCAGATGCTTGTA	*Taf7l* qPCR
Taf7l REV	CTGCCTTCCCTTCACTAATTC	*Taf7l* qPCR
Slx2 FOR	GACATTAACCGTGCTCTTAGT	*Slx2* qPCR
Slx2 REV	CTTCATTAAGCTGTGCCATTG	*Slx2* qPCR
Rhox13 FOR	TGCCACTGTCAAGGAGAG	*Rhox13* qPCR
Rhox13 REV	GGAGGAGTCGGAGGAGTC	*Rhox13* qPCR
Ccnb3 FOR	TTGGTGGAGATACAGGGAT	*Ccnb3* qPCR
Ccnb3 REV	CTTGCATTGTGCCTTCATTAG	*Ccnb3* qPCR
Cecr2 FOR	CGCACAAAGCCAGAGTT	*Cecr2* qPCR
Cecr2 REV	AGCATGGGAGTTTCCTCTA	*Cecr2* qPCR
Gapdh FOR	GGAGAAACCTGCCAAGTATG	*Gapdh* qPCR
Gapdh REV	AACCTGGTCCTCAGTGTAG	*Gapdh* qPCR

Appendix B: Additional RNA-seq information

Table B.1: RNA sequencing sample information. Sequencing information provided by the GenomeQuebec Nanuq server. MT refers to *Cecr2$^{GT/Del}$* samples, while WT refers to *Cecr2$^{+/+}$* samples. The numbers in the sample names are the original ID numbers of the mice. Quality refers to read quality, with values over 35 considered excellent.

Sample Name	Reads (millions)	Bases (millions)	Average Quality
MT_2043	42.44	8487.16	39
MT_2165	37.26	7451.6	39
MT_2166	44.23	8845.85	39
MT_2416	36.92	7383.03	39
MT_2425	34.72	6944.06	39
WT_2004	24.19	4838.3	39
WT_2005	44.31	8861.96	39
WT_2418	43.35	8669.94	39
WT_2430	35.37	7074.85	38
WT_2436	41.84	8367.82	39
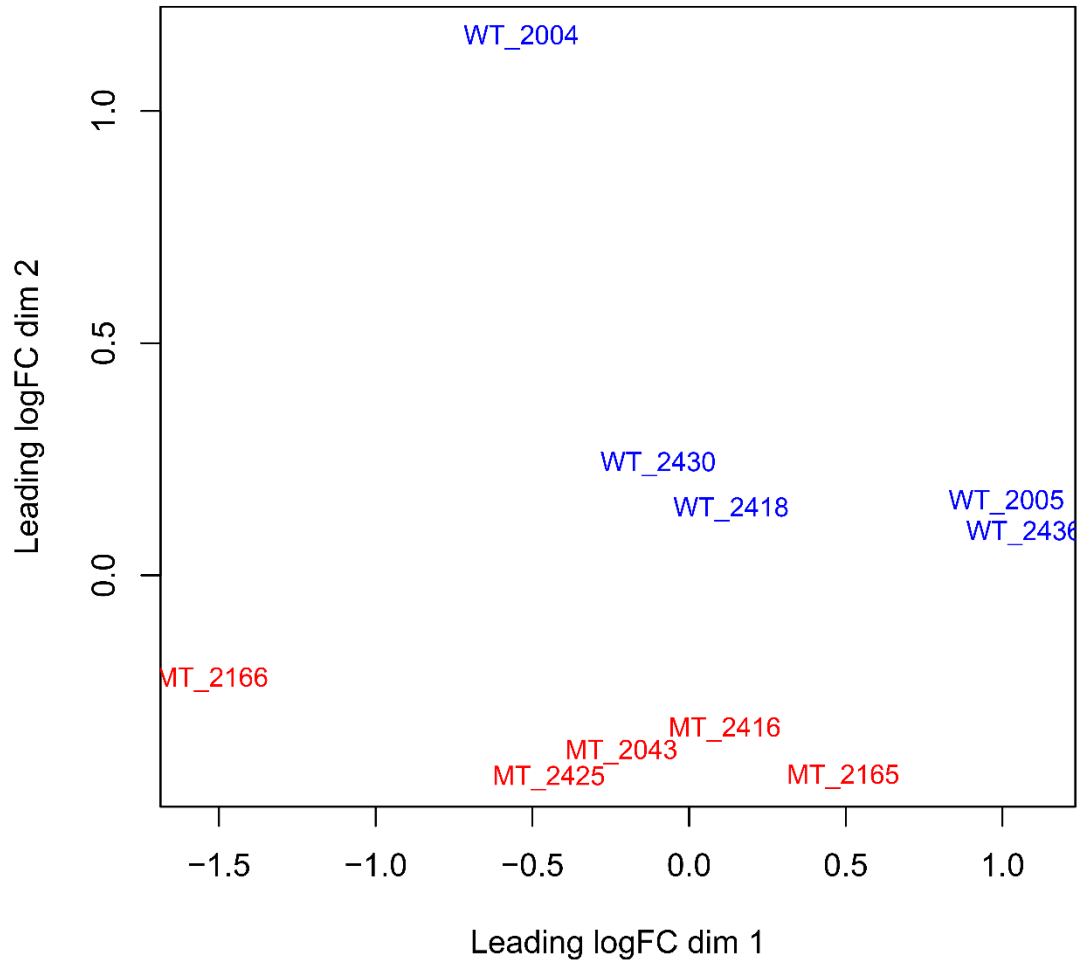
Figure B.1: Multi-dimensional scaling (MDS) plot of RNA-seq samples. *Cecr2+/+* (WT) and *Cecr2GT/Del* (MT) samples were plotted to assess their similarity. *(Dr. Arun Kommadath)*
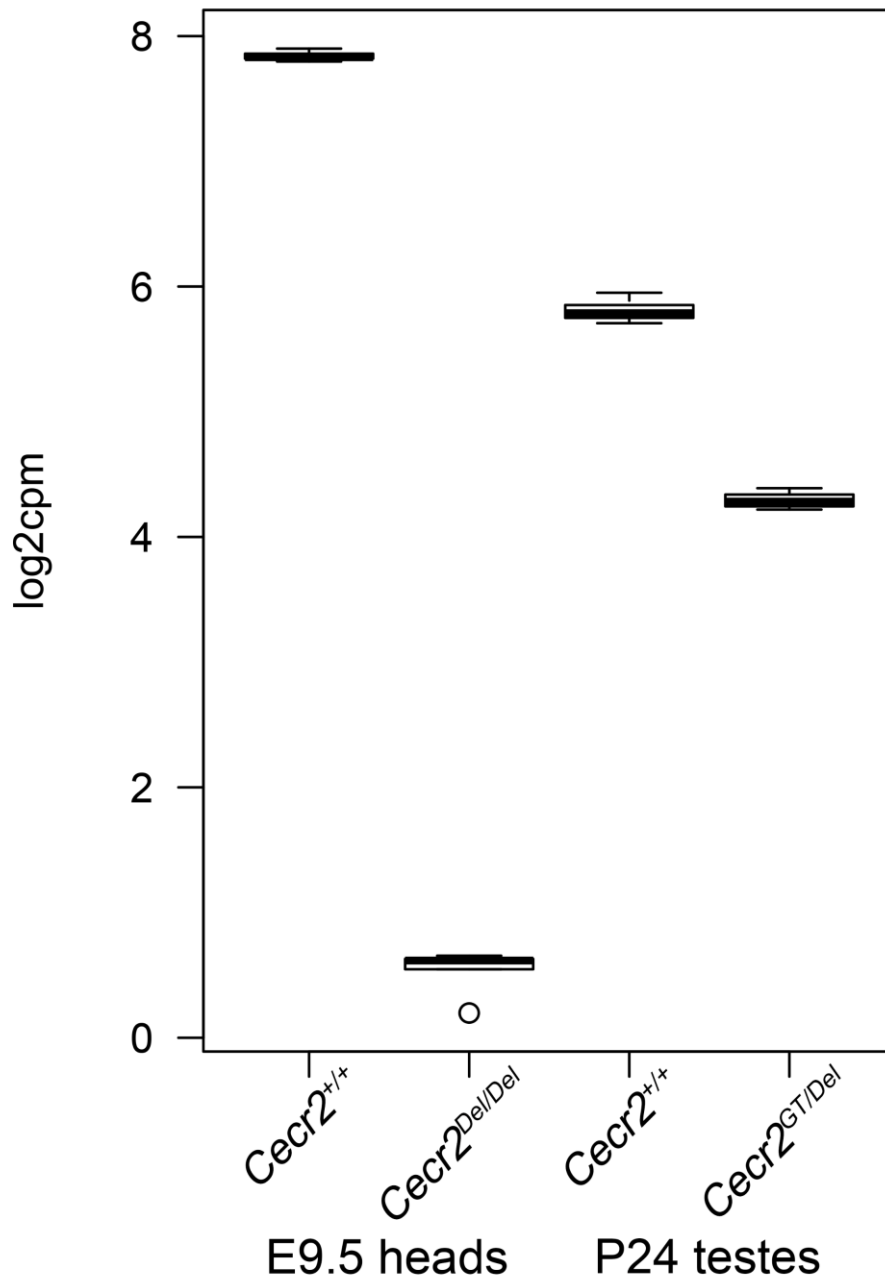
Figure B.2: Comparison of *Cecr2* expression levels between embryonic heads at the time of neurulation (E9.5) and P24 testes. In wildtype mice, *Cecr2* is expressed more highly in the head at E9.5 than in the testes at P24. Due to one copy of the *Cecr2^{GT}* allele in mutant testes, the expression is much higher than in the *Cecr2^{Del/Del}* head. *(Data is from both the RNA-seq in this study and Terpstra, 2018, figure generated by Dr. Arun Kommadath)*

Table B.2: Enriched GO terms for upregulated genes. Enrichment analysis was done using the Database for Annotation, Visualization, and Integrated Discovery (DAVID) v6.8 (Huang et al., 2009a, 2009b) with the assistance of Niall Pollock.

Term	Count	List Total	Pop. Hits	Pop. Total	BH p-value	Genes
GO:0007275 multicellular organism development	20	84	856	13380	6.42E-04	*L1cam, Prdm1, Sox11, Taf7l, Bmp7, Bex1, Dkk3, Dmbx1, Dab1, Dlx1, Draxin, Dcx, Ebf2, Hey2, Hhex, Hoxa7, Hoxd13, Ryr2, Tnfrsf12a, Zglp1*
GO:0007286 spermatid development	7	84	104	13380	1.62E-02	*1700013H16Rik, 3830403N18Rik, Taf7l, Xlr4a, Xlr5c, Xlr, Gm773*

Pop.= Population of expressed genes used as background, BH p-value= Benjamini Hochberg corrected p-value.

Table B.3: Enriched GO terms for downregulated genes. Enrichment analysis was done using the Database for Annotation, Visualization, and Integrated Discovery (DAVID) v6.8 (Huang et al., 2009a, 2009b) with the assistance of Niall Pollock.

Term	Count	List Total	Pop. Hits	Pop. Total	BH p-value	Genes
GO:0007275 multicellular organism development	24	135	856	13380	9.37E-03	*Eya4, Nat8f2, Pou5f1, D130043K22Rik, Radil, Tbx4, Tbx5, Celsr2, Chrd, Dppa4, Hemgn, Mtl5, Ntrk3, Pax9, Piwil1, Piwil2, Prm1, Prm2, Satb2, Trp63, Tnp2, Vax2, Wnt3a, Zfa-ps*
GO:0051321 meiotic cell cycle	8	135	94	13380	1.60E-02	*4930528F23Rik, Ccnb1ip1, Hfm1, Hormad2, Msh4, Piwil1, Piwil2, Spata22*

Pop.= Population of expressed genes used as background, BH p-value= Benjamini Hochberg corrected p-value.

Table B.4: Differentially expressed genes between _Cecr2_^{+/+} and _Cecr2_^{GT/Del} testes at P24.
Chr.= chromosome; FC= fold change, where FC>1 indicates higher expression in _Cecr2_^{GT/Del} testes; FDR= false discovery rate adjusted significance

Ensembl ID	Gene name	Chr.	Type	FC	FDR
ENSMUSG00000071226	Cecr2	6	protein coding	0.34	2.50E-56
ENSMUSG00000069743	Zfp820	17	protein coding	0.27	6.09E-40
ENSMUSG00000068349	Gml	15	protein coding	0.51	6.86E-24
ENSMUSG00000006906	Stambp	6	protein coding	0.47	3.52E-21
ENSMUSG00000051592	Ccnb3	X	protein coding	2.52	5.06E-21
ENSMUSG00000068600	Hemt1	15	protein coding	0.52	2.49E-20
ENSMUSG00000043300	B3galnt1	3	protein coding	0.50	1.07E-18
ENSMUSG00000085062	4933404O12Rik	5	lincRNA	0.55	1.83E-18
ENSMUSG00000024266	Adad2	8	protein coding	0.51	2.10E-18
ENSMUSG00000039198	Ptchd3	11	protein coding	0.53	1.33E-17
ENSMUSG00000024905	Mtl5	19	protein coding	0.61	1.56E-17
ENSMUSG00000005493	Msh4	3	protein coding	0.51	1.15E-15
ENSMUSG00000033644	Piwil2	14	protein coding	0.59	2.93E-15
ENSMUSG00000051984	Sec31b	19	protein coding	0.43	7.36E-15
ENSMUSG00000009596	Taf7l	X	protein coding	1.58	2.14E-14
ENSMUSG00000001819	Hoxd13	2	protein coding	4.90	1.48E-11
ENSMUSG00000023908	Pkmyt1	17	protein coding	0.65	2.94E-11
ENSMUSG00000024155	4930528F23Rik	17	protein coding	0.61	4.03E-11
ENSMUSG00000029576	Radil	5	protein coding	0.66	4.03E-11
ENSMUSG00000046101	6030422M02Rik	1	protein coding	0.51	5.55E-11
ENSMUSG00000009941	Nxf2	X	protein coding	1.61	9.93E-11
ENSMUSG00000045928	4933440M02Rik	7	protein coding	0.65	1.22E-10
ENSMUSG00000000037	Scml2	X	protein coding	1.58	1.32E-10
ENSMUSG00000021541	Trpc7	13	protein coding	0.35	1.35E-10
ENSMUSG00000073177	Gm773	X	protein coding	2.03	1.37E-10
ENSMUSG00000030510	Lass3	7	protein coding	0.62	1.75E-10
ENSMUSG00000029423	Piwil1	5	protein coding	0.66	1.96E-10
ENSMUSG00000047189	Gm9818	17	pseudogene	0.28	2.36E-10
ENSMUSG00000086635	4932415G12Rik	10	lincRNA	0.66	2.39E-10
ENSMUSG00000049576	Zfa	10	protein coding	0.45	2.41E-10
ENSMUSG00000020033	4930463O16Rik	10	lincRNA	0.52	3.81E-10
ENSMUSG00000087044	1700042G15Rik	4	lincRNA	0.63	6.63E-10
ENSMUSG00000075502	Gm5465	14	protein coding	0.59	1.02E-09
ENSMUSG00000020419	Hormad2	11	protein coding	0.60	1.60E-09
ENSMUSG00000032782	Cntrob	11	protein coding	0.63	1.78E-09

Ensembl ID	Gene name	Chr.	Type	FC	FDR
ENSMUSG00000037578	Pkd2l1	19	protein coding	0.60	2.05E-09
ENSMUSG00000060600	Eno3	11	protein coding	0.65	2.28E-09
ENSMUSG00000033318	Gstt2	10	protein coding	0.64	2.79E-09
ENSMUSG00000085601	Gm4969	7	protein coding	1.77	3.13E-09
ENSMUSG00000027221	Chst1	2	protein coding	0.62	5.85E-09
ENSMUSG00000070777	Ceacam20	7	protein coding	0.47	7.05E-09
ENSMUSG00000053873	Aym1	5	protein coding	0.51	9.26E-09
ENSMUSG00000068740	Celsr2	3	protein coding	0.62	1.04E-08
ENSMUSG00000043410	Hfm1	5	protein coding	0.59	1.44E-08
ENSMUSG00000009670	Tex11	X	protein coding	1.57	2.17E-08
ENSMUSG00000035964	Tmem59l	8	protein coding	0.60	2.50E-08
ENSMUSG00000050197	Rhox13	X	protein coding	1.78	2.96E-08
ENSMUSG00000021379	Id4	13	protein coding	0.63	3.08E-08
ENSMUSG00000074358	Ccdc61	7	protein coding	0.65	3.24E-08
ENSMUSG00000042271	Nxt2	X	protein coding	1.64	3.54E-08
ENSMUSG00000034391	Fbxo15	18	protein coding	0.58	3.99E-08
ENSMUSG00000008496	Pou2f2	7	protein coding	0.59	4.10E-08
ENSMUSG00000027811	4930579G24Rik	3	protein coding	0.63	4.37E-08
ENSMUSG00000024851	Pitpnm1	19	protein coding	0.65	4.63E-08
ENSMUSG00000051890	Klhdc1	12	protein coding	0.65	6.20E-08
ENSMUSG00000067629	Syngap1	17	protein coding	0.67	7.44E-08
ENSMUSG00000027180	Fbxo3	2	protein coding	0.65	8.16E-08
ENSMUSG00000031397	Tktl1	X	protein coding	1.61	1.03E-07
ENSMUSG00000087523	Gm12319	11	antisense	0.60	1.31E-07
ENSMUSG00000029121	Crmp1	5	protein coding	0.40	1.43E-07
ENSMUSG00000042386	Tex13	X	protein coding	1.59	1.58E-07
ENSMUSG00000030339	Ltbr	6	protein coding	1.60	1.71E-07
ENSMUSG00000020299	4930524B15Rik	11	protein coding	0.66	1.76E-07
ENSMUSG00000038738	Shank1	7	protein coding	0.60	1.87E-07
ENSMUSG00000026123	Plekhb2	1	protein coding	0.64	1.99E-07
ENSMUSG00000028874	Fgr	4	protein coding	0.34	2.00E-07
ENSMUSG00000046774	8030474K03Rik	X	protein coding	1.51	2.00E-07
ENSMUSG00000083773	Gm13394	2	pseudogene	0.60	2.81E-07
ENSMUSG00000086540	Scml1	X	lincRNA	1.93	3.08E-07
ENSMUSG00000073804	Nps	7	protein coding	0.45	3.33E-07
ENSMUSG00000035395	Pet2	X	protein coding	1.55	3.55E-07
ENSMUSG00000015787	Abo	2	protein coding	0.48	4.40E-07
ENSMUSG00000056771	Gm10010	6	protein coding	0.59	9.68E-07

Ensembl ID	Gene name	Chr.	Type	FC	FDR
ENSMUSG00000018168	Ikzf3	11	protein coding	2.63	1.05E-06
ENSMUSG00000072653	Zfp783	6	pseudogene	0.57	1.12E-06
ENSMUSG00000069825	Spata22	11	protein coding	0.61	1.26E-06
ENSMUSG00000035557	Krt17	11	protein coding	5.06	1.52E-06
ENSMUSG00000030772	Dkk3	7	protein coding	1.95	1.52E-06
ENSMUSG00000023443	Esx1	X	protein coding	1.60	1.58E-06
ENSMUSG00000041141	Pnmal1	7	protein coding	0.64	2.13E-06
ENSMUSG00000071470	Ccnb1ip1	14	protein coding	0.62	2.63E-06
ENSMUSG00000081348	Gm13878	2	pseudogene	0.42	3.18E-06
ENSMUSG00000057609	Lce1a1	3	protein coding	0.33	4.44E-06
ENSMUSG00000080901	Gm6215	X	pseudogene	1.92	4.80E-06
ENSMUSG00000020870	Cdc34-ps	11	protein coding	0.35	6.07E-06
ENSMUSG00000078932	CN725425	15	protein coding	0.59	6.53E-06
ENSMUSG00000050840	Cdh20	1	protein coding	0.49	7.62E-06
ENSMUSG00000086904	Gm13404	2	lincRNA	0.37	7.96E-06
ENSMUSG00000042401	Crtac1	19	protein coding	0.63	7.96E-06
ENSMUSG00000058317	Ube2e2	14	protein coding	0.61	8.39E-06
ENSMUSG00000027444	8030411F24Rik	2	protein coding	1.54	9.02E-06
ENSMUSG00000086503	Xist	X	non-coding	1.81	9.02E-06
ENSMUSG00000042066	Tmcc2	1	protein coding	0.55	9.83E-06
ENSMUSG00000085379	2310058D17Rik	11	lincRNA	0.62	1.70E-05
ENSMUSG00000031103	Elf4	X	protein coding	1.61	1.76E-05
ENSMUSG00000043419	A030009H04Rik	11	lincRNA	0.65	2.11E-05
ENSMUSG00000019810	Fuca2	10	protein coding	1.51	2.17E-05
ENSMUSG00000074674	Gm10742	3	protein coding	0.46	2.45E-05
ENSMUSG00000038331	Satb2	1	protein coding	0.56	2.58E-05
ENSMUSG00000052595	A1cf	19	protein coding	0.65	3.09E-05
ENSMUSG00000034777	Vax2	6	protein coding	0.52	3.09E-05
ENSMUSG00000006711	D130043K22Rik	13	protein coding	0.58	3.49E-05
ENSMUSG00000048155	1700014N06Rik	X	protein coding	1.86	3.95E-05
ENSMUSG00000041596	Vmn1r90	7	protein coding	0.66	4.82E-05
ENSMUSG00000061397	Krt79	15	protein coding	2.32	4.88E-05
ENSMUSG00000002325	Irf9	14	protein coding	1.55	4.96E-05
ENSMUSG00000029005	2610109H07Rik	4	protein coding	2.18	5.19E-05
ENSMUSG00000025813	Homer2	7	protein coding	1.72	5.35E-05
ENSMUSG00000030523	Trpm1	7	protein coding	0.60	5.68E-05
ENSMUSG00000008999	Bmp7	2	protein coding	1.61	5.72E-05
ENSMUSG00000025574	Tk1	11	protein coding	1.61	6.87E-05

Ensembl ID	Gene name	Chr.	Type	FC	FDR
ENSMUSG00000050132	Sarm1	11	protein coding	0.62	6.87E-05
ENSMUSG00000087146	Gm15205	X	lincRNA	2.03	7.54E-05
ENSMUSG00000020151	Ptprr	10	protein coding	0.59	7.54E-05
ENSMUSG00000079349	Magea5	X	protein coding	1.74	7.63E-05
ENSMUSG00000081743	Gm4911	X	pseudogene	2.19	7.79E-05
ENSMUSG00000037922	Bank1	3	protein coding	0.45	8.11E-05
ENSMUSG00000032323	Cyp11a1	9	protein coding	0.66	9.06E-05
ENSMUSG00000031093	Dock11	X	protein coding	1.54	9.56E-05
ENSMUSG00000055780	Usp26	X	protein coding	1.56	0.00010
ENSMUSG00000091119	Ccdc152	15	protein coding	0.64	0.00012
ENSMUSG00000079845	Xlr4a	X	protein coding	1.63	0.00013
ENSMUSG00000026822	Lcn2	2	protein coding	0.51	0.00013
ENSMUSG00000030474	Siglece	7	protein coding	0.59	0.00013
ENSMUSG00000051257	Trap1a	X	protein coding	1.52	0.00014
ENSMUSG00000060131	Atp8b4	2	protein coding	2.24	0.00016
ENSMUSG00000021318	Gli3	13	protein coding	1.53	0.00019
ENSMUSG00000030329	C530028O21Rik	6	protein coding	0.63	0.00022
ENSMUSG00000023806	Rsph3b	17	protein coding	0.67	0.00022
ENSMUSG00000080072	Gm14757	X	pseudogene	1.93	0.00023
ENSMUSG00000085843	A730085A09Rik	4	antisense	0.56	0.00025
ENSMUSG00000090440	Gm9732	14	protein coding	0.66	0.00025
ENSMUSG00000087522	Gm371	X	pseudogene	1.64	0.00025
ENSMUSG00000043259	Fam13c	10	protein coding	0.64	0.00028
ENSMUSG00000023905	Tnfrsf12a	17	protein coding	1.67	0.00031
ENSMUSG00000045326	Fndc7	3	protein coding	1.72	0.00031
ENSMUSG00000072923	Gm10439	X	protein coding	1.66	0.00042
ENSMUSG00000090354	Gm17556	3	lincRNA	1.63	0.00044
ENSMUSG00000038156	Spon1	7	protein coding	0.55	0.00045
ENSMUSG00000082925	Gm13135	4	pseudogene	0.66	0.00045
ENSMUSG00000085261	Gm13814	2	lincRNA	0.57	0.00046
ENSMUSG00000055746	Magea2	X	protein coding	1.89	0.00049
ENSMUSG00000020279	Il9r	11	protein coding	0.61	0.00051
ENSMUSG00000054727	1700013H16Rik	X	protein coding	1.54	0.00052
ENSMUSG00000063177	Klk1b27	7	protein coding	0.47	0.00056
ENSMUSG00000030724	Cd19	7	protein coding	0.58	0.00057
ENSMUSG00000079632	Rhox2f	X	protein coding	2.34	0.00061
ENSMUSG00000028519	Dab1	4	protein coding	1.62	0.00063
ENSMUSG00000034452	Slc24a1	9	protein coding	0.40	0.00063

Ensembl ID	Gene name	Chr.	Type	FC	FDR
ENSMUSG00000021999	Cpb2	14	protein coding	0.50	0.00065
ENSMUSG00000081179	Gm13136	4	pseudogene	0.63	0.00067
ENSMUSG00000062312	Erbb2	11	protein coding	1.53	0.00068
ENSMUSG00000078690	A230006K03Rik	7	protein coding	0.42	0.00071
ENSMUSG00000026147	Col9a1	1	protein coding	0.55	0.00071
ENSMUSG00000016496	Cd274	19	protein coding	0.60	0.00071
ENSMUSG00000030670	Cyp2r1	7	protein coding	0.60	0.00073
ENSMUSG00000079634	Rhox2d	X	protein coding	2.14	0.00083
ENSMUSG00000003273	Car11	7	protein coding	1.63	0.00088
ENSMUSG00000028268	Gbp3	3	protein coding	1.56	0.00088
ENSMUSG00000082593	Gm11331	13	pseudogene	1.94	0.00095
ENSMUSG00000025498	Irf7	7	protein coding	1.65	0.00096
ENSMUSG00000081960	Mageb17-ps	X	pseudogene	1.70	0.00099
ENSMUSG00000013668	4933402N03Rik	7	protein coding	0.22	0.00101
ENSMUSG00000091987	Gm3376	Y	protein coding	1.80	0.00109
ENSMUSG00000084128	Esrp2	8	protein coding	0.58	0.00111
ENSMUSG00000028859	Csf3r	4	protein coding	0.54	0.00112
ENSMUSG00000078955	Gm14222	2	sense intronic	1.78	0.00125
ENSMUSG00000029561	Oasl2	5	protein coding	1.63	0.00125
ENSMUSG00000050071	Bex1	X	protein coding	1.71	0.00131
ENSMUSG00000057439	Kir3dl2	X	protein coding	3.25	0.00136
ENSMUSG00000075611	Gm11545	11	pseudogene	1.57	0.00141
ENSMUSG00000051582	Otud6a	X	protein coding	1.58	0.00143
ENSMUSG00000093507	RP24-201C14.11	3	processed transcript	0.51	0.00148
ENSMUSG00000040856	Dlk1	12	protein coding	1.83	0.00154
ENSMUSG00000079711	Smok4a	17	protein coding	0.24	0.00162
ENSMUSG00000031434	Morc4	X	protein coding	1.59	0.00167
ENSMUSG00000007908	Hmgcll1	9	protein coding	0.56	0.00167
ENSMUSG00000063713	Klk1b24	7	protein coding	0.57	0.00167
ENSMUSG00000058550	Dppa4	16	protein coding	0.60	0.00167
ENSMUSG00000079350	Magea8	X	protein coding	1.69	0.00178
ENSMUSG00000054626	Xlr	X	protein coding	1.69	0.00199
ENSMUSG00000043453	Magea10	X	protein coding	1.63	0.00221
ENSMUSG00000027409	1700020A23Rik	2	protein coding	0.37	0.00221
ENSMUSG00000024109	Nrxn1	17	protein coding	0.65	0.00224
ENSMUSG00000084897	Gm14226	2	protein coding	1.54	0.00238
ENSMUSG00000034687	Fras1	5	protein coding	1.60	0.00245
ENSMUSG00000022510	Trp63	16	protein coding	0.60	0.00247

Ensembl ID	Gene name	Chr.	Type	FC	FDR
ENSMUSG00000028373	Astn2	4	protein coding	0.60	0.00248
ENSMUSG00000032566	1700080E11Rik	9	protein coding	0.19	0.00249
ENSMUSG00000087303	Lipo2	19	protein coding	0.60	0.00255
ENSMUSG00000050195	Scd4	19	protein coding	1.74	0.00266
ENSMUSG00000024107	Lhcgr	17	protein coding	0.57	0.00272
ENSMUSG00000029001	Fbxo44	4	protein coding	0.64	0.00275
ENSMUSG00000001497	Pax9	12	protein coding	0.63	0.00283
ENSMUSG00000041577	Prelp	1	protein coding	1.52	0.00300
ENSMUSG00000083027	Gm13140	4	pseudogene	0.60	0.00309
ENSMUSG00000031562	Dctd	8	protein coding	1.51	0.00314
ENSMUSG00000024986	Hhex	19	protein coding	1.51	0.00316
ENSMUSG00000024039	Cbs	17	protein coding	0.57	0.00324
ENSMUSG00000090764	Gm3127	14	protein coding	1.70	0.00324
ENSMUSG00000086296	D030055H07Rik	9	antisense	0.64	0.00331
ENSMUSG00000032502	Stac	9	protein coding	0.44	0.00360
ENSMUSG00000086810	Gm13110	4	lincRNA	0.57	0.00365
ENSMUSG00000045259	Klhdc9	1	protein coding	0.66	0.00373
ENSMUSG00000078365	Mos	4	protein coding	0.45	0.00378
ENSMUSG00000047757	Fancb	X	protein coding	1.93	0.00381
ENSMUSG00000019851	Perp	10	protein coding	0.53	0.00393
ENSMUSG00000067764	Xlr5c	X	protein coding	1.58	0.00403
ENSMUSG00000031125	3830403N18Rik	X	protein coding	1.51	0.00403
ENSMUSG00000023263	9530002B09Rik	4	protein coding	2.10	0.00405
ENSMUSG00000090470	2410012M07Rik	9	protein coding	1.81	0.00462
ENSMUSG00000080069	Gm41	X	pseudogene	1.54	0.00472
ENSMUSG00000021313	Ryr2	13	protein coding	1.73	0.00472
ENSMUSG00000085465	Gm15347	8	antisense	0.40	0.00486
ENSMUSG00000082082	Gm13230	4	pseudogene	2.34	0.00494
ENSMUSG00000084939	Gm830	4	processed transcript	0.37	0.00498
ENSMUSG00000049202	4930515G13Rik	17	pseudogene	0.58	0.00503
ENSMUSG00000024784	Gpha2	19	protein coding	0.52	0.00505
ENSMUSG00000085002	Gm12984	4	antisense	1.55	0.00512
ENSMUSG00000090381	Gm6158	14	protein coding	0.66	0.00517
ENSMUSG00000078486	2310042D19Rik	4	protein coding	0.65	0.00522
ENSMUSG00000073197	5730507C01Rik	12	protein coding	1.83	0.00535
ENSMUSG00000041828	Abca8a	11	protein coding	0.62	0.00580
ENSMUSG00000081885	Gm13231	4	pseudogene	0.62	0.00587
ENSMUSG00000054013	Tmem179	12	protein coding	1.65	0.00595

Ensembl ID	Gene name	Chr.	Type	FC	FDR
ENSMUSG00000087566	C920006O11Rik	9	lincRNA	0.66	0.00595
ENSMUSG00000066516	Klk1b21	7	protein coding	0.59	0.00601
ENSMUSG00000028707	Dmbx1	4	protein coding	1.68	0.00608
ENSMUSG00000063632	Sox11	12	protein coding	1.65	0.00608
ENSMUSG00000085419	Gm11734	11	lincRNA	0.55	0.00608
ENSMUSG00000087501	Gm12116	11	antisense	0.64	0.00613
ENSMUSG00000026354	Lct	1	protein coding	0.59	0.00613
ENSMUSG00000030107	Usp18	6	protein coding	1.66	0.00615
ENSMUSG00000051003	Olfr161	16	protein coding	0.56	0.00624
ENSMUSG00000063089	Klk1b8	7	protein coding	0.32	0.00641
ENSMUSG00000086075	Gm15728	5	lincRNA	0.66	0.00641
ENSMUSG00000027456	Sdcbp2	2	protein coding	0.66	0.00679
ENSMUSG00000086172	2700068H02Rik	4	antisense	0.58	0.00679
ENSMUSG00000052831	Rbmy1a1	Y	protein coding	1.85	0.00709
ENSMUSG00000039578	Fam190a	6	protein coding	0.44	0.00729
ENSMUSG00000049902	4921517D22Rik	13	protein coding	0.30	0.00731
ENSMUSG00000072932	Gm15128	X	protein coding	1.61	0.00754
ENSMUSG00000086574	Gm16960	9	lincRNA	0.59	0.00794
ENSMUSG00000069806	Cacng7	7	protein coding	0.66	0.00794
ENSMUSG00000026009	Icos	1	protein coding	2.30	0.00811
ENSMUSG00000032271	Nnmt	9	protein coding	0.48	0.00829
ENSMUSG00000093526	A930033C23Rik	5	antisense	0.63	0.00835
ENSMUSG00000033576	Apol6	15	protein coding	0.52	0.00848
ENSMUSG00000055816	Magea3	X	protein coding	1.57	0.00870
ENSMUSG00000028518	Prkaa2	4	protein coding	1.56	0.00876
ENSMUSG00000082332	Gm13384	2	pseudogene	0.57	0.00931
ENSMUSG00000044164	Rnf182	13	protein coding	0.64	0.00937
ENSMUSG00000054362	BC055111	4	protein coding	0.46	0.00952
ENSMUSG00000079681	Zglp1	9	protein coding	1.50	0.00953
ENSMUSG00000071773	Rhox1	X	protein coding	1.66	0.00970
ENSMUSG00000083732	Gm14197	2	pseudogene	0.43	0.00982
ENSMUSG00000058420	Syt17	7	protein coding	0.58	0.01054
ENSMUSG00000074895	Eif4e1b	13	protein coding	1.70	0.01090
ENSMUSG00000031285	Dcx	X	protein coding	2.26	0.01132
ENSMUSG00000053839	Gm9924	5	protein coding	0.54	0.01189
ENSMUSG00000063728	Magea6	X	protein coding	1.67	0.01210
ENSMUSG00000046008	Pnlip	19	protein coding	0.47	0.01222
ENSMUSG00000031085	Gm498	7	protein coding	0.27	0.01232

Ensembl ID	Gene name	Chr.	Type	FC	FDR
ENSMUSG00000079566	4930408F14Rik	X	protein coding	1.69	0.01236
ENSMUSG00000031698	Mylk3	8	protein coding	1.52	0.01242
ENSMUSG00000050876	Fam75d3	13	protein coding	0.54	0.01263
ENSMUSG00000071015	Gm136	4	protein coding	0.34	0.01263
ENSMUSG00000042678	Myo15	11	protein coding	0.64	0.01286
ENSMUSG00000074063	Osgin1	8	protein coding	0.63	0.01301
ENSMUSG00000027075	Slc43a1	2	protein coding	1.60	0.01309
ENSMUSG00000030098	Grip2	6	protein coding	1.76	0.01353
ENSMUSG00000022053	Ebf2	14	protein coding	1.59	0.01382
ENSMUSG00000033343	Magea4	X	protein coding	1.52	0.01388
ENSMUSG00000091401	Gm9252	7	pseudogene	0.36	0.01389
ENSMUSG00000087428	Gm15017	X	processed transcript	1.69	0.01435
ENSMUSG00000072919	4933437F05Rik	12	protein coding	0.60	0.01460
ENSMUSG00000034416	Pkd1l2	8	protein coding	0.66	0.01462
ENSMUSG00000046352	Gjb2	14	protein coding	1.82	0.01474
ENSMUSG00000038015	Prm2	16	protein coding	0.31	0.01487
ENSMUSG00000075389	2810410L24Rik	11	lincRNA	1.50	0.01488
ENSMUSG00000082154	Gm16464	7	pseudogene	0.54	0.01490
ENSMUSG00000051827	Rhox2a	X	protein coding	1.68	0.01497
ENSMUSG00000085486	Gm11634	11	antisense	0.26	0.01501
ENSMUSG00000019789	Hey2	10	protein coding	1.71	0.01552
ENSMUSG00000042498	D330045A20Rik	X	protein coding	1.51	0.01567
ENSMUSG00000086898	1700062I23Rik	17	antisense	0.29	0.01569
ENSMUSG00000061835	Olfr316	11	protein coding	0.49	0.01623
ENSMUSG00000078123	Gm5071	X	pseudogene	1.55	0.01679
ENSMUSG00000022501	Prm1	16	protein coding	0.33	0.01679
ENSMUSG00000036574	1700019O17Rik	1	pseudogene	0.39	0.01763
ENSMUSG00000041911	Dlx1	2	protein coding	1.60	0.01794
ENSMUSG00000043050	Tnp2	16	protein coding	0.34	0.01794
ENSMUSG00000040680	Kremen2	17	protein coding	2.12	0.01812
ENSMUSG00000068011	2510049J12Rik	6	protein coding	1.53	0.01818
ENSMUSG00000091405	Hist2h4	3	protein coding	0.57	0.01899
ENSMUSG00000079343	Gm5077	6	protein coding	0.65	0.01901
ENSMUSG00000074999	Gm10797	10	protein coding	0.42	0.01929
ENSMUSG00000040797	Iqsec3	6	protein coding	0.50	0.01929
ENSMUSG00000056940	Gm3629	14	protein coding	1.51	0.01950
ENSMUSG00000051036	Ttc24	3	protein coding	0.35	0.01971
ENSMUSG00000089396	U1	15	snRNA	0.65	0.01986

Ensembl ID	Gene name	Chr.	Type	FC	FDR
ENSMUSG00000031877	Ces2g	8	protein coding	1.56	0.02019
ENSMUSG00000038236	Hoxa7	6	protein coding	1.87	0.02029
ENSMUSG00000090118	Gm16163	8	processed transcript	0.60	0.02037
ENSMUSG00000050671	Ism2	12	protein coding	1.90	0.02071
ENSMUSG00000033981	Gria2	3	protein coding	0.47	0.02081
ENSMUSG00000049307	Fut4	9	protein coding	1.80	0.02134
ENSMUSG00000000094	Tbx4	11	protein coding	0.61	0.02219
ENSMUSG00000082728	Fam48b1	X	pseudogene	1.70	0.02225
ENSMUSG00000024738	Pga5	19	protein coding	0.43	0.02237
ENSMUSG00000079387	Luzp4	X	protein coding	1.83	0.02254
ENSMUSG00000085585	Gm12223	11	antisense	0.53	0.02277
ENSMUSG00000087111	Gm11399	11	antisense	0.67	0.02281
ENSMUSG00000067049	Unc93a	17	protein coding	0.44	0.02332
ENSMUSG00000033634	Cml2	6	protein coding	0.53	0.02366
ENSMUSG00000021966	Prss52	14	protein coding	0.31	0.02383
ENSMUSG00000081792	Anp32b-ps1	4	pseudogene	0.60	0.02419
ENSMUSG00000071770	Rhox4e	X	protein coding	1.95	0.02454
ENSMUSG00000074731	Zfp345	2	protein coding	0.58	0.02534
ENSMUSG00000029608	Rph3a	5	protein coding	0.42	0.02545
ENSMUSG00000034127	Tspan8	10	protein coding	0.65	0.02547
ENSMUSG00000006958	Chrd	16	protein coding	0.64	0.02552
ENSMUSG00000079627	Rhox2h	X	protein coding	2.17	0.02667
ENSMUSG00000091594	Gm17067	7	protein coding	0.37	0.02713
ENSMUSG00000079391	Gm2974	14	protein coding	1.64	0.02740
ENSMUSG00000059146	Ntrk3	7	protein coding	0.55	0.02781
ENSMUSG00000045053	Kcng3	17	protein coding	1.83	0.02805
ENSMUSG00000074849	4932441B19Rik	13	protein coding	0.36	0.02812
ENSMUSG00000085170	4930557C09Rik	11	antisense	0.50	0.02849
ENSMUSG00000045034	Ankrd34b	13	protein coding	1.71	0.02894
ENSMUSG00000032087	Dscaml1	9	protein coding	0.44	0.02913
ENSMUSG00000024406	Pou5f1	17	protein coding	0.54	0.02937
ENSMUSG00000074194	Zfp791	8	protein coding	1.58	0.02969
ENSMUSG00000053228	Ceacam3	7	protein coding	2.33	0.02979
ENSMUSG00000057137	Tmem140	6	protein coding	1.55	0.03037
ENSMUSG00000010461	Eya4	10	protein coding	0.58	0.03048
ENSMUSG00000039057	Myo16	8	protein coding	1.53	0.03059
ENSMUSG00000091088	4921514A10Rik	4	lincRNA	0.59	0.03070
ENSMUSG00000054074	2810030E01Rik	2	protein coding	1.61	0.03142

Ensembl ID	Gene name	Chr.	Type	FC	FDR
ENSMUSG00000020077	Srgn	10	protein coding	0.66	0.03143
ENSMUSG00000063684	Gm13910	2	pseudogene	0.60	0.03187
ENSMUSG00000073374	C030034I22Rik	17	protein coding	1.64	0.03189
ENSMUSG00000021640	Naip1	13	protein coding	0.62	0.03221
ENSMUSG00000031391	L1cam	X	protein coding	1.90	0.03274
ENSMUSG00000043068	Fam89a	8	protein coding	0.60	0.03280
ENSMUSG00000067215	Usp51	X	protein coding	1.56	0.03298
ENSMUSG00000018919	Tm4sf5	11	protein coding	0.45	0.03299
ENSMUSG00000064602	Snora41	1	snoRNA	0.48	0.03350
ENSMUSG00000076438	Oxct2b	4	protein coding	0.32	0.03470
ENSMUSG00000031302	Nlgn3	X	protein coding	1.55	0.03490
ENSMUSG00000024254	Abcg8	17	protein coding	0.59	0.03551
ENSMUSG00000038151	Prdm1	10	protein coding	1.92	0.03551
ENSMUSG00000028332	Hemgn	4	protein coding	0.32	0.03611
ENSMUSG00000028328	Tmod1	4	protein coding	0.56	0.03632
ENSMUSG00000029707	Fscn3	6	protein coding	0.37	0.03682
ENSMUSG00000071816	Ssxb5	X	protein coding	1.59	0.03691
ENSMUSG00000020401	Fam71b	11	protein coding	0.39	0.03700
ENSMUSG00000076315	Mir343	7	miRNA	0.65	0.03725
ENSMUSG00000092438	Gm18734	17	pseudogene	0.67	0.03728
ENSMUSG00000076436	Oxct2a	4	protein coding	0.32	0.03728
ENSMUSG00000084904	Gm14827	X	lincRNA	1.86	0.03781
ENSMUSG00000078160	Gm16503	4	protein coding	0.58	0.03795
ENSMUSG00000027482	Bpifa3	2	protein coding	0.35	0.03809
ENSMUSG00000087075	A230065H16Rik	12	protein coding	1.71	0.03875
ENSMUSG00000079638	Rhox2b	X	protein coding	1.89	0.03893
ENSMUSG00000074454	Defb33	8	protein coding	0.32	0.03893
ENSMUSG00000033060	Lmo7	14	protein coding	0.65	0.03929
ENSMUSG00000031709	Tbc1d9	8	protein coding	0.62	0.03973
ENSMUSG00000050526	4933406M09Rik	1	protein coding	0.46	0.04001
ENSMUSG00000091017	Fam71a	1	protein coding	0.41	0.04015
ENSMUSG00000074625	Arhgap40	2	protein coding	0.59	0.04034
ENSMUSG00000091737	Gm17543	1	lincRNA	0.52	0.04077
ENSMUSG00000026989	Dapl1	2	protein coding	0.45	0.04094
ENSMUSG00000085577	Mageb6-ps	X	pseudogene	1.62	0.04099
ENSMUSG00000039942	Ptger4	15	protein coding	1.59	0.04106
ENSMUSG00000011350	Gm5893	7	processed transcript	0.32	0.04140
ENSMUSG00000015962	1700016C15Rik	1	protein coding	0.35	0.04198

| Ensembl ID	Gene name	Chr.	Type	FC	FDR
ENSMUSG00000017720	Trp53tg5	2	protein coding	0.41	0.04329
ENSMUSG00000023192	Grm2	9	protein coding	0.46	0.04355
ENSMUSG00000072744	Gm8165	14	protein coding	1.69	0.04616
ENSMUSG00000030111	A2m	6	protein coding	1.82	0.04618
ENSMUSG00000048489	8430408G22Rik	6	protein coding	2.13	0.04672
ENSMUSG00000009900	Wnt3a	11	protein coding	0.54	0.04714
ENSMUSG00000026904	Slc4a10	2	protein coding	0.66	0.04850
ENSMUSG00000081402	Gm15455	1	pseudogene	0.57	0.04893
ENSMUSG00000026934	Lhx3	2	protein coding	1.70	0.04944
ENSMUSG00000018263	Tbx5	5	protein coding	0.43	0.04954

Appendix C: Supplemental Figures
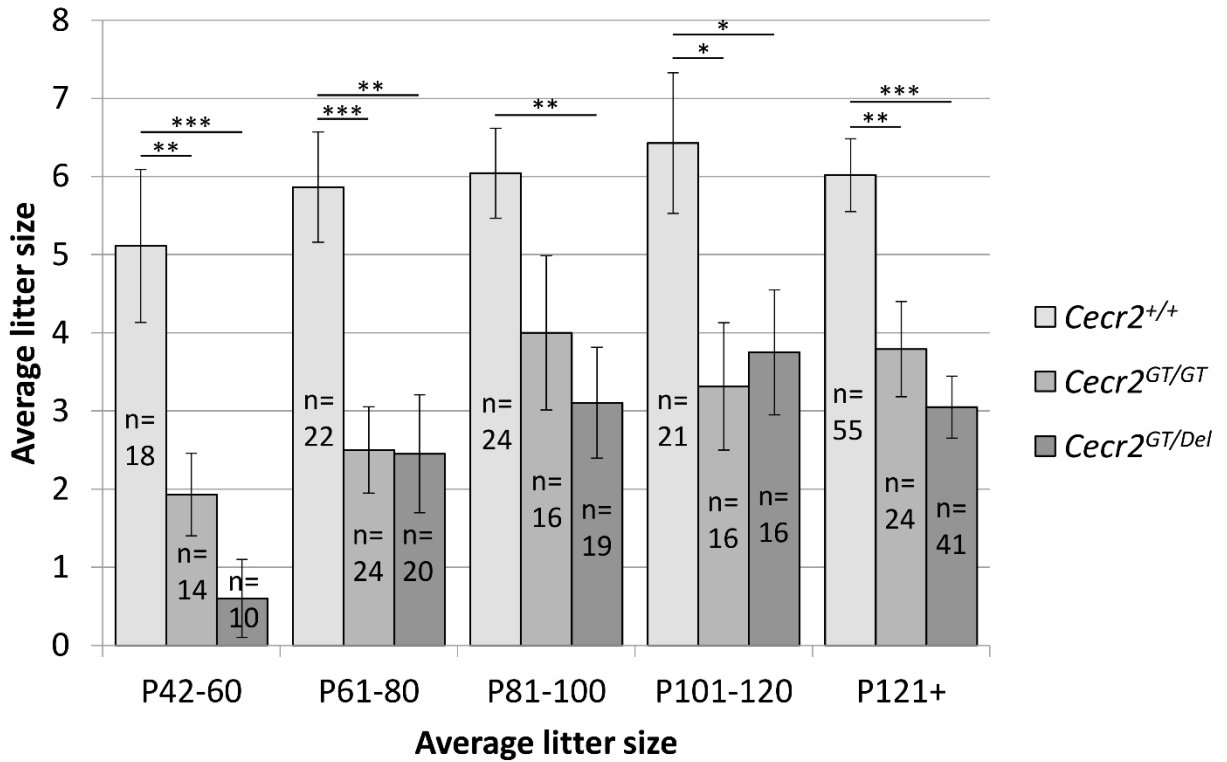
Figure C.1: Average litter sizes of *Cecr2* mutant males. This graph is the same as Figure 2.3 A, but with additional data from *Cecr2^GT/GT^* males. Levels of significance: *** $P \leq 0.001$, ** $0.001 \leq P < 0.01$, * $0.01 \leq P < 0.05$, and no asterisk indicates a lack of significance ($P > 0.05$). n= number of litters.

Appendix D: Supplemental Methods

D.1: Mouse husbandry

Approval was obtained from the University of Alberta Animal Care and Use Committee for all experiments involving mice (University of Alberta AUP 00000094). The colony was maintained daily by Science Animal Support Services (SASS) technicians. Mice were housed in ventilated cages (IVC Blue Line, Tecniplast, Buguggiate, Italy) except after exposure to non-ventilated air during surgery (see section 3.2.8), after which they were housed in filter top cages to avoid exposing the main colony to these mice that had a higher risk of contamination. They were maintained at 22±2°C with a 14 hour light/10 hour dark cycle with cardboard houses. Mice were generally euthanized using a HiRoad Euthanasia Chamber, which used isoflurane to anesthetize the mice before CO_2 euthanasia. Cervical dislocation was used for experiments requiring rapid dissection and tissue collection or mice under 3 weeks of age. Embryos collected late in gestation were euthanized by decapitation before they were dissected. The vast majority of this work was done using a BALB/cCrl strain of mice originating from Charles River Laboratories but maintained as a breeding colony within the University of Alberta for approximately 50 years. The protein work shown in Figure 2.1 C was done using an FVB/N strain originally from Jackson Laboratories, as FVB/N *Cecr2*^{Del/Del} mice are viable.

D.2: DNA extractions

Tissue samples were collected in 1.5 mL tubes and stored at -20°C until extraction. Ear notches were used for live mice, tails were collected from embryos, and tongue tissue was collected from adult mice at the time of dissection to confirm genotypes. Samples were then submerged in 75 µL of 50 mM NaOH and placed in a 95°C water bath for 1-3 hours (adapted from Lopez, 2012). Upon removal, they were vortexed and stored at 4°C until PCR reactions were complete. After this, samples were moved to -20°C for long term storage.

D.3: *Cecr2*^{GT} and Sry genotyping

A multiplexed PCR reaction was used to amplify the *Cecr2*⁺ allele, *Cecr2*^{GT} allele, and the male specific *Sry* gene to determine sex. The Mmu Intron7 F4, Mmu Intron7 R4, and pGT1R4 primers amplified a portion of the *Cecr2*⁺ allele (376 bp) and/or the *Cecr2*^{GT} allele (573 bp), while the SRY FOR and SRY REV primers amplified the *Sry* gene (266 bp) in males only. PCR reactions were 22 µL, containing a final concentration of 1X DreamTaq Buffer, 0.23 mM dNTPS, 0.91 µM of each primer, 1.5 U of DreamTaq (ThermoFisher, EP0705), and 2 µL of genomic DNA (unknown concentration, see D.2). These reactions were

amplified using a Bio-Rad T100 Thermal Cycler as follows: (1) 94°C for 3 minutes (2) 94°C for 15 seconds (3) 60°C for 20 seconds (4) 68°C for 40 seconds (5) repeat steps 2-4 36 times (6) 68°C for 5 min (7) hold at 4°C. Orange G was then added to load samples into a 2% agarose gel containing 0.1 µg/mL ethidium bromide. Gels were made and run in 1X TAE buffer (components) at ~130 V for 50 minutes. Bands were detected using an Alpha Innotech UV fluorescence gel imager.

D.4: Cecr2^{Del} genotyping

The IngeniousLox1, Ingenious SDL2, and LoxCECR2_DEL3R primers were used to amplify a portion of the *Cecr2+* allele (220 bp) and/or the *Cecr2^{Del}* allele (~450 bp). PCR and gel electrophoresis conditions were the same as for *Cecr2^{GT}* genotyping (see section D.3).

D.5: RNA extractions

RNA extractions were done using the Qiagen RNeasy lipid tissue kit (Qiagen, 74804) on previously frozen samples stored at -80°C. For uterus samples and testes under 42 days old, the entire tissue sample was used. For larger testes obtained from males 42 days or older, only approximately half of the tissue was used for extraction. The tunica albuginea was removed from all testes samples before beginning. Tissues were initially lysed and homogenized using a small plastic pestle in a 1.5 mL tube containing 1 mL of Qiazol lysis reagent, followed by vigorous pipetting using consecutively smaller pipette tips. The kit protocol was then followed as per manufacturer's instructions, and RNA was eluted using 60 µL (testis samples) or 40 µL (uterus samples) of nuclease-free H_2O. RNA concentration was then measured using the Qubit fluorometer at the MBSU, and a sample of RNA from each sample was treated with a DNA-free DNA removal kit (Invitrogen, #AM1906) as per manufacturer's instructions. After measuring RNA concentration again, samples were aliquoted into 1 µg aliquots and flash frozen in liquid nitrogen before storage at -80°C.